



Brunel
University
London

The Fundamentals of Pipeline Cleaning
with
Acoustic Cavitation

by

Ignacio María García de Carellán Esteban-Infantes

*A thesis submitted in partial fulfilment for the
degree of Doctor of Philosophy*

in the

Institute of Materials and Manufacturing
School of Engineering, Design and Physical Sciences

January 2016

Declaration of Authorship

I, Ignacio María García de Carellán Esteban-Infantes, declare that this thesis titled, “The Basics of Pipeline Cleaning with Acoustic Cavitation” and the work presented in it are my own. I confirm that:

- This work was done wholly or mainly while in candidature for a research degree at this University.
- Where any part of this thesis has previously been submitted for a degree or any other qualification at this University or any other institution, this has been clearly stated.
- Where I have consulted the published work of others, this is always clearly attributed.
- Where I have quoted from the work of others, the source is always given. With the exception of such quotations, this thesis is entirely my own work.
- I have acknowledged all main sources of help.
- Where the thesis is based on work done by myself jointly with others, I have made clear exactly what was done by others and what I have contributed myself.

Signed:



Date: 21/05/2019

"A good friend is not something that you have, is something that you are"

Myself

BRUNEL UNIVERSITY

Abstract

Institute of Materials and Manufacturing
College of Engineering, Design and Physical Sciences

Doctor of Philosophy

by Ignacio María García de Carellán Esteban-Infantes

This thesis undertakes the fundamentals of a new method for in-situ cleaning of industrial pipe fouling, which shows promising results on a hard commonly occurring fouling in process environment: Calcite. The presence of fouling causes a substantial increase in plant operation costs for a number of reasons, including efficiency reduction, and potentially causes contamination of products. The feasibility of cleaning Calcite fouling from industrial pipework using acoustic cavitation without having to dismantle the pipe network has been explained. For this, the existing theories of acoustic cavitation are related with the out-of-the-plane displacements occurring on the wall of sample pipes induced to vibration to analyse the cleaning process with acoustic cavitation. For the cavitation generation a modification of commercial high power transducers (HPT) is undertaken. The displacements of these HPT are analysed and compared with the displacements established in the theory required to produce transient cavitation. The cavitation produced by the modified HPT is measured with acoustic emission to improve the explanation of the phenomena responsible of the cleaning. Finally, sample pipes are cleaned with ultrasonic waves guided by the pipe wall while measuring the displacement of their outside wall using a 3D Scanning Vibrometer. The most effective cleaning occurs in the vicinity of antinodes and complete cleaning is only achieved when transient cavitation is generated.

Acknowledgments

I do feel grateful every single day of my life, is a must, for everything I have been given by nature and for all the persons I have met and have contributed to my personal growth, development, enjoyment, failures, etcetera. But, sometimes you have a special chance to say thank you, thank you very much! And then you realise that there are, and there has always been, some persons in your life that have given to it its real shape and, in a way, they are indeed part of yourself. Now I have that chance, and I would like to state my gratefulness like this.

I would like to start thanking all the placement students that have co-worked with me contributing with their effort, knowledge, and smiles to this hard way that is a PhD. Caumaghen Sannassy, Raghav Dave, Habiba Lais, and Zaidoun Baquain. Thanks a million!

To continue, I would like to thank my two supervisors that gave me this great opportunity and have given me the guidance towards success; Prof. Wamadeva Balachandran, Bala, and Prof. Tat-Hean Gan. Thank you very much for everything!

If we were talking just about the PhD in itself, the hardest moments, the tricky decisions, the frustration and motivation, the scientific discussions, the arguments! Then, I have to thank all my PhD colleagues from BIC, Pi or AFM. But, because the great gratitude that I feel, I have to do a distinct mention to two persons that have been really significant in this path. Because, more important than a massive knowledge in pipelines and in this particular field, I am taking two great, huge, and special FRIENDS that have become immortals in my mind. Bhavin Engineer and Keith Thornicroft. I “Keith” you guys! (Where “To Keith” means the strongest feeling that a person can have to another person, above love and below hate).

To my family. They have always been there no matter what, and they will be part of every single moment forever in my life. Especially to my indefatigable mother, I cannot remember a single moment in my life without her pushing me further like someone trying to roll a square rock. Thank you very much!

But, after all, my largest gratitude has to be given to her. My life, my support, my other half, the most amazing person the world has ever met. The one that makes me be the luckiest, the happiest, and the strongest. The first thing I want to see every single day of my life and the last one I want to hug before going to sleep. No-one has ever believed in me as much as you do, and no-one will ever make me feel as good you do. You definitely make me be a much better person and I am totally and absolutely in love with every single part of your being. Estefania Artigao Andicoberry, Fani, my Fani, thank you very much indeed!

The research leading to these results has received funding from the European Community's Seventh framework Programme managed by REA-Research Executive Agency <http://ec.europa.eu/research/rea> FP7/2007-2010, under grant agreement 262327.

Contents

Declaration of Authorship	i
Abstract	iii
Acknowledgements	iv
List of figures	viii
List of tables	xii
Abbreviations	xii
Physical Constants	xiv
Symbols	xv
1 Introduction	1
1.1 Motivation	1
1.2 Aims and Objectives	3
1.3 Methodology summary	4
1.4 Thesis Outline	6
1.5 Contribution to new knowledge	7
1.6 Publications	8
2 Literature review of pipe cleaning methods	10
2.1 Introduction	10
2.2 Non acoustic methods	11
2.2.1 Flushing	11
2.2.2 PIGging	12
2.2.3 Air Scouring	13
2.2.4 Chemical cleaning	13
2.2.5 Jetting	14
2.2.6 Cleaning and lining Rehabilitation	15
2.3 Acoustic methods	17
2.3.1 Patents	17
2.3.2 Technical investigations and technique proposed	18
2.3.3 Acoustic methods for biofouling prevention and removal	21
2.4 Summary	22
3 Creation of fouling on inner walls of pipe samples	24
3.1 Introduction	24

3.2	Objectives	25
3.3	Creation of fouling on pipes and plates using laboratory based tests.....	25
3.3.1	Electrochemical reaction.....	26
3.3.2	Sprayed deposition on heated plates	32
3.4	Results and interpretation	33
3.4.1	Electrochemical reaction composition analysis of Pipe 1	33
3.4.2	Electrochemical reaction composition analysis of Pipe 2	37
3.4.3	Electrochemical reaction composition analysis of Pipe 3	39
3.4.4	Spraying deposition on heated plates composition analysis.....	41
3.4.5	Adhesion quality analyses on sample plates.....	43
3.5	Summary	44
4	Theoretical background of acoustic cavitation.....	46
4.1	Introduction	46
4.2	Acoustic cavitation.....	47
4.3	Cavitation prediction	48
4.3.1	Rectified diffusion threshold.....	49
4.3.2	Blake threshold.....	49
4.3.3	Transient cavitation threshold.....	50
4.3.4	Inertial control radius	50
4.4	Cavitation prediction plots.....	51
4.5	Acoustic pressure generated by an oscillating wall	52
4.6	Cavitation prediction plots for further investigation.....	54
4.7	Summary	56
5	High Power Transducers (HPT) for the removal of fouling in pipelines	57
5.1	Introduction	57
5.2	Current HPT design.....	58
5.2.1	Transducers Selection.....	60
5.2.2	Transducers Modification.....	61
5.2.3	Attachment method and couplants.....	63
5.3	Transducer Analysis Techniques	64
5.3.1	Electrical Impedance Analysis.....	64
5.3.2	3D Scanning Vibrometer Analysis	66
5.4	Transducer Analysis Results	69
5.4.1	Resonant Frequencies.....	69
5.4.2	Modes of Vibration.....	77
5.4.3	Displacement	87
5.5	Summary	89

6	Cavitation detection in pipes generated by high power ultrasonic transducers	91
6.1	Introduction	91
6.2	Cavitation detection set-up and procedure	93
6.3	Spectral analysis results.....	94
6.3.1	Welch Method	95
6.4	Cavitation threshold detection and proposed.....	98
6.4.1	Conventional plotting method.....	99
6.4.2	Proposed plotting method.....	99
6.5	Summary	103
7	Cleaning of fouled pipes using high power ultrasonic waves.....	104
7.1	Introduction	104
7.2	Experimental procedure and set-up.....	106
7.3	Results and discussion	107
7.3.1	Pipe number 1)	112
7.3.2	Pipe number 2).....	119
7.4	Summary	124
8	Preindustrial trials.....	125
8.1	UltraCleanPipe collar and transducers test.....	125
8.2	Field trials in an industrial laboratory.....	134
8.2.1	Fouling creation for the field trails.....	134
8.2.2	Fouling creation setup	134
8.2.3	Procedure for the fouling creation	135
8.2.4	Fouling creation results	137
8.3	Field Trials set-up and procedure	137
8.4	Final trials procedure	140
8.5	Summary	146
9	Conclusions	147
9.1	Conclusions	147
9.2	Recommendation for future work.....	149
	References	151
	APPENDIX A	167
	APPENDIX B	173

LIST OF FIGURES

Figure 1.1. Example of a pipeline and laying maintenance by introducing a device inside the pipe.....	1
Figure 1.2. Example of different fouling accumulation in a 1 cm pipe section.....	2
Figure 1.3. Schematic idea of the UltraCleanPipe system for pipeline cleaning with ultrasounds.....	3
Figure 3.1. Corrosion process of steel in aqueous medium.....	27
Figure 3.2. Electrochemical deposition scheme.	29
Figure 3.3. Images of Sample Pipe 1, Before and After Undergoing Fouling Creation.....	30
Figure 3.4. Sample pipe prepared for being immersed into vessel.....	31
Figure 3.5. Set-Up of Fouling Creation Experimentation.....	31
Figure 3.6. Sprayed deposition on heated plates with atomizer set-up diagram.....	32
Figure 3.7. Results of Fouling Creation on Inner Walls of Pipe 1, a) is the picture taken from the bottom and b) is the picture taken from the top.....	34
Figure 3.8. Energy-dispersive X-ray spectroscopy (EDX) of one point location of the inner wall of a fouled pipe.	35
Figure 3.9. X-Ray Diffraction (XRD) of a sample scratched from pipe and the comparison with the expected results of copper (I) oxide, aragonite, Calcite and vaterite.	36
Figure 3.10. Scanning Electron Microscope (SEM) image of one point location of the inner wall of a fouled pipe.	36
Figure 3.11. Results of Fouling Creation on Inner Walls of Pipe 2, a) is the picture taken from the bottom and b) is the picture taken from the top.....	37
Figure 3.12. Energy-dispersive X-ray spectroscopy (EDX) of one point location of the inner wall of Pipe 2.....	37
Figure 3.13. X-Ray Diffraction (XRD) of a sample scratched form Pipe 2 and the comparison with the expected results of Calcite, aragonite, vaterite, and copper (I) oxide.....	38
Figure 3.14. Scanning Electron Microscope (SEM) image of one point location of the inner wall of Pipe 2.....	39
Figure 3.15. Results of Fouling Creation on Inner Walls of Pipe 3, a) is the picture taken from the bottom and b) is the picture taken from the top.....	39
Figure 3.16. Energy-dispersive X-ray spectroscopy (EDX) of one point location of the inner wall of a fouled pipe.....	40
Figure 3.17. X-Ray Diffraction (XRD) of a sample scratched form Pipe 3 and the comparison with the expected results of vaterite and Calcite.....	40
Figure 3.18. Scanning Electron Microscope (SEM) image of one point location of the inner wall of Pipe 3.....	41
Figure 3.19. Sample plates before and after the heating deposition with an atomizer method....	42
Figure 3.20. Energy-dispersive X-ray spectroscopy (EDX) of one point location of the inner wall of a fouled plate by heating deposition with atomizer method.....	42
Figure 3.21. X-Ray Diffraction (XRD) of a sample scratched form fouled plate and the comparison with a pure Calcite diffraction angles in purple.....	43
Figure 3.22. Scanning Electron Microscope (SEM) image of one point location of the inner wall of a fouled plate.....	43
Figure 4.1. Represents the cavitation prediction plot for an acoustic field of 10 kHz with a water with a saturation value $C=1$. Picture taken from [151]. Equation (4.6) is represented by R_D , equation (4.8) is represented by R_B , equation (4.9) is represented by R_T , and equation (4.11) is represented by R_I . The three regions A, B and C are highlighted with an orange square.....	51
Figure 4.2. Illustration of a vibrating wall in contact with a fluid generating an acoustic wave in the fluid.....	53

Figure 4.3. Cavitation prediction plots for tap water with a gas saturation of 1 for 30 kHz ultrasonic excitation that corresponds with the typical condition applied in further investigations preformed in this work.	55
Figure 5.1. High Power Langevin transducer typical configuration.	59
Figure 5.2. 1D Vibrometry analysis of the contact surface of a HPT. a) Shows the vibration at the main resonant frequency in which the entire contact surface is vibrating at the same phase. b) and c) illustrate resonant frequencies with different phase distribution that could be considered to be used depending on the application, d) and e) present the random vibration of the surface at those frequencies.	60
Figure 5.3. Schematic illustration of the contact surface of a flat and concave transducer.	62
Figure 5.4. Transducers under analysis, a) T43 transducer with concave surface, b) contact surface of T43.	62
Figure 5.5. Detailed dimensions of transducer T43 machined to fit on pipe of external radius of 25.54mm.	63
Figure 5.6. Representative circuit of a HPT.	64
Figure 5.7. Impedance analysis setup for one single transducer.	65
Figure 5.8. 3D scanning vibrometer setup for the analysis of one HPT vibration.	67
Figure 5.9. Schematic representation of the relative location of the three heads of the 3DSV and the contact surface of a HPT submitted to a vibrometry analysis.	68
Figure 5.10. Impedance analysis of T41 HPT. The frequencies under analysis are marked.	70
Figure 5.11. Impedance analysis of T43 HPT prior to the machining method.	70
Figure 5.12. Impedance of T43 with a concave surface after being machined.	71
Figure 5.13. Impedance Analysis Comparison of T43 Transducer before and after being machined.	72
Figure 5.14. Axis orientation, origin and contact surface of a HPT under the 3DSV analysis.	73
Figure 5.15. Displacement measurement per frequency of the transducer T41 with the vibrometer.	74
Figure 5.16. Comparison between the frequency analysis of the impedance analysis and the 3DSV for T41.	75
Figure 5.17. Axis orientation, origin and contact surface of a concave HPT under the 3DSV analysis.	75
Figure 5.18. Displacement measurement per frequency of the transducer T43 concave with the 3DSV.	76
Figure 5.19. Frequency analysis comparison between the impedance and FFT vibrometer analysis for T43 concave.	76
Figure 5.20. Points location on the two transducers surface for T41 a) and T43 b).	77
Figure 5.21. Mode of vibration analysis at the two opposite instants of maximum amplitude at resonant frequency 1 for T41 a) and c), and T43 b) and d).	78
Figure 5.22. Mode of vibration analysis at the two opposite instants of maximum amplitude at resonant frequency 2 for T41 a) and c), and for T43 concave b) and d).	80
Figure 5.23. Mode of vibration analysis at the two opposite instants of maximum amplitude at resonant frequency 3 for T41 a) and c), and T43 concave b) and d).	82
Figure 5.24. Mode of vibration analysis at the two opposite instants of maximum amplitude at resonant frequency 4 for T41 a) and c), and T43 concave b) and d).	84
Figure 5.25. Mode of vibration analysis at the two opposite instants of maximum amplitude at resonant frequency 5 for T41 a) and c), and T43 concave b) and d).	86
Figure 5.26. Average displacement of the contact surface of T41 on the “Z” direction vs power drained by T41. Each point is the average of 100 measurements with the 3DSV.	88
Figure 5.27. Average displacement of the contact surface of T43 concave on the “Z” direction vs power drained by T43. Each point is the average of 100 measurements with the 3DSV.	88

Figure 5.28. Comparison of average displacement of the contact surface of T41 and T43 excited with sine and square signals.	89
Figure 7.1. Classic ultrasonic cleaning device and principle.	105
Figure 7.2. Example pipe statements used for the experimentation.	106
Figure 7.3. Axis orientation, origin and displacement visualization with the 3DSV.	107
Figure 7.4. Relation between the scanning area measured with the vibrometer and the cleaning area to be compared, a) presents outside of the pipe where the reflective beads are highlighted, b) presents the inner location of the scanning area which is the location that is going to be compared below.....	108
Figure 7.5. 3DSV results obtained from the measurement of the vibration of the scanning area at the same time that the cleaning is being performed.	109
Figure 7.6. Schematic explanation of the conversion of the displacement obtained by the vibrometer to the vibrations in the radial direction.	111
Figure 7.7. Representation of the necessary angles for the calculation of the displacement in the radial direction on the plane x-z for each point on the contact surface.	111
Figure 7.8. FFT analysis of the scanning surface for pipe number 1 to find the frequency that produces the largest displacements in the Z direction.	112
Figure 7.9. Inside wall of pipe number 1 halved after the cleaning.....	114
Figure 7.10. Inner surface of the pipe after the cleaning procedure and representation of the cleaning areas related with the nodes and antinodes of the vibration.....	115
Figure 7.11. Displacement representation obtained with the 3DSV and the relation with the cleaning areas of pipe 1).	115
Figure 7.12. Cavitation prediction plot for the conditions applied in the investigation of pipe number 1) experimentation.....	117
Figure 7.13. Comparison between the cleaning results and its relation with the P/Po per point of the scanning area for the pipe 1).....	118
Figure 7.14. FFT analysis of the scanning surface for pipe number 2) to find the frequency that produces the largest displacements in the Z direction.	119
Figure 7.15. results of cleaning in pipe 2).	120
Figure 7.16. Inner surface of the pipe after the cleaning procedure and representation of the cleaning areas related with the nodes and antinodes of the vibration of pipe 2.....	121
Figure 7.17. Displacement representation and the relation with the cleaning area of pipe 2)...	122
Figure 7.18. Cavitation prediction plot of the conditions applied in the investigation of pipe number 2) experimentation.....	123
Figure 7.19. Comparison between the cleaning results of and its relation with the P/Po per point of the scanning area for pipe 2).	123
Figure 8.1. FFT analysis of the scanning surface for pipe number 3) to find the frequency that produces the largest displacements in the Z direction.	126
Figure 8.2. Inside wall of pipe number 3 halved after the cleaning.....	127
Figure 8.3. Inner surface of the pipe after the cleaning procedure and representation of the cleaning areas related with the nodes and antinodes of the vibration of pipe 3).	128
Figure 8.4. Displacement representation and the relation with the cleaning area. Specification of the maximum displacement and the threshold points selected.....	129
Figure 8.5. Cavitation prediction plot for the conditions applied in the investigation of pipe number 3).....	130
Figure 8.6. Comparison between the cleaning results and its relation with the P/Po per point of the scanning area for pipe 3).....	131
Figure 8.7. Remaining Calcite on pipe 3) inner wall with the impact of a cavitation.	132
Figure 8.8. Metallography of the cross-section of pipe 3).....	133
Figure 8.9. Setup for creation of fouling.....	135

Figure 8.10. Images of the objects used to introduce the solution in the pipe. a) Funnel, hose and solution. b) Wood stoppers with a hole in the middle to allow introduction of the high concentration solution.	136
Figure 8.11. Even distributed CaCO_3 on the inner wall of the 1.5 m pipe.....	137
Figure 8.12. Field trials set-up in a real industry laboratory facility.	138
Figure 8.13. Frequency Sweep from 20 kHz to 80 kHz applied on the pipe for the optimal frequency selection.	139
Figure 8.14. Relative position of the second HPT referred to the location of the first HPT for the field trials.	139
Figure 8.15. Amplitude of the signal for each position of the second transducer.	140
Figure 8.16. HPT transducers attached with low acoustic attenuation couplant silicone and UCP support clamped to a 1.5 m pipe for the field trials for the non-flow experimentation.	141
Figure 8.17. Results of the cleaning in the pipe with no flow conditions.	142
Figure 8.18. UltraCleanPipe transducers and support attached for the field trials. Flow of 230 l/min.	143
Figure 8.19. Sections of the pipe cleaning with flow.	144
Figure 8.20. Inner section of the pipe cleaned with a flow of 230 l/min and a pressure of 0.5 bar.....	145

LIST OF TABLES

Table 2-1. Schematic representation of pipeline cleaning methods.	16
Table 2-2. Qualitative ranking of cleaning processes in terms of selected attributes, as high (H), medium (M) and low (L).	23
Table 4-4-1. Values used in the equations from (4.6) to (4.11) for the calculation of the curves: R_D , R_B , R_T and R_I cavitation prediction plots	54
Table 5-1. Transducers selection for the feasibility study of use of ultrasonic waves for the removal of fouling from pipelines. The transducers were manufactured by HESENTEC in China. Highlighted with grey the transducers presented in this chapter.	61
Table 5-2. Representative frequencies selected for the analysis.	69
Table 5-3. Normalised displacement of T41 and T43 concave at resonant frequency 1 at the representative points under analysis.	79
Table 5-4. Normalised displacement of T41 and T43 concave at resonant frequency 2 and at the representative points under analysis.	81
Table 5-5. Normalised displacement of T41 and T43 concave at resonance frequency 3 at the representative points under analysis.	83
Table 5-6. Normalised displacement of T41 and T43 concave at resonance frequency 4 at the representative points under analysis.	85
Table 5-7. Normalised displacement of T41 and T43 concave at resonance frequency 5 at the representative points under analysis.	87
Table 7-1. Parameters of the excitation of pipe number 1.	112
Table 7-2. values used of the calculation of the cavitation prediction plots of pipe 1) experiments.	116
Table 7-3. Parameters of the excitation of pipe number 2.	119
Table 7-4. Values used of the calculation of the cavitation prediction plots of pipe 2) experiments.	122
Table 8-1. Parameters of the excitation of pipe number 2.	125
Table 8-2. Values used of the calculation of the cavitation prediction plots of pipe 3) experiments.	129
Table 8-3. Frequency sweep parameters for the optimal frequency selection.	138
Table 9-1. Differences between current ultrasonic cleaning and the new method presented in this thesis.	149

ABBREVIATIONS

U.S.	United States
GNP	Gross National Product
MW	Mega Watt
UK	United Kingdom
HPT	High Power Transducers
OD	Outside Diameter
ID	Inside Diameter
3DSV	3D Scanning Vibrometer Laser
EDM	Electrical Discharger Machining
SEM	Scanning Electron Microscope
XRD	X-Ray Diffraction
PIGgin	Pipeline Intervention Gadget
EDX	Electron Diffraction Spectroscopy
FRP	Fibre-Reinforced Polymers
CIP	Cleaning-in-place
PVC-U	Unplasticized Polyvinyl Chloride
SAW	Surface Acoustic Waves
SEF	Supercritical Fluid Extraction
EDM	Electrical Discharge Machining
FFT	Fast Fourier Transform
NDT	Non-Destructive Testing
FSI	Focus Stacked Image
UCP	UltraCleanPipe
PZT	Langevin Piezoelectric Transducers

PHYSICAL CONSTANTS

$\sigma_{20\text{ }^{\circ}\text{C}}$	Surface tension of water at 20°C	72.10 <i>N/m</i>
$c_{20\text{ }^{\circ}\text{C}}$	Speed of sound at 20 °C and 101325 Pa	1,482 <i>m/s</i>
$\kappa_{20\text{ }^{\circ}\text{C}}$	Ratio of specific heats of air at 20 °C	1.401
$\rho_{\kappa_{20\text{ }^{\circ}\text{C}}}$	Density of water at 20 °C	997 <i>kg/m³</i>
$P_{0\text{ }20\text{ }^{\circ}\text{C}}$	Atmospheric pressure at room conditions	101,325 <i>Pa</i>

SYMBOLS

M_{eff}	Effective mass of the sphere	kg
ρ	Fluid density	kg/m^3
ρ_o	Fluid density at $t = 0$	kg/m^3
t	Time	s
μ	Liquid viscosity	Ns/m^2
σ	Surface tension	N/m
R	Radius of sphere	m
R_o	Initial bubble radius	m
R_D	Rectified diffusion bubble radius	m
R_B	Bubble radius	m
R_T	Bubble transient cavitation radius	m
R_I	Inertial control bubble radius	m
R_{RES}	Bubble resonant radius	m
P_o	Ambient pressure	P_a
P_i	Internal Pressure of a cavity	P_a
P_I	Inertial radius pressure	P_a
P_v	Pressure of condensable part	P_a
P_G	Pressure of non-condensable part	P_a
P_a	Acoustic pressure	P_a
P_A	Acoustic pressure amplitude	P_a
P_D	Rectified diffusion pressure	P_a
P_e	External Pressure	P_a
P_B	Blake pressure	P_a
P_T	Transient pressure	P_a
P_f	Ratio P_T/P_o	-
P_n	Ratio P_I/P_o	-
P_R	Pressure of bubble radius R	N/m^2

f	Frequency	Hz
f_R	Resonant frequency of the bubble	Hz
f_D	Resonant frequency of a bubble of radio R_D	Hz
κ	Ratio of specific heats	-
ω	Angular frequency	rad/s
X_D	Proportion $2\sigma/P_oR_D$	-
X_B	Proportion $2\sigma/P_oR_B$	-
X_r	Proportion $2\sigma/P_oR_r$	-
v_s	Speed of sound	m/s
v_{part}	Particles speed	m/s
$v_{\text{part}_{\text{max}}}$	Particles maximum speed	m/s
F	Force	N
S	Cross-sectional area	m^2
A	Amplitude of the wall vibration	m
C	Saturation of gases	—
k	Effective stiffness	N/s^2
S_t	Cross-sectional area of the transducer	m^2
E	Young's modulus	P_a
L_t	Length of the transducer	m
Z	Impedance	Ω
R	Resistivity	Ω
jX	Reactance of imaginary part	Ω
D_{tv}	Total displacement of a vibration point	m
D_x	Displacement in X direction	m
D_z	Displacement in Z direction	m
D_{x-z}	Projection of D_{tv} on XZ plane	m
D_r	Displacement in radial direction	m

Dedicated to my sons

1 Introduction

This chapter will give an insight into the requirement for new cleaning methods to address the problem of fouling on the interior of liquid carrying pipelines. The economical and production costs related with existing cleaning procedures and associated halting of production processes are highlighted. The remainder of this chapter outlines the objectives, the methodology applied, the scope for the work of this thesis, followed by structure and approach of this document and a finally a summary of the contributions to knowledge.

1.1 Motivation

There are thousands of kilometres of pipes in the world. For example the total length of high pressure transmission pipelines around the world has been estimated at 3,500,000 km [1]. These simple structures are not only responsible for fluid transport but they are also considered as the instrument that controls all the process variables such as flow, temperature, pressure and concentration. Therefore, adequate maintenance of pipelines is a must in industry. Inspection, replacement and cleaning are vital maintenance activities applied to a pipeline and great investment is needed (Figure 1.1). For example, in 2007 the U.S Environmental Protection Agency calculated that public water pipes infrastructure needs a twenty-year capital improvement totalling \$334.8 billion [2].



Figure 1.1. Example of a pipeline and laying maintenance by introducing a device inside the pipe.

Fouling is one of the main reasons for maintenance. It is an undesirable build-up of matter on the inner wall of pipelines, which leads to a number of unwanted economic, environmental and

operational problems and has been pointed out as a major industrial problem [3]. In advanced industrialised countries fouling costs between 0.25 and 0.30 percent of the gross national product (GNP) [4]. Studies in 2010 revealed that American oil refineries spend in excess of \$2 billion per year combating fouling [5] and therefore researchers around the world are looking for different approaches to reduce the costs and the complications associated with these problems.

The decreased throughput of industrial processes due to the pipe blockage by fouling accumulation is an expected problem. The reduction of the inner pipe diameter due to the fouling accumulation (Figure 1.2) brings another complication associated with the increase of the cost of pumping and increased use of fossil fuels and thus CO₂ generation [6]. Rupture, deformation, regular replacement and contamination of products and raw materials are other potential problems associated with fouling. These may lead to major incidents such as explosions, threats to human life and plant destruction [7].

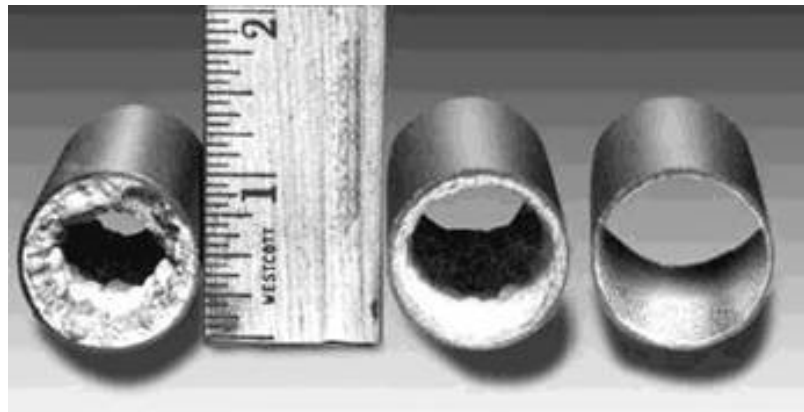


Figure 1.2. Example of different fouling accumulation in a 1 cm pipe section.

Several methods have been tried to reduce the accumulation of deposits in industrial metallic surfaces such as pipes or heat exchangers like electromagnetic treatment of water or coatings [8] but none of them can stop the growth of scale. Therefore, cleaning is the technique in use worldwide to solve the problem. The existing methods of cleaning produce an environmental hazard both because of the aggressive chemicals (acids or alkalis) used for the cleaning and the sludge produced during the washing process. A literature review of these methods is presented in Chapter 2.

Current cleaning methods incur high costs due to the methods themselves and also due to the required temporary shutdown of the process plant. For example, the estimated cost of a one day shut-down of a 1,300 MW power plant is around \$ 500,000 and the losses in a large oil refinery are about \$1.5 million per day [9]. In 1978, it was estimated that the annual cost of fouling in the UK was £370-400 million [10], in which the cost due to the halt in production was around £100 million, i.e. over 25 percent of the total cost. Therefore, a method in which production can

continue during the cleaning process would mean an important increase to the operational economics and environmental health benefits.

In this thesis a new method to clean fouling in pipes based on an ultrasonic approach is presented. The proposed technique alleviates the need to stop production because the cleaning system is mounted on the outer surface of the pipeline at a convenient location at any time during the process. The transducer selection, system design and experimental results obtained are explained in Chapters 4, 5, 6, and 7.

This work has been carried out in parallel to the European funded project UltraCleanPipe (UCP), grant agreement 262327. The project aim was to develop a working prototype based on an ultrasonic method to remove the undesired built-up in industrial pipes by attaching an array of modified high power (HPT) transducers on the outside wall of a pipeline and propagating an ultrasonic wave through the pipe. A schematic diagram of the project's idea is depicted as shows Figure 1.3.

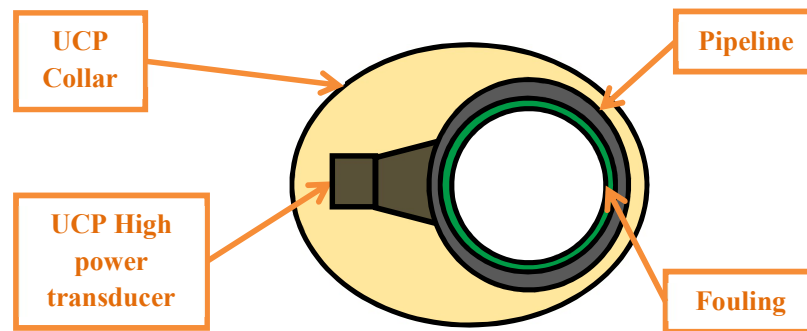


Figure 1.3. Schematic idea of the UltraCleanPipe system for pipeline cleaning with ultrasounds.

1.2 Aims and Objectives

This research aims to probe a new potential method for the removal of hard scale fouling from pipelines with the use of ultrasonic propagation through the pipe wall. This can be applied while production is ongoing and without damage to the structural health of the pipe or any pipe components. To achieve this aim the following specific objectives were studied:

Specific Objectives

- To carry out a literature review of the state-of-the-art of pipe cleaning methods in general and in particular, ultrasonic cleaning methods.
- To establish a reliable and reproducible method to produce hard scale fouling of calcite on the inner surface of pipe sections. Using the established method, produce a number of test samples for testing with high power ultrasonic transducers.

- To modify the existing high power transducers (HPTs) to improve surface contact and facilitate the attachment method to a working pipeline and perform an analysis of the corresponding ultrasonic excitation.
- To explain the physical mechanism of the cleaning method based on the theory of cavitation and the measured of the vibrations applied to the test samples

1.3 Methodology summary

To achieve all these objectives different techniques have been utilised. In this Section the methodology for each type of experimentation is briefly explained.

To create a hard scale fouling in a reproducible way, an electrochemical deposition has been utilised (Chapter 3). Two kinds of experiment were performed. For a small pipe 30cm long, 50.08 mm Outside Diameter (O.D.) and 1.5 mm wall thickness stainless steel 316L pipes and 100x150x1.5 mm stainless steel 316L plates, two types of electrochemical reaction were used: the hydrolysis of water and oxygen reduction in water. Both of these were used to increase the pH in the locations next to the metallic surface to produce the precipitation and the adhesion of Calcite in the sample pipes and plates. These reactions are explained in the Chapter 3.

For the electrochemical reaction, sample pipes were immersed in a highly concentrated solution of Calcium Carbonate to generate scale on the inside wall of the pipe. An “*ACM Instruments RP01 research potentiostat*”, was used to apply a constant voltage in the electrochemical cell to grow the allotropic form of Calcium Carbonate dependent on the temperature and voltage. The experiments are presented in Chapter 3. For the heating deposition, the highly concentrated solution was aggregated constantly to the sample surface. The solution was instantaneously evaporated, leaving a residue which was analysed to ensure the desired coating of Calcite was formed on the inner surface of the sample pipes and plates. To investigate the proper adhesion of the fouling, two different tests were done. A tape adhesion test and a pull-off test were carried out on the plates and well-established methods to analyse the quality of the adhered coating (Appendix A) were implemented.

In order to explain the science involved in the cleaning process, a theoretical background to acoustic cavitation is presented in Chapter 4. This presents the equations necessary to plot the cavitation predictions dependent on the liquid properties such as density, viscosity, and temperature, as the ratio of acoustic pressure to atmospheric pressure (P_a/P_o) vs. the ratio of bubble radius to resonant radius at that frequency, R/R_{RES} (see Section 4.3). In addition, Chapter 4 includes the calculations necessary to transform the displacement of the outside surface of the pipe into an acoustic pressure in the water inside the pipe (see Section 4.5). This pressure is related then to the cavitation prediction plots to find the minimum displacement needed to generate stable and transient cavitation.

In parallel, modified HPTs were created and analysed for their efficacy of pipe excitation. For this, conventional commercially available HPTs were selected with a range of resonance frequencies and powers. These transducers were analysed first with an impedance analyser to find their resonance frequencies and the impedances in the vicinities of the resonance frequencies. The transducers' performance was analysed with a "PSV-500-3D Scanning Vibrometer Laser" (3DSV) to visualise the actual vibration at different frequencies and their responses. This was compared with the impedance analysis results, Section 5.4.1. The 3DSV was also used for modes of vibration analysis at different frequencies and the measurement of the total displacement in the Z direction (perpendicular to the pipe wall) with different signal waveforms - square and sinusoidal. The results for the total displacement were compared with the theory presented in Chapter 4. For the transducer excitation, the Vibrometer signal generator was used to generate the signal and a power amplifier *Electronics & Innovation Ltd., 1040L RF Boarband Power amplifier.* was used to amplify the signal to the level required to drive the transducers.

Once the selected transducers were analysed they were machined to increase their contact area with the pipe surface. Flat-faced transducers have a small coupling contact with the pipe surface and are difficult to attach to the pipe. The transducers were appropriately shaped using Electrical Discharger Machining (EDM). This method, also known as spark machining, uses recurring current discharges between two electrodes separated by a dielectric liquid which removes material from the pieces submitted to the machine. The transducers were machined to have the same curvature radius as the outside radius of the sample pipes (see Chapter 5).

The machined curved transducers were submitted to the same test as the flat ones to compare their vibration characteristics using impedance and Vibrometer analysis. Modes of vibration, resonance frequencies, total displacement, and response to the type of signals, square and sinusoidal were compared for four pairs of transducers to understand how the change in the horn length and shape influence the transducer behaviour (See Chapter 5).

Once the capabilities of the machined transducers were analysed and it was demonstrated that they can produce even higher displacements on the contacted surface, they were attached to a pipe to analyse the possibility of producing cavitation inside the pipe. These tests were performed with the machined transducers mounted on a water filled pipe. The transducers were excited by signals generated by a signal generator, *Agilent Technologies DSO-X 2012A*, and amplified to the desired level by a power amplifier, *Electronics & Innovation Ltd., 1040L RF Boarband Power amplifier.* At the same time an acoustic sensor was immersed in the water inside the test Section. The drive signal was systematically increased at different resonance frequencies to identify the cavitation threshold due to the acoustic emission generated by the cavitation's vibration.

In parallel, a vibration analysis with the 3D-Vibrometer laser, Polytec was performed on one 30cm 316L stainless steel mentioned above with the machined transducers attached to the outer surface. The cavitation threshold could then be correlated with the displacement.

Based on the findings of the tests described above, the experimental procedure was extended to conduct further experiments on pipes with artificially created fouling. The high power transducers were attached to pipes filled with tap water and submitted to vibration. After 30 min the experiments were halted and allowed to dry for two days. Then the samples that were submitted to vibration were analysed in multiple ways; Scanning Electron Microscope SEM, X-Ray Diffraction XRD and Electron Diffraction Spectroscopy EDX. The results obtained in the cleaning areas were compared with the Vibrometer results. The pipes and the remaining fouling were analysed with SEM, XRD, EDX and metallography to find the pattern of cleaning on the surface and the structural health of the pipes walls. The samples submitted to the cleaning method were analysed by metallography and SEM to probe whether or not the cavitation damages the pipe walls or causes any problem to the pipe's structural health (Chapter 7).

After completing the laboratory experiments, field trials were performed in the Heinz food process plant, Wigan, UK. In this case two 1.5 m stainless steel pipes with 51.02 cm of OD and 50.78 cm of ID were submitted to the cleaning procedure. These were attached to a representative Section of an industrial plant in two different conditions: i) tap water, no flow, 0.5 bars pressure, 5 high power transducers and ii) tap water, 70l/min flow, 4 power transducers. The fouled pipes were induced to vibrate for 30 min with the high power transducers excited at their resonance frequency. After the cleaning procedure the pipes were cut and analysed. The results of the cleaning were compared with the 3D-Vibrometer analysis done in similar conditions (Chapter 8).

1.4 Thesis Outline

This thesis is divided in nine Chapters. Chapter 1 presents an introduction and overview of the thesis. The aim is to give a concise scope of this study with overall ideas and rationale. A literature review of current pipe cleaning methods and the technologies applied in this thesis are explained in Chapter 2. Non acoustic and acoustic methods in use for pipe cleaning are explained and compared with the new proposed technique.

Chapter 3 is dedicated to the explanation of fouling. In this chapter a methodology used to create limescale in a reproducible way is explained as well as the importance of the generation of good samples to clean. An analysis of the fouling created and its strength are also presented in this chapter.

In Chapter 4 an explanation of the phenomenon of acoustic cavitation is given. Also in the chapter the mathematical method to calculate the cavitation prediction plots is presented and the cavitation prediction plot regions are explained. Also presented is the relationship between the displacement measured with the 3DSV and the acoustic pressure generated in the water inside the pipe. In addition, a cavitation plot for the typical conditions used in the lab is produced to calculate the minimum displacement necessary to produce transient cavitation in the sample pipes.

The modification of HPTs for fouling removal of pipelines is presented later (Chapter 5). For this, commercial HPTs available for ultrasonic cleaning were analysed with an impedance analyser, *Agilent 4294A 110MHz Precision Impedance Analyser*, and 3DSV. Then, these transducers were modified. The existing HPTs were cut to the same internal radius as the outside radius of the pipes investigated, increasing the contact area between the transducers and the pipes. This also increases the power transmitted to the pipe. The new transducers were analysed with an impedance analyser and the 3DSV to compare their capabilities with the original ones. Displacement in all direction, resonance frequencies, modes of vibration, response to different signals were compared (Chapter 5).

After comparing the capabilities of the new and the classic HPTs, the concave one was mounted on a pipe filled with water to study their capabilities for cavitation generation inside the pipes. The cavitation threshold determined at the main resonance frequencies this is presented in Chapter 6.

Chapter 7 includes the results for the practicality of cleaning pipes with ultrasonic guided waves. This will be presented for different laboratory conditions. A further analysis of the pipe after the cleaning is presented, showing that cavitation impact does not affect the health structure of the pipe while removing lime-scale.

The field trials performed in a food processing industry and the analysis of the results are presented in Chapter 8.

In Chapter 9 the conclusions obtained in this thesis and recommendations future work are presented.

1.5 Contribution to new knowledge

Associated with the objectives presented above each technical chapter presented in this thesis contains a contribution to new knowledge and a summary is presented here.

Critical review of previous investigation on pipeline cleaning with ultrasound. A technical review of previous investigation in the possibility of using ultrasounds for pipeline cleaning highlighting their advantages and disadvantages is presented. The review highlights the importance of generating a similar fouling existing in industry for further analysis.

Development of a new technique to create lime-scale deposition in pipelines. A new technique for Calcite formation inside stainless steel pipe sections was presented. The details of the methodology used are presented. This can be achieved in a reliable and repeatable way to obtain desired arbitrary fouling conditions needed for experimentation.

Modification of a new HPT for pipe cleaning: A modification of an HPT to a new type of concave HPT is presented and analysed. These new transducers, after cutting, present a variation in the resonance frequencies as well as a change in impedance at resonance. The 3d-Vibrometer analysis shows different type of vibration of the transducers and higher displacements of the contact surface can be achieved.

Cavitation threshold in tubular pipes excited with complex transducers. The cavitation threshold inside pipes submitted to vibration is detected with a new type of plotting and a procedure to increase the accuracy of the measurement is given.

New method for the removal of fouling with ultrasonic waves. Comparison of the wave propagation and the cleaning zones is presented. The cleaning area's distribution is compared with the surface displacement, proving that it is the wave traveling through the pipe sample that is responsible for the pipe cleaning rather the wave propagated through the liquid.

Type of cavitation necessary for the removal of hard scale fouling. The removal of fouling is compared with the cavitation prediction plots and it is demonstrated that under the conditions applied only transient cavitation can remove hard scale fouling from the inner wall of a pipe.

1.6 Publications

G. de C., Ignacio, C., Phil, S., Cem& G. Tat-Hean “Methods for detection and cleaning of fouling in pipelines” *5th International Conference on Emerging Technologies in Non-Destructive Testing*, Ioannina, Greece, 19th-21st September, 2011. 231-236. (www.gbv.de/dms/tib-ub-hannover/687798590.pdf)

G. de C., Ignacio, C., Ray “Removal of crystal fouling from metallic surfaces using ultrasonic vibration” *5th Annual Student Research Conference*, Uxbridge, London, UK, 18th-20th June 2012 M14-M15.

(http://www.brunel.ac.uk/__data/assets/pdf_file/0003/189264/ResCon_Abstract_Book_2012_v9.pdf)

G. de C., Ignacio, C., Phil, G. Tat-Hean, & S., Cem “Laser vibrometry to identify resonances of coated substrates” *British Institute of Non-Destructive Testing Conference*. Daventry, Northamptonshire, UK. 11th-13th September 2012. (ISBN: 978-1-62276-437-2 (www.gbv.de/dms/tib-ub-hannover/745589154.pdf))

M. Leggn, M.K. Yücel, I. Garcia de Carellan, V. Kappatos, C. Selcuk, T.H. Gan “Acoustic methods for Biofouling Control: A review” *Ocean Engineering* 103 (2015) 237–247.

G. de C., Ignacio, M., Serafeim, L., Mathew, D. Raghav, K., Vassilios, S., Cem, J., Pierre-Oliver, J., K., Hans, S., Jan “Characterization of the Ultrasonic Wave Propagation in the Application of

Prevention of Fouling on a Ship's Hull" *International Conference on Maritime Technology*. Glasgow, UK, 7th-9th July 2014`

G. de C., Ignacio, S., Cem, K., Vassilios& G. Tat-Hean "Investigation of the lime-scale removal from inner wall of pipelines using ultrasonic waves" *Ultrasonics 2014 Conference*. Costa Da Caparica, Portugal, 15th-17th September 2014.

2 Literature review of pipe cleaning methods

2.1 Introduction

Fouling deposits on industrial process pipes are difficult to avoid, and the current cleaning and preventing methods are rarely optimised [11], and pose a significant problem for plant operators. There are a number of varieties of fouling that may occur, involving different elemental compositions and chemical structures (Chapter 3). There are almost limitless combinations of elements that make up fouling deposits, determined by the process itself.

To avoid this problem, different tools have been developed to remove fouling [12] and a large number of patents (>300) can be found in the literature. These methods can be divided into six groups which generally are minimally optimised because of the lack of understanding of the ways in which the surfaces are cleaned and how the cleaning procedure is affected by the process variables [13]. It can be said that there is a dearth of knowledge in scientific pipe cleaning methods. Currently it is difficult to find a process which can indicate when to apply the cleaning procedure and for how long it has to be applied. The change in the raw materials and environmental variables make it very difficult to predict when to apply the cleaning method.

Very few investigations have been done based on the effectiveness and duration of current pipeline cleaning procedures and the process of designing an appropriate cleaning protocol for each situation is still considered semi-empirical [14]. It has been investigated and proved that high flow velocity increases the cleaning efficiency and therefore decreases the time consumed, and that generally there is a decrease in cleaning time as temperature increases [15]. Further, the time taken to clean is also a function of the chemical agent concentration [16]. This has been calculated but it is hard to find a final conclusion as to when the cleaning process is considered complete, and the cleaning processes are often automated with set flows at set times [14]. Therefore, the existing techniques may be regarded as `conventional` because they employ simple water solutions or gases for an arbitrarily chosen periods based more on experience rather than exhaustive scientific experimentation.

Many of the existing procedures rely on production outages and require the use of a large amount of chemicals. This is an obvious environmental concern with an associated economic impact mainly because the production stops and the increase in the costs of pumping due to the decrease of the inner pipe diameter. Other problems such as contamination of products and raw materials, rupture, deformation, corrosion are intimately associated with the fouling problem.

In parallel to these efforts in the development of cleaning processes, new construction materials and lining rehabilitation have been explored to reduce the accumulation of fouling inside pipelines. Teflon®, nanocomposites, plastics, Fibre-Reinforced Polymers (FRP), and alloys, which discourage fouling deposits from forming. New tools in PIGging (Pipeline Intervention Gadget) have been used such as ultrasonic inspection equipment, for not only cleaning, but also for detecting failures and corrosion, or to verify the cleaning efficiency. The idea of using ultrasound for removal of fouling has also been studied previously [17], [18].

The prevention of fouling can be considered another possibility to resolve this problem. A common practice is the use of “Acid treatment”, also called pH control, applied in large chemical plants. It consists of adding strong acid to the water solution that produces the CO_3^{2-} to transform it into CO_2 such that it can be removed as a gas. This has been reported as producing too much corrosion due to the high acidity [19]. Addition of certain chemical agents such as polyelectrolytes or copolymers of low concentration added to process water is another fouling prevention technique [20]. Also, the use of magnetic fields for the prevention of calcium carbonate deposits in any industry carrying water is a well know technique with good results reported [21], [22]. The selective growth of Aragonite inside the water prevents the accumulation of Calcite polymorph scale build-up. Electric fields have also been reported as a method for the prevention of biofouling in pipelines [23]. Finally the catalytic growth of calcium carbonate crystals in the water phase or using turbulent processes to enhance the growth of crystals in solution have been reported [24].

A new method to avoid the problem of fouling in pipelines is presented in this thesis and compared with existing ones in this chapter. A literature review of the current cleaning methods is first presented below.

2.2 Non acoustic methods

In the following Section the current cleaning method are explained pointing out the advantages and disadvantages of each. A schematic resume with graphic drawings of each method is presented in Table 2-1.

2.2.1 Flushing

This method is very common in all sizes of liquid pipeline and requires an increased flow of water or process product through the pipe to clean the pipe interior. That is an advantage because it does not need to stop the production. The method is commonly used in pipelines which have a slow flow rate that leads to an excessive retention in the system, or have had an operation disturbance due to bacterial growth or sediment impurities. The flushing technique can be considered in two broad categories: conventional and unidirectional. Conventional flushing consists of opening all the valves of one area and/or all hydrants, in the case of water. This method is not very powerful but can be managed easily and without substantial manpower and is known

to clean up to one year's worth of loose sediment (a '1 year expected life benefit'). Unidirectional flushing however isolates a particular pipe Section or loop with a unique direction of flow that removes the loose sediment and biofilm. This method is more powerful than conventional flushing and removes 1-3 years of sediment but needs manpower and control over the direction of the flow. Flushing does not however work properly for pipes of diameters over 25 mm. Flushing is limited to fluid velocity rates of 1 m/s, but can cover long distances, between 3-5 km and can be used in all kinds of pipe with any structural conditions [25]. It has been shown that increasing the flow of a pipeline enhances the removal of fouling [26]–[32]

2.2.2 PIGging

This technique requires the introduction of a solid device inside the pipe, normally bullet shaped, so the pipe needs entry and exit points. In non-stop production PIGging, the process is carried out with a launcher and a catcher [33]. The device typically travels through the pipe removing even hard scales such as calcium carbonate, hydroxyapatite, barium sulphate, aluminium oxide, and phosphates, due to the high friction forces between solid-solid surfaces. Fluid then removes the debris. Initially this technique was very rudimentary, needing a rope to pull the device through the pipe, or a motor inside the PIG. More recently, fluid pressure itself is used to move the PIG or swabs through the pipe and so this technique needs pressurised equipment. With this technique, PIGs of varying sizes and properties are introduced to gradually remove scale from the pipeline and restore the internal bore to the original size, even when the pipe is initially completely blocked [34]. A PIG with the same dimension as the pipe bore will provide the best cleaning for this technique. This allows removal of hard scale from the pipe and can be applied in all kind of pipelines. It is specially recommended for large diameter pipes (over 0.6 m) and long distances. However, because the method introduces a solid device inside the pipe, there is a risk that damage may be caused to the pipe or its attachments. If the pig shape is created sharper, the technique is called abrasive pigging working in the same way as normal PIGging. It employs tungsten studs or an abrasive wire mesh to cut rust, scale, or paraffin deposits off the inside of the pipe [35]–[37]. This technique can only be used in iron or steel pipes and the structural conditions should be good, with no history of leaks or breaks. Other problems associated with Abrasive PIGging relate to how the removed scale itself induces damage to pipe accessories. Although this technique is more expensive than conventional PIGging, it is more effective, with an expected pipe life benefit of 3-10 years [38].

One improvement is the non-stop-pigging method with which the pigs are used without stopping production, introducing the PIG at intervals depending on the process and the requirements. For this technique, the pipeline needs a PIG launcher and a PIG catcher, cannot use butterfly valves, and ball valves must be specified with the same diameter as the rest of the pipeline [39]. This method is not restricted to the type of pipes but to the type of process, because of the requirement

of the launcher and the catcher. It has been shown that this technique is capable of removing parts of the fouling layer at the early stage of the fouling deposition process [40], [41].

Extensive experience with PIGs led to “Smart PIGging”, which not only cleans the pipe but also ultrasonically inspects the pipe, monitoring its conditions, such as wall thickness, leaks, scales, failures, corrosion, etc. Smart PIGging is commonly used in oil and gas industries and does not need to stop production [42]–[45].

There is a relatively new PIGging technique which uses abrasive crushed ice in suspension with water, which can travel through the pipe without plugging it. This can therefore access otherwise challenging shapes like elbows, flanges, valves, reducing tees, reducers, venture meter, and hex bushings. The technique offers 3-10 years of expected life benefit and can be used in a variety of pipes. A disadvantage to Ice PIGging is that the production needs to be stopped prior to application but it can be used to remove soft fouling and deposits from a pipe even with difficult forms [46]–[54].

2.2.3 Air Scouring

This technique is an advanced version of flushing, which is ineffective in low-pressure areas and large diameter mains where velocities are low. It is also an improvement on pigging, as a PIG can become lost, torn or jammed [39]. This technique introduces a ‘slug flow’ which is compounded of cool air that is introduced to a water pipeline under high pressure. The slug flow travels through the pipe removing impurities, fouling, sedimentation and bacterial growth. It is estimated that air scouring can remove three times the normal sediment volumes removed by normal flushing methods. This method is specifically for water treatment but can be used in other processes. It gives 1-5 years of expected life benefit and can cover 3-5 km per day removing friable scale. The pipe must be in a fair structural condition, but the technique needs less water than flushing and swabbing. It also requires more equipment, including a compressor, filters and baffle boxes. Environmental considerations are necessary with this slug produced because of its high concentration of impurities, sedimentation, scale, microorganism and chemicals products from the process [12], [55].

2.2.4 Chemical cleaning

This type of cleaning use a mix of chemicals, heat and water to clean machinery, vessels or pipe work without dismantling the plant [30], [31], [56], [57]. If the cleaning procedure is done with a system installed in the process it is call cleaning-in-place (CIP) [58], [59].

Chemical cleaning is typically used for smaller diameter lines. This method produces a very clean pipeline and can remove loose corrosion. Many patents exist based on the compositions of a solution which will depend on the process, like drain-pipes or industrial process pipes [60]–[64].

The cleaning method is accomplished by the driving forward by injection of a batch of cleaning solution, which is then flushed with water. It is then necessary to apply a neutraliser and a passivator, all separated by PIGs, through the pipeline. This method provides very good results on the interior of pipelines with 3-10 years of expected life benefit and can cover 0.1-1 km per day removing hard scale.

Depending on the nature of the fouling different types of solution can be used. If the fouling needs a specific alkalinity, the cleaning agent can be acid [65]–[67] or caustic [68], [69]. This is commonly used for cleaning pipes that cannot be cleaned by normal PIGging. The method is designed to clean thoroughly the interior of the pipe but has the disadvantage that it can deteriorate the pipe's walls because of the corrosive nature of the chemicals used. Also, there is the risk of residual acid remaining in the pipe following the cleaning process, which can cause future degradation of the pipe. It is difficult to totally remove or neutralise all such corrosive chemicals. This technique has been used even for disinfecting sanitary equipment like haemodialysis machines because the disinfectant properties that the alkali solutions possess [66], [67].

Organic solvents are also used specifically for cleaning small pipelines with organic fouling due to the high costs of the chemicals and the environmental risks. The solution very often carries hazardous chemicals such as xylene and toluene, making it difficult to manage and requires qualified personal to apply. These types of solvent are normally very flammable and harmful so they require extreme precautions when applying under high pressures or temperatures [59], [70]–[72].

Soaps are commonly used for cleaning oil from gas lines. The solution consists of degreasing agents and detergents and is easily diluted by line fluids because it reacts with the fouling and makes it soluble in water [73], [74]. This means there is a lack of penetration and solids are not carried far, and so may reattach to the pipe surface. As such, this is only an effective cleaning substance when used over relatively short distances.

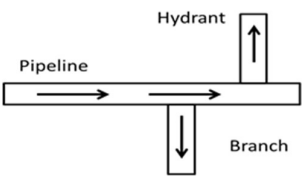

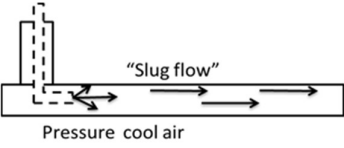
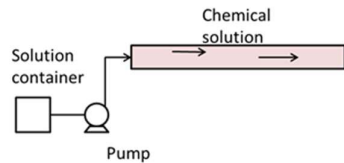
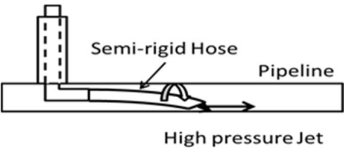

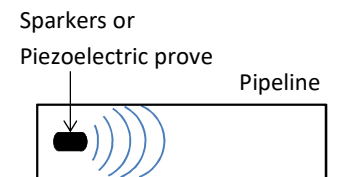
2.2.5 Jetting

This method has been improved and uses a pressurized stream of water by introducing a semi-rigid hose inside the pipe, removing scales and sediment. This technique can be used in all kinds of pipelines and diameters from 200 mm to 1000 mm due to the dimensions of the hose, but the pipe cannot have any history of leaks or breaks. This method has 3-7 years of expected life benefit and can cover 0.5-1.0 km per day removing friable scale. Some water jetting systems use acid to soften the scale, but this limits the applicability of the system depending on the pipe materials and environmental conditions. Other systems use sand as an abrasive agent, increasing the cleaning ability, but the sand can damage the pipe wall [75]–[77].

2.2.6 Cleaning and lining Rehabilitation

For this technique, a lining which rehabilitates the pipe is introduced, increasing the durability and preventing problems of corrosion and fouling. This method can be applied in pipes above 70mm bore and increases the expected life of the pipeline. It is possible to apply non-structural linings only to pipes in good condition, i.e. no history of leaks or breaks. Here, a coating is laid inside the pipe, which will significantly extend the pipe's life. The most common internal linings are cement mortar or epoxy resins. Structural linings can be applied at all levels of structural health because this technique provides a total rehabilitation through PVC-U profiles. This method will increase the pipe strength and enlarge the expected life of benefit 25-50 years [78], [79].

Table 2-1. Schematic representation of pipeline cleaning methods.

Method	Types	Characteristics	Diagram
Flushing 2.2.1	-Conventional flushing -Unidirectional flushing	- Remove lost sediment and Biofilm. - 1 year expected life of benefit. -Any Type of pipeline with fair structural conditions. - 3-5 km per day.	
Pigging 2.2.2	-Nonstop Pigging -Abrasive Pigging -Smart Pigging -Ice Pigging	- Remove hard scale. - 3-10 year expected life of benefit. -Any Type of pipeline with good structural conditions. - 1-1.5 km per day.	
Air Scouring 2.2.3		- Remove friable scale. - 1-5 Year expected life of benefit. -Any Type of pipeline with fair structural conditions. - 3-5 km per day.	
Chemical Cleaning 2.2.4	-Acid and Caustic Cleaning -Solvents -Soaps	- Remove friable scale. - 3-10 years expected life of benefit. -Any Type of pipeline with fair structural conditions. - 0.1-1 km per day.	
Jetting 2.2.5		- Remove friable scale. - 3-7 year expected life of benefit. -200-1000 mm pipelines with good structural conditions. - 0.5-1 km per day.	
Cleaning and Lining Rehabilitation 2.2.6	-Lining -Structural lining	- Increase the pipe strength. - 25-50 Year expected life of benefit. -Any Type of pipeline from 75 mm - 60-90 m per day.	
Acoustic methods 2.3	-Sparkers -Piezoelectric probes	-Prevention and removal of biofouling. -5-10 days of expected life benefit. -Any Type of pipeline with fair structural conditions. -System has to be constantly running.	

2.3 Acoustic methods

The use of acoustic waves for cleaning pipelines is the topic of this thesis therefore an analysis of the previous experiments using acoustics waves are described with special emphasis in this Section.

2.3.1 Patents

There are a number patents in the literature that use acoustic waves to remove fouling from tubular shape structures. Drains, sewers, or wells have the same geometry as a pipeline therefore any acoustic method applied to those structures is considered.

In 1969 Jacks [80] proposed a method and apparatus for cleaning a pipe with sonic energy. This explains how a resonating horn with a belt-shape is introduced inside a vertical tube. The horn is excited by an electro-acoustic transducer which generates waves in the sonic and ultrasonic range typically of 20 kHz in the liquid inside a pipe. This produces acoustic cavitation in the surrounding area removing the unwanted fouling inside the duct. The patent does not give technical information regarding the power, time or other variables related to the cleaning technique and it does not give any theoretical explanation about how the cleaning process occurs. With this patent the device has to be introduced inside an open pipeline hanging down from a cable. This will interrupt the production to perform the cleaning method. On the other hand the pipe has to be full of liquid for the cavitation generation to perform the cleaning.

Another similar tool consisting of a device introduced into a tube-shaped structure was patented in 1976 by Keenan [81]: “Sonic cleaning of wells”. This device consists of a sonic generator placed in a liquid layer within the underground of the well next to the fouling formation. It transmits sonic energy in the sound and ultrasound regions through the surrounding liquid to get to the entire reservoir so as to break up hard tars and create new fissures in the surrounding raw materials that can stimulate also the production of the well. It is self-propelled and powered through electrical cable. In this case the production does not have to be stopped because the device has been designed for cleaning wells. The patent does not have any explanation about the physics involved in the cleaning mechanism.

In 1981 Bodine [82] proposed the “Sonic apparatus for cleaning wells, pipe structures and the like”. This patent refers to wells and exploits rotatory motion with quadrature related vibration components. This rotation oscillates at sonic frequency. The movement of the liquid inside the tube removes the dirt by friction generated by the surrounding liquid. It needs therefore liquid inside the pipe to clean. The patent contains flapper valves that allow the entrance of debris storing them till the device is extracted from the tube. The device is used only applied to vertical tubes. It does not explain the sciences involved in the cleaning method.

A “Venturi flow nozzle ultrasonic cleaning device” was patented by Loose et al [83] in 1988. This patent describes an array of four transducers attached to a Venturi flow nozzle. This apparatus aims is to remove the accumulation of fouling from the Venturi nozzle without stopping the production by applying acoustic waves in the pipeline in the ultrasonic range. The transducers are attached to horns which improve the contact with the Venturi nozzle. They are no details given regarding the underpinning science involved in the cleaning. The authors claim that production does not need to be stopped and that is a low cost with low maintenance equipment.

The last patent that can be found in the literature makes use of pressure drop and the shock wave generated by it. Hutchins [84] developed a “Method for cleaning water pipe” in the 1993. This method consists of a rapidly opened and closed valve. This generates an increase and decrease of the pressure inside of the pipe depending on the level of water accumulated in the reservoir. This is due to the change in the static head of the liquid. The scientific explanation is that the flow cannot be stopped suddenly, therefore, the water keeps moving inside the pipe. Furthermore the static pressure increases due to an increase in the height of the liquid in the reservoir. The oscillation makes the pipe walls expand and contract. This effect removes the fouling inside of a pipe.

2.3.2 Technical investigations and technique proposed

In addition to the previous patents there are some technical publications related with the uses of ultrasonic cleaning of pipelines or similar structures. From that point of view, the first publication regarding cleaning without stopping the production was done in 2005. Benzinger et al [85] investigated the use of ultrasound in a microstructure heat exchanger, a stereolithographic formed microstructured device (60 mm length x 40 mm width x 5 mm height) with 21 channels (22 mm length x 800 μm width x 100 μm height). A flow of 1.5 Kg/h of an aqueous solution of $\text{Ca}(\text{NO}_3)_2/\text{NaHCO}$ was pumped through the microchannels of the heat exchanger. The temperature causes the precipitation of calcium carbonate due to reverse solubility [86]. The accumulation of fouling in the inner surface can be detected by the reduction of the efficiency of the heat transfer coefficient that is calculated with the difference of temperature of the solution at the entrance and the exit. The authors applied pulses with a sonotrode of 20 kHz and 35 W of power over 1 min to remove the fouling ultrasonically. The effect on the removal was observed by changes in the heat transfer coefficient which increases after each ultrasonic pulsation due to the removal of fouling which is a thermal insulator. This is calculated with the variation in the water temperature change inside the heat exchanger. In this publication, the comparison shows that the efficiency of the heat transfer is reduced with every cycle because the overall accumulation of fouling keeps increasing gradually. This can be due to the distribution of the zones that are cleaned with the ultrasound propagation. The node and antinode distributions generated by the type of wave propagated can be the reason for the zones being completely cleaned or not cleaned. Finally it is important to highlight the authors’ claim that the power applied is below the cavitation

threshold but detailed explanation is not given. The literature [87], [88] indicates that it should be above the cavitation threshold. Also the experiments explained in Chapter 5 evidence that 35W is powerful enough to produce cavitation under this condition.

Nakagawa et al [18] performed some experiments closely related with the studies performed in this thesis. The authors used a bolt-clamped Langevin transducer of 28.0 kHz resonant frequency to excite a stainless-steel 186 mm pipe with 27.2 mm OD and 21.4 mm ID to prove the concept of removing fouling from the inner wall. In the paper there is an analysis of the possible waves propagated through a 186 mm sample pipe with a 3-dimensional finite-element-method to find the best frequency and mode of excitation. This is used in combination with vibration velocity measured with a laser Doppler vibrometer used for the final selection of the best frequency to be applied, 26.5 kHz, based on the out-of-plane displacement of each wave mode that generates a standing wave with that pipe length. The authors claim that except for the nodes of the flexural wave, the fouling by calcium carbonate deposits was removed completely. This was done for scale up to 2.0mm thickness. It was concluded that pipes can be cleaned ultrasonically without the use of water or other liquids inside the pipe during the cleaning process. Therefore, no cavitation was generated.

The absence of liquid evidences that the cleaning process takes place without the generation of cavitation. Also, in the publication of Nakagawa, the procedure for the fouling creation seems to be producing sedimentation fouling which is least strongly adhered and softer than a hard fouling (Chapter 3). Therefore, the results obtained could have removed a soft scale not comparable with industrial fouling. This justifies the importance of the analysis of the precise fouling. The adhesion of the fouling film to the substrate is a key factor for later investigations. If the fouling is easier to remove than common industrial fouling, the results in cleaning may not be sufficient to solve existing problems of industrial or domestic fouling. In Chapter 3 a method to create fouling for further removal is developed and explained.

In 2012 Legay et al [85] published work on the inner pipe of a tubular heat exchanger cleaned with ultrasound. The publication presents cleaning results of cylindrical structures by the production of acoustic cavitation.

The authors create the samples by spray painting black paint to simulate the fouling. It ensures a homogeneous distribution of an analogous fouling in the pipe and provides a reproducible method. Painting has a number of important dissimilarities with the fouling, Calcite, investigated here: physical, mechanical, acoustic and chemical properties are noticeably different. Even though the analysis of the results and the wave generation are closely connected to the ones explained in this thesis since the patents of cleaning are related with the nodes and antinodes of the wave propagated.

Different pipes are used in these experiments; glass pipes of 380 mm length and 9-12 mm internal-external diameters respectively and two different for stainless steel both of 380 mm length and with two different wall thicknesses. One of 2 mm with an ID of 10 mm and 12 mm of OD and other with 0.4 mm of wall thickness with 5.6 mm of ID and 6 mm of OD. The painted areas of the pipes are submitted to the cleaning procedure. The waves are generated on the inner surface of the outside tube of a tubular heat exchanger, which is called a resonator, and propagated through the liquid contained between the two tubes. This kind of resonator is used with other industrial applications as described in Chapter 5. Cavitation is generated surrounding the inside tube and both the inner and outside surfaces are cleaned in different proportion depending on the pipe material and diameter. The efficiency is higher in the outside surface of the tube in most cases. Also presented is the distribution of cleaned and not cleaned areas that can be related to the location of the nodes and antinodes of the compressional wave traveling through the liquid. The extent of cleaning increases over time presenting the best capabilities after 25 min of ultrasonic excitation. Only the glass pipe presents a 100% efficiency after 25 min. It is important to highlight that the cavitation was not detected with any method and was assumed to be happening. Here (see Chapters 6 and 7) the detection of cavitation is done both by acoustic emission and by the analysis of the impact of cavities on the remaining fouling after the cleaning to ensure that this is the cleaning mechanism responsible for the results (Chapter 7).

The efficiency of the ultrasonic cleaning is evaluated by visual analysis and by measuring the overall heat transfer coefficient. This depends on the temperature of the two liquids both in the entrance and in the exit. The improvement of the heat transfer is related to the removal of fouling which produces an important resistance to the heat transfer. This efficiency is improved after ultrasonic cleaning with a frequency of 35 kHz and a power around 100 W. It is known that ultrasound can increase the overall heat transfer coefficient [85] that could have been the reason of the increase in the heat transfer coefficient, but further visual analysis of the painted pipes exhibited good results on cleaning and therefore the improvement of the heat transfer is also produced by the fouling removed.

It is important to highlight that in the above publication the painted pipe subjected to the cleaning procedure was always inside another pipe within which piezoelectric high power transducers were attached. This means that the cleaning was occurring inside a structure, like in classic ultrasonic cleaning, in a solvent, in this case, water. Therefore, a compressional wave was producing acoustic cavitation and cleans an object inside a container, the resonator. This mechanism is comparable to a classic ultrasonic bath in which the acoustic waves travel through a liquid in which the object submitted to the cleaning procedure is submerged. In this thesis the mechanism is different, a wave is propagated through a pipe wall producing the cleaning of the same wall in which the acoustic wave propagates. It is the vibration of the structure what cleans the structure. In Chapter 7 a comparison between the cleaning results areas and the measurements of the actual displacement due to the vibration of the pipe is presented.

2.3.3 Acoustic methods for biofouling prevention and removal

Although in this thesis the fouling removed is a hard scale fouling by Calcite (Chapter 3), the ultrasonic prevention or removal of biofouling in tubular structures has been briefly considered.

Biofouling can be defined as the undesirable formation of organic matter on surfaces immersed in water. This has important differences from mineral fouling with respect to adhesion, hardness, fragility and chemical composition. A review of the use of ultrasound in the removal or prevention of this type of fouling is presented below.

In the literature, the most common method for the prevention of biofouling with acoustic waves can be “Acoustic sparkers”, also referred as pursers, plasma sparker, or plasma jet; it generates impulsive wide frequency bandwidth acoustic waves in water. This has been documented in patent [89] and papers during the last twenty years [90]–[92]. The sparkers generate a large voltage stored in a capacitor. This voltage is released rapidly between two electrodes in water. This exceeds the water dielectric breakdown level and the surrounding water may be vaporized producing an acoustic wave between 100Hz – 150 kHz and power densities around 4 W/ft² [93]. The propagation of the wave may prevent the growth of any microorganism in the water. This has been reported to have success in preventing the growth of mussels up to 100% in pipes of 16” diameter and 1800 ft. length with pulses every 3s for four years [94]. This technique is generally used for the prevention of Zebra mussels in sea water structures [89], [95]–[97].

Other uses of ultrasound for biofouling removal different to plasma sparkers can be found in the literature. For example the biofilm removal in lab trials in a glass tube showing that ultrasound can reduce, in some cases, the growth of biofouling by applying pulses between 20-320 kHz of 30 s in glass tubes [98]. In this investigation, the most important achievement was for a 50 cm tube with 33 kHz where a 87.5% mineralized biofilm was removed. In these experiments the wave is traveling through water and the cleaning procedure occurs in the objects immersed in that water. This is similar to classic ultrasonic cleaning. In addition, it is important to consider that mineralized biofilm gives a stronger adhesion and hardness than just biofouling.

In 2003 Oulahal-Lagsir et al [99] showed that the use of ultrasound can improve the performance of the enzyme treatments for the removal of biofilm from a stainless steel surface. This is because the ultrasound may enhance the activity of certain enzymes or because of the enhancement of the diffusion in the biofilm. One disadvantage of this method is the use of enzymes itself. If the idea is to clean structures offshore it would be quite difficult to avoid the dispersal of the enzymes in the marine environment that could have a serious impact on the environment.

It has been shown that surface acoustic waves (SAW) of 100 kHz can enhance the antimicrobial activity of antibiotics and therefore its antifouling properties. This is due to the enhancement of the antibiotic diffusion through the biofilm and potentially because of the bioacoustic cellular

response of some bacteria to SAW [100]. This method would still need the use of chemical like the antibiotic for the removal.

Also, ultrasound has been used in combination with oxidants to kill cyst, larvae and adults of Brine Shrimp. Ultrasound at 1.4 MHz presented the capability of killing 50, 90 and 100% of cyst, adults and larvae respectively. Also ultrasound with the same frequency enhances the results of oxidants such as H_2O_2 up to 75, 80, and 95% of mortality of cyst, larvae and adults respectively, or O_3 up to 80, 80, and 100% of mortality of cyst, larvae and adults respectively. Also ultrasound killed up to the 35% of unicellular green algae and increased the effectiveness of H_2O_2 and O_3 up to 70% and 80% respectively [101].

In general it can be said that the combination of ultrasound with any other biocide improves the performance of the biocide. In tubes of 18 mm ID and 1 m length, 20 kHz ultrasound was applied with a reduction of 8 μm in the biofouling thickness. Also the use of ultrasound in combination with O_3 presented a difference in the accumulation of 111 μm for the O_3 only and 7 μm for the combination [102].

2.4 Summary

This completes the review of the methods for pipeline cleaning Table 2-2 summarises the advantages and disadvantages of all the methods in comparison with that proposed in this thesis.

It has been explained that the type of fouling and its creation in previous investigations have not been treated as in this thesis where the fouling creation is an important factor. It has been explained that not all fouling adheres well to the substrate and its chemical and physical properties can mean an important difference from real conditions. And therefore the fouling to be removed must adhere well and should be similar to typical fouling in industry. The method will be useful under any type of fouling conditions. And therefore the method of fouling removal with ultrasound can be validated. Here a full analysis of the fouling creation is done to ensure that the results can be used to remove one of the most challenging fouling in the industry, Calcite.

In the literature, the cleaning of any tubular structure with ultrasound required the use of a specific transducer with different resonators. These are not analysed prior to the cleaning and has been used as a tool for cleaning. Here a new type of transducers and its analysis is presented. The performance of each transducer at each frequency and the effects produced by its modifications are explained in Chapter 4.

Regarding previous investigations of the removal of fouling of pipelines, the analysis of the physics involved in the removal are not fully explained and no method for the detection of cavitation is used. Here the cavitation detection as well as the cavitation threshold has been studied

to verify and explain the physics required for minimum energy cleaning. This guarantees the lowest power consumption resulting in cleanings.

Also analysis of the types of wave's propagation through the samples are generally not investigated and not considered an important feature. Here the actual wave propagation is measured and related to the cleaning procedure since this work claims that it is the wave propagating through the structure which is responsible for the cleaning procedure and not the wave transferred to a solvent as in classic ultrasonic cleaning.

Finally, non-cleaning results under real conditions exist in the literature. Here in Chapter 7 the results for cleaning with an array of transducers are presented and compared with the actual vibration of the pipe subjected to the cleaning procedure.

Table 2-2. Qualitative ranking of cleaning processes in terms of selected attributes, as high (H), medium (M) and low (L).

Cleaning Method	Intrusiveness	Geometrical constraints	Effectiveness	Cost
Flushing	M/H	L	M/H	L
Swabbing or PIGging	H	L/M	M/H	L/M
Non-stop production PIGging	M/H	H	H	M/H
Abrasive PIGging	H	M/H	H	M/H
Smart PIGging*	L/M	H	H	M/H
Ice PIGging	L/M	L	M/H	L/M
Air Scouring	M/H	L	H	M/H
Chemical cleaning	M/H	M/H	H	H
Jetting	M/H	L/M	H	M/H
Lining and rehabilitation	H	M/H	H	H
Proposed ultrasonic method*†	L/M	M/H	‡	L

*Also used for inspection

† Anticipated outcome

‡ In progress

3 Creation of fouling on inner walls of pipe samples

In Chapter 1 fouling was presented as a problem of high importance in industry and of economic impact in industrialised countries. In Chapter 2 a review of previous investigations into the removal of fouling from pipelines and heat exchanger tubes using ultrasound was presented, where a gap in the research was identified regarding the type of fouling created for later removal. This chapter discusses a method to create fouling on inner walls of sample pipes to study the removal efficiency using ultrasonic excitation (Chapter 7). The fouling is analysed by crystallographic methods and is subjected to adhesion tests to prove its quality and attachment properties.

3.1 Introduction

Accumulations of dirt inside pipelines can occur in different ways and some of them are easy to remove and are poorly adhered to the substrate. A simple increase in the flow, as like in flushing cleaning method (Chapter 2) can remove this type of fouling and therefore, its elimination with ultrasound would not necessarily be representative as a solution of industrial scale. As Chapters 4 and 7 explain, different types of dirt cleaning need different types of cavitation excitation. Therefore high importance has been given here to the generation of hard, well adhered fouling similar to that found in industrial and domestic pipelines, such as Calcite, hydroxyapatite, or some sulphates. However, the focus in this work is to create Calcite fouling in pipe samples. Moreover, this approach, is different to previous investigations in the removal of fouling using ultrasonic wave guided (this concept is explained in Section 7.1).

Calcite is considered by some authors as the most common fouling in industry around the world [103]–[105]. This type of fouling strongly adheres to the substrate surface, is highly insoluble and is hard enough to be a difficult challenge to remove. Therefore, if the acoustic cleaning method works with Calcite, it is expected to work with any other challenging fouling found in industry.

Calcium carbonate is a chemical compound that exists in different allotropic forms in solid state. The most important are Calcite, aragonite and vaterite, but monohydrocalcite, and ikaite may also occur [106], [107]. These can coexist inside pipelines and grow with different proportion and speed depending on the process and its variables such as pipe material, previous surface treatments, temperature, pH, and solution composition [108]–[111]. Aragonite can be in larger concentration at the early stages but it tends to convert to Calcite gradually over time [112]. In fact, all the allotropic forms tend to convert to Calcite over time [107], [112]–[115]. This is because

Calcite is the most stable polymorph of calcium carbonate [107]. Also, it is known that aragonite has higher density and it is less prone to form hard scale [22] than Calcite. Moreover, aragonite is needle-like and adheres less well than the rhombohedral Calcite crystals. Therefore, among all calcium carbonate polymorphs, Calcite is the most common one in industrial processes and is the one of concern worldwide [116]. Here a selective growth of Calcite in pipelines and plates is presented with two different methods.

In order to verify that Calcite is the allotropic form that has adhered to the substrates, a crystallographic analysis of the fouling is performed in some of the representative samples Section 3.4. For that three different techniques are applied: Energy-dispersive X-ray spectroscopy (EDX), X-Ray Diffraction (XRD) and Scanning Electron Microscopy (SEM).

Finally two different types of adhesion test are performed to classify and quantify the union of the fouling to the substrates. For that, “adhesion by tape”, ASTM D3359-97, and “pull off” tests, EN ISO 4624:2002 are performed on a sample.

3.2 Objectives

In order to verify that the samples generated are suitable for the investigation (use of ultrasound for the removal), the following objectives have been established:

- The methods have to be reproducible.
- The fouling has to be well adhered to the surface of pipe walls and sample plates.
- The chemical composition and the polymorph created have to be equal to one existing in the industry.
- The fouling has to be evenly distributed on the walls.
- The sample pipes have to be representative of existing parts of industrial components.

3.3 Creation of fouling on pipes and plates using laboratory based tests

In opposition with the idea of considering Calcite fouling as an industrial problem, it has been considered that calcium carbonate deposits in pipelines are a good method for corrosion protection and it has been proposed as a good lining (see Section 2.2.6) protection material [117]–[119].

Related with this, a few patents have been created for the rapid coating of steel pipelines [120]–[123]. All these patents are based in circulating a high concentrated solution of calcium carbonate into the pipes subjected to the coating process maintaining a high concentration of calcium carbonate and increasing gradually the pH.

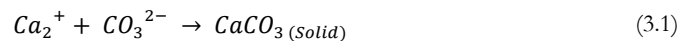
Furthermore, the growth of Calcite in pipes has been studied with different purposes. In 2007 Chen et al [124] used a pipe of 1 mm of ID and 9.4 mm length, filled with a saturated solution of calcium carbonate to analyse the process of scale deposition of the different allotropic forms of calcium carbonate. It was measured with X-Ray Diffraction (XRD) that the remaining allotropic form in the scale formation was Calcite even though other forms were created in the preliminary stages as explained in Section 3.1.

Later on, Umoru et al (2012) [125] investigated the anticorrosion properties as a coating of calcium carbonate, magnesium carbonate and a combination of both. For this, the pipes were submerged in high concentrated solution for a period of twenty four hours to allow for the precipitation on the sample surface. It was proven that magnesium carbonate is better as an anticorrosion lining material but calcium carbonate is still better than the bare Steel.

Applying a similar method to the one occurring in chemical plants processes, Muryanto et al (2014) [126] used a flowing ring built in house system to evaluate the effects of flow rates, temperatures and malic acid on the mass and the morphology of the calcium carbonate scale.

The methods presented above are different to the one used here, which is based on an electrochemical reaction (Section 3.3.1). This electrochemical reaction has been used in the past but in small flat samples, of less than 20 cm² [127]–[130]. Here the sample pipes were coated with a layer of Calcite, as presented in Section 3.3.1.

All the methods to create Calcite as an artificial fouling depend on the chemical reaction (3.1). The chemical kinetics of this reaction can be modified by adjusting temperature, electrode potential, pH, and concentrations of the reactants. With this, the rate of the fouling accumulation can be increased.



Here two different methods are presented: one based on an electrochemical reaction (Section 3.3.1) and the other based on the inverse solubility of calcium carbonate (Section 3.3.2). The aim is to generate Calcite as fouling that satisfies the objectives previously established in Section 3.2.

3.3.1 Electrochemical reaction

Pipelines are inevitably deteriorated due to the spontaneous corrosion processes of the metallic surface. Figure 3.1 explains the process of corrosion on metallic surfaces in contact with water. This consists on a reduction-oxidation reaction. In this case, the reduction reaction is the chemical reaction (3.2) (Figure 3.1) in which the oxygen reacts with the surrounding water and with the

electrons given by reaction (3.3) to produce hydroxyl ions. These electrons are given by the iron from the alloy as per the oxidation (3.3).

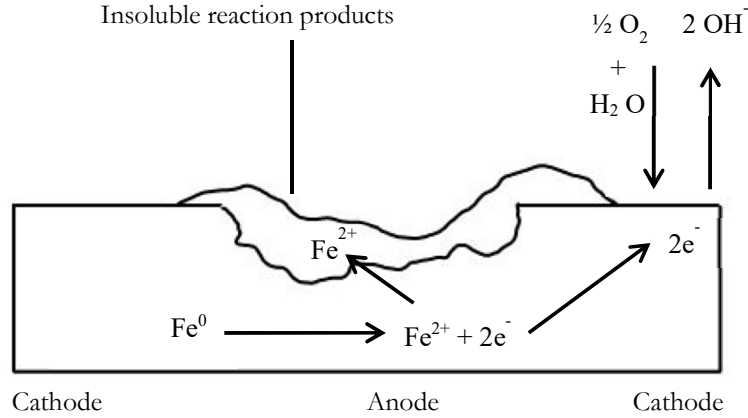
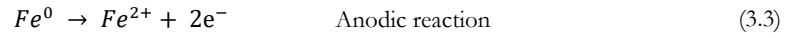
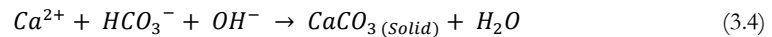


Figure 3.1. Corrosion process of steel in aqueous medium.

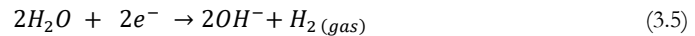
The corrosion of steel can also lead to the generation of insoluble solids e.g. iron oxides as a product of the presence of Fe^{2+} produced by the electrochemical reaction (3.3) Figure 3.1.

In addition, other fouling can occur based on the Le Châtelier principle [131] e.g. the generation of Calcite by the presence of OH^- due to the electrochemical reaction (3.2), which leads to the generation of calcium carbonate scales, in the presence of Ca^{2+} and HCO_3^- in the solution, chemical reaction (3.4) [132].



Consequently, the precipitation of $CaCO_3(soli)$ can be forced to be generated on the metallic surface if the pH is raised in the solution in contact to it, and by having a high concentration of Ca^{2+} and HCO_3^- in this solution. Here the generation of Calcite in the inner wall of the pipe and plate samples is done by increasing the concentration of OH^- , and therefore the pH, by an electrochemical method similar to the corrosion process presented in Figure 3.1.

The process consists of two different electrochemical reactions that increase the pH, the electrolysis of oxygen (3.2) and the electrolysis of water, also called hydrolysis (3.5):



Reaction (3.5) starts at a potential below -0.8277 V [133] but previous work in the selective growth of calcium carbonate scales recommends -1.6 V . Reaction (3.2) occurs at even lower potentials. Therefore, to increase the speed of these reactions, potentials around -1.6 V have to be applied.

In addition, it is important to consider that it has been proved by J. Martinez-Cruz et al [130] that it is possible to control the allotropic form of calcium carbonate (Calcite, aragonite, vaterite) at a microscale on metallic surfaces by modifying the composition of the solution, temperature, and electrode potential E^0 in the electrochemical cell used. Calcite is more prone to be created at 40°C and The pH of 7.8 was established to be the optimal for the creation of Calcite [132].

Electrochemical procedure and set-up

Figure 3.2 shows a schematic diagram of the set-up for the creation of fouling. A large glass vessel is filled with 20 litres of a high concentrated solution of calcium carbonate. This is heated to 40°C and kept constant while it is continuously agitated using a magnetic stirrer.

A plastic disc is placed on top of the vessel with access ports to connect all instrumentation and to seal off any water vapour escaping. A condenser is added to ensure that the water evaporated within the mixture is not lost and the solution is kept in equilibrium at atmospheric pressure.

Extra oxygen is pumped inside the vessel to substitute the oxygen consumed by the electrochemical reaction (3.2). This is done by the air supplier which has a diffuser at the end to improve the transfer of oxygen into the solution; carbon dioxide and some water are also added with the air supply.

To control the voltage, three different electrodes are used for the electrochemical reaction; i) the working electrode, which is the pipe, ii) a counter electrode, which is a copper wire placed directly in the middle of the pipe, and iii) a reference electrode which is electrically connected to the solution by a salt bridge.

All these electrodes are connected to a potentiostat¹ to maintain the working electrode at a constant voltage of -1.6 V in the electrolytic cell, Figure 3.2.

A negative voltage is then applied to the sample pipe which is distributed across the entire wall surface whereas the counter electrode (copper wire) has a positive voltage and is placed through the centre of the sample, ensuring there is no contact with the sample as shown in Figure 3.4. The reaction is maintained at a constant voltage (-1.6V) and temperature of 40°C for 16 hours. The results of the fouling creation are presented below.

¹ Potentiostat is a device for controlling or maintaining constant the potential difference between the electrodes in an electrochemical cell.

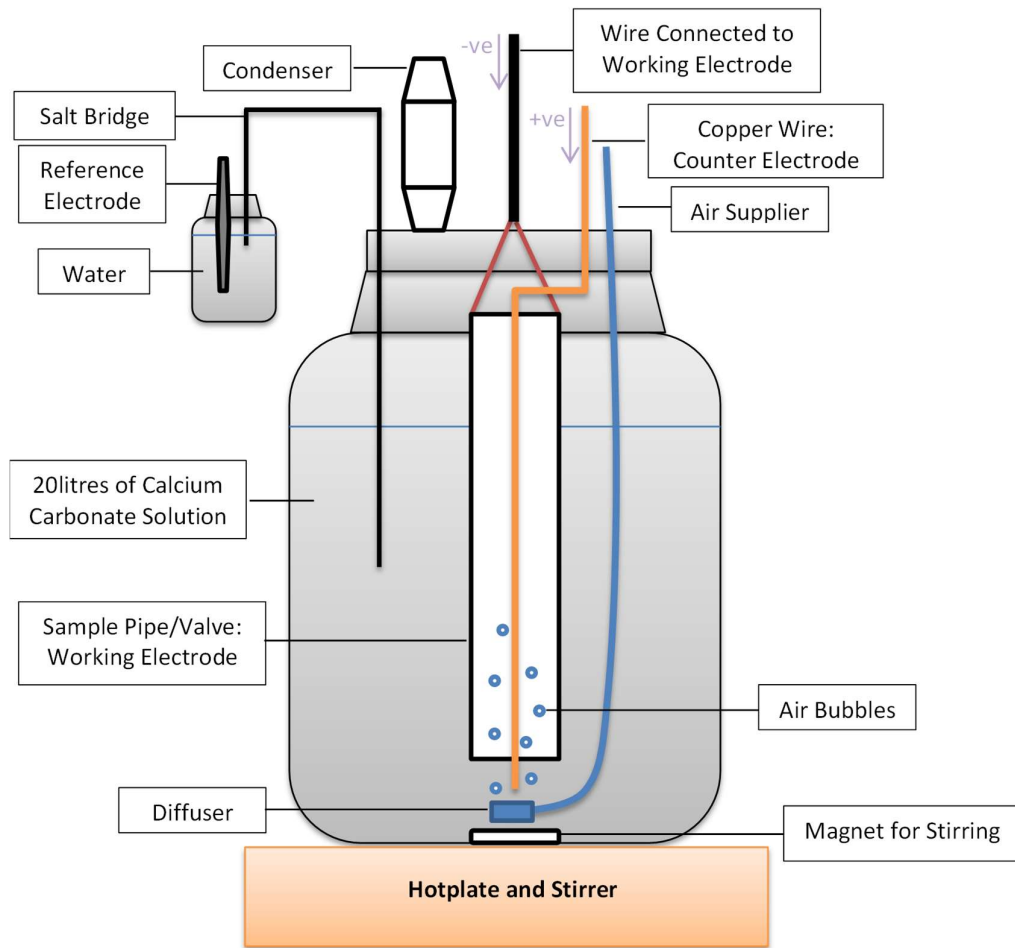


Figure 3.2. Electrochemical deposition scheme.

Sample pipe

The sample pipes need to be prepared to induce the fouling creation only on the inner wall of the pipes. For that, the pipes are wrapped with hand stretch black film of 25 microns thickness to protect the outside wall of fouling growth, Figure 3.3. Each sample pipe is photographed before and after undergoing fouling creation (see Section 3.4).

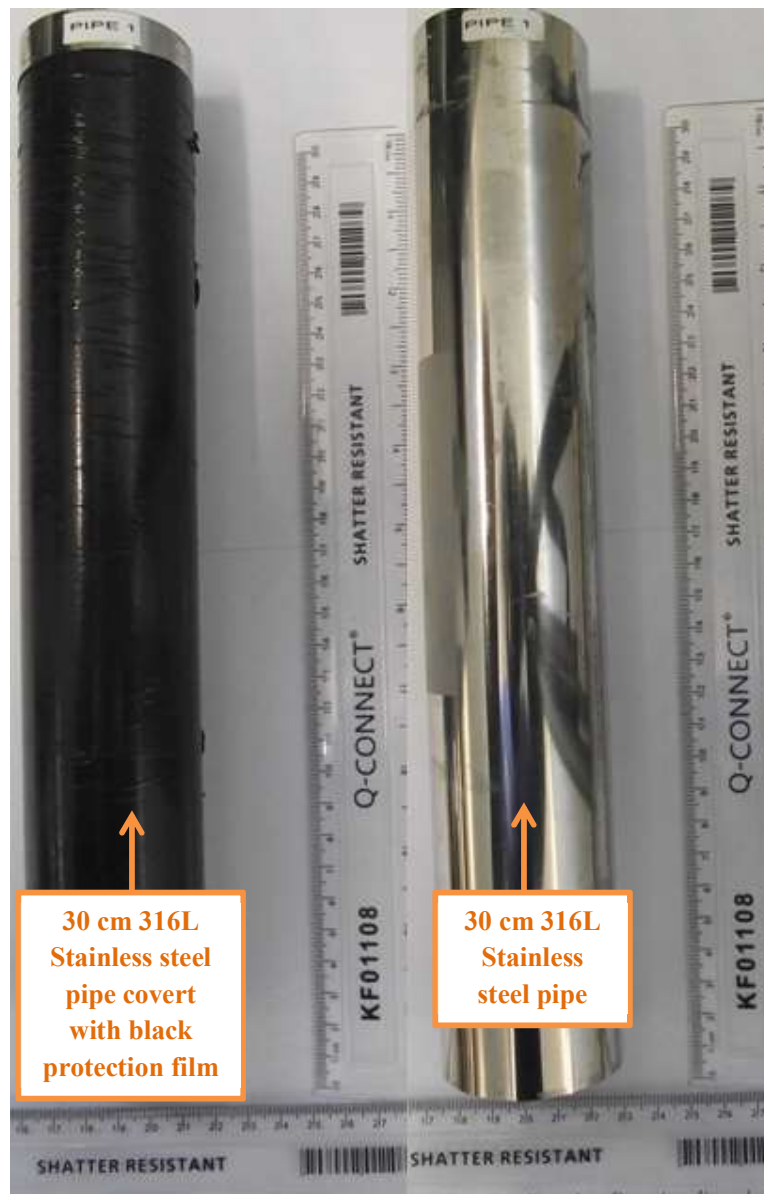


Figure 3.3. Images of Sample Pipe 1, Before and After Undergoing Fouling Creation.

After protecting the outside wall of the pipes, four cables are attached with a separation of 45° in four different locations to maintain the top and the bottom cross Section of the pipe horizontal. The four cables, also applied a constant voltage to the working electrode, the pipe as showing, Figure 3.4. A jubilee clip is used to secure the wire onto the pipe as the wire will suspend the pipe from above into the solution. A copper wire is introduced through the middle of the pipe and is held in place using plastic brackets to remain out of contact with the pipe and wires. Figure 3.4 shows the notation of the preparation of the pipe.

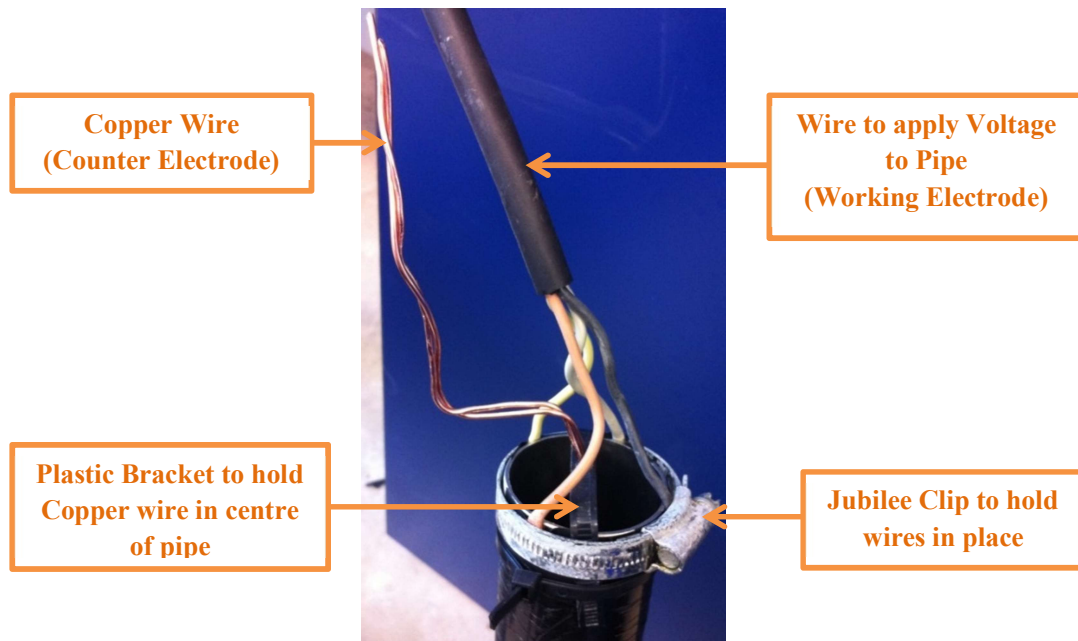


Figure 3.4. Sample pipe prepared for being immersed into vessel.

As a counter electrode, a copper wire is placed through the centre of the sample, ensuring that there is no contact with the working electrode to avoid electrical short-circuit.

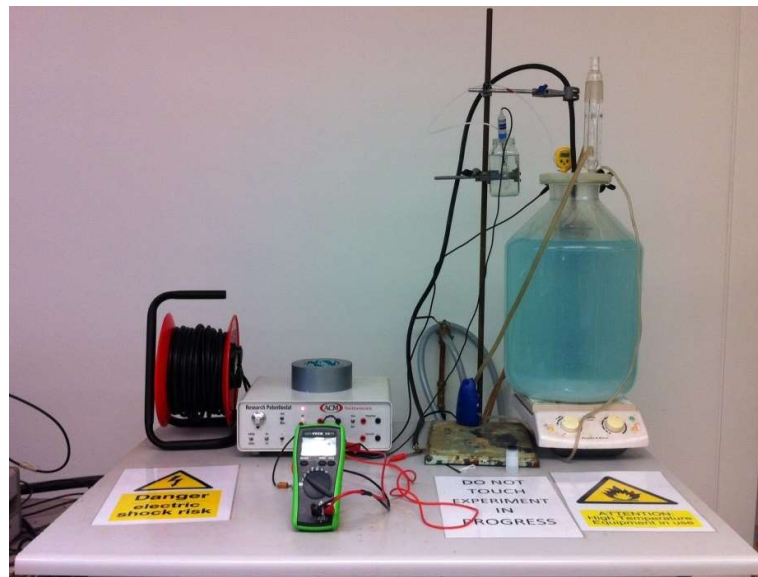


Figure 3.5. Set-Up of Fouling Creation Experimentation.

Figure 3.5 shows a sample pipe which is immersed into the vessel using a thick wire that holds the sample into the solution whilst applying a current. The pipe is not fully immersed since the locations where the wires are attached must be kept above the surface of the solution.

3.3.2 Sprayed deposition on heated plates

It is widely known that calcium carbonate decreases in solubility when the temperature rises, and that is why the deposition of calcium carbonate is a common problem in all kinds of heated processes. This basic idea has been used to generate fouling in sample plates.

In this case the chemical equation to be considered would be equation (3.1) and the chemical principle is an inverse solubility process. Therefore, by increasing the temperature of substrate and adding a solution of calcium carbonate, it is expected to precipitate. The higher the concentration of the solution the higher the accumulation rates of calcium carbonate on the metallic surface.

It has been considered that all the allotropic forms of calcium carbonate tend to convert to Calcite (Section 3.1) and Calcite forms hard scale well-attached. A domestic water atomiser was used to spray the high concentrated solution on a metallic surface to produce fouling.

Sprayed deposition on heated plates procedure and set-up:

To generate Calcite on a stainless steel of 150x100x1.5mm a sample plate was introduced in an empty vessel maintained at a temperature of 120°C. When the plate was at that temperature a high concentration solution was sprayed on the sample every ten seconds during a period of six hours, as depicted in Figure 3.6.

For these experiments it was necessary to use the following equipment:

- Heater
- Stainless steel plate
- Recipient
- Saturated solution
- Atomizer

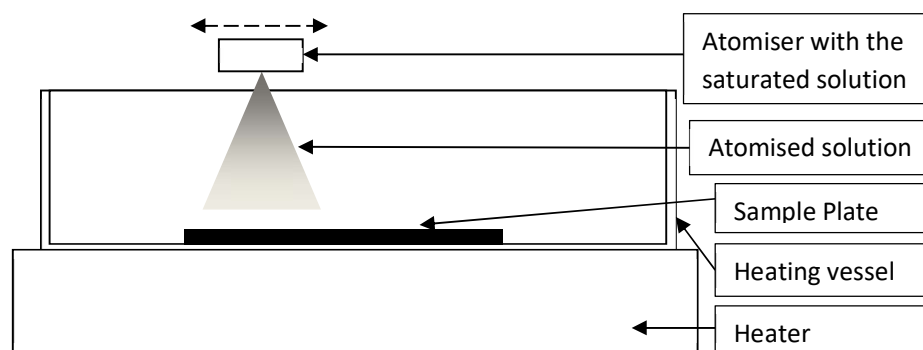


Figure 3.6. Sprayed deposition on heated plates with atomizer set-up diagram.

The plate is placed on a heating vessel and the temperature raised up to 120°C and then the concentrated solution is atomized onto the plate several times.

3.4 Results and interpretation

The analyses of the fouling created on the pipes were performed after the cleaning procedure presented in Chapter 7. This is to avoid the potential removal or modification of the fouling created by cutting the samples for the analyses. The three different techniques for chemical and crystallographic composition analyses listed are described below:

Scanning Electron Microscope (SEM) is a type of electron microscope that produces images of a sample by scanning its surface with a focused beam of electrons. The electrons interact with the atoms in the sample, producing various signals that contain information about the sample's surface topography and composition. This technique has been used before for the analysis of Calcite and other allotropic polymorphs of calcium carbonate [127], [130].

Energy-dispersive X-Ray spectroscopy (EDX)² is an analytical technique used for the elemental analysis or chemical characterization of samples. It is that each element has a unique atomic structure and therefore it produces a unique set of emission peaks after the X-Ray excitation. The EDX is performed in a SEM which excites a sample with X-Rays and measured the the emission on the X-Ray spectrum. This is a qualitative method which only gives information on the presence of an element on a sample but it cannot quantify the amount of the element on the sample [134].

X-Ray Diffraction (XRD) is an analytical technique that relies on the dual wave-particle nature of electromagnetic waves, in this case X-Rays, to obtain information about the structure and composition of crystalline materials. A primary use of the technique is the identification and characterization of the crystallographic composition of a sample based on its diffraction pattern. [110], [135]

In addition to the chemical and crystallographic analyses, two standardised measurements have been applied to the samples created to validate the quality of the adhesion of the fouling created on the samples: “Adhesion by tape” and “Pull-off adhesion” tests (see Section 3.1)

3.4.1 Electrochemical reaction composition analysis of Pipe 1

The first analysis is a visual one to see that the entire pipe is covered by an even distribution of fouling. Figure 3.7 shows the inner wall of a pipe covered with fouling.

² In this thesis the EDX analyses have been performed without controlling specimen's geometry (size, shape, and location inclination) what makes the counts per second of the “y” axes meaningless [205] and therefore are not included in the plots.

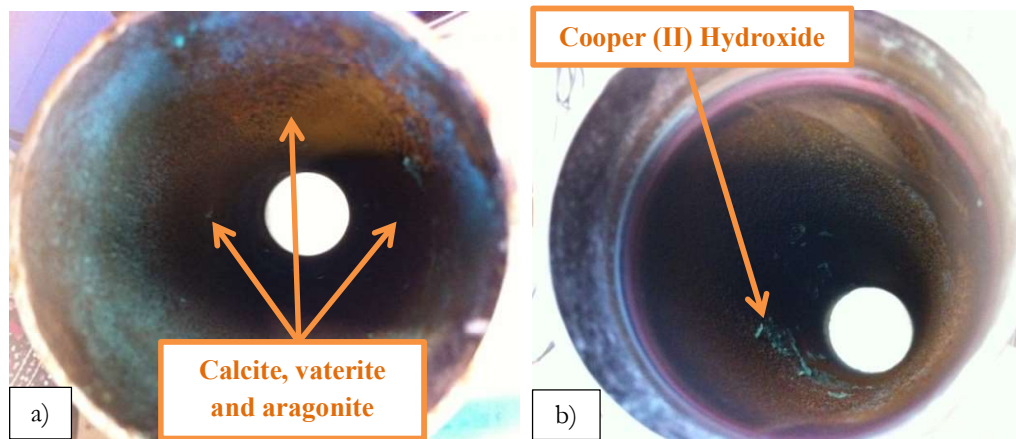


Figure 3.7. Results of Fouling Creation on Inner Walls of Pipe 1, a) is the picture taken from the bottom and b) is the picture taken from the top.

Further analyses are needed to verify the actual composition of the fouled coating. Firstly the chemical composition must be known. The solution used was a high concentration of calcium carbonate but other ions such as Cl^- and Na^+ could have been precipitated as sodium chloride, for example. But these are more unlikely to form a precipitation since the concentration of these ions in the solution is well below the solubility product of this salt which is 35.9g/ml. Also the electrolysis of sodium chloride needs higher negative potential ($E^0 = -2.7$ V) to produce sodium hydroxide. Therefore sodium chloride is not expected to be generated as fouling in the samples. Either way, other elements from the steel, air, or the black cover could have created other solids, therefore chemical analysis is needed.

Figure 3.8 presents the EDX analysis of Pipe 1 fouled with the electrochemical reaction method of fouling creation. It can be seen that the scale created is formed mainly by calcium, carbon, and oxygen, which is the elemental composition of Calcite, and has traces of iron and copper. The iron may come from the steel or other sub-products of the electrochemical reactions such as Fe_2O_3 Iron (II) oxide or other iron oxides. The copper is presented in the solution due to the oxidation of the copper electrode.

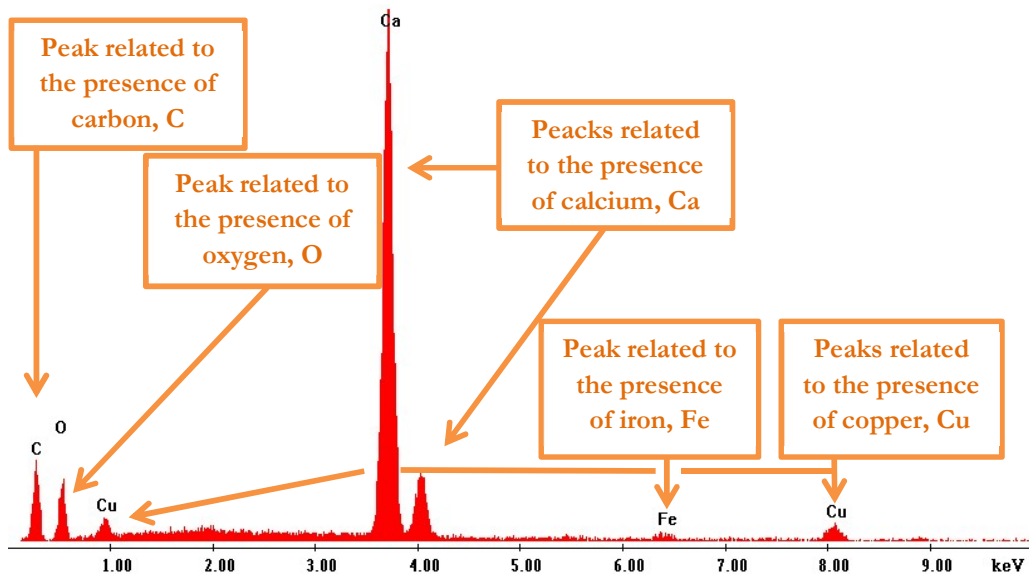


Figure 3.8. Energy-dispersive X-ray spectroscopy (EDX) of one-point location of the inner wall of a fouled pipe.

This chemical composition does not determine that the fouling created is Calcite. Therefore further analyses were proposed. A method that can analyse the samples from a crystallographic perspective is XRD. This measures the diffraction angles of a sample, and by providing the angles and the intensity of the reflected beams it gives a three-dimensional picture of the density of the electrons within the crystal and therefore, its atomic and molecular structure. Comparing the sample XRD results with the XRD database of known samples, the crystallographic composition of the scratching fouling can be concluded.

Figure 3.9 shows the XRD of a sample scratched from the inner wall of a fouled pipe. It can be seen that the reflected beam and their intensity match with a combination of Calcite (purple in the graph), vaterite (blue), and traces of aragonite (yellow) and copper (I) oxide (green). This composition gives to the sample its red-brown colour due to the Calcite, vaterite [136], [137].

In addition, there can be seen a blue coloured solid which has not been detected after the cleaning. This is most likely due to the Copper (II) Hydroxide complex which is a typical product of electrochemical reaction that includes copper [138].

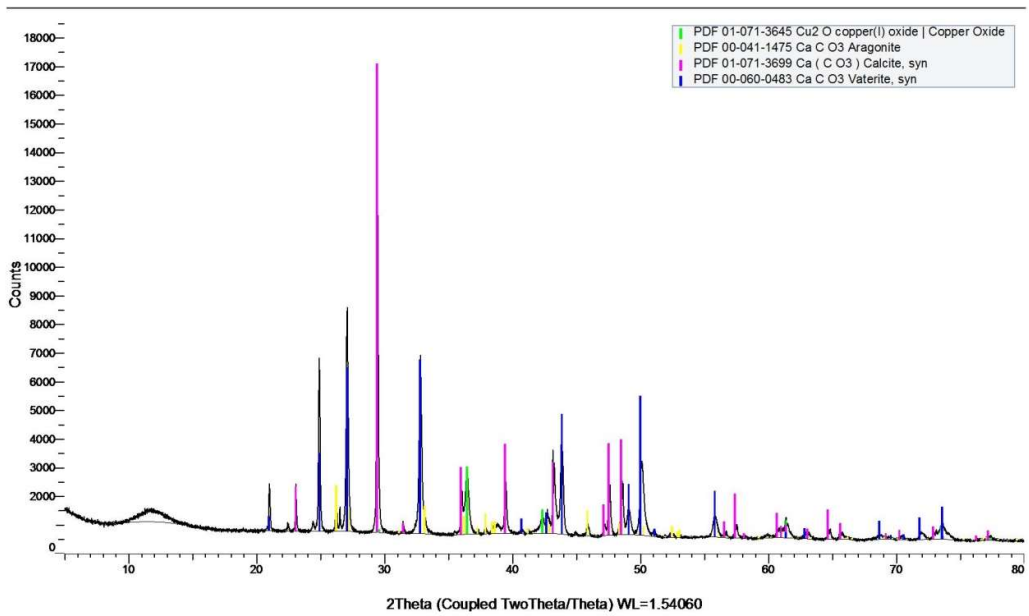


Figure 3.9. X-Ray Diffraction (XRD) of a sample scratched from pipe and the comparison with the expected results of copper (I) oxide, aragonite, Calcite and vaterite.

Finally a SEM scan was done in different locations to evaluate the crystals' distribution in the surface. Figure 3.10 presents the SEM of one-point location on the inner wall of a sample pipe. The Calcite crystals are evenly distributed among the sample. It can be seen that the Calcite is the substrate for other semi-amorphous depositions that can be the vaterite or any other of the minerals presented in the XRD.

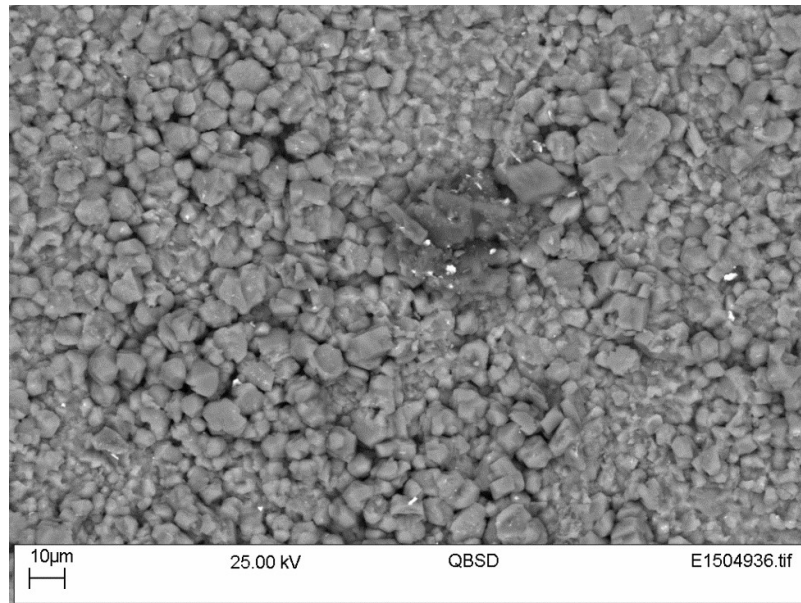


Figure 3.10. Scanning Electron Microscope (SEM) image of one-point location of the inner wall of a fouled pipe.

Considering all the above, it can be concluded that the most abundant allotropic form created is Calcite, and it is evenly distributed, which was the aim of this fouling creation experiments.

3.4.2 Electrochemical reaction composition analysis of Pipe 2

The first analysis is a visual one to see that the entire pipe is covered by an even distribution of fouling. Figure 3.11 shows the inner wall of a pipe covered with fouling.

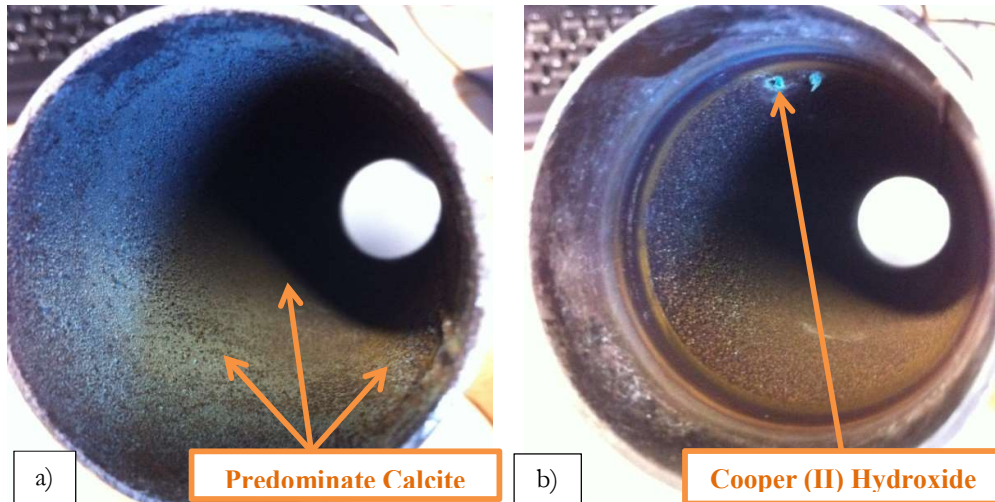


Figure 3.11. Results of Fouling Creation on Inner Walls of Pipe 2, a) is the picture taken from the bottom and b) is the picture taken from the top.

Figure 3.12 presents the EDX analysis of the fouling created on Pipe 2 by the electrochemical method. It can be seen that the scale created is very similar to the one created on Pipe 1, but in this case the EDX does not detect any Iron on the sample.

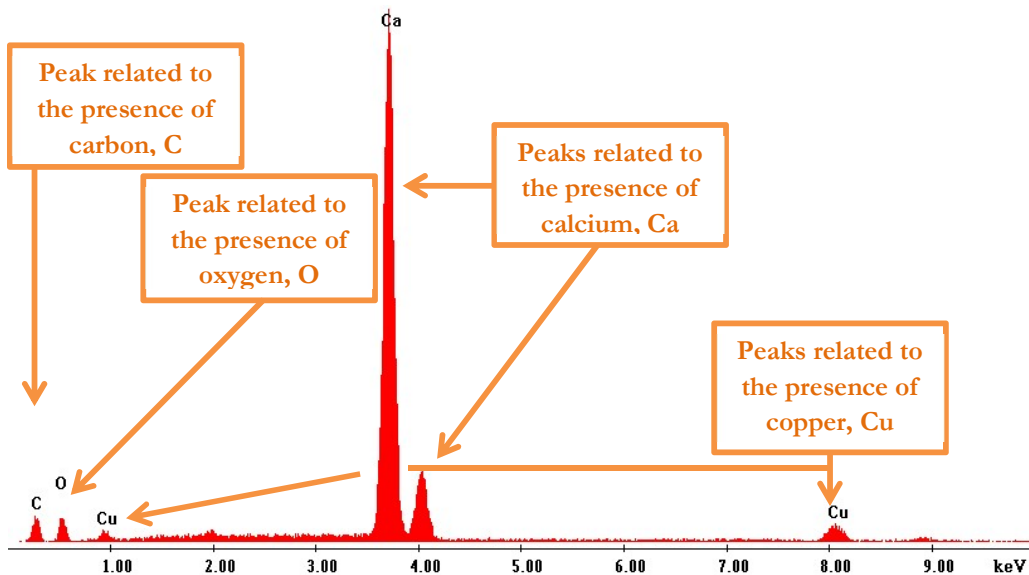


Figure 3.12. Energy-dispersive X-ray spectroscopy (EDX) of one-point location of the inner wall of Pipe 2.

Figure 3.13 shows the XRD of a sample scratched from the inner wall of a fouled pipe. It can be seen that the reflected beam and their intensity match with Calcite (purple in the graph), some vaterite (blue), and traces of aragonite (green) and copper (I) oxide (yellow). The composition is similar to Pipe 1 and it has also a similar colour. Pipe 2 also has a blue colour presented in Figure 3.11 due to the Copper (II) Hydroxide complex.

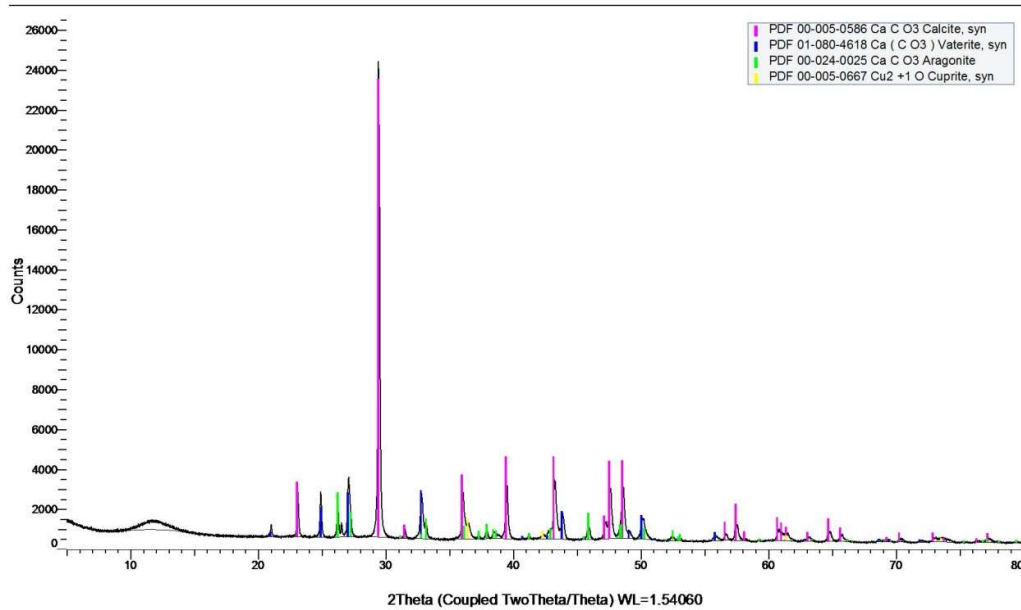


Figure 3.13. X-Ray Diffraction (XRD) of a sample scratched form Pipe 2 and the comparison with the expected results of Calcite, aragonite, vaterite, and copper (I) oxide.

Finally, a SEM scan was done in different locations of the surface to evaluate crystal distribution. Figure 3.14 presents the measured SEM of one-point location of the inner wall of a sample pipe. The fouling is evenly distributed across the sample. It can be seen that the Calcite is the substrate for other semi-amorphous depositions that can be the vaterite or any other of the minerals presented in the XRD.

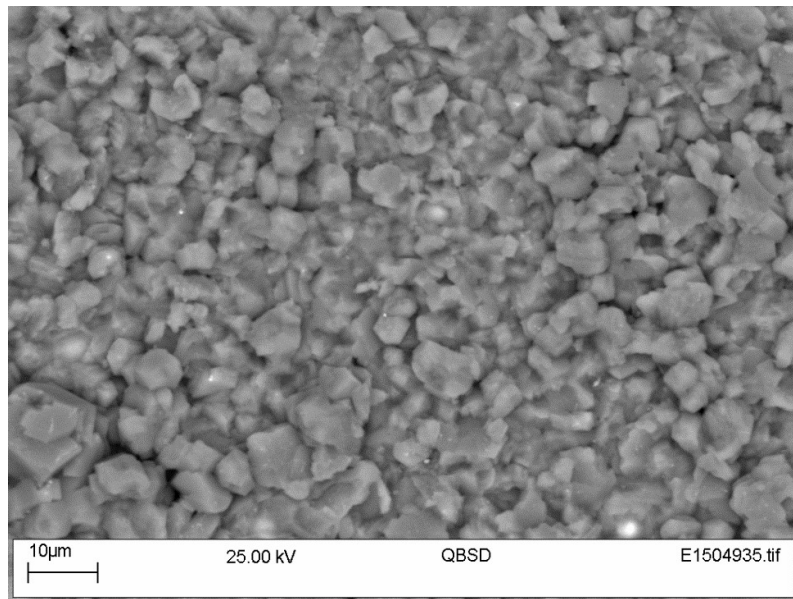


Figure 3.14. Scanning Electron Microscope (SEM) image of one-point location of the inner wall of Pipe 2.

It can be concluded that in Pipe 2 the most abundant allotropic form created is Calcite, and the fouling is evenly distributed which was the aim of this fouling creation experiments.

3.4.3 Electrochemical reaction composition analysis of Pipe 3

As in the previous cases, initially a visual inspection of the fouled pipe is done Figure 3.15 shows the inner wall of Pipe 3 covered with fouling.

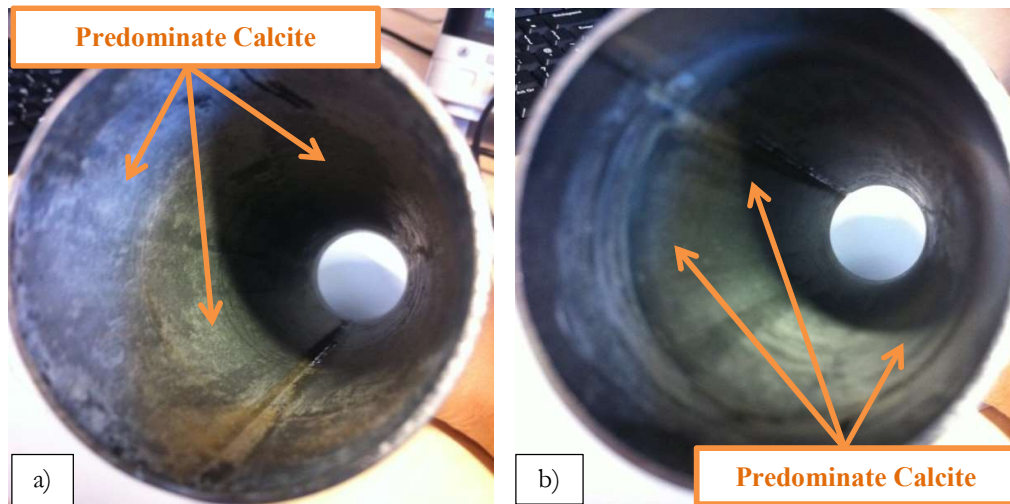


Figure 3.15. Results of Fouling Creation on Inner Walls of Pipe 3, a) is the picture taken from the bottom and b) is the picture taken from the top.

Figure 3.16 presents the EDX analysis of Pipe 3 after fouling by the electrochemical reaction method. It can be seen that the scale created is formed mainly by calcium, carbon, and oxygen, which is the elemental composition of Calcite, and has traces of iron and copper. The iron and

copper from the pipe and the electrode like pipes 1 and 2. Pipe 3 also presents traces of chromium that comes from steel alloy.

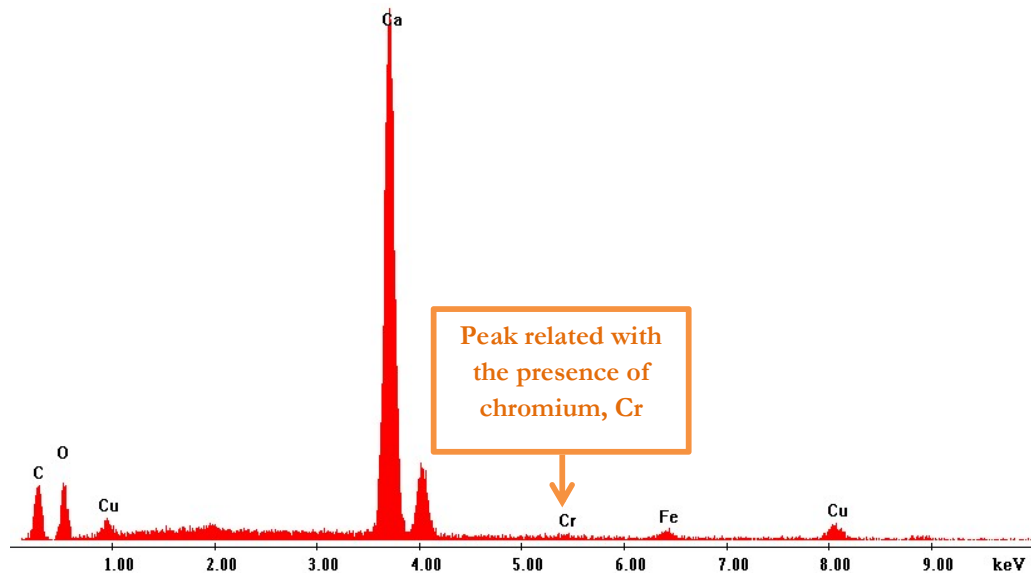


Figure 3.16. Energy-dispersive X-ray spectroscopy (EDX) of one-point location of the inner wall of a fouled pipe.

Figure 3.17 shows the XRD of a sample scratched from the inner wall of a fouled pipe. It can be seen that the reflected beam and their intensity match with a combination of Calcite (green in the graph), vaterite (blue). The existence of these two components gives the brown colour to the sample [137] as shown in Figure 3.15.

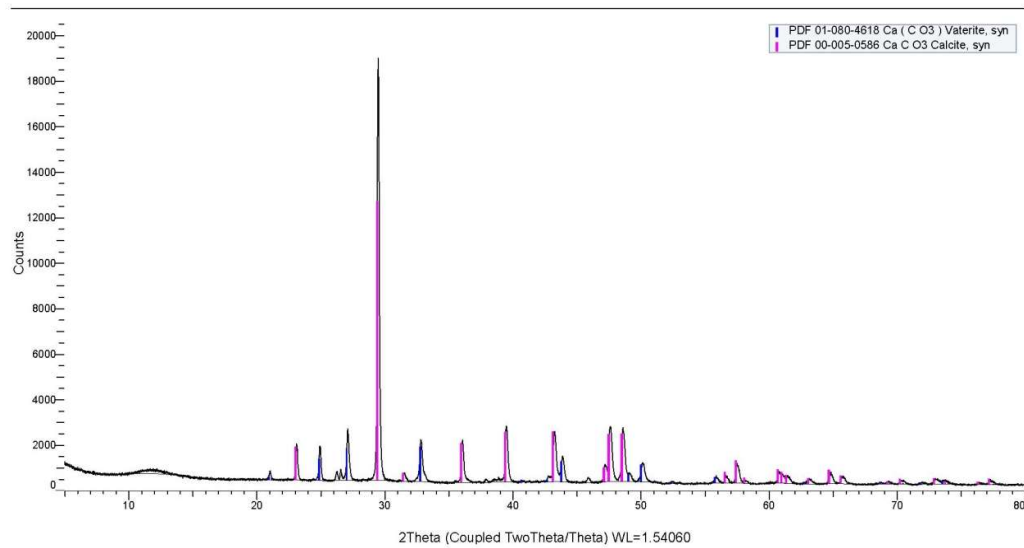


Figure 3.17. X-Ray Diffraction (XRD) of a sample scratched form Pipe 3 and the comparison with the expected results of vaterite and Calcite.

Finally a SEM scan was done in different locations of the surface to evaluate the crystals distribution in the surface. Figure 3.18 presents the SEM of one-point location of the inner wall of a sample pipe. The Calcite crystals are evenly distributed across the sample. In this case more proportion of cubes of Calcite can be seen. In this sample Calcite is also the substrate for other semi-amorphous depositions that can be the vaterite or any other of the minerals presented in the XRD.

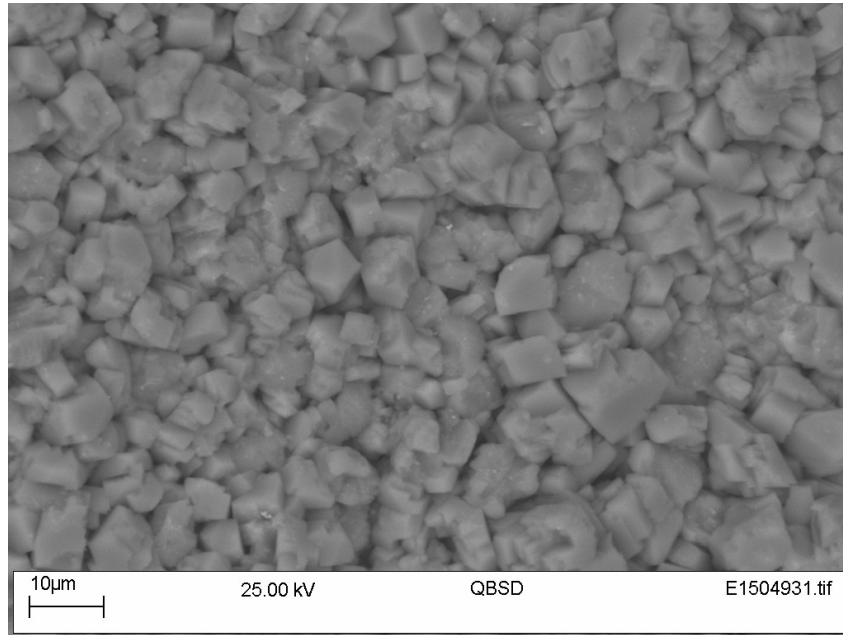


Figure 3.18. Scanning Electron Microscope (SEM) image of one-point location of the inner wall of Pipe 3.

It can be concluded that the most abundant allotropic form created is Calcite, and it is evenly distributed which were the aims of this fouling creation experiment.

3.4.4 Spraying deposition on heated plates composition analysis

In the same way as in the previous case, a crystallographic analysis to the fouling created has been done for the spring deposition on a heated plate with atomizer.

In this case, the solution used for the fouling creation had the same composition as the solution for the electrochemical reaction but the potential products are different since no electrochemical reactions are expected and the concentration of the sodium chloride will be over saturation due to the evaporation of the water.

The plates subjected to this method present an even distribution of fouling. Figure 3.19 shows the comparison of two plates with and without Calcite fouling created on one of the surface.

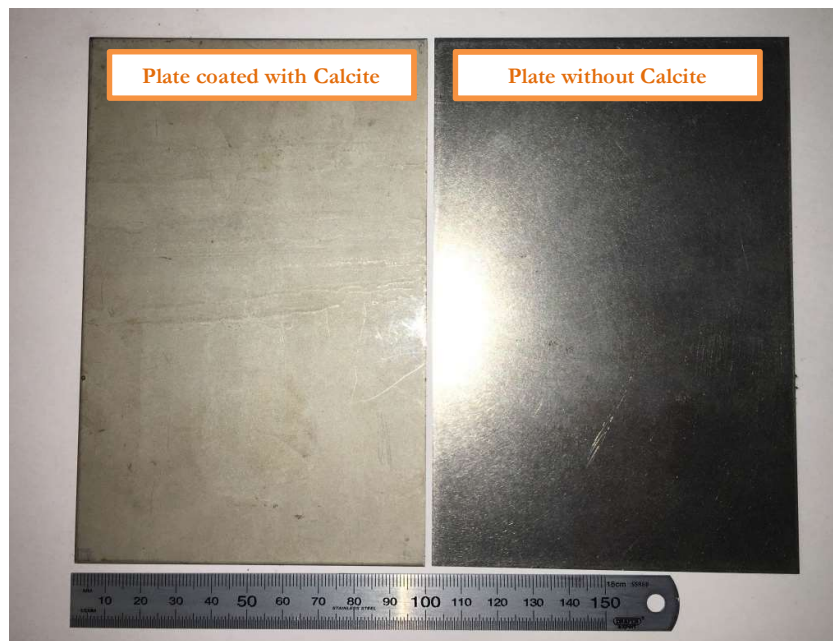


Figure 3.19. Sample plates before and after the heating deposition with an atomizer method.

Like in the electrochemical reaction the first test applied was EDX. It can be seen in Figure 3.20 that the plate has all the elements of calcium carbonate and also traces of chlorine, chrome and iron which may come from the solution and the steel plate.

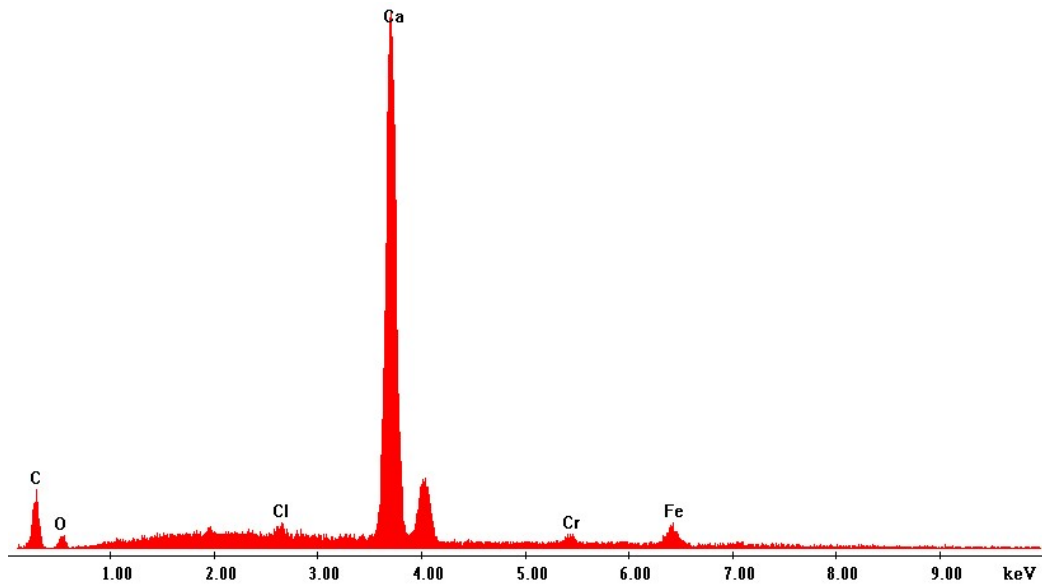


Figure 3.20. Energy-dispersive X-ray spectroscopy (EDX) of one-point location of the inner wall of a fouled plate by heating deposition with atomizer method.

Again for a crystallographic analysis an XRD measurement was performed on a sample plate to find out the calcium carbonate polymorph that was created. Once again in this case it can be seen that Calcite is the predominant allotropic form of calcium carbonate in the sample, Figure 3.21.

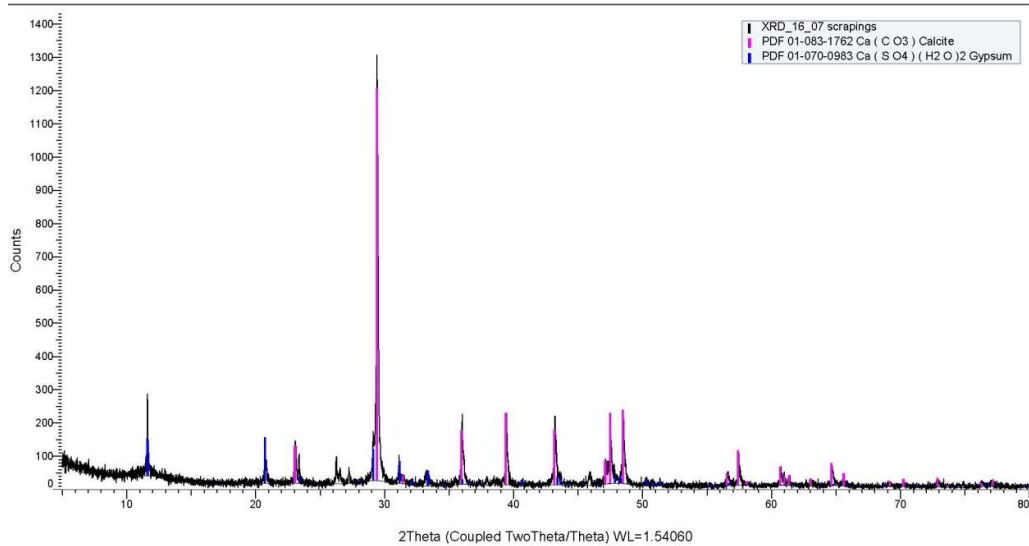


Figure 3.21. X-Ray Diffraction (XRD) of a sample scratched from fouled plate and the comparison with a pure Calcite diffraction angles in purple.

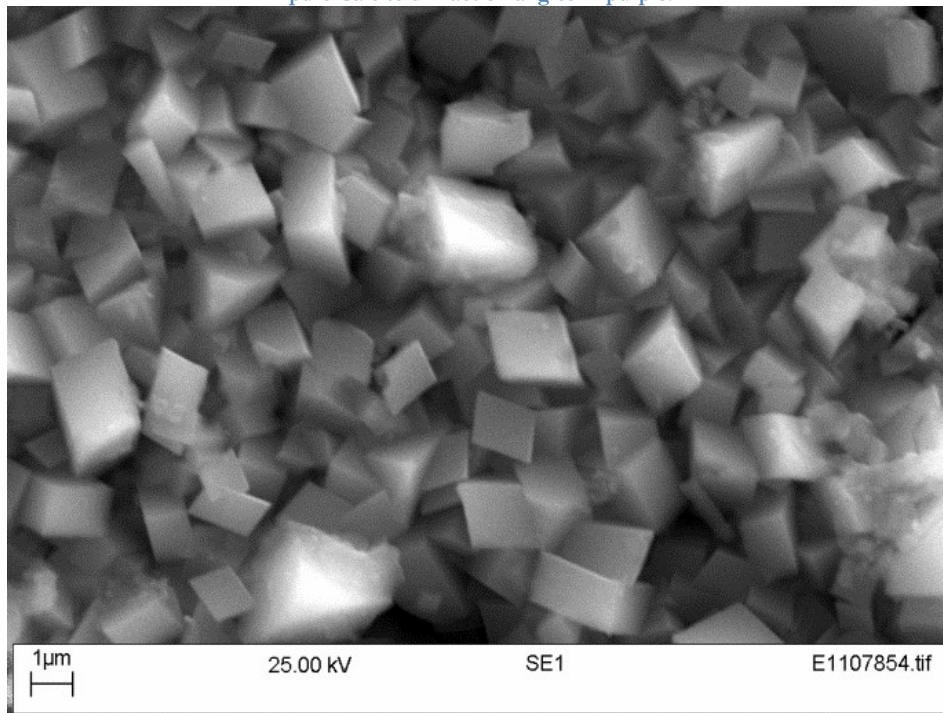


Figure 3.22. Scanning Electron Microscope (SEM) image of one-point location of the inner wall of a fouled plate.

Finally, SEM was performed on the plate. Figure 3.22 presents the cubic formation of Calcite crystals on the plate.

3.4.5 Adhesion quality analyses on sample plates

The importance of the type of fouling attached to a pipe has been explained for further experimentation and also why the generation of Calcite means the generation of a appropriated

fouling that can be found in a number of different industrial processes and domestic pipelines. But the reactions can occur within the solution and not in the samples.

The preliminary observation of the samples presented a well adhered fouling that could not be removed easily from the substrates and a sharp metallic object was needed to remove a small amount. But a standardised measurement has been applied in order to quantify the adhesion, referred to the values given by the standards, of the fouling created on the samples. For that to methods were used: “Adhesion by tape” and “Pull-off adhesion” tests.

Adhesion by tape test

The adhesion by tape test, which has the ASTM standards designation: D 3359-97, evaluates the adhesion of a coating on a metallic surface in a qualitative manner. This is done by scratching the coated surface generating a squared division of the coating, and then pasting a standardised tape one-inch (25-mm) wide, semi-transparent, pressure-sensitive, and taped for 60 seconds to ensure good adhesion. Finally, the tape is removed and the coating remaining on the substrate is analysed.

The fouling created on a sample plate has been analysed. Results evidence a coating with an adhesion factor of 5 over 5 in the adhesion by adhesion by tape test. This means that around 0% of the coating had been removed during the test meaning that it is high quality coating.

Pull-off adhesion test

This test falls under the standard EN ISO 4624:2002, and evaluates the adhesion of a coating to a substrate in a quantitative manner. This is done by applying an adhesive to a dolly and attaching it to the coating. Then the dolly is pulled off while the force applied is measured. This is done with a pull-off adhesion tester that can measure the force under which the coating has been removed from the substrate. By knowing the contact surface and the force needed, the stress needed can be calculated.

The dolly used for this experimentation was a 20mm diameter grit blasting and the adhesive Loctite super glue.

The result of the test was 4.30 MPa what evidences that very high stresses have to be applied for the fouling to be removed.

3.5 Summary

This chapter describes why Calcite has been selected as the fouling to be grown for later removal with the use of ultrasound.

Two different methods to generate Calcite fouling in sample pipes and plates were presented: electrochemical reaction and spray deposition on heated plates. All the methods produce an even distribution of fouling in the samples for further analysis.

In order to validate the fouling created through the different methods, several tests have been conducted on the samples: crystallographic and composition analyses (Scanning Electron microscope, X-Ray Diffraction, and Energy-dispersive X-ray spectroscopy).

Furthermore, the adhesion of the Calcite coating to the samples has been tested by both qualitative (adhesion by tape test) and quantitative (pull-off adhesion test) means to measure the quality of the adhesion.

All the analyses lead to the conclusion that the fouling created is of high quality and very well adhered to the samples, hence it is considered representative of the actual fouling found in the industry.

4 Theoretical background of acoustic cavitation

A fouling creation method to generate real industrial fouling on pipes that will be used as samples was presented in Chapter 3. Previously in Chapter 2, the use of Acoustic Cavitation was proposed as a method for the removal of fouling, based on a literature review of current cleaning methods. In the present chapter the theoretical background to understand the cavitation phenomena is given. Cavitation prediction graphs are presented, and prediction plots that provide information on the displacement needed for generation of two types of cavitation are produced.

4.1 Introduction

Cavitation can be defined as the sudden formation and bursting of bubbles in a liquid due to a rapid decrease of pressure. It has been calculated that this bubble's collapse can produce liquid jets and shock waves with pressures above 8 GPa [139] and temperatures of at least 5000 K [140].

This phenomenon was first described by Osborne Reynolds in a publication dated 1894 [141] by the observation of erosion in British torpedo boats. Moreover, cavitation is a typical cause of failure in different industrial devices such as propellers, pumps, engines and control valves. Since cavitation is considered as an important problem in industry, different mechanisms are being used or under development for its prevention or mitigation of its unwanted effects [142]. In contrast, cavitation has a number of advantageous industrial applications and is used in different engineering sectors such as chemical synthesis, water and effluent treatment, biotechnology, sono-crystallisation, atomization, cleaning, and sono-chemistry.

Undoubtedly, these industrial applications use cavitation under control producing it with different methods such as acoustic cavitation, optic cavitation, acoustic sparkers or pulsers, and particle cavitation. Each of them has its advantages and disadvantages. For example optic cavitation can be formed in free liquids without any disturbing parts, where the exact location of the bubble and the instant of generation can be known [143], but it can only be produced in a single point, as it also happens in particle cavitation and sparkers [93], [144]. In this thesis acoustic excitation is selected essentially because it can be generated in larger areas such as a pipelines and it is considered as the most important source of cavitation for practical proposes [145]. Moreover, acoustic cavitation can be applied from the outer wall of a pipe without interacting with the inner process of the pipe. In this case, the acoustic energy is guided by the pipe wall and it is transferred to the liquid right next to the inner wall of the pipeline, generating the decrease of pressure for the cavitation formation and subsequent fouling removal.

At this point, an explanation of the acoustic cavitation phenomenon and the theory necessary to explain the results obtained in the experimentation is given. In addition, the mathematical equations required to calculate the acoustic pressure generated in the liquid by a vibrating wall are presented, which are based on Newton's second law of motion.

Finally, an example of the cavitation prediction plot generated based on the conditions applied in the investigation is given, as well as the minimum displacement required to generate cavitation in all the areas.

4.2 Acoustic cavitation

According to the given definition of cavitation, if the sudden decrease of pressure is produced by an acoustic wave traveling through a liquid it is called acoustic cavitation, and it is referred both to the creation of new cavities and to the expansion of pre-existing ones. These minuscule bubbles can be trapped in the liquid, attached to particles immersed in the fluid or confined in microscopic fissures in the liquid-solid boundary surface [146].

The acoustic cavitation phenomena can be really complicated to understand since both the pressure and velocity field in a two phase gas-liquid medium has to be determined along with the motion of a bubble wall, under the effect of an oscillating pressure [147]. Also it is important to consider that the most general case is where a cavity is not spherical but has an arbitrary shape. Therefore, the common practice, as found in the literature, is based on the description of the motion of a single cavity considering it spherical and symmetric.

In fluid and bubble dynamics the most common equation to describe the motion of a single bubble is called the "Rayleigh-Plesset" equation (4.4). This describes the dynamics of a single spherical bubble immersed in an infinite liquid. In the case of multiple bubble systems like that generated by an acoustic field, some collateral effects are ignored and the most general practice is to ignore their effects. In essence, the energy balance necessary to reach this equation is obtained as follow;

$$\left[\begin{array}{c} \text{Kinetic energy} \\ \text{of the influenced} \\ \text{mass} \end{array} \right] - \left[\begin{array}{c} \text{Energy dissipated} \\ \text{due to the} \\ \text{viscosity} \end{array} \right] = \left[\begin{array}{c} \text{Work of the} \\ \text{internal} \\ \text{pressure} \end{array} \right] - \left[\begin{array}{c} \text{Work of the} \\ \text{external} \\ \text{pressure} \end{array} \right] - \left[\begin{array}{c} \text{Work} \\ \text{of the surface} \\ \text{tension} \end{array} \right]$$

Here the kinetic energy of the mass of fluid influenced by a sphere of radius R immersed in a liquid is given by equation (4.1) [148];

$$\frac{1}{2} M_{eff} (R')^2, \text{ where } R' \equiv \frac{dR}{dt}, \quad (4.1)$$

and M_{eff} is the effective mass of the sphere;

$$M_{eff} = 3\rho \left(\frac{4\pi}{3}\right) R^3, \quad (4.2)$$

Where ρ is the density of the liquid. Then the balance yields;

$$\frac{1}{2}M_{eff} \left(\frac{dR}{dt}\right)^2 - \int_{R_0}^R \left(-\frac{4\mu}{R} \frac{dR}{dt}\right) 4\pi R^2 dR = \int_{R_0}^R \left(P_i - P_e - \frac{2\sigma}{R}\right) 4\pi R^2 dR, \quad (4.3)$$

Where μ is the liquid viscosity and R_0 is the initial bubble radius. If this energy balance is differentiated with respects to R and divided by $4\pi R^2 \rho$, it results in;

$$RR'' + \frac{3}{2}(R')^2 + \frac{4\mu}{\rho} \frac{R'}{R} + \frac{2\sigma}{\rho R} + \frac{P_o - P_i}{\rho} = 0. \quad (4.4)$$

In equation (4.4) the two first terms refer to the inertia of the cavity, the third is referred to the viscosity, the fourth to the surface tension, and the remaining one is related with the pressure both inside and outside the bubble. Here the internal pressure P_i is split into a condensable part P_v of the vapour and a non-condensable part P_G of the gas dissolved in the liquid; $P_i = P_v + P_G$. Also, the term for the external pressure P_e can be decomposed into the atmospheric pressure P_o and a time varying part or acoustic pressure P_a . For a continuous ultrasonic sinusoidal excitation with single frequency, this can be written as;

$$P_a = -P_A \sin \omega t. \quad (4.5)$$

Where P_A is the acoustic pressure amplitude, and assuming negative half-cycle happens at first place of a bubble growth.

4.3 Cavitation prediction

It is known that there are two types of acoustic cavitation: (i) stable cavitation and (ii) transient cavitation [140], [149]. i) Stable cavitation happens when a cavity oscillates under a variable pressure for a number of cycles. This can be dissolved back in the liquid, merged with other cavities producing a large one, or collapse. ii) Transient cavitation is when a bubble bursts, often violently, within a single cycle or small number of cycles. In this case the bubbles collapsing can produce nuclear reactions and light emissions. These two types of cavitation are also known as inertial and non-inertial cavitation respectively, and will have different types of effects in a solution, having therefore different applications in industry. For example transient cavitation is desirable in industrial applications of macro-sound such as emulsification or sono-chemistry, while stable cavitation is used for degassing or ultrasonic cleaning [147], [150].

In the current work, a new application of cavitation for cleaning pipelines is presented where controlling the type of cavitation plays a primary role.

To know which type of cavitation is going to be produced based on the acoustic pressure, Apfel et al 1981 [151] proposed a plotting method, unifying in one graph the different thresholds that

the cavitation phenomenon has depending on the ultrasonic pressure. All the equations required to plot the three different thresholds and the inertial control radius are explained as follows.

4.3.1 Rectified diffusion threshold

The mechanism related with the minimum pressure to have a bubble growth in liquids is the mass transfer through the bubble wall; this is called “rectified diffusion” [152]–[155]. Safar M.H. (1969) [153] introduced the effects of heat conduction in the motion of a bubble described by the equation (4.6) for a bubble of radius R_D (referred to as rectified diffusion) in a liquid of surface tension σ and with a gas filling the bubbles with a ratio of specific heats κ . Then, the minimum pressure P_D for an acoustic pressure frequency f is given by;

$$\frac{P_D}{P_o} = \frac{[3\kappa(1+X_D)-X_D][1-(f/f_D)^2](1-C+X_D)^{1/2}}{[6(1+X_D)]^{1/2}}, \text{ where } X_D = \frac{2\sigma}{P_o R_D}, \quad (4.6)$$

C is the saturation of gases in the liquid and f_D is the resonant frequency of a bubble of radius R_D that can be calculated by [156];

$$f_D = \frac{1}{2\pi R_D} \left\{ \frac{3\kappa P_o}{\rho} \left[1 + X_D \left(1 - \frac{1}{3\kappa} \right) \right] \right\}^{1/2}. \quad (4.7)$$

Equation (4.6) is one of the equations used to create the cavitation prediction plots. This is represented by the curve R_D in Figure 4.1, for the values found in the literature [151], and in Figure 4.3, as an example of the typical conditions applied in the experimentations presented in this work (Sections 5.4.3 and 7.4).

4.3.2 Blake threshold

The next threshold is known as the “*Blake threshold*” [157]. The growth in this case is by mechanical means (with little gas transport) due to the inertia of the liquid surrounding the bubble, known as “liquid felt”. Blake proposed an equation that predicts the minimum acoustical pressure P_B for a bubble of radius R_B under an atmospheric pressure P_o in a liquid of surface tension σ . This is written as follow;

$$P_B/P_o = 1 + \frac{4}{9} X_B \left[\frac{3X_B}{4(1+X_b)} \right]^{1/2}, \text{ where } X_B = \frac{2\sigma}{P_o R_B}. \quad (4.8)$$

Equation (4.8) is used also to create the cavitation prediction plots, Figure 4.1 and Figure 4.3, and is represented by the curve R_B .

4.3.3 Transient cavitation threshold

Thirdly, the threshold from which a bubble will collapse in a short number of cycles is called the “transient threshold”. Consequently, transient cavitation is generated. This threshold is of vital importance since the highest pressures and temperatures are generated when transient cavitation occurs. It is also known that the pressures are that high that can generate atomic reactions with light emissions [158]–[160]. For this, the “*Rayleigh–Plesset*” equation (4.4) was derived by Apfel in 1981 when a bubble reaches a size approximately twice the original size in a few cycles [148], [151] to produce equation (4.9) for this threshold.

In this case the calculations done refer to the radius of a bubble R_T , which is the minimum radius that a bubble needs to become transient giving an acoustical pressure of P_T under an acoustic pressure field with a frequency f on a liquid of surface tension σ and density ρ . The equation is written as follows [151];

$$R_T = \frac{0.13}{f} \left(\frac{P_o}{\rho} \right)^{1/2} \left[\frac{P_f - 1}{\sqrt{P_f}} \left[1 + \frac{2}{3} (P_f - 1) \right]^{1/3} \right]; \quad P_f \leq 11 \quad (4.9)$$

$$R_T = \frac{0.3}{f} \left(\frac{P_o}{\rho} \right)^{1/2} \left(\frac{2}{3} (P_f - 1) \right)^{1/2}; \quad P_f \geq 11 \quad (4.10)$$

Where;

$$P_f \equiv \frac{P_T}{P_o}$$

It is important to bear in mind that this equation is only valid for incompressible liquids and assumes that it breaks down in the final stages of the cavity collapse in case of the interfacial velocity approaching the speed of sound in the liquid. Another assumption is that there are no large thermal effects (large viscous or latent heat effects), no mass transport (the gas content remains essentially constant), and constant inertial pressure in the whole cavity at any instant in time, which can be considered a good approximation if the wavelength of sound in the gas is noticeably larger than that of the bubble diameter. When any of these assumptions are not met, more complex theory must be applied [148].

4.3.4 Inertial control radius

Finally Apfel in 1981 [148], [151] also included the definition of a minimum radius of a bubble R_I from which bubble growth is driven by inertial control under an acoustic pressure field of amplitude P_I and frequency f . The equation (4.11) yields [148];

$$R_I = \left(\frac{4}{6\pi f} \right) (P_n - 1) \left(\frac{2P_o}{\rho P_n} \right)^{1/2}; \quad P_n \equiv \frac{P_I}{P_o} \quad (4.11)$$

Equation (4.11) is the last equation necessary to create the cavitation predictions plots (see Section 4.4). With the previous equations: (4.6), (4.8), (4.9) or (4.10) (depending on the value of P_f (Section 4.3.3)) and equation (4.11), the cavitation plots can be generated. For that the curve described by equation (4.11) is represented by R_I in Figure 4.1 and Figure 4.3.

4.4 Cavitation prediction plots

If all the equations explained above are plotted in the same graph it is possible to define the different zones where the different types of cavitation are more likely to occur.

Then computing all the equations from (4.6) to (4.11) it is possible to obtain the cavitation prediction plots, shown in Figure 4.1. This describes the types of cavitation expected at different acoustic operated pressures for a specific liquid and felling-bubble gas³. Three different potential cavitation regions can be seen for the three thresholds described above.

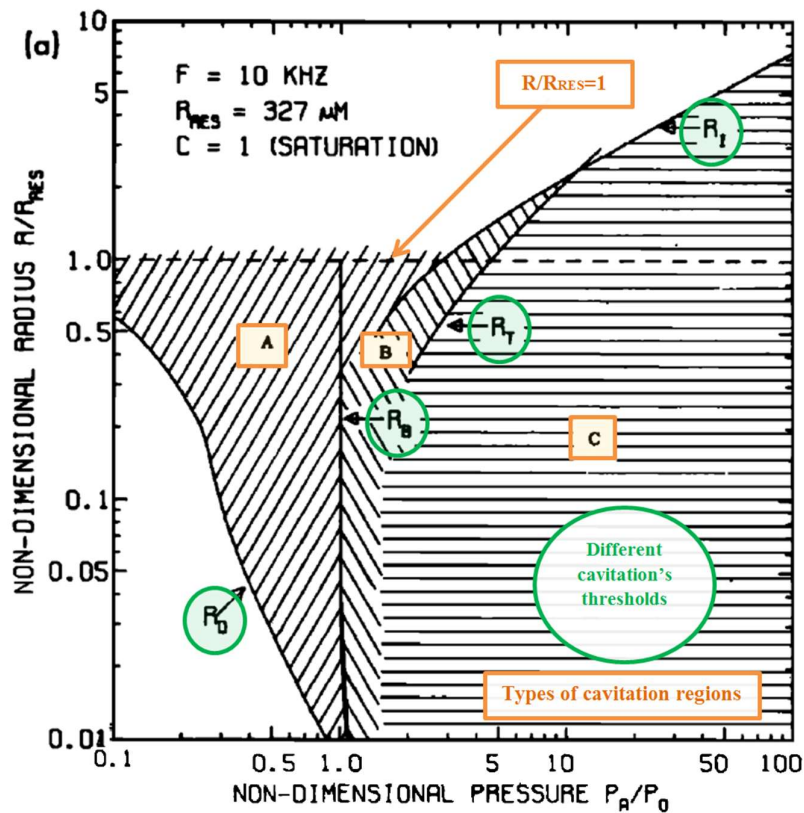


Figure 4.1. Represents the cavitation prediction plot for an acoustic field of 10 kHz with a water with a saturation value $C=1$. Picture taken from [151]. Equation (4.6) is represented by R_D , equation (4.8) is represented by R_B , equation (4.9) is represented by R_T , and equation (4.11) is represented by R_I . The three regions A, B and C are highlighted with an orange square.

³ Felling-bubble gas is the existing gas solved in the liquid that fells or can fell the bubbles generated by the acoustic pressure oscillation.

The interpretations of the three regions found in Figure 4.1 are explained below as follows:

Region A: The growth of the bubble is only due to rectified diffusion. When the bubble reaches a size it will go into a more violent oscillation and may split into micro-cavities. It is not expected to produce erosions in hard materials such as Calcite in this region due to the cushioning effect of the entrapped gas even though this type of cavitation is used for degassing and for classic ultrasonic cleaning. This is because of the shock wave generated by the microbubble oscillation under the variable acoustic field, Figure 4.1.

Region B: In this case the growth is due either or both to the rectified diffusion and/or mechanical means, and the initial bubble will not be transient. If the bubble reaches the resonant radius, it can shatter into micro-bubbles and if those bubbles are smaller than the original one, they can fall in Region C and become transient. It is important to note that curves R_T and R_I are not valid for $P_f < 2$. This type of cavitation has the same properties as Region A, but if the bubble becomes unstable and goes to a catastrophic collapse it can lead to fragmentation into smaller bubbles and fall into Region C, Figure 4.1.

Region C: This is the transient region where cavities will rapidly collapse producing extremely high pressures and heat. In this location it is expected to damage any solid by the jets generated during the implosion, Figure 4.1.

It has been proven in this work that the transient cavitation, region C, is the type of cavitation capable to remove hard scale fouling from the inner wall of a pipe (see Section 7.4).

4.5 Acoustic pressure generated by an oscillating wall

The acoustic pressure can be measured in different ways. Here, since the proposed method depends on wave propagation through the pipe wall, the investigation is carried out based on the displacement produced in the inner wall of the pipeline. This displacement then needs to be converted into pressure to be analysed with the graphical method proposed in Section 4.3 since the graph plots the ratio of acoustic pressure and atmospheric pressure vs the ratio of bubble radius and resonant radius of a bubble at the frequency of the excitation. The transformation from displacement to acoustic pressure can be explained based on Newton's Second Law as follows:

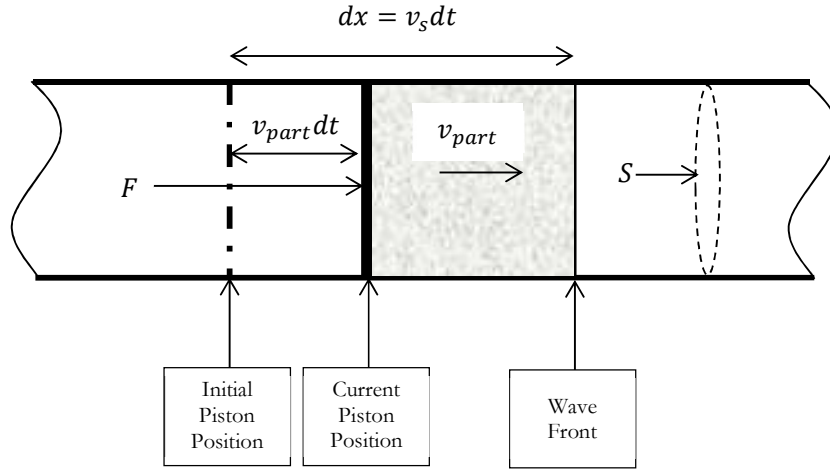


Figure 4.2. Illustration of a vibrating wall in contact with a fluid generating an acoustic wave in the fluid.

Consider a vibrating piston at the end of a long tube with a cross-sectional area S , as shown in Figure 4.2. Originally, the piston remains in a static equilibrium. Now consider applying a force F to the piston. This will make the piston move to the other end generating a compression force whose wave front will move a distance dx during a short interval of time dt . Since the wave front travels at the speed of sound in the fluid it satisfies $dx = v_s dt$. The particles themselves, however, move at different speed v_{part} driven by the piston. By considering that the distance from the piston to the wave front is differentially small, it can be assumed that the particles in the volume affected by the piston have the same speed. Here the total mass of fluid moving to the right is $dm = \rho_o S dx$ where ρ_o is the density of the fluid at $t = 0$, and therefore has a linear moment of;

$$dp = \rho_o S v_s dt v_{part}, \quad (4.12)$$

By applying Newton's Second Law then,

$$P \equiv \frac{F}{S} = \frac{1}{S} \frac{dp}{dt} = \rho_o v_s v_{part}. \quad (4.13)$$

Now considering the piston governed by simple harmonic motion with an angular frequency ω , the velocity of the particles can be found by,

$$v_{part} = -A\omega \cos(\omega t), \quad (4.14)$$

And

$$v_{part_{max}} = A\omega, \quad (4.15)$$

Where A is the amplitude of the wall vibration. Then the pressure amplitude generated by an oscillating wall yields,

$$P = \rho_o v_s A \omega, \quad (4.16)$$

For an excitation with a constant frequency f ,

$$P = 2\pi\rho_o v_s A f. \quad (4.17)$$

4.6 Cavitation prediction plots for further investigation

After describing how to generate the cavitation prediction plots it is necessary to determine the frame for the investigation. Later on in Chapter 7, acoustic cleaning of pipelines with ultrasound is performed using tap water and HPT at resonant frequencies of 30 kHz. Therefore, for transducer design (see Chapter 5) it is necessary to establish the displacement needed to generate the different types of cavitation, stable or transient.

As an example a cavitation prediction plot for tap water with a frequency of excitation of 30 kHz is presented in Figure 4.3. The three locations explained in Section 4.4 determine which type of cavitation is expected to be generated. To generate this plot, two vectors both for the bubble radius and the acoustic pressure are generated and substituted along with the values presented in Table 4-4-1 in the equations from (4.6) to (4.11) to produce the curves: R_D , R_B , R_T and R_I . R_{RES} can be calculated with equation (4.7) by substituting f_D by the frequency of excitation, 30 kHz for Table 4-4-1, and considering $R_{RES} = R_D$.

Table 4-4-1. Values used in the equations from (4.6) to (4.11) for the calculation of the curves: R_D , R_B , R_T and R_I cavitation prediction plots.

Magnitude	Symbol	Value	Units
<i>Surface tension of water at 20 °C</i>	$\sigma_{20\text{ }^\circ\text{C}}$	7.20E – 02	<i>N/m</i>
<i>Ratio of specific heats of air at 20 °C</i>	$\kappa_{20\text{ }^\circ\text{C}}$	1.401	–
<i>Density of water at 20 °C</i>	$\rho_{\kappa_{20\text{ }^\circ\text{C}}}$	997	<i>kg/m³</i>
<i>Atmospheric pressure at room conditions</i>	$P_{0/20\text{ }^\circ\text{C}}$	101,325	<i>P_a</i>
<i>Saturation on air gases</i>	C	1	–
<i>Frequency of excitation</i>	f	30.00	<i>kHz</i>
<i>Resonant radius</i>	R_{RES}	82.28	<i>μm</i>

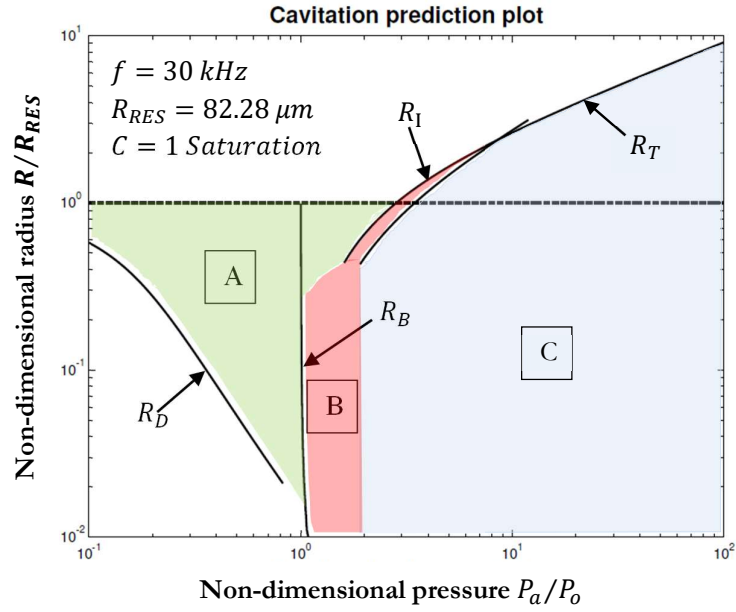


Figure 4.3. Cavitation prediction plots for tap water with a gas saturation of 1 for 30 kHz ultrasonic excitation that corresponds with the typical condition applied in further investigations performed in this work.

It can be seen from Figure 4.3 that the minimum non-dimensional pressure P_a/P_0 to generate transient cavitation is a ratio of 1.9. Therefore, the minimum displacement at that pressure and frequency can be obtained by using equation (4.17) as follows;

For,

$$P_a/P_0 = 1.9,$$

Then for an atmospheric pressure of $101,325 P_a$,

$$P_a = 1.9 \times 101,325 = 192,517.5 Pa.$$

Substituting in (4.17) for a water density at 295 K of $\rho_o = 997 K_g/m^3$ and considering the speed of sound in water at the same temperature $v_s = 1482 m/s$ then

$$A = \frac{P}{2\pi\rho_o v_s f} = 5.18 \times 10^{-7} m = 0.518 \mu m.$$

This is the amplitude value of the displacement that needs to be reached in order to generate transient cavitation.

4.7 Summary

This chapter has defined the cavitation phenomenon and its properties related to the capabilities of cleaning different types of scales. Two types of acoustic cavitation, stable and transient, have also been explained, commenting on the effects that each of them can produce on fluids and solids.

In parallel, the explanation of the governing equation of a spherical bubble has been given, starting from the energy balance. In addition, this equation has been written in a non-dimensional form.

After considering the basics of cavitation, the chapter explains a method to predict the types of cavitation that can occur depending on the acoustical pressure, the frequency of excitation and the density of the liquid. The method contains the equations for the different cavitation thresholds unifying them in one plot.

A method to calculate the acoustic pressure generated by an oscillating wall depending on the displacement of the wall has then been presented.

Finally, an example with a cavitation prediction plot is given for a generic ultrasonic excitation. From this plot has been obtained the minimum displacement of the oscillating inner wall of the pipe that is needed for the different types of cavitation. This will be used in the following chapters for the transducers selection and for the experimentation.

5 High Power Transducers (HPT) for the removal of fouling in pipelines

This chapter contains the analysis and comparison of a HPT modified for pipeline cleaning and the same HPT transducer without modification. This is done by analysing three characteristics; resonance frequency, modes of vibration and maximum displacement.

5.1 Introduction

Using the cavitation prediction multi-plot presented in the previous chapter (Section 4.5) and equation (4.20), it was possible to set the minimum displacement necessary to produce the transient cavitation for a driven frequency of 30 kHz that will result in the removal of fouling. Such displacement must be therefore achieved by the selected transducers.

Acoustic cavitation in ultrasonic cleaning baths (or classic ultrasonic cleaning) is produced by the vibration generated by Langevin bolt-clamped HPT [161]–[163]. These transducers are also used and under development in different industrial sectors worldwide for other applications such as welding, stimulation of chemical activity, or sono-chemical destruction on living cells, crystallization and freezing, emulsification, cleaning, filtration and drying, and chemical reaction activation [164], [165], [163].

The literature describes different modifications of the HPT. For example transducers for wire bonding [166] present HPT with large resonators, or high power composite transducers to be used in several power ultrasonic applications [167]. The radiator, or front mass, shape modifications are another adjustment to the conventional HPT. For example, the use of plates with square or circular shape as radiator to improve the performance of ultrasound in deforming, drying, supercritical fluid extraction (SEF), and other processes [163]. Similar to the present study are transducers with a cylindrical radiator to generate an even distribution of the acoustic field inside a radiator tube [168]. A large capacity ultrasonic device for complex vibration, which is a combination of six Langevin transducers bolt-clamped to a vibrating disc, has been developed to produce stepped complex transverse vibration in a rod [169]. Also transducers with different loading mass in both ends that can satisfy multiple resonant frequencies increasing the high power transmitting capability [170] are an existing modification to classic HPT transducers designs.

For the present work it is important to consider that currently HPTs have a flat contact surface to be attached to plane containers. Here, a redesign of HPTs with a concave contact surface is necessary so that they can be attached to pipes. The solution is proposed in Figure 5.3. This is a

modification of the existing Langevin HPT with a concave cut in the resonator to generate a curved contact surface and improve the attachment and the transduction of acoustic energy. This geometrical adjustment affects key parameters of the transducers such as modes of vibration, resonant frequencies, impedance values, and maximum displacement. These variations are analysed experimentally below.

5.2 Current HPT design

HPTs are designed to produce the largest possible displacements in the contact surface, Figure 5.1. These are assembled by bolting the front mass and the back mass on both ends of stacked piezoelectric ceramics, and gluing them with an epoxy-resin to improve the excitation. They can be made of different materials such as steel, aluminium, bronze, or titanium alloy and others to confer the transducers different properties both mechanical and chemical [171].

The most common configuration of HPT is a front mass, piezoelectric ceramics, back mass and a bolt, Figure 5.1. A piezoelectric ceramic element is excited with an AC current with the desired frequency to induce the ceramic to vibrate. This produces a linear interaction between the electrical and the mechanical state of the material. The waves generated are propagated through the front mass and transferred by the contact surface to the object that is to be excited.

In order to generate the largest possible displacement, these transducers are designed and excited at their resonant frequency $f = \omega/2\pi$. For this, the front mass m_1 , and the back mass m_2 must have a proportion given by equation (5.1)[172]:

$$\omega^2 = \frac{k(m_1+m_2)}{m_1m_2}, \quad (5.1)$$

Where k is the effective stiffness of the transducer's material and can be calculated as follows:

$$k = \frac{S_t E}{L}, \quad (5.2)$$

where S_t is the cross-sectional area of the transducer in the plane in contact with the piezoelectric ceramics, E is the Young's modulus of the two masses, and L_t is the length of the transducer.

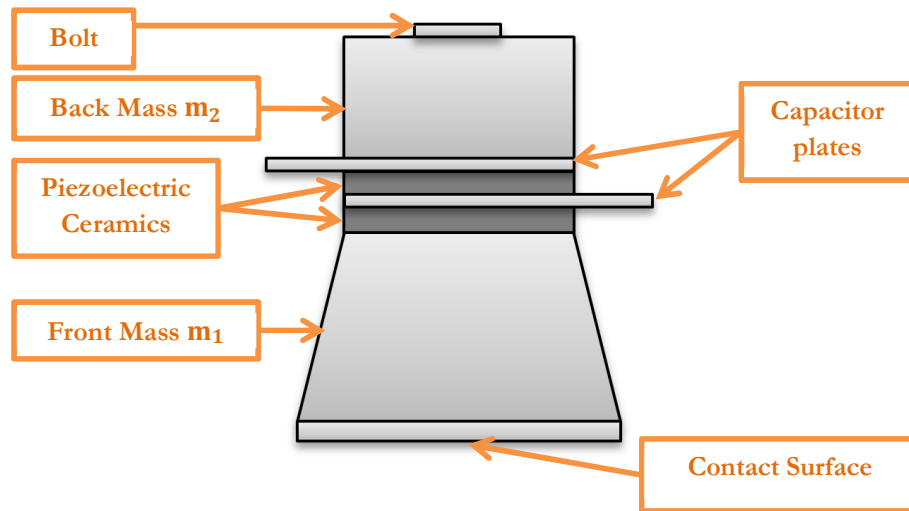


Figure 5.1. High Power Langevin transducer typical configuration.

Although the HPTs are designed to have one optimal frequency, these can resonate at more than one. This fact can be seen by the contact surface vibration analysis with the 1D scanning Vibrometer laser. This evidences different modes of vibration depending on the frequency of excitation. Figure 5.2 shows the 1D-Vibrometer analysis of one HPT contact surface, which is the surface of the transducers that is to be attached to the object to induce the vibration. It can be seen that the resonant frequencies a), b), and c) have a rhythmic distribution of vibration. At the resonant frequency a) the entire surface vibrates with a coherent displacement producing a strong piston like vibration. This leads to a better transduction of energy. Secondly, at b) and c) all the points on the surface do not vibrate in a coherent way. These different modes of vibration could be used for different applications. Any other random frequencies such as d), or e) present a *pell-mell* distribution of vibration and should not be considered as high power ultrasound excitation due to the low displacements produced in the contact surface. The number of resonant frequencies and the complexity of the modes of vibration are even more complex when the transducers have a contact surface modification (see Sections 5.4.1 and 5.4.2).

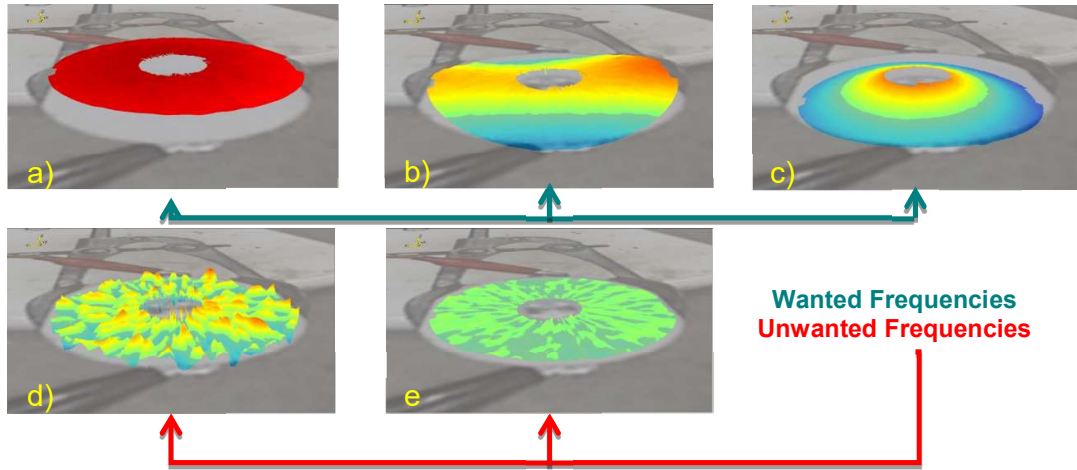


Figure 5.2. 1D⁴ Vibrometry analysis of the contact surface of a HPT. a) Shows the vibration at the main resonant frequency in which the entire contact surface is vibrating at the same phase. b) and c) illustrate resonant frequencies with different phase distribution that could be considered to be used depending on the application, d) and e) present the random vibration of the surface at those frequencies.

As evidenced in Figure 5.2, these other frequencies have a mode of vibration that could be not optimal for the high power ultrasonic excitation for the absence of a rhythmic vibration. Depending on the transducer design any other frequency different to the key resonant frequency can produce smaller displacements, may need higher voltages to be excited, and can have lower efficiency. Currently each commercially available transducer is sold with a specific frequency which delivers the largest power and displacement but in this thesis the analysis of other resonance frequencies is done to study the capabilities of HPT at those frequencies. The measurements of the actual displacement of the contact surface for HPT before and after modification are presented here.

5.2.1 Transducers Selection

As commented above, HPTs are devices that are operated at their key resonant frequency. At this frequency the HPT is supposed to produce larger displacements and generate the highest output powers. At any other resonant frequency the displacements and the total power output is supposed to be much lower.

Since there are no broadband high power transducers, some transducers with a narrowed, determined broadband have been selected for this investigation. Here four HPTs have been selected. These are HPTs used for classic ultrasonic cleaning with frequencies of 28, 40, 100 and 120 kHz. Table 5-1 shows the four pairs of transducers selected and their key specifications.

⁴ It is considered 1D vibration in the case presented at Figure 5.2, because the measurements were done with one laser beam and therefore only one direction of vibration can be measured and presented.

Table 5-1. Transducers selection for the feasibility study of use of ultrasonic waves for the removal of fouling from pipelines. The transducers were manufactured by HESENTEC in China. Highlighted with grey the transducers presented in this chapter.

Transducer Group	Material	Power	Nomenclature	Resonance Frequency
T21-T23	Stainless Steel	50W	T21 T23	40kHz
T31-T36	Stainless Steel	60W	T31 T33	100kHz
T41-T43	Stainless Steel	60W	T41 T43	28kHz
T51-T53	Stainless Steel	80W	T51 T53	120kHz

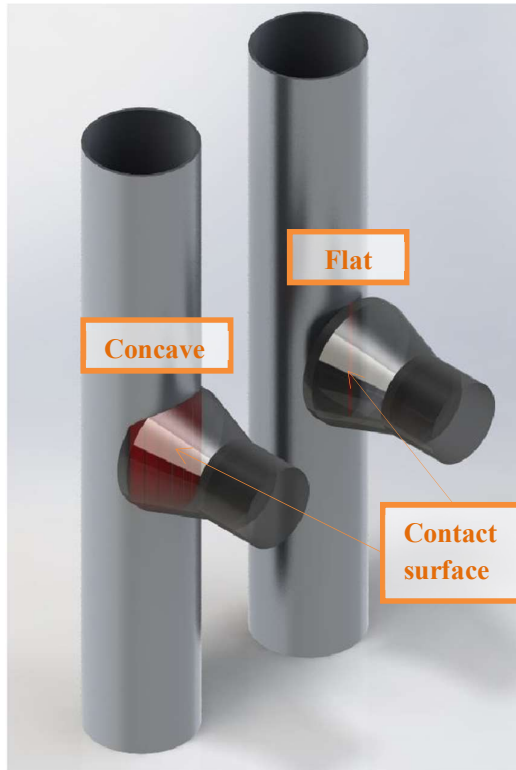
Table 5-1 presents the transducers selected for the investigation. The nomenclature applied is arbitrary. The naming system consists of the letter 'T' to indicate the object is a transducer. Then the first number assigned refers to a group of transducers which are identical. For instance, T2 is a stainless steel transducer which operates using 50W at 40 kHz in comparison to T3 which is a stainless steel transducer which operates at 100 kHz using 60W. An increase on the first digit indicates an increase in the power consumption of the transducer. The second number used for naming the transducer is indicative of the unique identifier from the batch that has been manufactured. For example, T21, T22 and T23 are identical transducers which indicate a quantity of 3 has been purchased.

5.2.2 Transducers Modification

Existing commercial transducers have a flat contact surface, Figure 5.1, hence a line contact would be the only interaction between a commercial transducer and the pipe after being attached together. This will result in a low energy transmission, Figure 5.3. Therefore, a modification of the existing transducers is proposed here in order to increase the contact surface and hence the transduction of energy.

The modification of the transducer is done to match the fouled pipes generated in Chapter 3 that will be used for the fouling removal investigation (Chapter 7). The specifications of the pipes can be found in Chapter 3.

Figure 5.3. Schematic illustration of the contact surface of a flat and concave transducer.



This modification of the existing HPT facilitates the attachment to the pipes and also increases the amount of energy transfer to the pipe by increasing the contact surface. Figure 5.3 evidences the difference in the contact surface of a plane and a concave transducer. Figure 5.3 above shows the drawings of a classic HPT transducer modified to have a concave surface. Figure 5.4 shows one of the selected transducers after machining. It is important so see that the contact surface (Figure 5.4) has a threaded hole which is the most common method for HPT attachment to flat surfaces [173]. The attachment methods and the couplants used in this thesis are explained in Section (5.2.3), and Figure 5.5 presents the detailed dimensions after cutting.

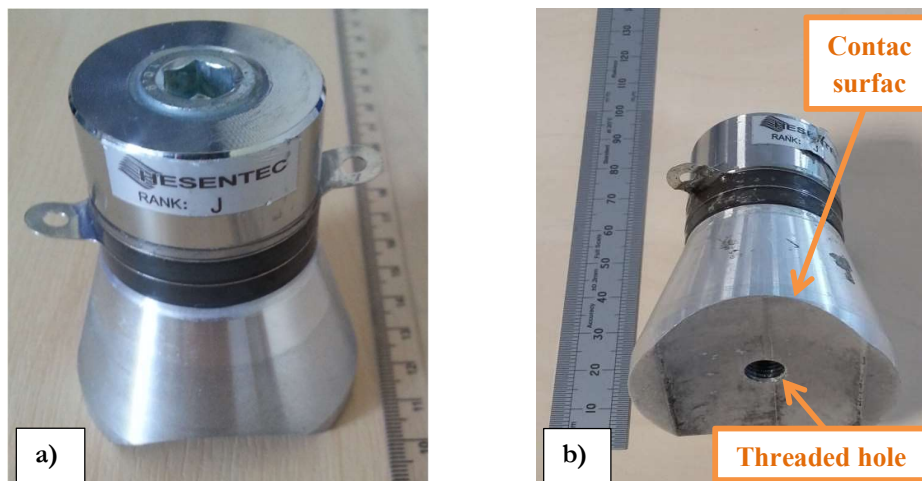


Figure 5.4. Transducers under analysis, a) T43 transducer with concave surface, b) contact surface of T43.

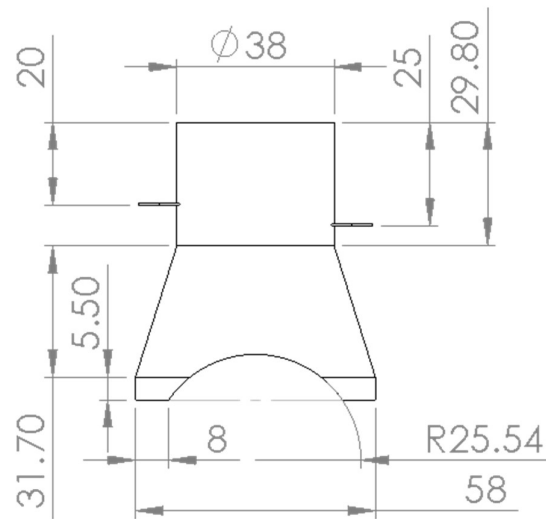


Figure 5.5. Detailed dimensions of transducer T43 machined to fit on pipe of external radius of 25.54mm.

Machining method

The technique used for cutting the transducers is Electrical Discharge Machining (EDM). Although mechanism of material erosion in EDM is still arguable, it is accepted that the principle is the conversion of electrical energy into thermal energy through a series of separated electrical discharges taking place between the electrode and the work piece immersed in a dielectric fluid [174]. This increment of the temperature can gradually remove matter from the surface.

5.2.3 Attachment method and couplants

In classic ultrasonic cleaning the most common method used for the attachment is by bolt welded on the plate to be excited and on it the HPT is both bolt clamped and glued to the surface to improve the acoustic energy transduction. That is why HPT have a thread hole (Figure 5.4.). The most common glue is a dual component Epoxy resin.

In this thesis the attachment method is different. Here the transducers are attached to the pipes using a ratchet strap or the collar designed (APPENDIX A) during the project UltraCleanPipe (see Section 1.1). To improve the acoustic energy transduced to the pipe two types of couplants are used in all cases:

- Ultrasonic couplant gel “Sonotech Soundsafe”
- Low acoustic attenuation couplant silicone.

5.3 Transducer Analysis Techniques

The modification applied to the HPTs is expected to change their properties. Two different techniques are proposed for the characterisation of the modified transducers: Electrical Impedance Analysis and Vibration Analysis.

5.3.1 Electrical Impedance Analysis

In order to calculate the resonant frequencies of the transducers before and after machining an impedance analysis is performed for each transducer.

Electrical impedance is the measurement of the opposition that a circuit presents to the passage of a current when a voltage is applied. Similarly, mechanical impedance is a measure of how much a structure resists motion when subjected to a harmonic force.

Subsequently, if a transducer is a device that can convert electrical energy to mechanical energy and vice versa, an electrical impedance analysis can give also the mechanical impedance of a mechanical structure with a transducer attached. The minima in impedance will occur when the energy travels more easily in the mechanical system under study, and that happens at the natural or resonant frequencies.

Therefore, impedance analysis can be used as one of the methods to find the resonant frequencies of an HPT. At these resonant frequencies the displacement will be much higher than at other frequencies and so will be the power output. These frequencies are the ones that should be excited following the explanation given in 5.2.

Piezoelectric transducers have complex input impedance and this impedance affects their driving response, bandwidth, sensitivity and power output. It is therefore convenient to approximate the ultrasonic transducer by an electrical model. Figure 5.6 presents the representative circuit of a transducer [175].

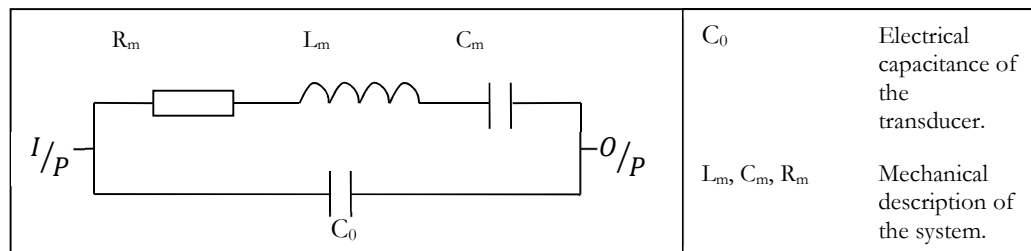


Figure 5.6. Representative circuit of a HPT.

All transducers behave as a circuit and, depending on the frequency applied, the reactance and inductance change in value. Both the capacitance and the inductance determinate the imaginary factor of the impedance and consequently the mechanical power output.

$$Z = R + jX, \tag{5.1}$$

Where Z is the impedance, R is the resistivity, or the real part, and jX is the reactance, or the imaginary part.

Impedance analysis provides information on the minimum impedance which occurs when the phase between the voltage and the current change from -90 to 90 degrees. In this condition the nature of the circuit changes from inductive to capacitive, therefore the imaginary part undergoes an important change from negative to positive and it is zero at the resonant frequency [175]. The real part of the impedance, the resistance, is close to zero at the first minimum [176], thus converting most of the electrical energy to mechanical energy and giving the transducer the biggest power output.

Impedance analysis set-up

The following equipment was used for the experiments:

- Impedance analyser: Agilent 429A Precision Impedance Analyser.
- High power piezoelectric transducers, T41 and T43.
- BNC Cables.
- Laptop.

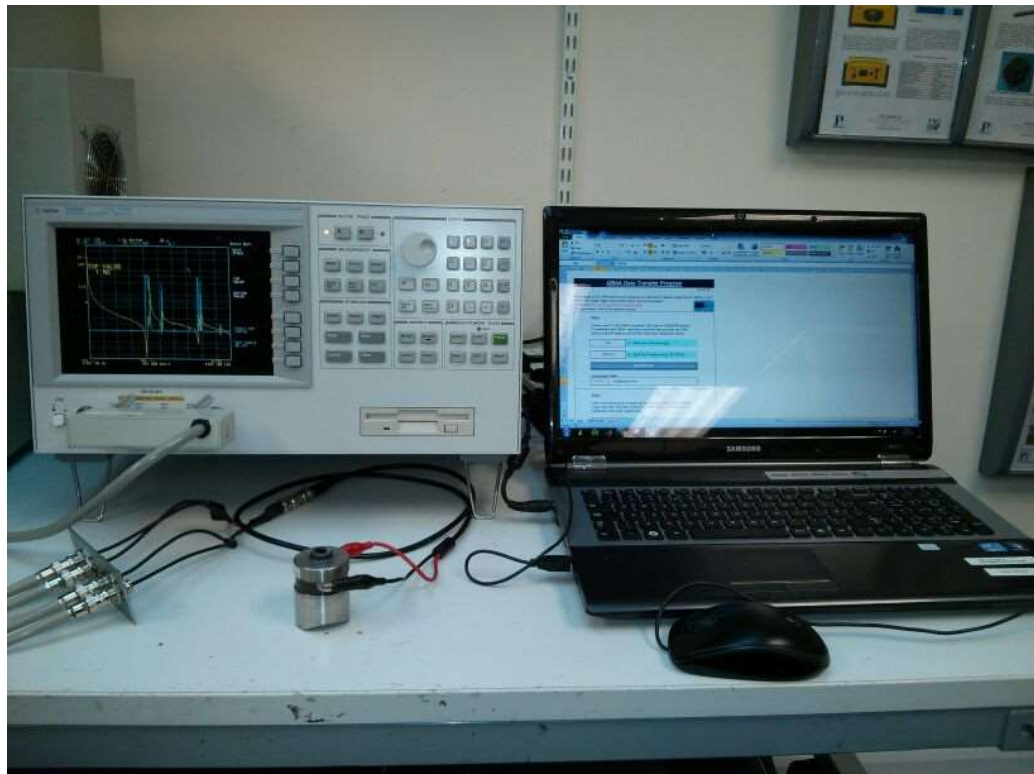


Figure 5.7. Impedance analysis setup for one single transducer.

Electrical Impedance analysis procedure

The piezoelectric transducers were connected to an impedance analyser. This impedance analyser generated a frequency sweep between 1 and 100 kHz with a constant voltage. It measured the impedance, transmittance and phase of the circuit at each frequency, the results for which are given in Section 5.4.1.

For each experiment an auto calibration of the circuit used for the measurement was performed to compensate the electrical impedance of the cables.

5.3.2 3D Scanning Vibrometer Analysis

Another technique to calculate the resonant frequencies of a HPT is the vibratory analysis performed with the 3D Scanning Vibrometer laser 3DSV (Polytec, PSV-500-3D-V Scanning Vibrometer VHF, Appendix B). It measures the variation of the velocity of a number of points on the surface under analysis. With three laser beams projected on the sample it can measure the changes produced in the frequency of the light beams reflected back to the vibrometer heads due to the Doppler Effect. Then, processing the signal acquired by each head it can give the velocity of each point under analysis (x, y and z). The vibrometer can also calculate by interpolation of the actual movement of the surface and plot the results in a 3D video or image at any moment in time. It has an accuracy of 2nm and the laser beams have a frequency of 4×10^{14} Hz. This accuracy represents an error of less than the 0.04% of the displacement calculated in Chapter 4 for the transient cavitation threshold and thus, the accuracy of the 3DSV is well above that required.

Other data such as the FFT (Fast Fourier Transform) of each point or the average FFT of the surface can be produced, having as amplitude the displacement and the acceleration, in addition to the velocity. In this thesis the FFT plots with the average of the entire surface and single point displacements will be used to analyse the vibration of the HPT before and after being machined. Later, in Chapter 7, it will be used to measure the displacement of the outside wall of the pipes subjected to the cleaning procedure.

3D Scanning Vibrometer Setup

The following equipment was used for the experimentation:

- Laser Scanning Vibrometer 3DSV.
- High power piezoelectric transducers.
- BNC Cables.
- Arbitrary signal generator.
- E&I 1040L power amplifier.

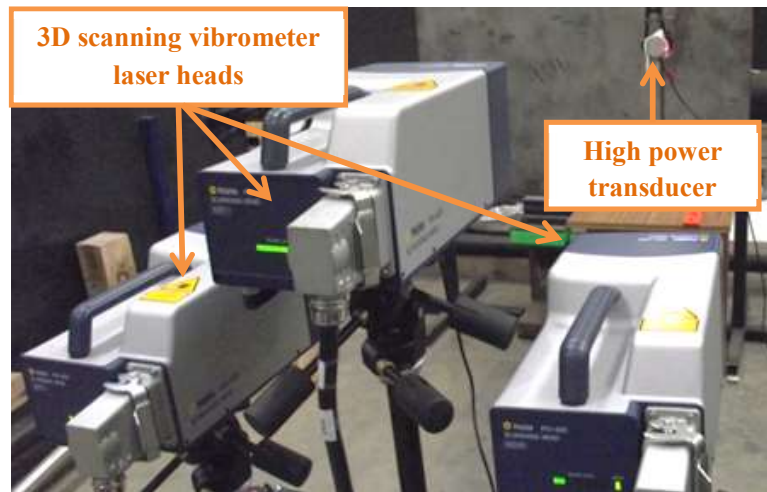


Figure 5.8. 3D scanning vibrometer setup for the analysis of one HPT vibration.

3D Scanning Vibrometer Procedure

For the experimentation, the vibrometer heads are placed forming an equilateral triangle with the plane containing the triangle facing the samples. Then the object under analysis is placed $99 \text{ mm} + n204 \text{ mm}$ (specified by the supplier) from the centre of equilateral triangle where n is a natural number ($n=1, 2, 3\dots$) Figure 5.9.

For this experimentation an HPT is attached to a clamp with the contact surface facing the centre of the equilateral triangle. In this case at 1527 mm (equivalent to $n = 7$). Then, the 3DSV is calibrated to consider the contact surface of the HPT the $x - y$ plane, with the normal vector to the surface \hat{k} (unit vector of Z axis). The out-of-the-plane displacements produced by transducers will be along the "z" axis and the in-plane displacements of the transducer will be along the "x" and "y" axes. This is calibrated by a 2D and 3D alignment of the 3DSV.

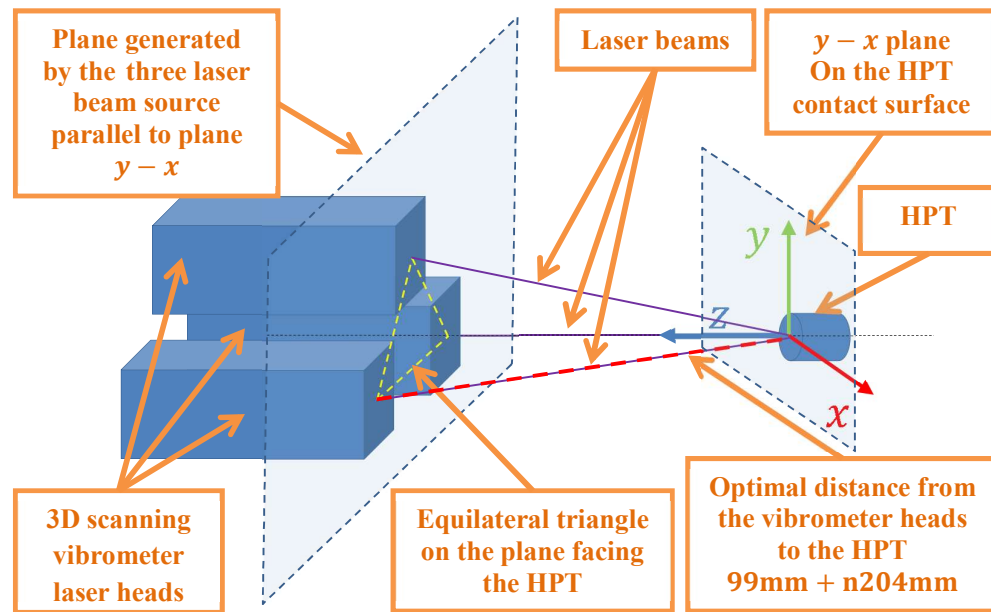


Figure 5.9. Schematic representation of the relative location of the three heads of the 3DSV and the contact surface of a HPT submitted to a Vibrometry analysis

Finally, prior to the experimentation, the number of points in the scanning area are determined. The number of points generally depends on the wavelength of the wave excited in the sample but in the case of the contact surface of an HPT a different approach is needed. Figure 5.2 showed how an HPT can have a rhythm distribution of displacement and with the same phase in the entire scanning area. This would therefore need fewer points to characterise the actual vibration. Otherwise, it would be expected to have a larger wavelength distribution for lower frequencies but, as was presented in Figure 5.2, any frequency different to a resonant frequency can vibrate with a disordered distribution and with “infinite number of phases”. Therefore, high density point areas are applied to understand the mode of vibration of each frequency. In this experimentation a density of 20 points per square centimetre is applied.

Once the 3DSV is ready, the HPT is connected with a BNC (Bayonet Neill–Concelman) cable to a power amplifier which applies 55dB of amplification to the signal. The signal is generated by the 3DSV signal generator. Depending on the type of analysis different types of signals are generated. Here, three different types of signal are applied:

- a) A frequency sweep between 20 and 150 kHz to find the resonant frequencies. The aim of these experiments is to find the resonant frequencies and to analyse the mode of vibration at the most important ones.
- b) A sinusoidal wave at the resonant frequency with different voltage inputs.
- c) A square signal at the resonant frequency with the same voltage inputs.

Once everything is arranged, the experiments start. An internal trigger of the 3DSV coordinates the generation of the signal to the HPT and the measurements of the motion of its surface. An average of 50 collections is done per point location.

5.4 Transducer Analysis Results

In order to characterize the modified HPTs two types of analyses have been proposed (Impedance Analysis and Vibration Analysis) that will provide information on the resultant resonant frequencies, modes of vibration and displacement in the 3D directions.

5.4.1 Resonant Frequencies

To find the resonant frequencies of the HPTs, impedance analysis is the most common practice, here a vibrometer analysis is also applied for further investigation of the actual motion of the contact surface of the transducers.

Impedance Analysis

Based on the opposition of the current to flow in an electrical circuit an impedance analyser can find the resonant frequencies where the opposition is at its minimum. Figure 5.10 and Figure 5.11 present the impedance analysis of the two original HPTs, before the machining method. It can be seen that the key resonant frequencies can be found at 38.2 kHz and 38.36 respectively. As commented in 5.2, more than one resonant frequency can be found in a single HPT observed at each minimum in the impedance analysis. Also, disordered behaviours can be found in any other random frequency. Therefore, five frequencies have been selected for the analysis. These frequencies are presented in Table 5-2. They are a representative selection of resonant and non-resonant frequencies, being these a), c) and d) resonant, and b) and e) two random frequencies.

Table 5-2. Representative frequencies selected for the analysis.

	Manufacturer specifications		T41 Flat		T43 Flat		T43 Concave	
	Frequency (kHz)	Impedance (Ω)	Frequency (kHz)	Impedance (Ω)	Frequency (kHz)	Impedance (Ω)	Frequency (kHz)	Impedance (Ω)
1)	28 \pm 0.5	\lesssim 20	28.45	19.99	28.61	59.05	33.00	54.19
2)	<i>unspecified</i>	<i>unspecified</i>	39.66	934.10	39.83	896.80	40.15	1067.00
3)	<i>unspecified</i>	<i>unspecified</i>	46.00	97.48	46.65	57.00	45.35	86.54
4)	<i>unspecified</i>	<i>unspecified</i>	84.84	16.29	85.33	7.21	88.09	28.84
5)	<i>unspecified</i>	<i>unspecified</i>	100,30	499.50	100.1	462.9	99.95	501.1

Table 5-2 presents the values of the frequencies at resonance of T41 and T43 before and after the cut and the value provided by the supplier. The difference presented between the transducers of the same type is reasonably consistent. In case of T43 before and after the machining process, it can be seen a sweep to a higher frequency except for frequency 3). This can be due to the change of the mode of vibration (see Section 5.4.2).

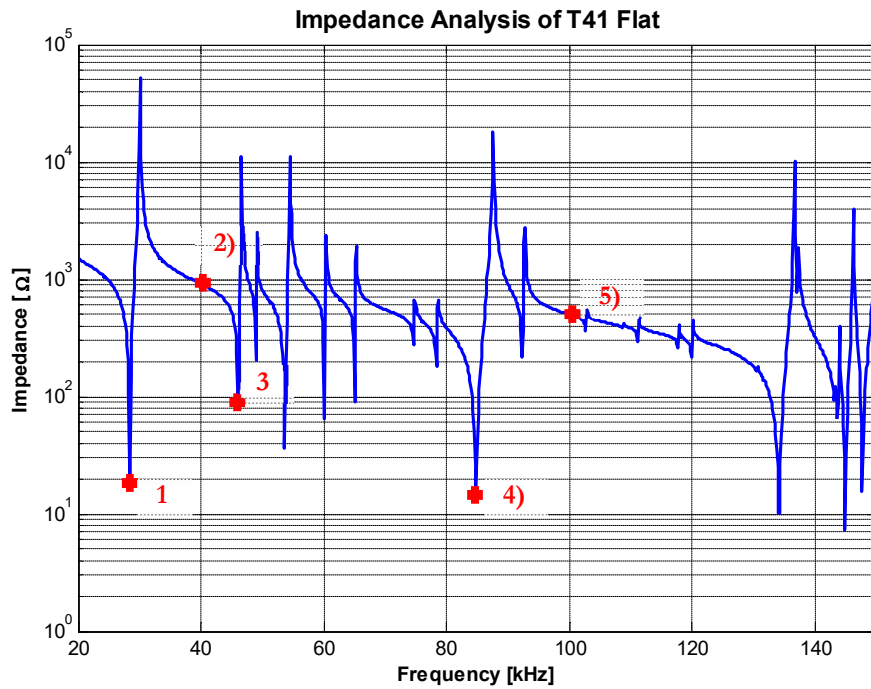


Figure 5.10. Impedance analysis of T41 HPT. The frequencies under analysis are marked.

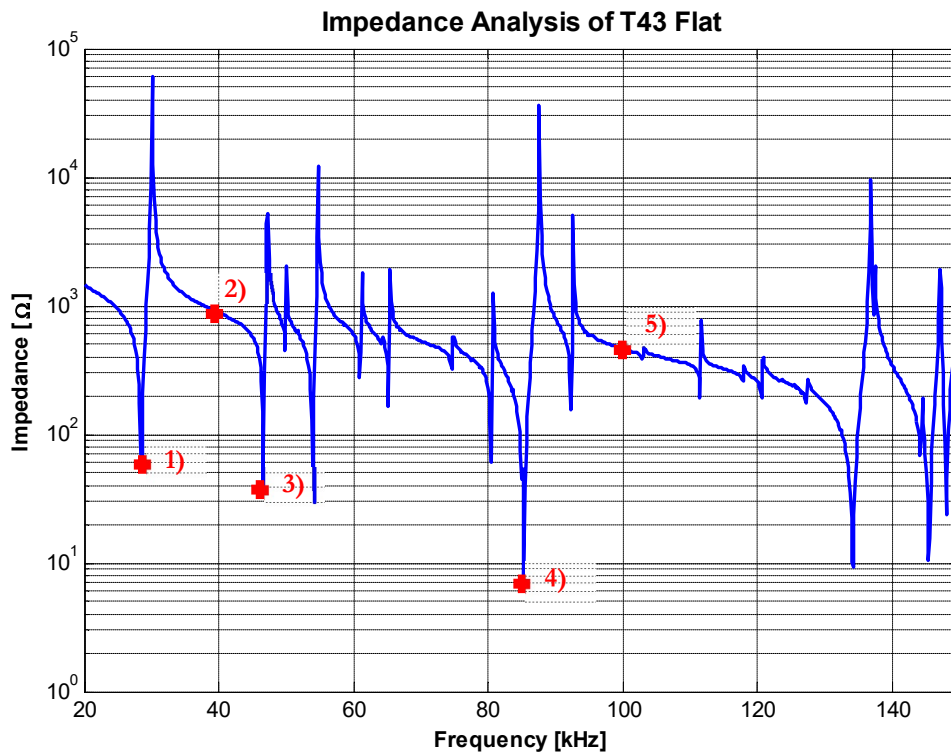


Figure 5.11. Impedance analysis of T43 HPT prior to the machining method.

After machining, as Figure 5.12 and Figure 5.13 present, the resonant frequencies of T43 are shifted to higher frequencies. Also, the impedance at resonant frequencies has changed to higher

values. This means that the dissipation of energy due to a change in the geometry has increased and therefore more voltage is needed for the excitation.

Another result of the modification of the transducer geometry is the occurrence of new modes of vibration. In case of a HPT transducer with a concave surface a larger number of modes are generated since the contact surface has now larger number of degrees of freedom. Thus, T43 concave presents at least 20 resonant frequencies in contrast with the T41 and T43 flat which have only 10 in the frequency range between 20 kHz and 150 kHz. Therefore, a vibration analysis is needed for a better understanding of each transducer characteristics.

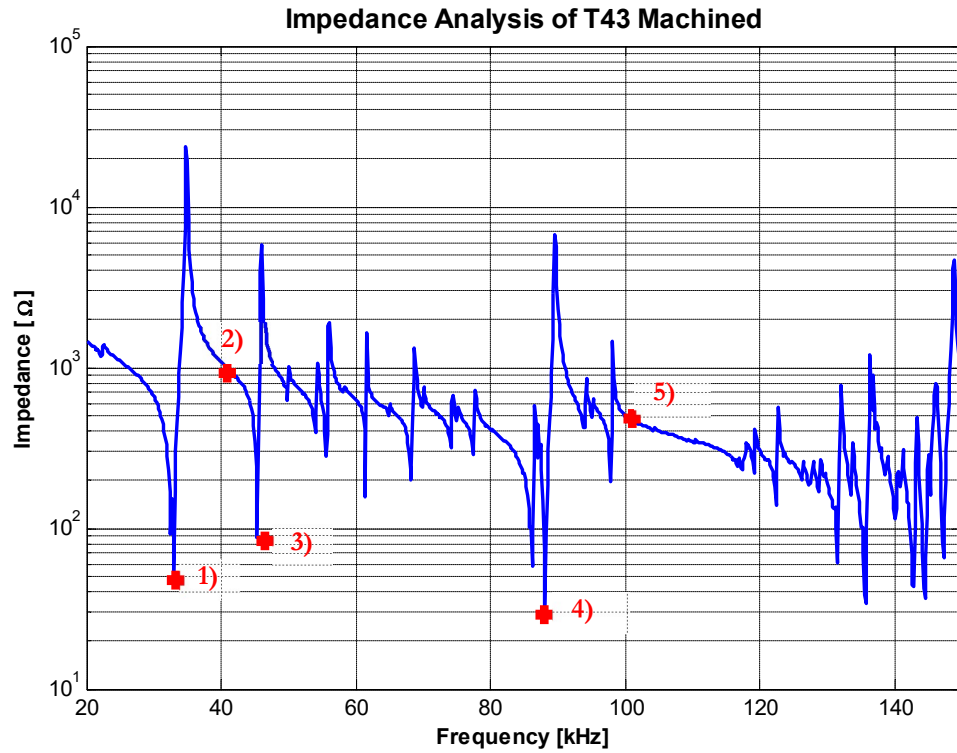


Figure 5.12. Impedance of T43 with a concave surface after being machined.

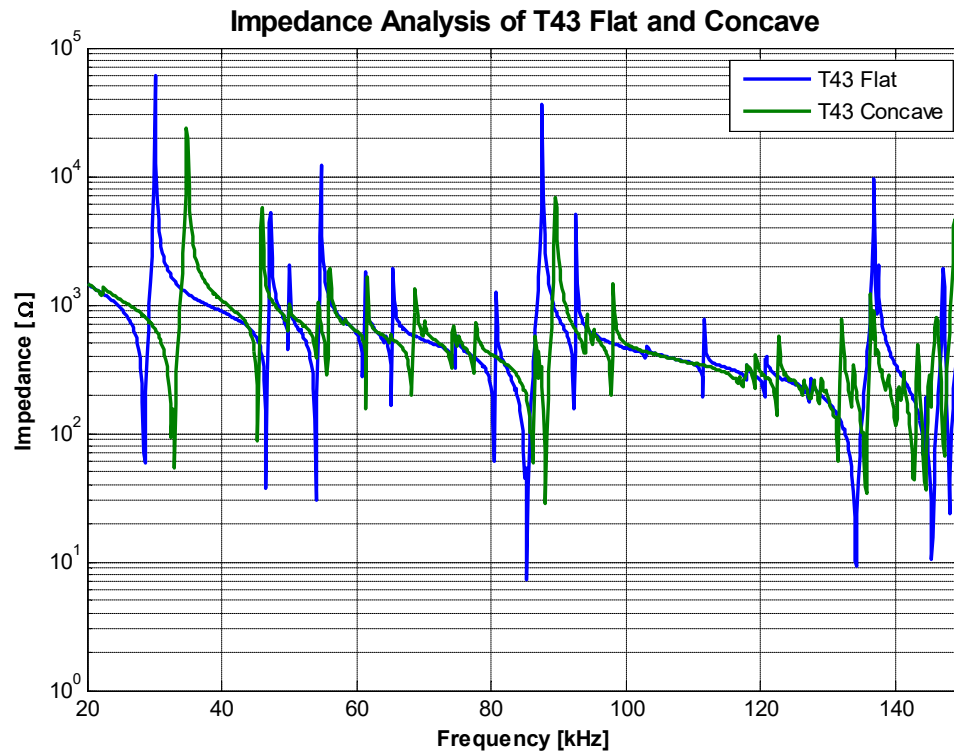


Figure 5.13. Impedance Analysis Comparison of T43 Transducer before and after being machined.

3D Scanning Vibrometer Analysis

Following the previous discussion, parameters such as the displacement and modes of vibration cannot be determined by the previous analysis. To obtain these parameters the first step is to use the 3DSV for FFT analysis.

Since the following explanations consider the oscillations in the three-dimensional space directions, an illustration of the axes location with regards to the contact surface of the HPT under analysis is needed. Figure 5.14 presents the visualization of the displacement of the contact surface, the origin of the surface and the image of the contact surface of the HPT in the back and the 3D axes orientation. The orientation of the axes related to the vibrometer heads is presented in Figure 5.9.

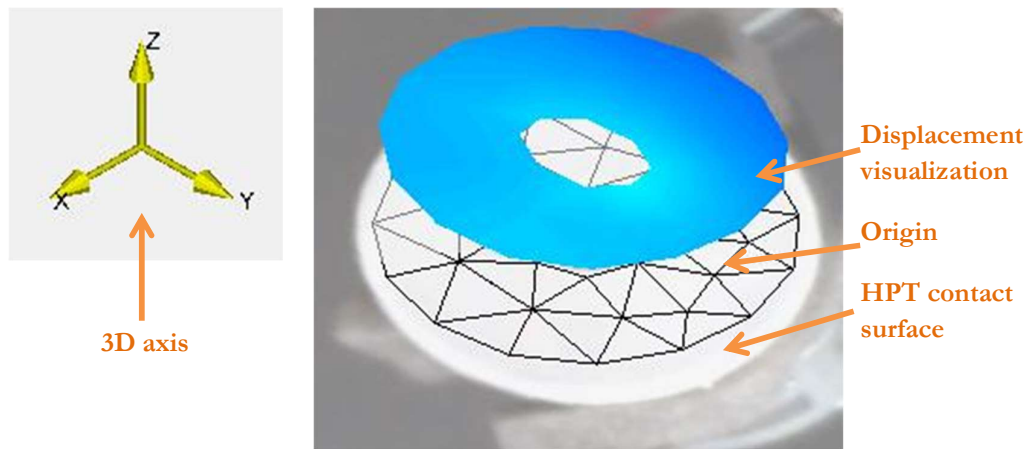


Figure 5.14. Axis orientation, origin and contact surface of a HPT under the 3DSV analysis.

Each frequency presented in Table 5-2 can now be analysed in terms of the displacement of the contact surface. Figure 5.15 presents the average displacement of each frequency for the three-dimensional space directions. As it can be seen, the displacement has different values for each direction at each frequency. For example, for T41 the first resonant frequency, 1), presents the larger displacement in the “Z” direction normal to the contact surface, which is the displacement presented in Figure 5.14. This would generate a compressional wave in the “Z” direction. The second frequency under analysis, 2), has a very low displacement. 3), results in large displacements in “X” and “Y” direction and lower in “Z”. 4) has an even distribution of displacements and finally 5), as 2), has negligible displacement in comparison with the other three. The visualization of the contact surface at all the 5 frequencies is presented in 5.4.2.

It is important to highlight that a) is the only resonant frequency that has predominant displacement in the “Z” direction in addition to be the one with the larger value for the displacement. It is expected to be the most suitable to produce acoustic cavitation, as explained in Chapter 4.

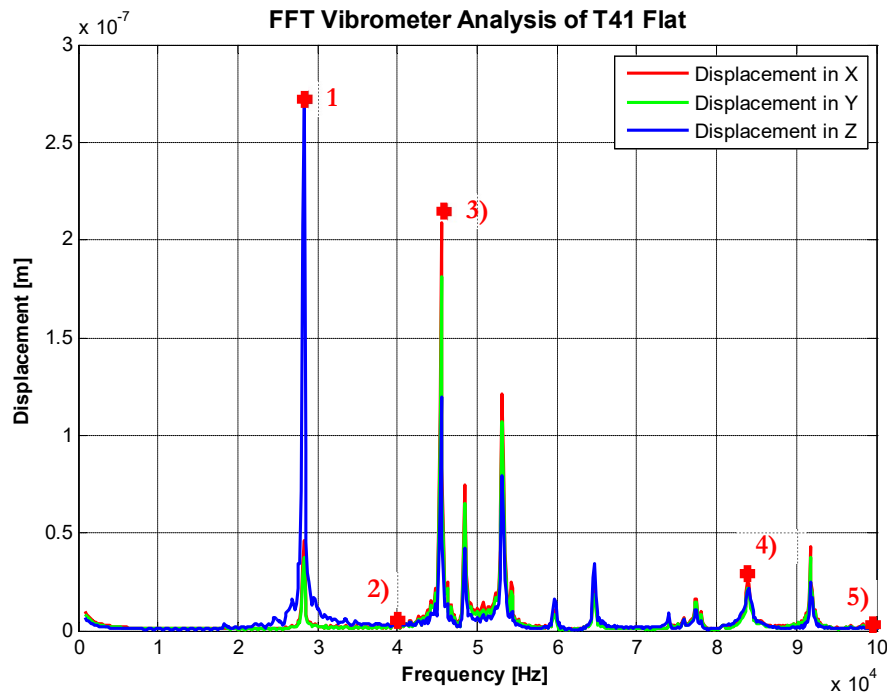


Figure 5.15. Displacement measurement per frequency of the transducer T41 with the vibrometer.

It is interesting to compare the two frequency analyses by plotting both of them in the same graph. Figure 5.16, presents the impedance analysis and the FFT vibrometer analysis of T41. It can be seen that each minimum in the impedance analysis has a corresponding maximum in the vibrometer analysis. Moreover, it is important to realise that the values of the impedance have no relation with the actual displacement and therefore it is not possible to know, just with an impedance analysis, if a resonant mode would produce enough displacement for some applications. For example, one of the resonant frequencies under analysis, 4), has a sharp minimum in the impedance but it produces small displacements.

Comparison between Impedance and Vibrometer Analysis of T41 Flat

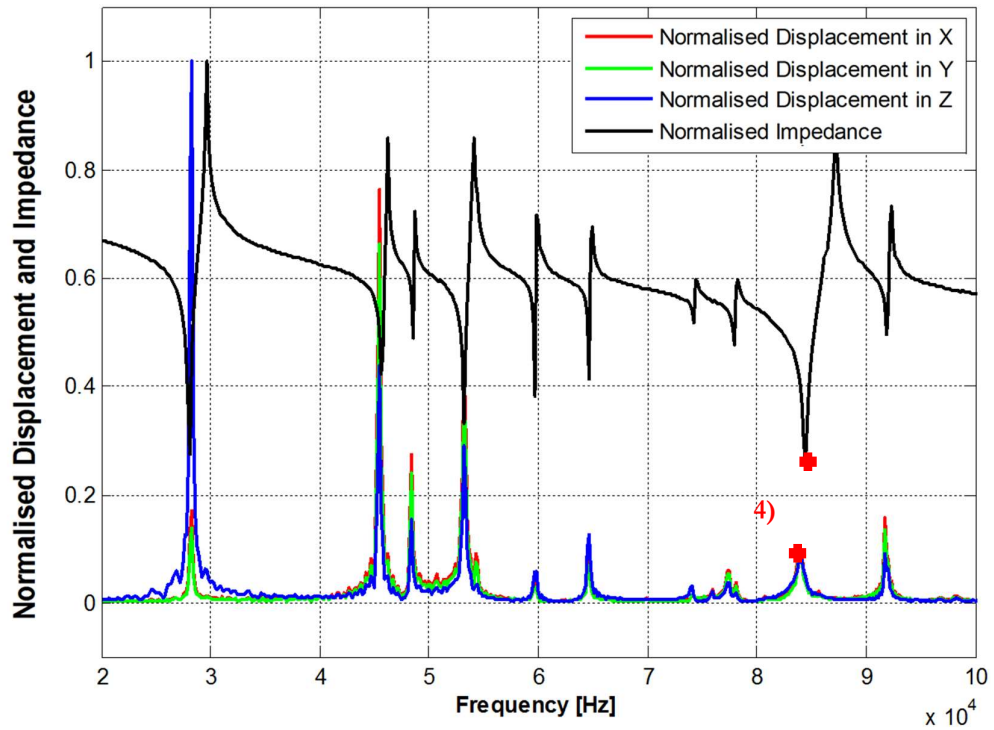


Figure 5.16. Comparison between the frequency analysis of the impedance analysis and the 3DSV for T41.

For an HPT with a concave surface the axes were configured as presented in Figure 5.17. It is important to note that the origin now has a concave shape in the same way that the contact surface of the HPT does. In this case the “Z” axes would be in the radial direction of the pipe with the HPT attached.

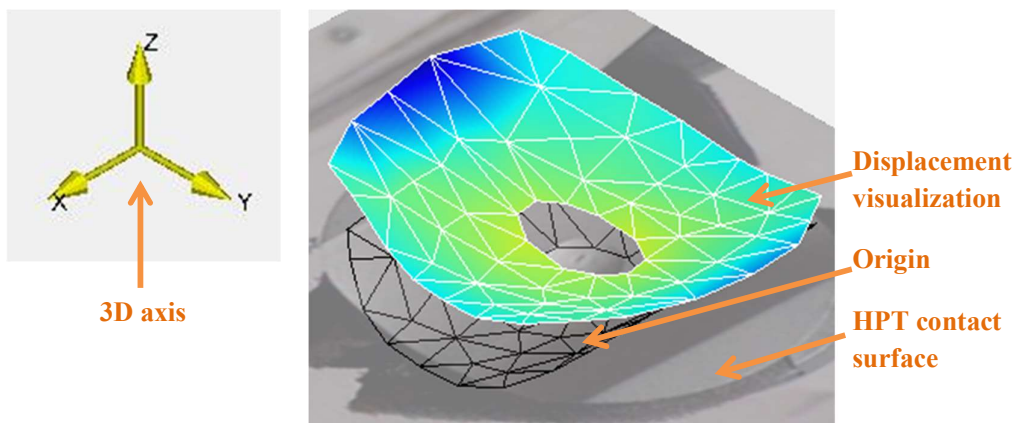


Figure 5.17. Axis orientation, origin and contact surface of a concave HPT under the 3DSV analysis.

Then, performing an FFT analysis on a T43 concave, the results yield as follow.

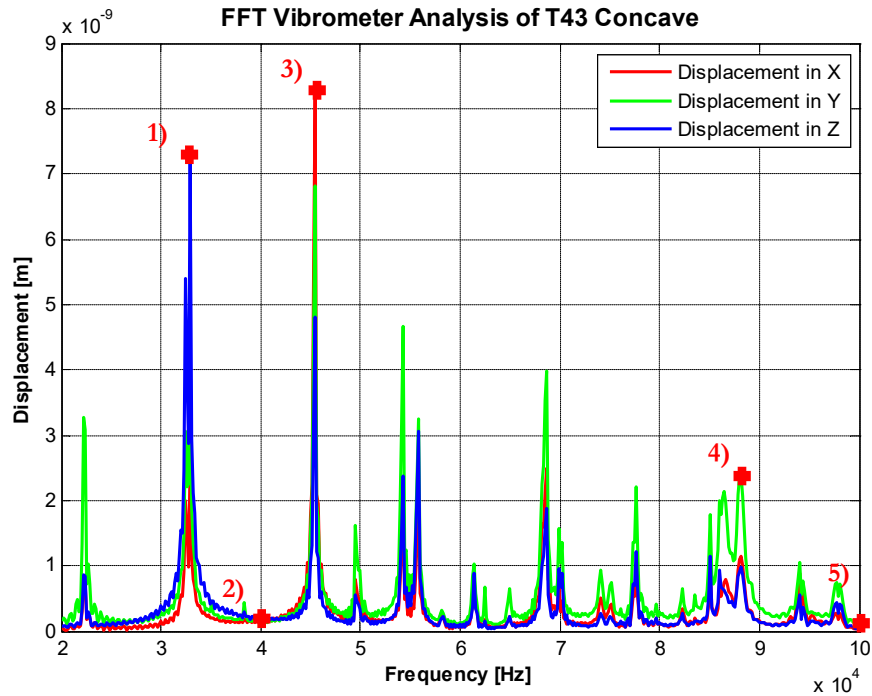


Figure 5.18. Displacement measurement per frequency of the transducer T43 concave with the 3DSV.

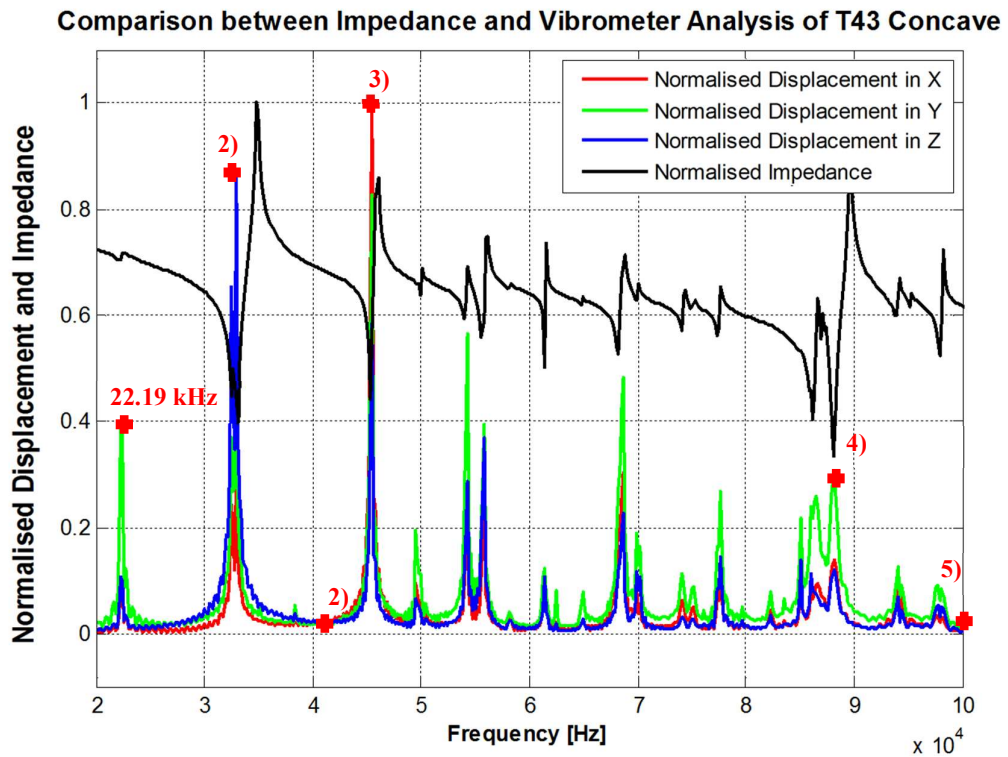


Figure 5.19. Frequency analysis comparison between the impedance and FFT vibrometer analysis for T43 concave.

In contrast with T41 flat, T43 concave presents higher displacements in the “Y” direction in the majority of the resonant frequencies but not in the resonant frequency 1) which has shifted to

30.00 kHz presents again larger displacements in the “Z” direction, Figure 5.18 and Figure 5.19. Frequency 2) presents low displacements in the three dimensional directions, frequency 3), in this case behaves with a larger displacement than frequency 1) but it is done in the “X” direction due to the mode of vibration generated (further analysis in Section 5.4.2). 4), has been divided in three different peaks with predominant displacement in the “Y” direction. Finally, 5), like 2), present low displacements in the three directions, as was expected since they are not resonant frequencies of the transducers. Therefore, these frequencies are not suitable for cleaning.

5.4.2 Modes of Vibration

These FFT analyses give the value of the average displacement of the contact surface of T41 and T43, but each point in the surface can have different displacements in the three axes depending on the wave mode produced at each frequency. Therefore, further analysis to know the 3D displacement is needed.

For the mode analysis it is necessary to define a number of points on the contact surface to facilitate understanding of the displacement and its direction during the vibration. Figure 5.20 presents the location of the points on the two transducers under analysis. The view is parallel to the “Z” axis and the orientation of “X” and “Y” is consistent in the remaining figures below for a better understanding. Also a set of four colours have been applied: blue (1, 2) for the two ends in the “Y” axis, red (3, 4) for the two ends in the “X” axis, orange (5, 6, 7, 8) in the two diagonals between “X” and “Y” axes, and green (9, 10, 11, 12) in the middle of the transducers. The following tables in this subchapter will have the same distribution of colours.

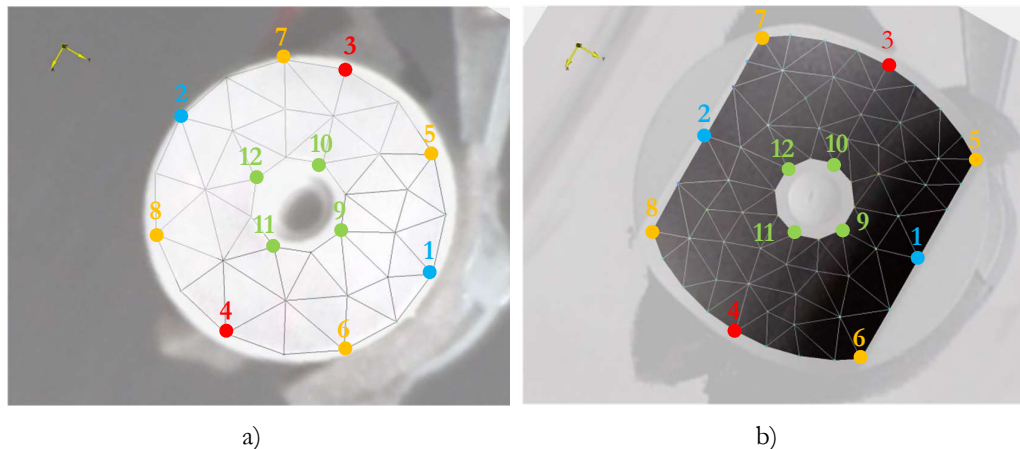


Figure 5.20. Points location on the two transducers surface for T41 a) and T43 b).

Solids can have different resonant frequencies depending on the material properties but also depending on its geometry. These resonant frequencies will vibrate at different modes. A mode of vibration can be defined as the characteristic manner in which a system oscillates with a certain characteristic and pattern of motion at one frequency.

The displacement found in the three space directions will be analysed for five different frequencies for transducers T41 and T43.

Frequency 1

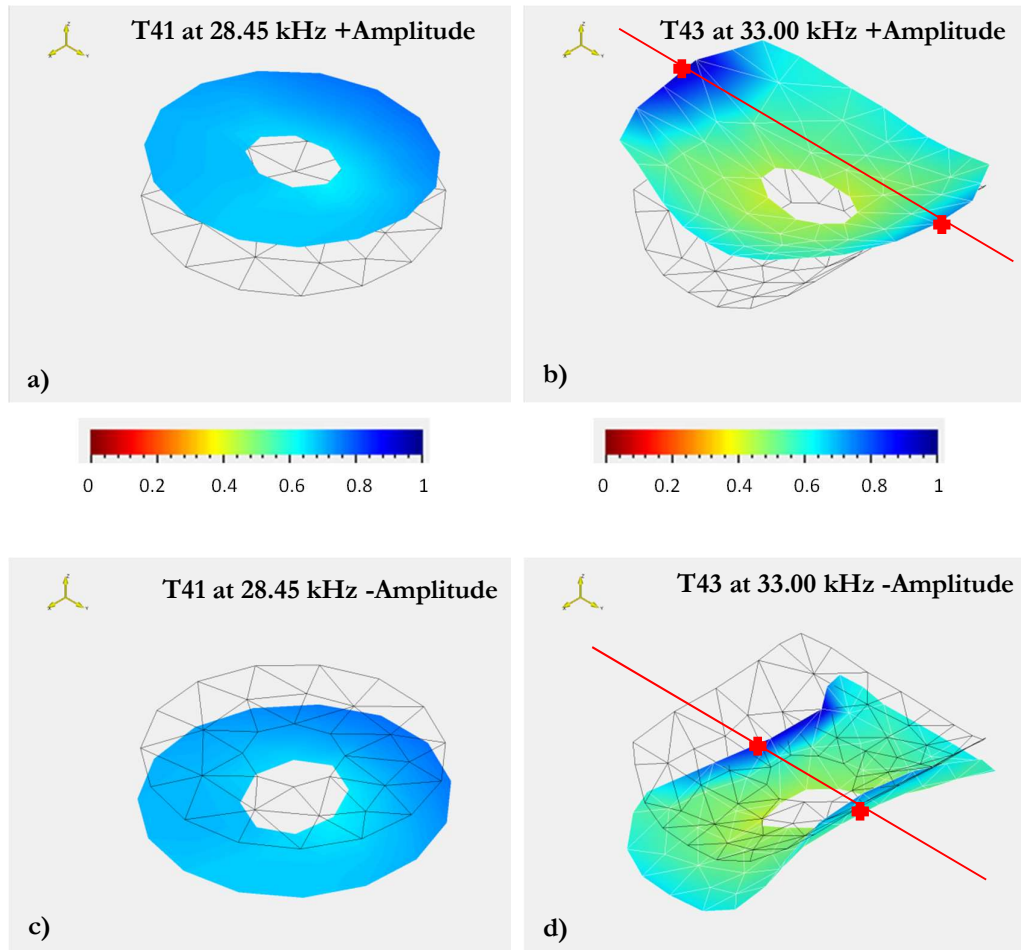


Figure 5.21. Mode of vibration analysis at the two opposite instants of maximum amplitude at resonant frequency 1 for T41 a) and c), and T43 b) and d).

Frequency 1 occurs at 28.45 kHz for T41 and 33.00 kHz for T43. The displacement is predominant in the “Z” direction for both T41 and T43, but T43 has also high displacements in the “Y” component. Figure 5.21 a) presents the displacement pattern of the contact surface of T41. As it can be seen, all the points of the surface vibrate at the same phase and with similar displacement in the three axes. Table 5-3 presents the normalized displacement of the surface. This evidences that the displacement is even in the “Z” direction for the all the points on surface. In contraposition it can be seen that the centre of the transducer has larger displacements in the “Y” direction (points 9 and 12) than in the “X” direction (10 and 11).

The analysis of T43 at frequency 1 evidences a different type of vibration. Here the largest displacement occurs on the two ends of the “Y” axis (points 1 and 2). This is in contraposition with the total average displacement which is larger in the “Z” direction (Figure 5.18). The

transducer is expanding at the highest amplitude and a contraction in the minimum amplitude, Figure 5.21.

The displacement in the “Y” direction may contribute to the generation of compressional waves in the radial direction, and therefore cavitation, inside of the pipe. This will be discussed in Chapter 7.

Table 5-3. Normalised displacement of T41 and T43 concave at resonant frequency 1 at the representative points under analysis.

Point on the surface	T41 28.45 kHz			T43 33.00 kHz		
	X	Y	Z	X	Y	Z
1 (28)	0,07	0,05	0,94	0,01	0,63	0,40
2 (21)	0,03	0,04	0,97	0,16	1,00	0,26
3 (34)	0,24	0,19	0,99	0,25	0,10	0,55
4 (6)	0,22	0,19	0,88	0,28	0,06	0,57
5 (2)	0,27	0,11	0,99	0,16	0,21	0,49
6 (11)	0,11	0,17	0,88	0,15	0,29	0,44
7 (18)	0,16	0,17	1,00	0,12	0,46	0,38
8 (13)	0,20	0,12	0,93	0,16	0,44	0,40
9 (23)	0,07	0,04	0,84	0,03	0,18	0,42
10 (30)	0,26	0,20	0,82	0,11	0,39	0,36
11 (24)	0,23	0,19	0,90	0,12	0,33	0,40
12 (25)	0,06	0,05	0,90	0,02	0,21	0,39

Frequency 2

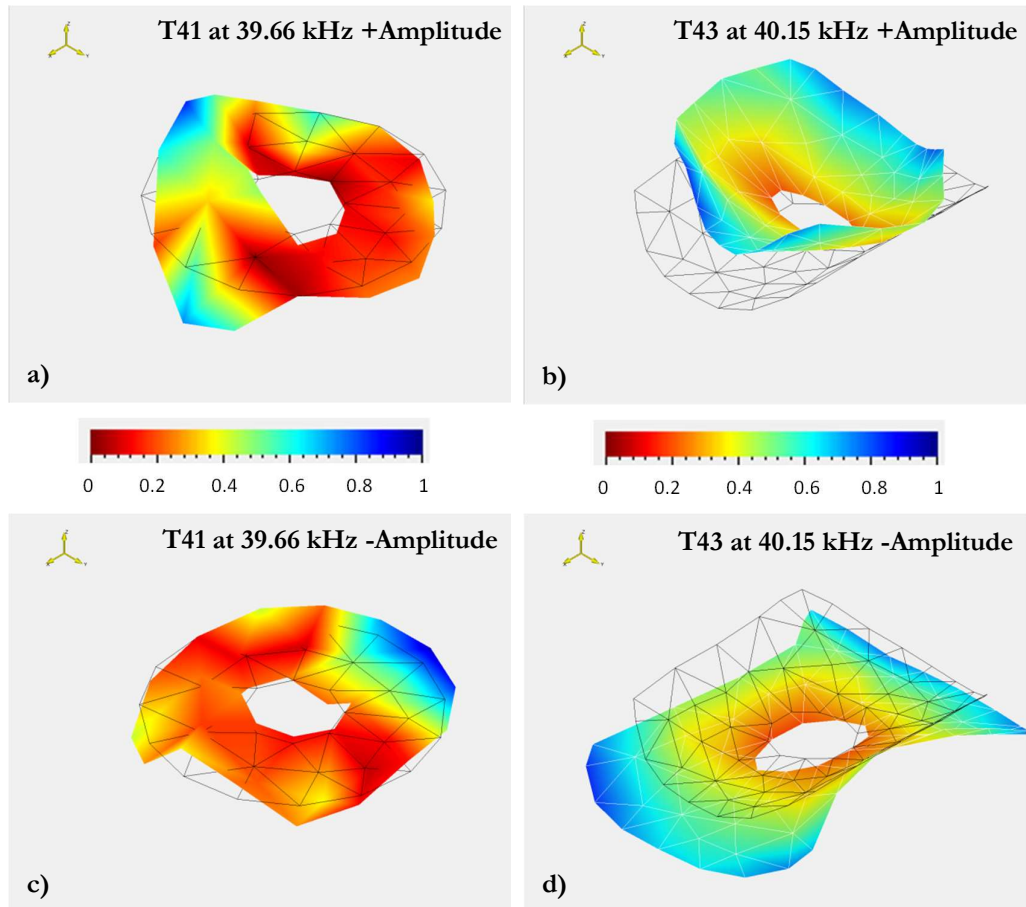


Figure 5.22. Mode of vibration analysis at the two opposite instants of maximum amplitude at resonant frequency 2 for T41 a) and c), and for T43 concave b) and d).

The second frequency under analysis, frequency 2), has been selected at 39.66 kHz in T41 and at 40.15 kHz in T43. This frequency presents a disorder distribution for T41 in the contact surface. This was expected since it is a non-resonant frequency. In contraposition, a rhythm vibration can be seen for T43 with large displacements in the corner of the transducers (points 5, 6, 7, 8) both in “Y” and “X” axes, Table 5-4. Even though, high displacements will not be expected at this frequency, Figure 5.19.

Table 5-4. Normalised displacement of T41 and T43 concave at resonant frequency 2 and at the representative points under analysis.

Point on the surface	T41 39.66 kHz			T43 40.15 kHz		
	X	Y	Z	X	Y	Z
1 (28)	0,27	0,07	0,62	0,03	0,96	0,47
2 (21)	0,16	0,16	0,83	0,17	0,86	0,32
3 (34)	0,77	0,71	0,51	0,69	0,16	0,87
4 (6)	0,85	0,75	1,00	0,70	0,19	0,87
5 (2)	0,83	0,50	0,49	0,64	0,73	0,91
6 (11)	0,44	0,57	0,81	0,60	0,63	0,91
7 (18)	0,51	0,63	0,64	0,58	1,00	0,94
8 (13)	0,70	0,40	0,98	0,77	0,51	0,99
9 (23)	0,16	0,14	0,15	0,13	0,33	0,27
10 (30)	0,87	0,74	0,08	0,39	0,32	0,23
11 (24)	0,76	0,77	0,43	0,43	0,39	0,29
12 (25)	0,23	0,16	0,32	0,09	0,26	0,25

Frequency 3

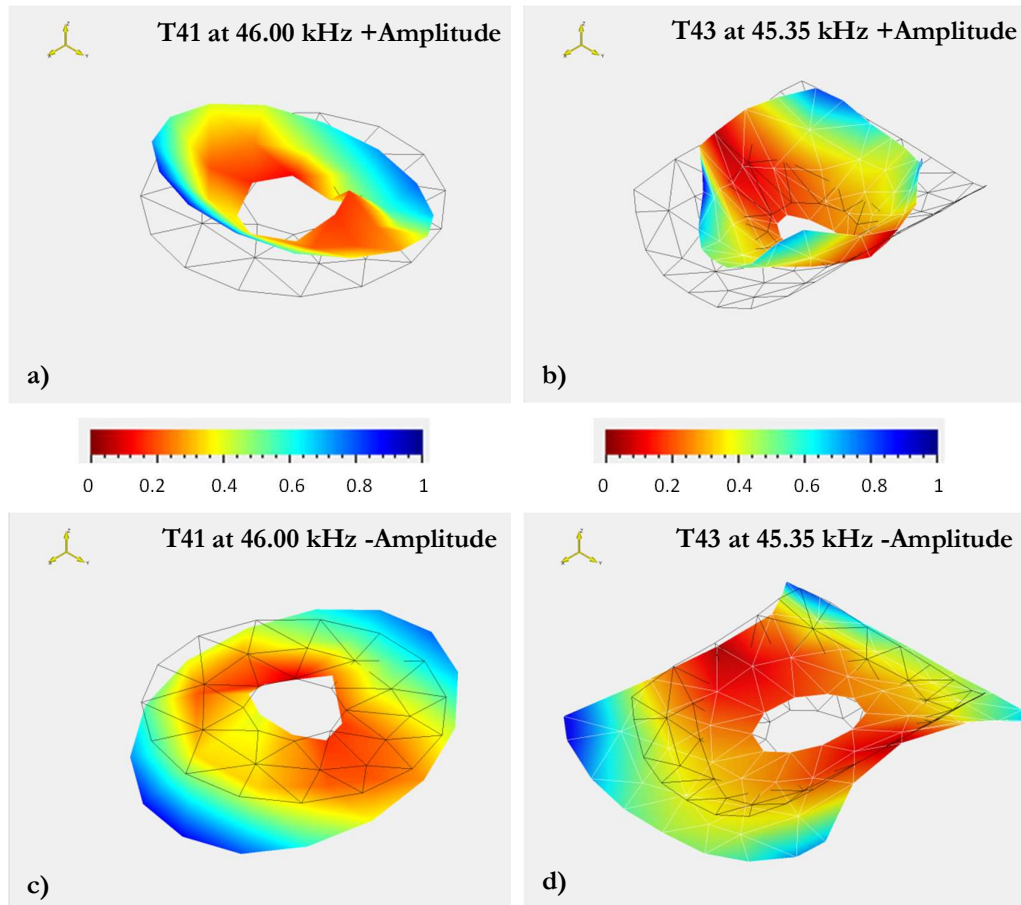


Figure 5.23. Mode of vibration analysis at the two opposite instants of maximum amplitude at resonant frequency 3 for T41 a) and c), and T43 concave b) and d).

In this case frequency 3 appears at 46.00 kHz for T41 and at 45.35 kHz for T43. In the two cases the transducers present a rhythmic vibration distribution since both are resonant frequencies.

For T41 the largest displacements occur in the “X” and “Y” directions at the two ends of the “X” axis (points 3 and 4). Table 5-5. In opposition the two points on the two ends of the “Y” axis present almost zero displacement in the three space directions.

For T43 the points located in the two ends of the “Y” axis present again almost no-displacement in the three space directions. The highest displacements can be found in the points located in the three corners of this transducer, being predominant in the “Y” axis and very similar and even in both “X” and “Z” directions.

Table 5-5. Normalised displacement of T41 and T43 concave at resonance frequency 3 at the representative points under analysis.

Point on the surface	T41 46.00 kHz			T43 45.35 kHz		
	X	Y	Z	X	Y	Z
1 (28)	0,25	0,09	0,42	0,03	0,20	0,01
2 (21)	0,18	0,19	0,68	0,03	0,12	0,01
3 (34)	0,94	0,88	0,25	0,41	0,08	0,28
4 (6)	1,00	0,90	0,80	0,44	0,08	0,35
5 (2)	0,99	0,62	0,20	0,51	0,95	0,35
6 (11)	0,50	0,67	0,63	0,43	0,72	0,37
7 (18)	0,57	0,71	0,37	0,47	0,99	0,52
8 (13)	0,87	0,53	0,83	0,59	1,00	0,53
9 (23)	0,18	0,12	0,32	0,09	0,12	0,21
10 (30)	0,98	0,87	0,50	0,27	0,12	0,22
11 (24)	0,90	0,80	0,04	0,32	0,15	0,20
12 (25)	0,28	0,09	0,06	0,06	0,06	0,22

Frequency 4

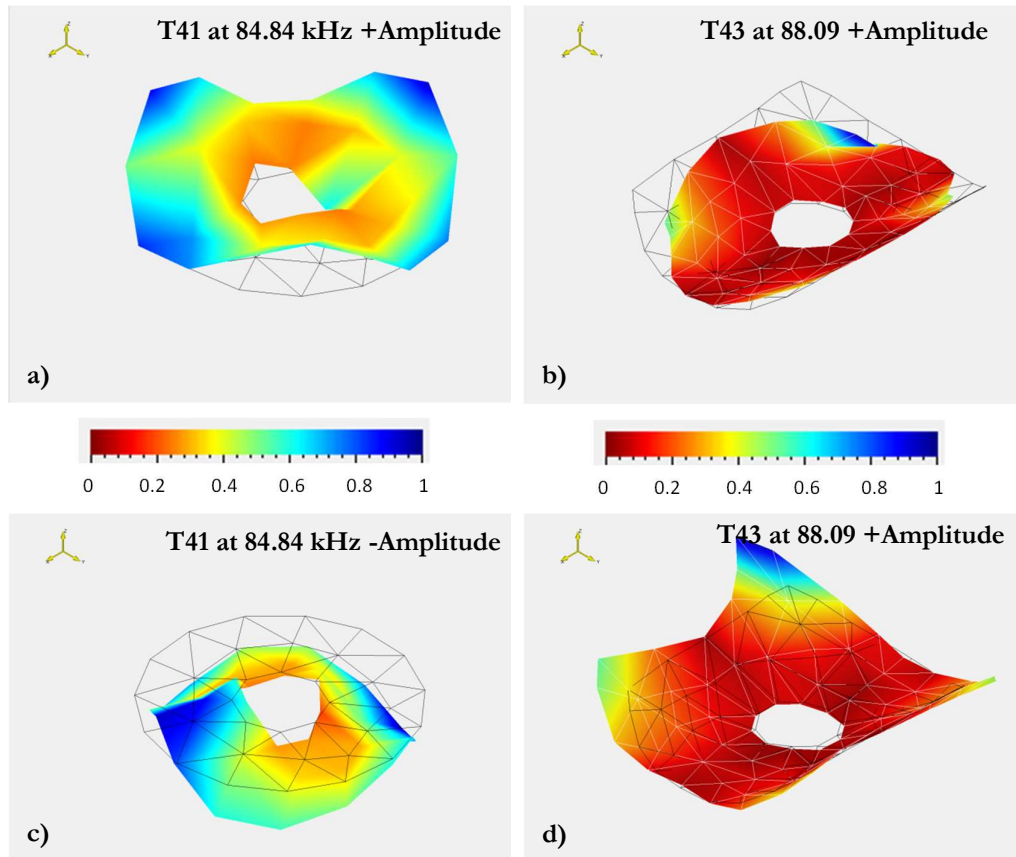


Figure 5.24. Mode of vibration analysis at the two opposite instants of maximum amplitude at resonant frequency 4 for T41 a) and c), and T43 concave b) and d).

Frequency 4 occurs at 88.84 kHz in T41 and at 88.09 kHz in T43. It is important to realise that frequency 4 has three different potential peaks in T43 and the one selected for the comparison is the peak with highest average displacement, Figure 5.18.

For T41 the vibration presents a rhythmic distribution but with different displacement patterns of vibration in the different representative points. It has the largest displacements in the middle points of the “X” axis (points 10 and 11). It can also be seen that the surface do not vibrates on a coherent way.

In case of T43 the surface presents low displacements in comparison with the corners of the transducer (points 5, 6, 7, 8). At these points the displacements occur mainly in the “Y” direction.

Table 5-6. Normalised displacement of T41 and T43 concave at resonance frequency 4 at the representative points under analysis.

Point on the surface	T41 84.84 kHz			T43 88.09 kHz		
	X	Y	Z	X	Y	Z
1 (28)	0,67	0,56	0,43	0,02	0,17	0,10
2 (21)	0,46	0,39	0,54	0,03	0,17	0,07
3 (34)	0,29	0,44	0,58	0,15	0,09	0,05
4 (6)	0,53	0,60	0,45	0,12	0,02	0,03
5 (2)	0,34	0,46	0,69	0,17	0,39	0,33
6 (11)	0,67	0,42	0,62	0,05	0,46	0,38
7 (18)	0,67	0,38	0,53	0,16	1,00	0,39
8 (13)	0,31	0,37	0,41	0,10	0,56	0,38
9 (23)	0,24	0,11	0,30	0,02	0,03	0,05
10 (30)	1,00	0,73	0,25	0,03	0,07	0,07
11 (24)	0,92	0,80	0,30	0,02	0,04	0,03
12 (25)	0,11	0,22	0,29	0,02	0,04	0,10

Frequency 5

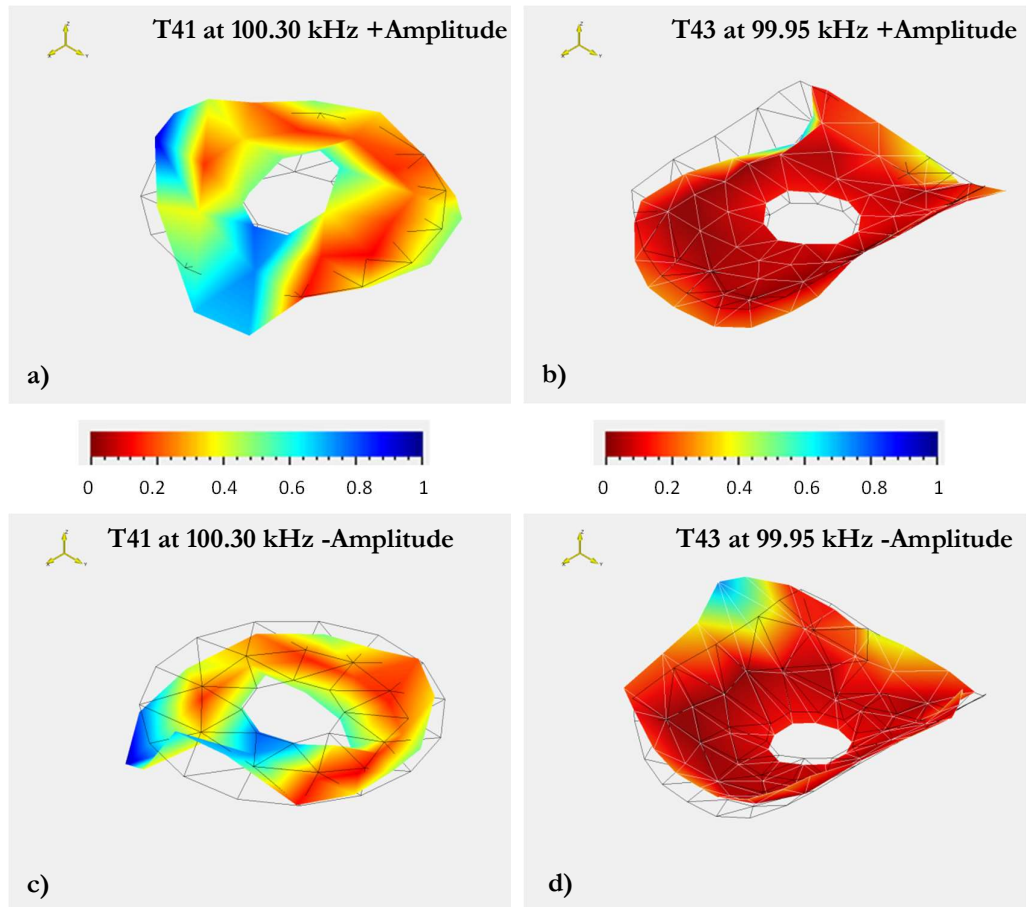


Figure 5.25. Mode of vibration analysis at the two opposite instants of maximum amplitude at resonant frequency 5 for T41 a) and c), and T43 concave b) and d).

Finally, frequency 5 is selected at 100.30 kHz for T41 and at 99.95 for T43. This case is very similar to frequency 2 where a disorder distribution of vibration is found.

Table 5-7. Normalised displacement of T41 and T43 concave at resonance frequency 5 at the representative points under analysis.

Point on the surface	T41 84.84 kHz			T43 88.09 kHz		
	X	Y	Z	X	Y	Z
1 (28)	0,85	0,48	0,33	0,03	0,15	0,12
2 (21)	0,35	0,19	0,62	0,06	0,24	0,08
3 (34)	0,50	0,48	0,28	0,11	0,29	0,15
4 (6)	0,74	0,77	0,46	0,13	0,19	0,19
5 (2)	0,62	0,36	0,37	0,10	0,27	0,02
6 (11)	0,28	0,43	0,43	0,08	0,14	0,03
7 (18)	0,43	0,57	0,25	0,07	0,19	0,05
8 (13)	1,00	0,73	0,65	0,10	0,28	0,03
9 (23)	0,34	0,30	0,70	0,02	0,09	0,07
10 (30)	0,22	0,27	0,69	0,04	1,00	0,08
11 (24)	0,63	0,46	0,47	0,03	0,09	0,07
12 (25)	0,85	0,48	0,33	0,02	0,10	0,07

5.4.3 Displacement

Following the calculations done in Chapter 4 to find the minimum displacement required to generate transient cavitation for a typical excitation, it is important to ensure that the modified HPT can generate this displacement.

From all the frequencies described above the key resonant frequency is frequency 1, hence the analysis will be carried out at this frequency. This frequency is expected to produce the highest displacement for cleaning and should be sufficient to analyse whether or not cavitation can clean Calcite attached to the inner wall of a pipe.

Figure 5.26 presents the displacement generated in T41 with different values of power. It can be seen that the displacement necessary to generate transient cavitation is reached at any value of power used for the excitation. Also, it can be seen that the slope of the sine excitation is higher than the square signal but both of them reached a maximum in a close value: 1.758 μm at 26 W for the sine excitation and 1.676 μm at 65 W for the square signal.

In the case of the machined transducer, the minimum value to obtain transient cavitation is reached also at any power applied, Figure 5.27. In contrast to T41, T43 does not present a maximum in the displacement and larger values of displacement can be obtained. Also a change in the slope can be appreciated at powers close to the maximum in the displacement presented in T41.

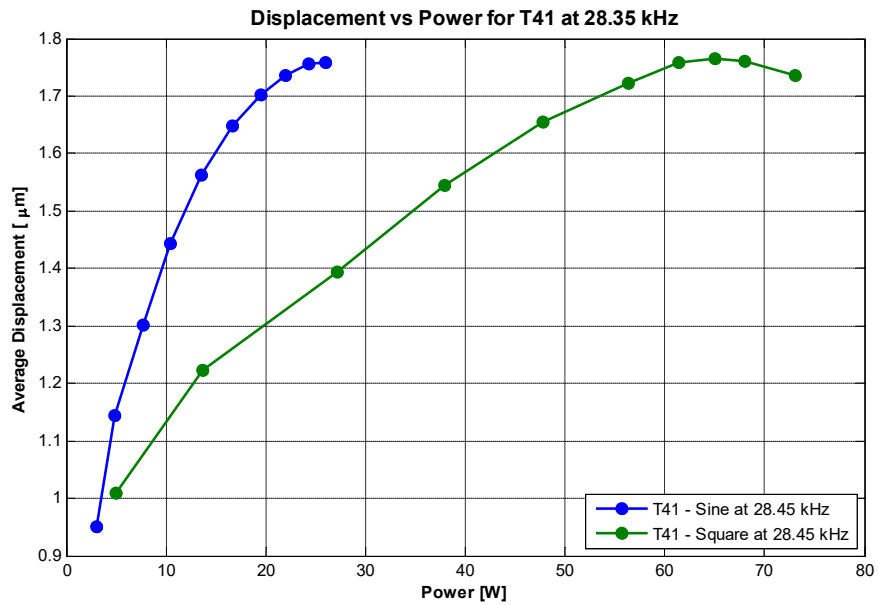


Figure 5.26. Average displacement of the contact surface of T41 on the “Z” direction vs power drained by T41. Each point is the average of 100 measurements with the 3DSV.

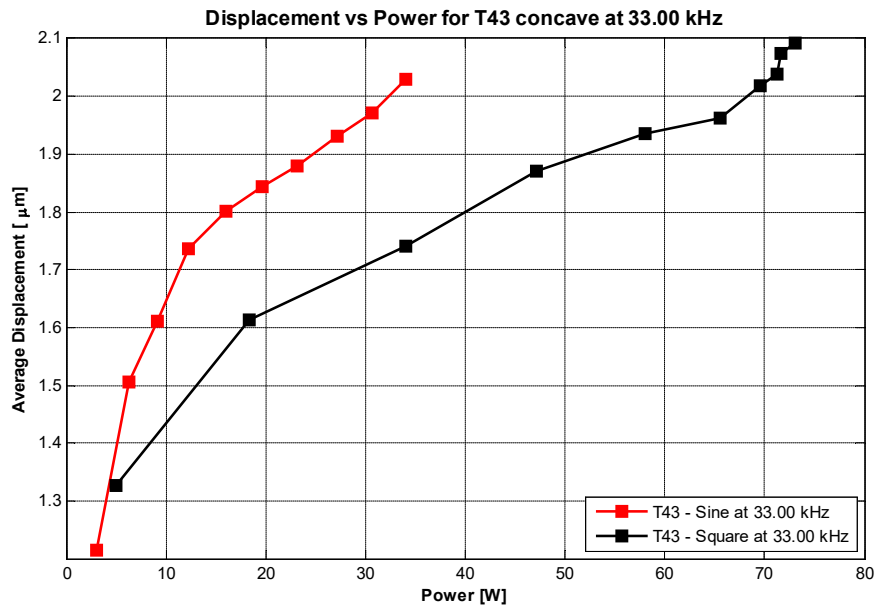


Figure 5.27. Average displacement of the contact surface of T43 concave on the “Z” direction vs power drained by T43. Each point is the average of 100 measurements with the 3DSV.

Figure 5.28 presents the comparison of two transducer displacements at different values of power. It can be seen that T43 needs less power to obtain larger values of average displacement in the contact surface.

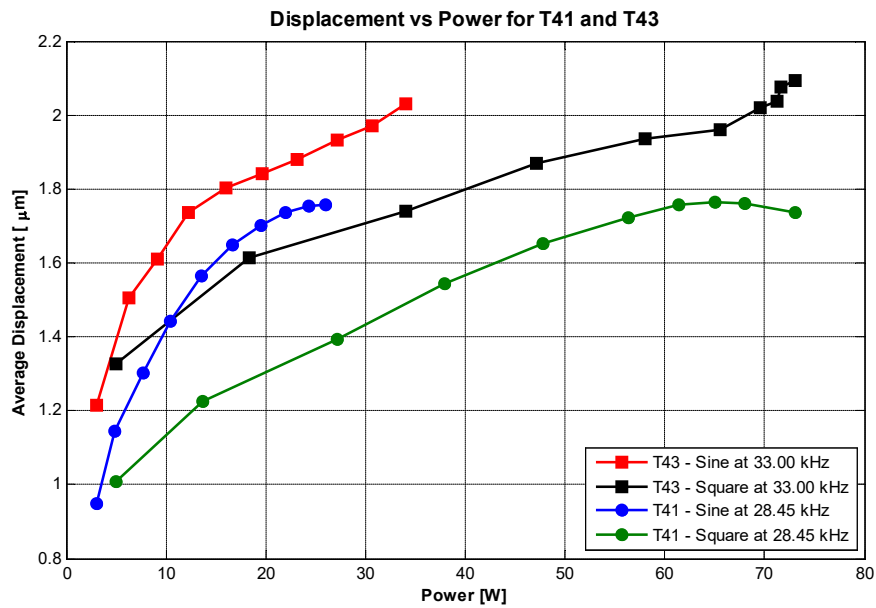


Figure 5.28. Comparison of average displacement of the contact surface of T41 and T43 excited with sine and square signals.

The values of the displacement presented have been obtained for the transducer on its own. It is important to note that those values can change when the transducer is attached to the sample pipe for cleaning. Hence the vibration analysis and the direction of the excitation will be analysed again in Chapter 7 to verify that the displacement required is still met under the new condition, i.e. after attaching the transducer to the pipe.

5.5 Summary

This chapter has given an explanation of the current understanding of high power transducers and the modifications that have been made to the resonator for different industrial purposes.

The HPTs existing in the market have been machined to facilitate the attachment to a pipe and to increase the contact surface between HPT and the pipe.

A resonance frequency analysis for a flat and a concave HPT has been done both with an impedance analyser and a 3DSV. This has shown that resonant frequencies are shifted to higher values due to the decrease of the resonator length. In addition, it has been seen that the new HPT still present low value of impedance in the resonant frequencies as well as large displacements.

It has been shown that the impedance analysis is insufficient to know which frequencies vibrate with the largest displacements. Also, the HPTs present arrhythmic modes of vibration at some

resonant frequencies. Therefore, a method to analyse the entire vibration distribution and the displacements obtained has been presented to understand the HPT contact surface.

Finally, it has been shown that the modified transducers still present displacements high enough to produce cavitation based on the results presented in Section 4.6. Although this displacement is generated in a different direction in the majority of the frequencies, the key resonant frequency continues to have predominant displacement in the desired “Z” direction. In addition, it has been shown that sinusoidal signals required less power for the excitation.

6 Cavitation detection in pipes generated by high power ultrasonic transducers

This chapter explains the detection of the cavitation phenomena in the pipes under analysis to verify that the modified HPTs presented in Chapter 5 are producing cavitation. It also explains a method to find the first cavitation threshold based on existing signal processing techniques.

6.1 Introduction

Acoustic cavitation detection is essential for a range of industrial applications such as in sonochemistry to improve the chemical effects produced by ultrasounds due to the generation of cavitation or, in ultrasonic cleaning baths to measure the energy at each point to map the energy distribution and characterize the efficiency of the cleaning effect. The detection of cavitation can also show the capabilities of the HPT used for different engineering uses like pipelines cleaning.

This investigation aims to prove that hard scale fouling inside pipelines can be removed with the use of acoustic cavitation. Therefore, the detection of cavitation inside the pipes under analysis is a must. Chapter 4 contains the theory to explain the cavitation phenomena and also covers the math's necessary to generate the cavitation prediction plots to estimate the cavitation threshold and the type of cavitation that is more likely to occur under a specific acoustic excitation. But, since cavitation phenomenon occurs at the microscopic scale it can be difficult to observe with the naked eye. Therefore, it is necessary to use a proven experimental method for its detection.

In the literature different methods for cavitation detection have been reported. These can be categorised depending on the effects produced by the cavitation. In this manner, previous investigators have relied on:

- 1) Optical or visualisation methods such as the presence of bubbles [177] or advanced optical techniques such as micro-photos with high speed cameras to visualise the cavitation generation and its bursting acoustic fields [147], [178], [179]. Related with this, the measurement of the light emission produced due to the nuclear reaction that can occur in a transient cavitation at such high temperatures and pressures have been used. This is called sonoluminescence [180]–[182].
- 2) Based on the shock waves generated in the liquid by the cavitation two subcategories can be found, the detection of subharmonics and ultraharmonics due to the nonlinear oscillation of stable cavitation in which vibration produces acoustic emissions [183]–[185], and the shock

waves produced due to transient cavitation has also been measured [158], [186]. The decay of the sound pressure due to the decrease of cavitation produced by the degassing of the liquid has been used [187], The audible burst of gas cavities produced by transient cavitation have been used [188].

- 3) Another possibility is the measurement of the changes in temperature in classic ultrasonic cleaning baths that are supposed to be produced by cavitation [189], this rise in temperature is in fact used for the cancer treatment in humans [183].
- 4) The presence of cavities in the liquid can be detected also by the changes in the velocity of the acoustic wave propagation within the liquid [187].
- 5) The electrical detection of cavitation by the measurement on electrical admittance variations of the emitters has also been reported [190]. vi) Another method is based on the measurements of concentration of the products of a chemical reaction catalysed, what is called sono-chemistry [190].
- 6) Finally, cavitation can also be detected by visualizing the effects of the erosion produced on the solid surfaces immersed in the fluid [191], [192]. The results obtained in this thesis could fall within this method since the Calcite is removed by the use of cavitation in the locations where a threshold related with the displacement is found.

Acoustic emission detection of cavitation

The acoustic emission detection of cavitation is based on the analysis of the presence of subharmonics and ultraharmonics in the acoustic emission produced by oscillating bubbles under sinusoidal oscillating pressure. Therefore, based on this, only stable cavitation can be detected since transient cavitation only lasts one cycle or a short number of them. Consequently, transient cavitation has not been detected by the generation of subharmonics and ultraharmonics so far.

Cavitation bubbles oscillate at the same frequency as the applied acoustic pressure, which produces acoustic emissions at that frequency, and also they can produce oscillation at the harmonics like $n \cdot f$ where n is a natural number ($n = 1, 2, 3, 4, \dots$) and f is the frequency of acoustic pressure applied, ultraharmonics at $n \cdot f/m$ where m is a natural number ($m = 1, 2, 3, 4, \dots$), or subharmonics f/n where n is a natural number ($n = 1, 2, 3, 4, \dots$). This phenomenon is explained by Church's model [193], [194]. Esche, R. (1952) [195] was the first to observe this behaviour by the presence of the subharmonic spectral components of cavitation bubbles under an acoustic field.

Based on this principle it is possible to observe the generation of cavitation by the spectral characteristic of the acoustic emission. Here, the cavitation threshold for the key resonant frequencies of both flat and concave transducers is analysed with two proposes, to prove that cavitation is generated at different frequencies and to evaluate that concave transducers are more appropriated for pipes excitation.

6.2 Cavitation detection set-up and procedure

The cavitation detection set-up consists of two different systems working in parallel. Figure 6.1 shows the experimental arrangement to investigate cavitation generation on a 30cm pipe filled with water.

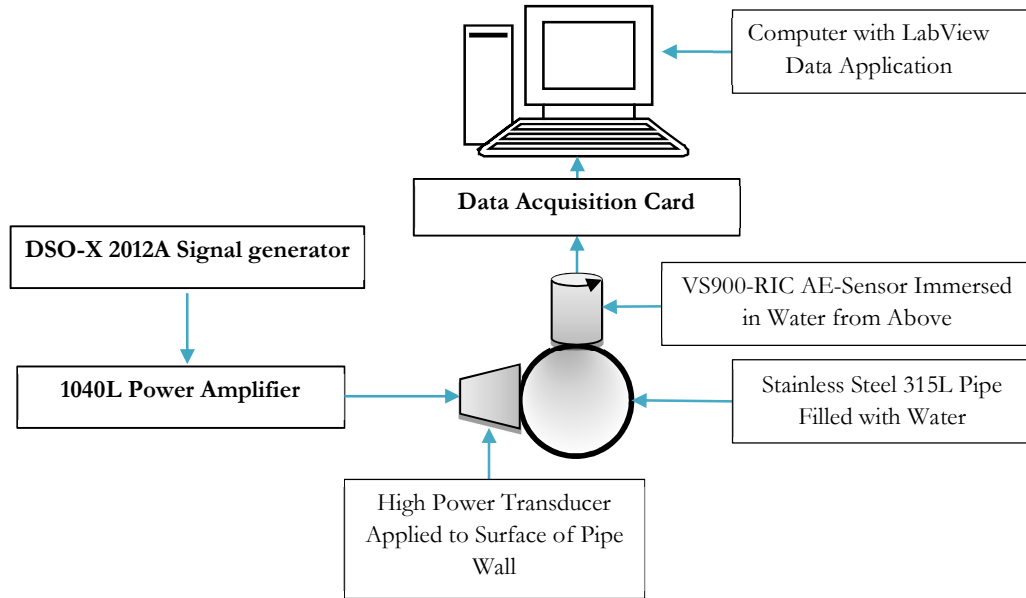


Figure 6.1. Cavitation detection set-up schematic diagram.

Acoustic cavitation generation unit

This part of the set-up consists of an oscilloscope (DSO-X-2012A) for the signal generator, 10 Hz frequency resolution tuning and therefore only increments of 10 mV can be applied. The signal generated is amplified 55 dB by a power amplifier (1040L, RF Power Amplifier) of 400 W. The generated signal excited a HPT that can be flat or concave depending on the experiment. These are attached to a clean 30 cm pipe filled with water at room conditions (see Section 3.3), Figure 6.2.

Acoustic emission measurement unit

The acoustic emission measurement unit consists of an acoustic emission broad-band sensor with the contact surface immersed in the water of the pipe (VS900-RIC AE-Sensor), Figure 6.2. The data acquisition card used was ADlink PCI-9816, with a maximum sampling rate of 10 MSamples/sec, 16-bit resolution and $\pm 5V$ input range. This is controlled with a computer with LabView software for the data processing and storage.

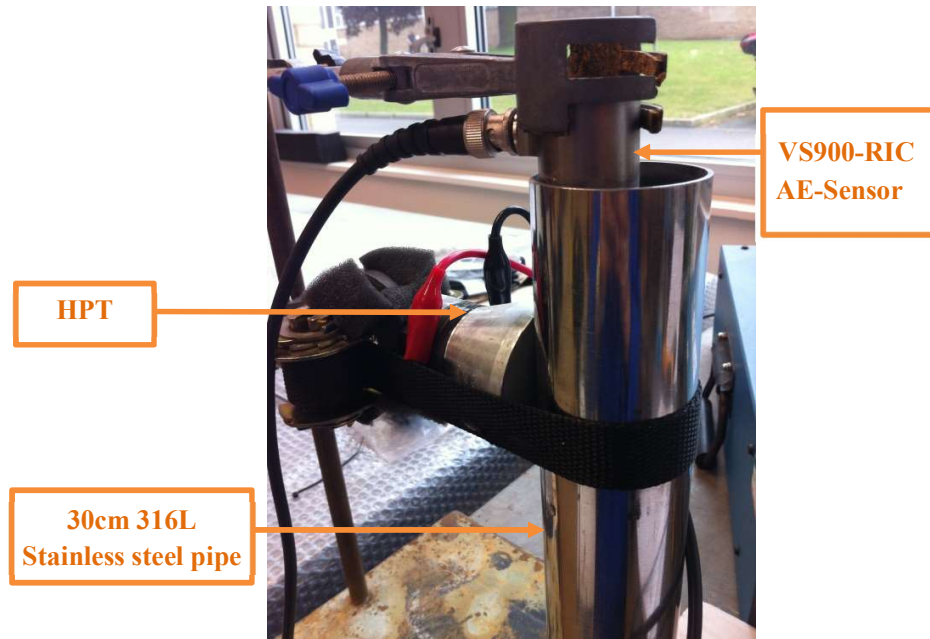


Figure 6.2 Image of the HPT attached to the side of a 30cm pipe with a ratched strap and with couplant gel (see Section 5.2.3) and acoustic emission sensor with the contact surface immersed in the water.

With the setup ready, the pipe is filled with water at room temperature. The temperature is controlled to be the same in all the experiments from the temperature of the tap water and the same tap water at 100 °C by the following equation:

$$m_{tap} \cdot cp_{tap} \cdot \Delta T_{tap} = m_{boiled} \cdot cp_{boiled} \cdot \Delta T_{boiled} \quad (6.1)$$

Where m_{tap} and m_{boiled} are the masses required of tap water and boiled water respectively, cp_{tap} and cp_{boiled} are the specific heats of tap water and boiled water respectively and ΔT_{tap} and ΔT_{boiled} are the increment of the tap water and boiled water respectively.

With equation 6.1 it is possible to calculate the mass of the two water samples necessary to form a litre of water with the desired temperature.

With the pipe filled with water, and a HPT attached to the pipe, it is excited at a resonant frequency increasing the voltage applied to the power amplifier in steps of 10 mV or 100 mV depending on the experiment purpose. This is done starting at 0 and finishing at 1000 mV. At the same time the cavitation detection unit is collecting the acoustic emissions produced in the system at each voltage increase. The acoustic emission detection system is recording information for one second each time.

6.3 Spectral analysis results

The signals collected from the experiments described above are processed with two different methods to prove the generation of acoustic cavitation.

6.3.1 Welch Method

Also known as modified average periodogram this is used for estimating the power that a signal has at different frequencies. This is based on the concept of using periodogram spectrum estimates, as a result of converting a signal from the time domain to the frequency domain [196].

In an average periodogram signal plot, where there is a large peak that is not aligned with one of the distinct frequencies such as $f/2$, this is due to the leakage phenomenon. This means that due to a peak not being concentrated at a single distinctive point, the peak has spread over into its adjacent frequencies [197].

Welch 1967 [196] suggested the modification of the average periodogram plot to reduce this leakage. When doing the Welch signal processing in the square window, the computed subsignal can be considered as finding the Fourier coefficients of the periodic extension. This can sometimes lead to a discontinuity which leads to the Gibb's phenomenon of the Fourier series, causing ringing or oscillations near the discontinuity after the signal has been reconstructed through Welch. Welch proposed other windows to be used which consist of a gradual decrease to zero instead of a sudden decrease as found in the rectangle window to stop discontinuities [197]. This work will use the spectrum function in the Hann window as it consists of a gradual increase and decrease to/from zero to eliminate jump discontinuities.

The Welch method for cavitation detection has been used before by D. Zmarzly, M. Szmechta 2008 [198]. Here a Matlab toolbox is used for the analysis. The script loops each instant of data obtained through acoustic emissions and generates a graph which plots Frequency (MHz) vs Power/Frequency (dB/Hz) for each image of data taken and displays the voltage input also with power at each instant.

Acoustic Spectrum Analysis

For the analysis of these signals the Welch parameters established were Hanning window, with a period length of 100,000 values and an overlapping of 50%.

Through the Welch Signal Processing method, a plot for each voltage applied to the HPT is produced. Figure 6.3 is an example of a plot with an excitation of 40 mV. In this figure only the harmonics due to the HPT vibration are presented. These harmonics are a multiple of the applied frequency $n \cdot f$. The presences of these harmonics are not considered to be produced by cavitation oscillation but due to the standing waves generated in the transducer.

$$1st\ harmonic: nf = 1 \times 33.46\ kHz = 33.46\ kHz$$

$$2nd\ harmonic: nf = 2 \times 33.46\ kHz = 66.92\ kHz$$

$$3rd\ harmonic: nf = 3 \times 33.46\ kHz = 100.38\ kHz$$

$$4th\ harmonic: nf = 4 \times 33.46\ kHz = 133.84\ kHz$$

$$5th\ harmonic: nf = 5 \times 33.46\ kHz = 166.20\ kHz$$

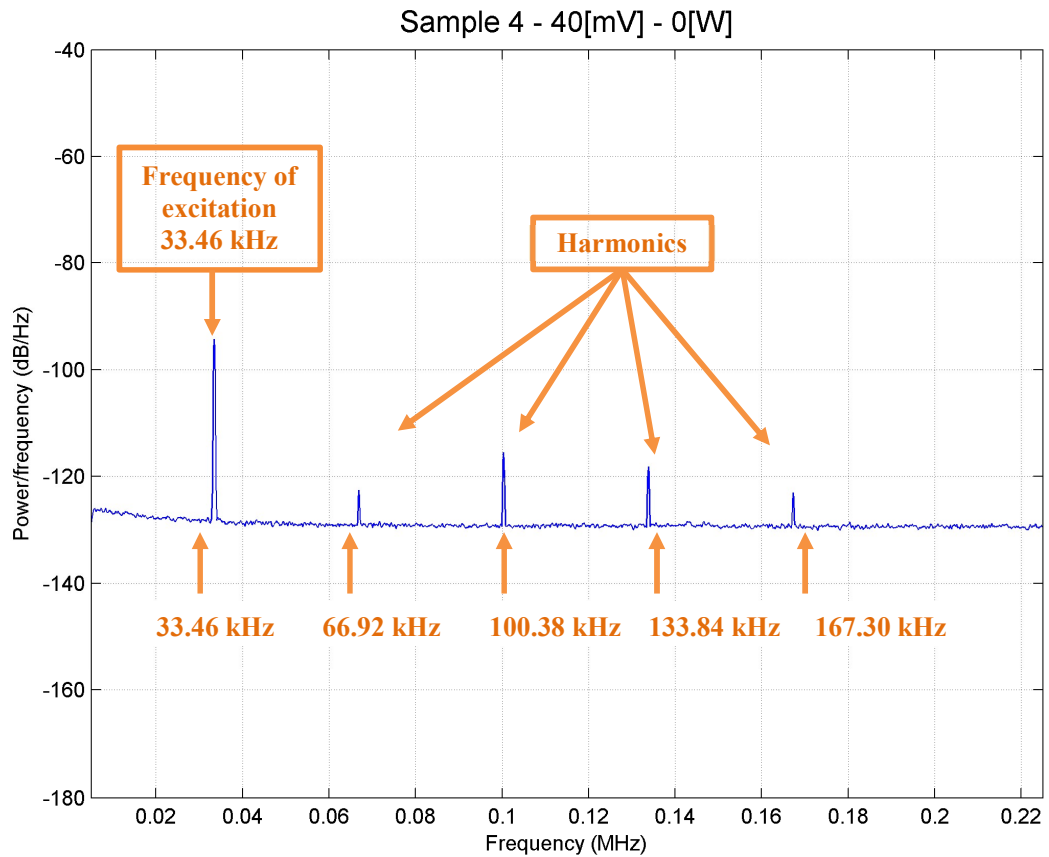


Figure 6.3. Welch Signal Processing of T43 excited at 33.46 kHz at 40mV.

At some point, when the power supplied to the HPT reaches, the cavitation threshold, additional subharmonics or harmonics can appear. Figure 6.4 presents a Welch Signal Processing of transducer T43 excited at 33.46 kHz at 270 mV. At this voltage input and due to the impedance mismatching, the energy absorbed per second is 6 W. In this case, the ultraharmonics of the excitation frequency appears at $n \cdot f/m$ but in this case the first subharmonic $f/2$ is not present and the ultraharmonic $3 \cdot f/2$ is not clear in the graph which makes it difficult to detect onset of cavitation. Therefore, based on the literature it cannot be considered as the cavitation threshold.

$$\text{Ultraharmon} : nf/m = 5 \times \frac{33.46}{2} \text{ kHz} = 83.65 \text{ kHz},$$

$$\text{Ultraharmonic: } nf/m = 7 \times \frac{33.46}{2} \text{ kHz} = 117.11 \text{ kHz},$$

$$\text{Ultraharmonic: } nf/m = 9 \times \frac{33.46}{2} \text{ kHz} = 150.57 \text{ kHz}.$$

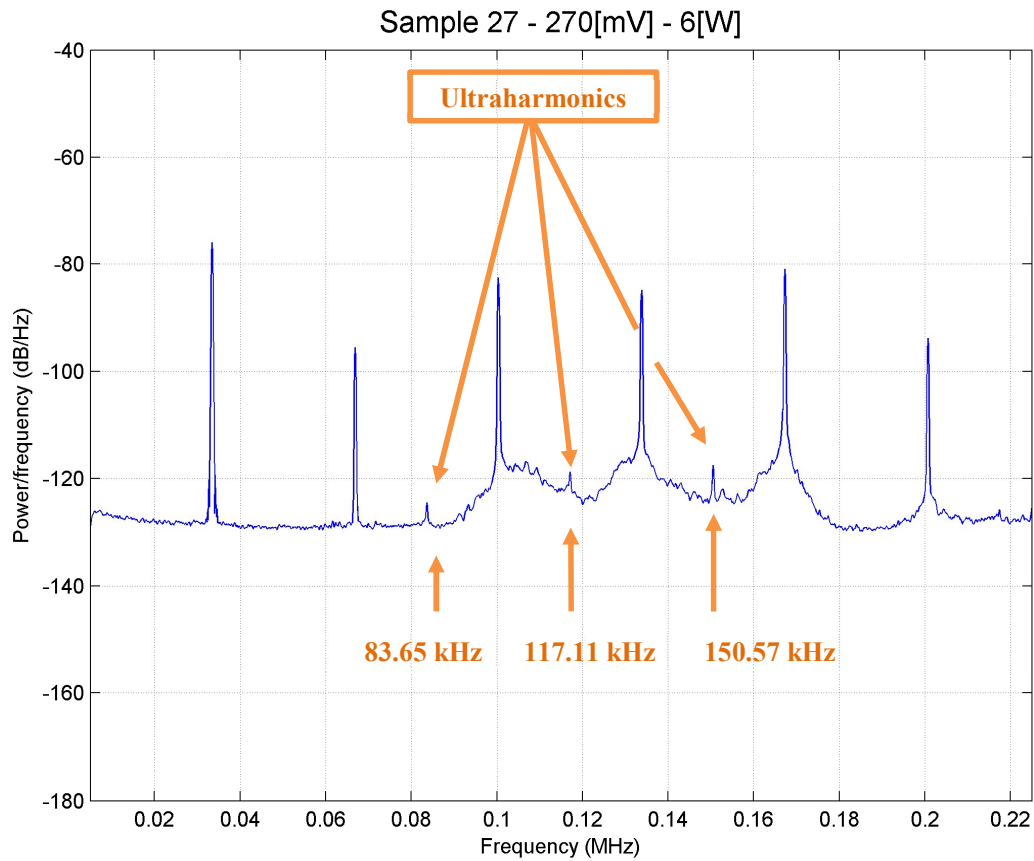


Figure 6.4. Welch Signal Processing of T43 excited at 33.46 kHz at 270 mV; Harmonics with some acoustic emissions.

After increasing the voltage input to 280 mV, with a power drained by the HPT of 6 W, which is the difference between the power delivered from the high power amplifier to the transducer minus the power reflected back to the power amplifier. The peaks related with the subharmonic $f/2$ and the harmonic $3 \cdot f/2$ are clearly visible. This could be considered now as the cavitation threshold. Figure 6.5 presents the location of the first subharmonic and the ultraharmonic $3f/2$.

$$1st\ subharmonic: f/2 = \frac{33.46}{2} kHz = 16.73 kHz,$$

$$Ultraharmon : 3f/2 = 3 \times \frac{33.46}{2} kHz = 50.19 kHz.$$

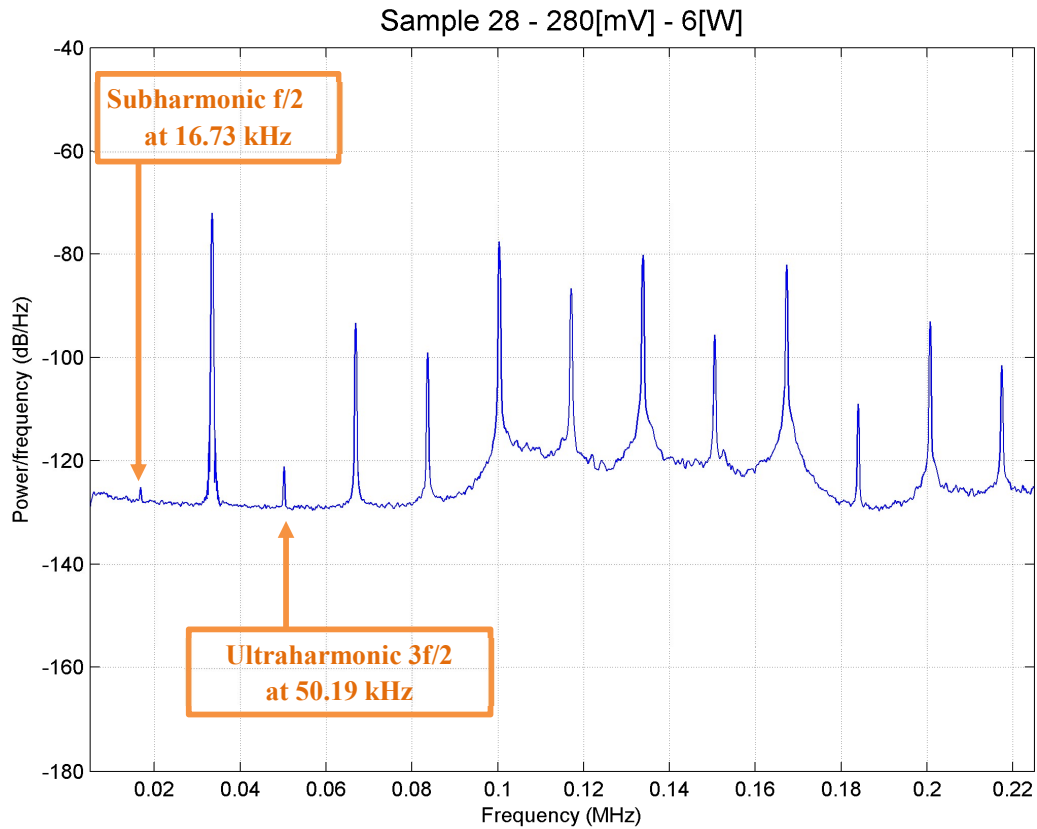


Figure 6.5. Welch Signal Processing of T43 excited at 33.46 kHz at 280mV; Subharmonics with more acoustic emissions.

Figure 6.5 presents the Welch process to the signal acquired in test three at 280 mV. This presents the existence of the first subharmonic $f/2$ and the ultraharmonic $3f/2$. To obtain the value of the minimum voltage to the power amplifier necessary to generate cavitation it has been necessary to produce a plot for each value of voltage. In the following Section two methods to find the cavitation threshold are discussed.

6.4 Cavitation threshold detection and proposed

As discussed above, it can be tedious to detect a peak produced by a subharmonic in the Welch plotting method and also it may need a number of graphs to find the threshold of cavitation. Here all the signals acquired in one graph after applying the FFT analysis, the peaks of the subharmonic or the ultraharmonic, are plotted in two different ways. FFT is proposed similar to the one proposed by S. Yoshizawa 2008 [185].

In this case a step increase of 10 mV is applied from 20 mV to 1000 mV, this would produce 100 different plots that would need to be analysed independently. Instead, all the signals are plotted in two different ways as follows.

6.4.1 Conventional plotting method

In the 2008 S. Yoshizawa [185] proposed a method consisting of plotting all the values of the subharmonic $f/2$ peak at the different excitation powers. This provides a graph in which the threshold can be found when the intensity of the peaks is just different from the noise. Figure 6.6 presents the cavitation threshold for the three experiments done under the same conditions.

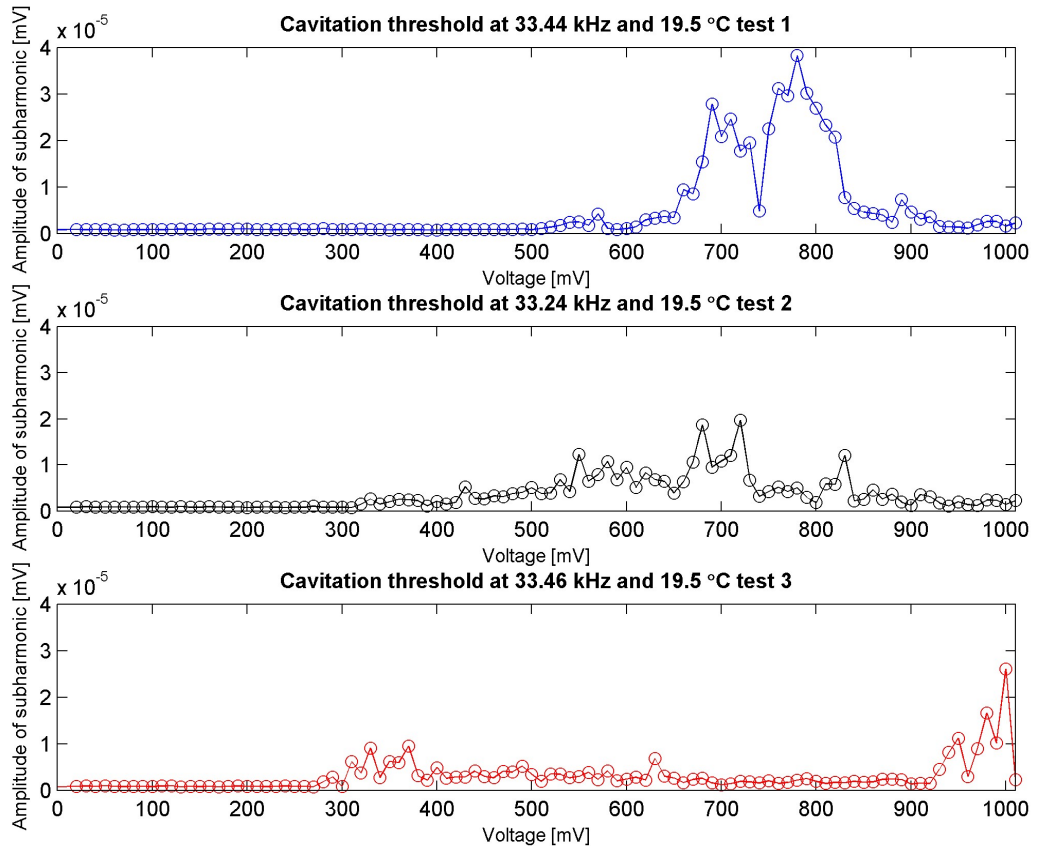


Figure 6.6. Cavitation threshold detection in a pipe excited with T43 at different frequencies around 33.40 kHz at 19.5 C.

It can be seen in Figure 6.6 that the threshold in test 1 is around 530 mV, in test 2 it is around 330 mV and in test 3 around 280 mV, but in all the cases it is difficult to define since it can be considered fluctuations of the value of the noise in subharmonic location. Therefore, a different method is proposed.

6.4.2 Proposed plotting method

This method plots all the normalized values of the FFT of the frequencies around the subharmonic and the ultraharmonic. This is done as follows:

1. Each signal is converted to the frequency domain by an FFT Matlab tool.
2. The resonant frequency of each step of excitation is located in the FFT.

3. Two windows of data are created with a frequency range for the subharmonic $f/2$ and the ultraharmonic $3f/2$ respectively.
4. The data of each window is normalized. This will set as 1 the maximum in that frequency range.
5. Finally, all the normalized data of the FFT windows are plotted in the same graph adding $n + 1$ to each component of the FFT of each signal. Where “ n ” is the number of the experiment in chronological order.

Considering that the separation between plots is one unit, if the maximum in the window is at the subharmonic or the ultraharmonic it will create a straight line e.g. considering that after the threshold all the steps should have a maximum at the harmonics, this produces a graph with a line that determines the threshold of the cavitation.

If this type of plotting is compared with the method in which just the values of the peak at each value of voltage are represented, it can be seen that the appearance of the threshold can be doubted. For that reason, the combination of the two methods has been chosen as the solution.

Figure 6.7, is an example of the plotting method for test 1. It can be seen that it gives a picture of the cavitation generation at different powers. When the subharmonic $f/2$ or the ultraharmonic $3f/2$ occurs, there will be a maximum in the frequency range and therefore the value will be “one” and will generate a concatenated series of “ones” and therefore a line.

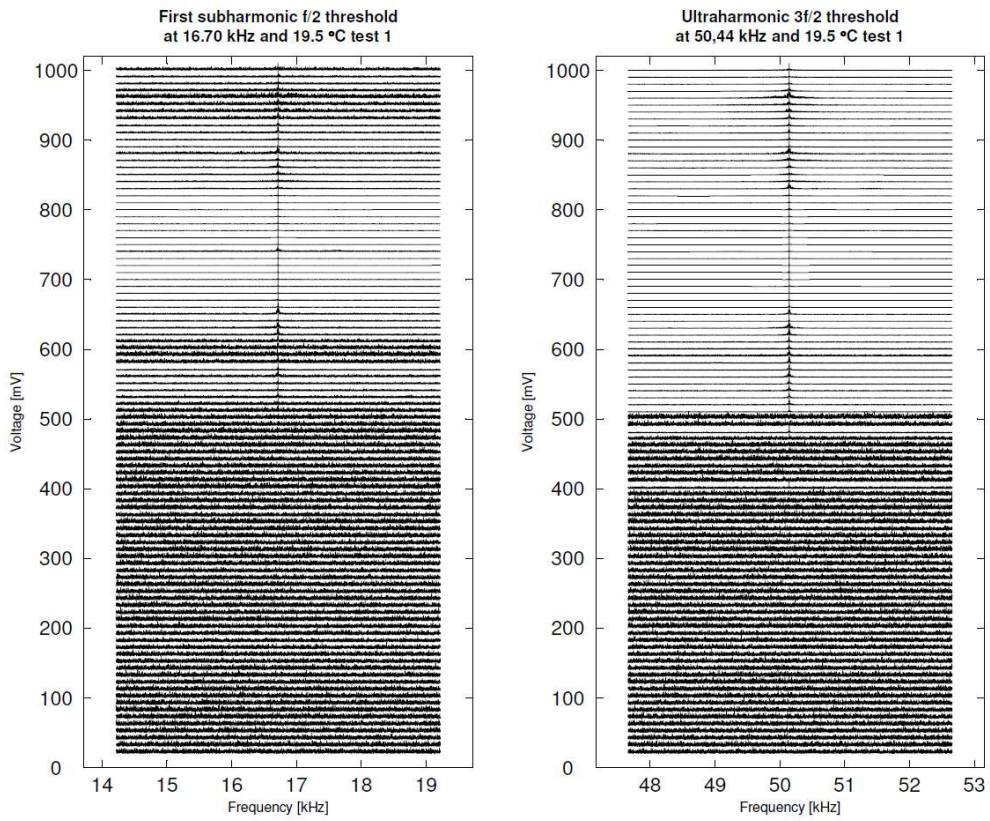


Figure 6.7. Cavitation threshold in a pipe induced to vibration with T43 concave transducer at 33.44 kHz and 19.5 °C.

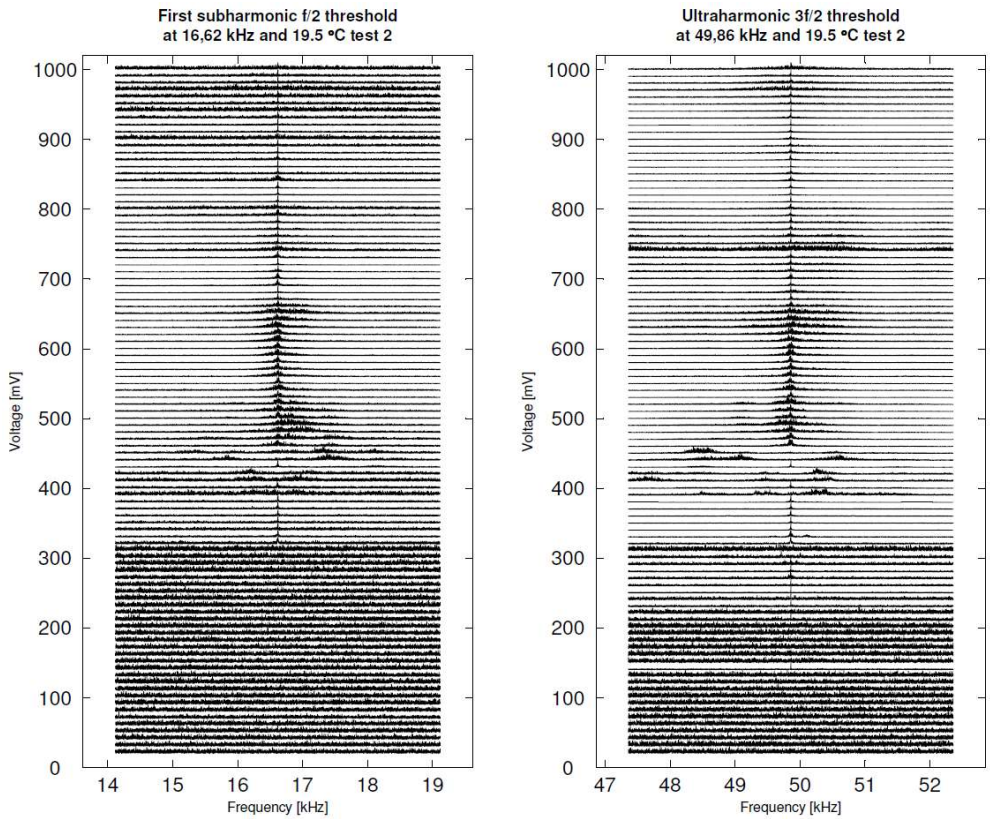


Figure 6.8. Cavitation threshold pipe induced to vibration with T43 concave transducer at 33.24 kHz and 19.5 °C.

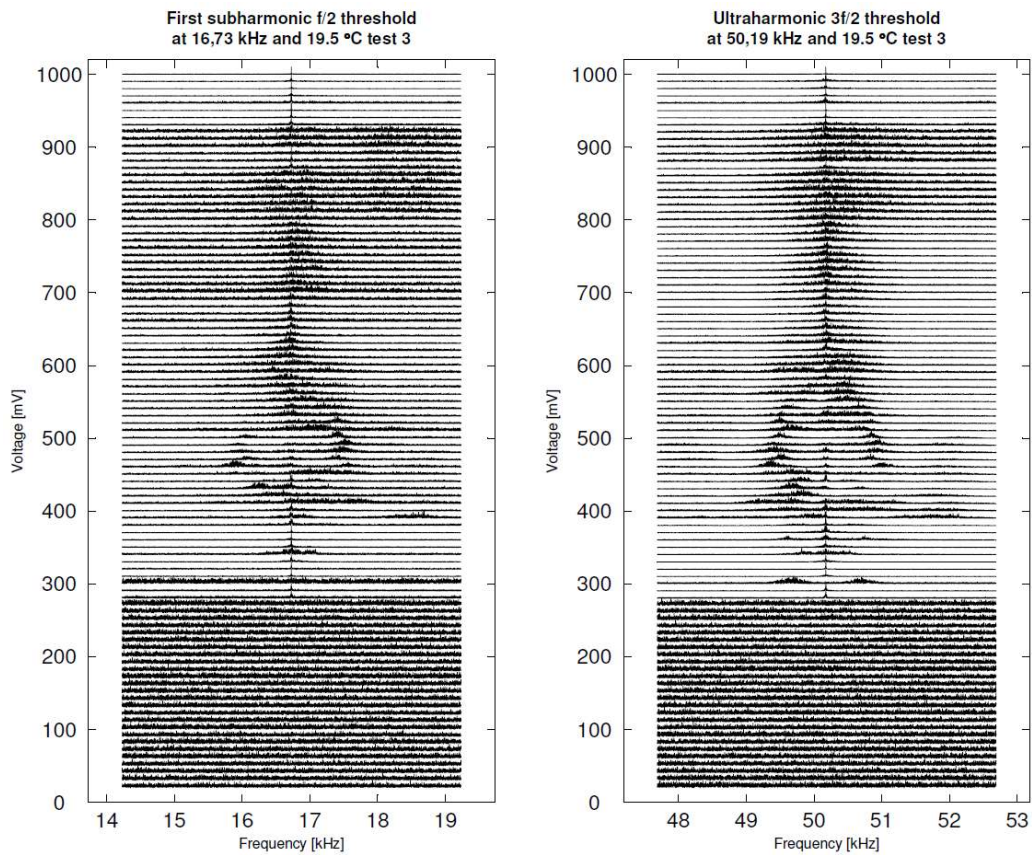


Figure 6.9. Cavitation threshold in a pipe induced to vibration with T43 concave transducer at 33.46 kHz and 19.5 °C.

The figures above present the results in the three tests performed to find the cavitation threshold in a pipe excited with the transducer T43 at the first resonant frequency.

Figure 6.7 presents a threshold at 520 mV in the first subharmonic and at 400 mV in the ultraharmonic $3f/2$.

Figure 6.8 presents the threshold at 330 mV in the subharmonic $f/2$ and 150 mV for the ultraharmonic $3f/2$. The question is which subharmonic or ultraharmonic has to be considered as a threshold. In the literature the presence of the subharmonic $f/2$ is considered as the acoustic cavitation unique indication but the results presented here suggest that further investigation related with the presence of ultraharmonics of higher order may change the conception of the cavitation onset measurement with acoustic emission. In addition, the ultraharmonic is not presented in all the values of voltage after the threshold. Also, it can be seen that in the higher values of voltage the noise makes it more difficult to visualize the line generated by the concatenation of “ones”.

Figure 6.9 shows the results of test 3 in which the threshold is presented in the same location for both the subharmonic and the ultraharmonic at 280 mV. Again the presence of other

ultraharmonics presented in Figure 6.6 could be considered as the actual threshold of cavitation since it has been proved that cavitation oscillation can produce any ultraharmonic [193].

6.5 Summary

An explanation of the existing methods for the detection of cavitation has been given based on the phenomena produced by detected cavitation. Within all the methods, the detection of the subharmonics and harmonics vibration with acoustic emission has been selected.

This method has been used to detect the existence of cavitation and to determine its threshold in different conditions for the machined HPT used in this work.

In addition, it has been proposed that the analysis of the different subharmonics and the ultraharmonics for the use of acoustic emission as a cavitation threshold detection technique.

7 Cleaning of fouled pipes using high power ultrasonic waves

This chapter contains the results of ultrasonic cleaning of fouled pipes induced to vibrate with the machined transducers presented in this thesis. A 3D scanning vibrometer laser is used to measure the actual displacement of the outside wall of the pipes, the displacement is converted to the acoustic pressure generated by the oscillating wall and this is related with the performance of the results in the cleaned pipes.

7.1 Introduction

All the information presented in the previous chapters has been used to carry out the experiments that are presented in this chapter. In this chapter, the capabilities of the identified high power ultrasonic transducers generating sonic waves to successfully remove fouling in pipelines used in industry have been analysed. A theoretical explanation to the results obtained is given based on the theory presented in Chapter 4.

Five fouled pipes are induced to vibrate under controlled conditions while the actual displacement of the outside wall of the pipe is measured with the 3DSV. Later the displacements generated during the cleaning process were compared with the clean zones obtained. The results are also related with the theory presented in Chapter 4 for its validation.

Cleaning principle and wave modes

Classic ultrasonic cleaning in immersion tanks is commonly used in industry. This works using a compressional wave produced by a number of HPT's attached to the tank surface. In this manner, a solvent contained in the ultrasonic cleaning bath is excited to produce cavitation in the whole volume. The cavities vibrate at the excitation frequency and the shock wave generated removes the dirt of the object such as grease and other oily build-up. Figure 7.1 represents a typical ultrasonic cleaning bath configuration.

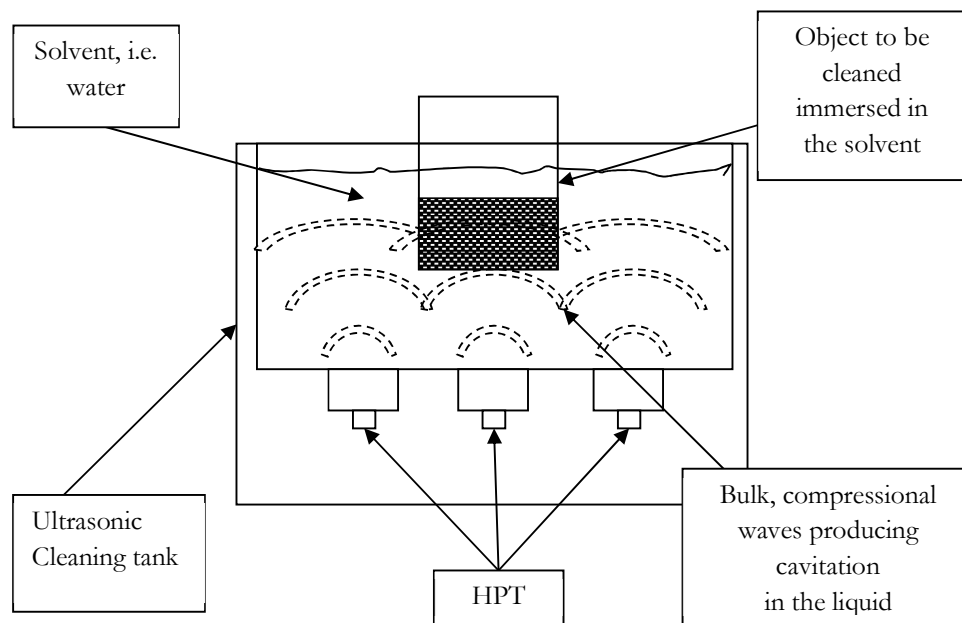


Figure 7.1. Classic ultrasonic cleaning device and principle.

The potential vibrations of the object submitted to the classic cleaning procedure are not of concern and do not affect the cleaning method. This is in total contrast to the technique under development here, where the pipe vibration is responsible for its own cleaning. Therefore, it depends on the capabilities of the vibration to generate cavitation in the vicinities of the inner wall of the pipe. Taking this into account, the type of wave of concern is not a bulk wave since it travels through the thickness of the pipe wall in a mode similar to a guided wave.

A guided wave can be defined as a wave of which energy is concentrated nearby a boundary or between parallel boundaries separating materials with different acoustic impedance and that has a direction of propagation parallel to these boundaries. This type of wave can travel further than bulk waves and are commonly used in non-destructive testing (NDT) [199]–[201]. These types of waves are different to waves generated in this thesis for the cleaning proposes and rather than been called either bulk waves or guided waves can be called waves guided. This is because they do not have the properties as either bulk or guided waves. They difference with bulk waves is that they are not propagating in an infinite volume and the velocity will depend on the number and types of diffractions [199] and are not guided waves because the wave generation and the modes generated are not the ones described by the dispersion curves for a the type of pipe used [199]. Therefore, the concept to be applied is wave guided. And this is in contrast to the classic cleaning, excitation does not consider the wall in which the transducers are attached and the wave that is propagated through this wall.

7.2 Experimental procedure and set-up

For the investigation one concave HPT is attached to a pipe fouled with Calcite (Chapter 3) with a stretch strap or a collar specifically developed to improve the transducer's attachment (Appendix C). The pipe with the transducers is attached vertically with a stand and is filled with water. To stop the water leaking from the bottom a cover made with latex film and American tape is used. Reflective beads "P-RETRO Retroreflective Glass Beads" are attached to the scanning area to improve the scattering properties of the surface under analysis. Figure 7.2 presents one of the pipes attached to the stand.

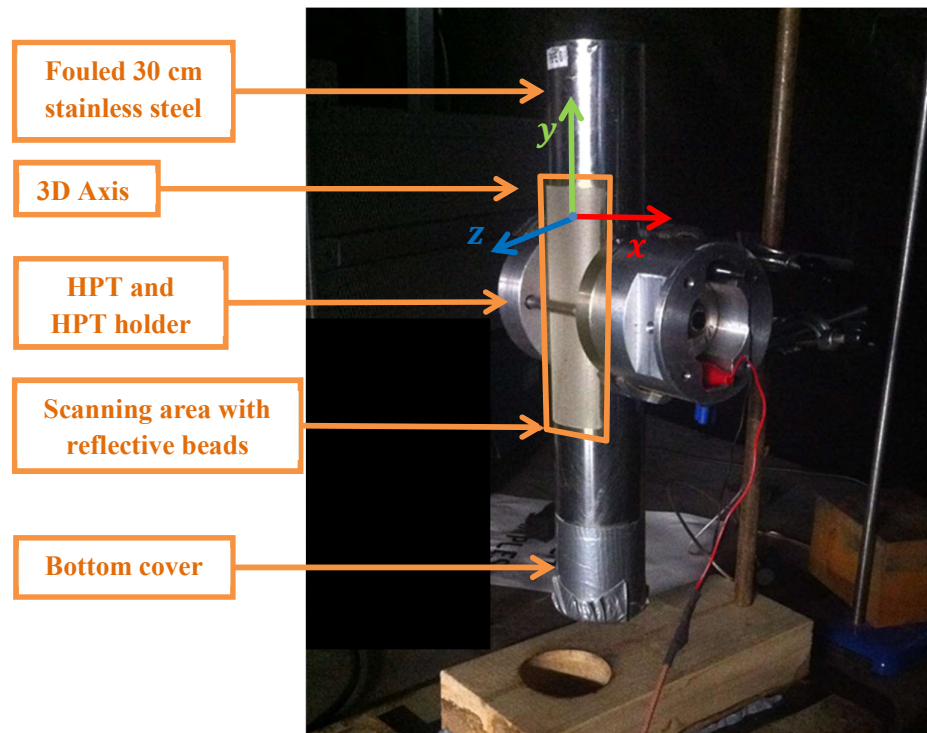


Figure 7.2. Example pipe statements used for the experimentation.

For the excitation the signal generator of the 3DSV is used. The input constant signal is amplified with a 1040L Power Amplifier (55dB). The output of the amplifier is connected to the HPT attached to the pipe.

To measure the actual vibration of the pipe while being cleaned, a 3DSV is placed in front of the pipe subjected to the cleaning. This is calibrated applying a configuration to the three-dimensional axis as shown in Figure 7.3.

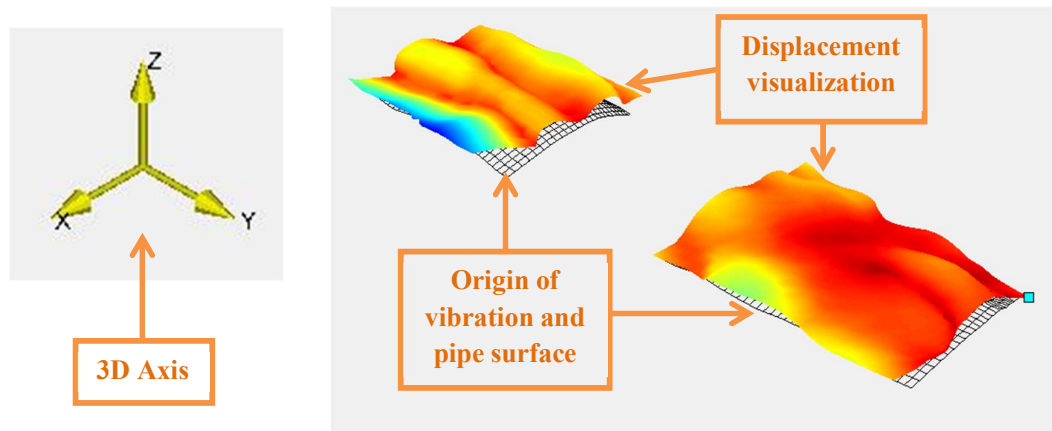


Figure 7.3. Axis orientation, origin and displacement visualization with the 3DSV.

In this manner, the out of the plane displacements will be related with the “Z” axis in the visualization of the pipelines vibration.

When all the equipment is connected and the pipe is filled with water, the vibrometer calibration is done as per Figure 7.3. In order to ensure that no modification occurs in the fouling, a FFT analysis with a low power sweep is applied with the vibrometer in order to find the resonant frequencies of the system composed by the transducer and the filled pipe and holder. The vibrometer is setup to collect 50 signals per scanning point.

From the FFT the frequency with largest displacement in the “Z” direction is selected for the cleaning.

The selected frequency is applied with full power during 30 minutes while the 3DSV measures the actual displacement of the contact surface. Once the experimentation is finished the pipes are emptied and left to dry for cutting and further analysis.

7.3 Results and discussion

After the cleaning procedure, the pipes are cut and a focus stacked image (FSI) of the cleaned surface area is taken from the opposite side of the scanning area. The FSIs are compared with the results obtained during the cleaning process.

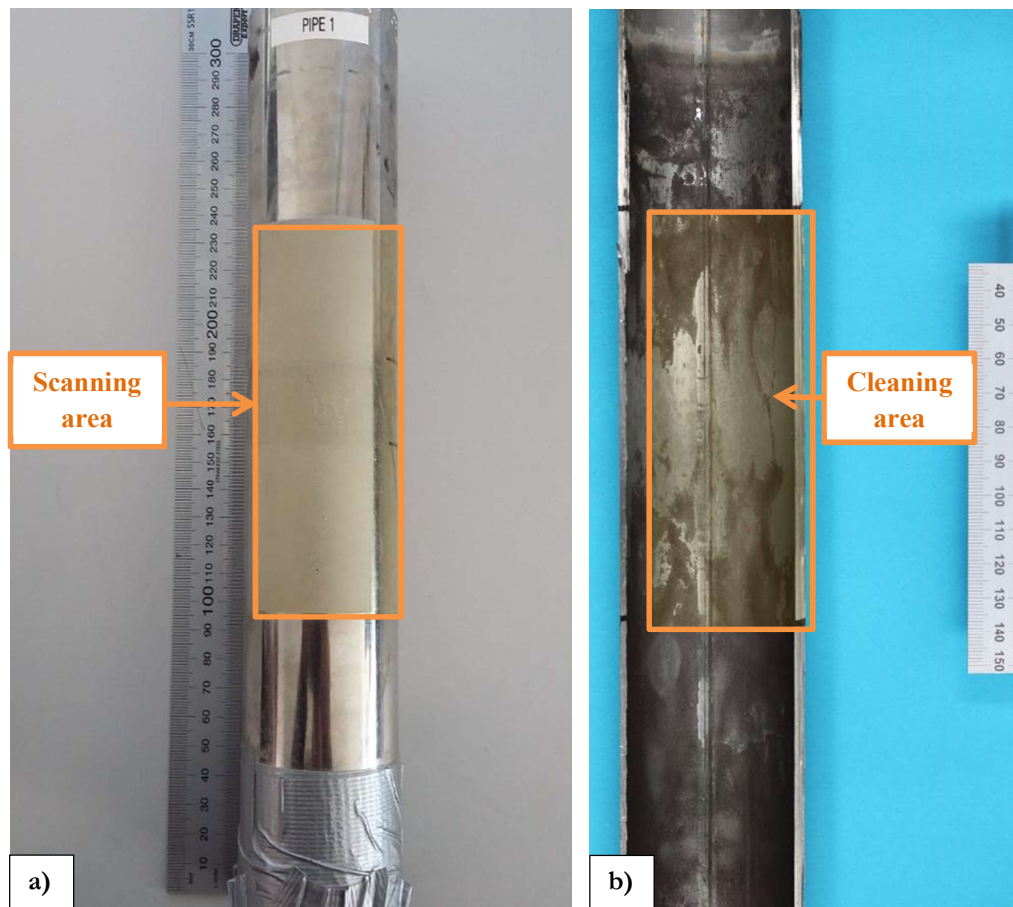


Figure 7.4. Relation between the scanning area measured with the vibrometer and the cleaning area to be compared, a) presents outside of the pipe where the reflective beads are highlighted, b) presents the inner location of the scanning area which is the location that is going to be compared below.

The cleaning results and the scanning area can be related as presented in Figure 7.4. This measurement produces 3D images of the average measured displacement while the pipes were cleaned. Figure 7.5 presents one example of the visualisation of pipe 1 average displacements measured. As it can be seen, the scanning area is divided in two parts. This is because the attachment method needs to hold the pipe around the same location of the transducer. This division appears in all the results presented in this thesis.

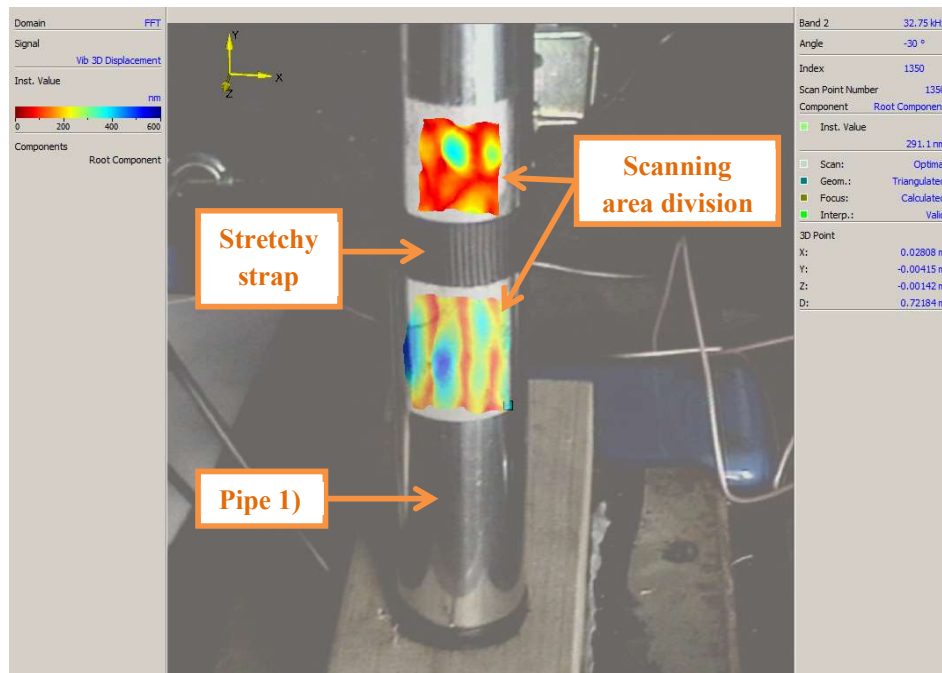


Figure 7.5. 3DSV results obtained from the measurement of the vibration of the scanning area at the same time that the cleaning is being performed.

Figure 7.5 presents the results given by the laser vibrometer for pipe 1) as an example, but the displacements of concern in this study are the displacements in the radial direction. The calculation of the displacements in the radial direction that will be applied in the analysis of all the pipes used in the investigation is explained as follows.

Calculation of the displacement in the radial direction

In order to link the displacement measured with the vibrometer and the cavitation prediction plots it is necessary to calculate the displacement in the radial direction. This is because the type of wave that has to be generated is a compressional wave and it has to be generated perpendicularly to the inner wall of the pipe. Therefore, the values given by the vibrometer along the three-directional axes have to be converted in the radial component of the vibrating point. With this the acoustic pressure generated next to the boundary between the water and the pipe wall can be calculated. The calculations for the conversion are presented below (Figure 7.6 and Figure 7.7).

For a vibration point on the inner wall of a pipe (x, y, z) with a total displacement measured by the 3DSV equal to D_{tv} , can be calculated its projection of the plane $x - z$ that contains (x, y, z) by;

$$D_{x-z} = \sqrt{D_x^2 + D_z^2}, \quad (7.1)$$

Where D_{x-z} is the projection of D_{tv} on the plane $x - z$ and D_x , and D_z , are the displacements measured by the 3DSV in that point on the x and z axes respectively. It is important to note that

the component D_y does not affect the projection of D_{tv} on the plane $x - z$ and therefore it is not included in the calculations, Figure 7.6. Then, D_{tv} will have associated displacement in the radial direction D_r which is the projection of D_{x-z} on the radial axis of the pipe. This is the shorter distance between the point and the axis of the pipe.

Then, by knowing the angle between the radial axis of the pipe and D_{x-z} , D_r can be calculated as follows (Figure 7.7);

For

$$\beta = \tan^{-1} \left(\frac{D_x}{D_z} \right), \quad (7.2)$$

And

$$\sigma = \tan^{-1} \left(\frac{d_x}{d_z} \right), \quad (7.3)$$

If

$$\alpha = |\beta| - \sigma. \quad (7.4)$$

It is important to note that for the calculation of α it is necessary to use the absolute value of β since α is always the difference between β and σ . In contraposition α can be either positive or negative since $\cos(\alpha)$ equals $\cos(-\alpha)$.

Then

$$D_r = D_{x-z} \cos(\alpha). \quad (7.5)$$

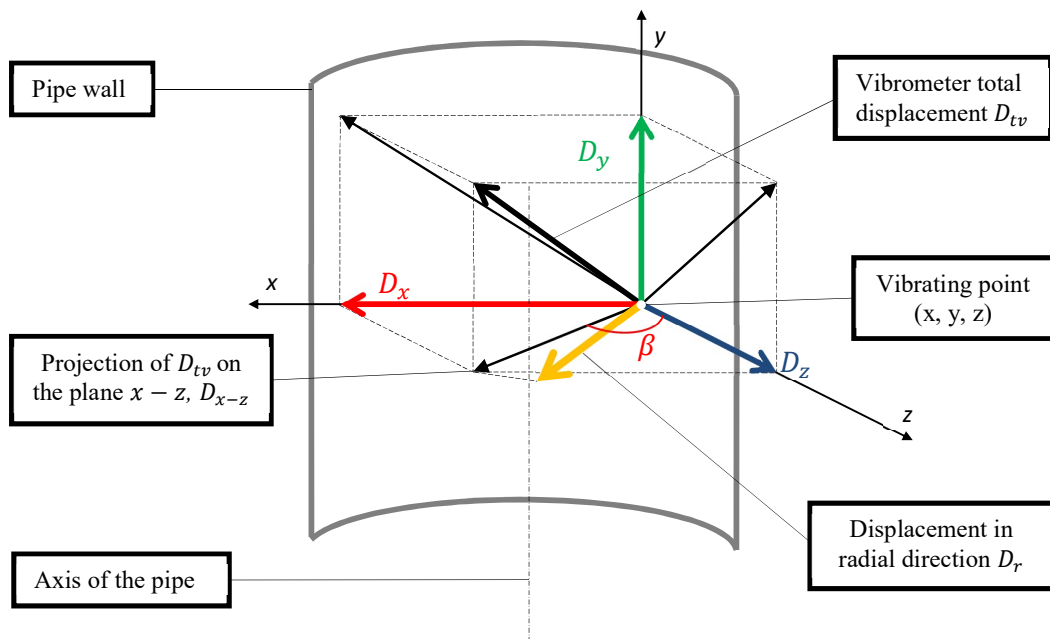


Figure 7.6. Schematic explanation of the conversion of the displacement obtained by the vibrometer to the vibrations in the radial direction.

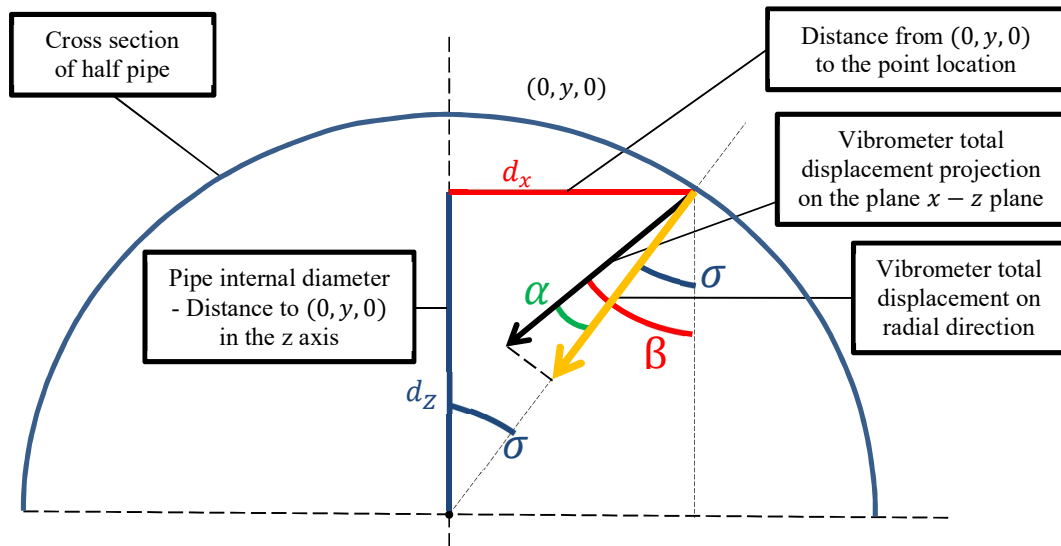


Figure 7.7. Representation of the necessary angles for the calculation of the displacement in the radial direction on the plane x-z for each point on the contact surface.

By applying the calculations explained above it is possible to obtain the value of the displacement generated in the radial direction and therefore the value of the acoustic pressure generated in the liquid. With this it is possible to calculate P/P_o for each point for further analysis of the cavitation prediction plots.

7.3.1 Pipe number 1)

Pipe number 1) was excited with T43 concave transducers for 30 min. The frequency selected for the cleaning process was 32.7 kHz. This was selected by doing a FFT analysis of the scanning surface looking for the frequency with largest displacement in the Z direction. Figure 7.8 presents the average displacement FFT of the contact surface for the selection of the optimal frequency in pipe 1). The HPT used for the excitation was T43 and the pipe was excited during 30 min with a total power drained by the transducer of 65W. The parameters of the excitation are presented in Table 7-1.

Table 7-1. Parameters of the excitation of pipe number 1.

	Value of the parameter
Transducer	T43
Power Input	65W
Excitation Frequency	32.7 kHz
Duration of the excitation	30 min

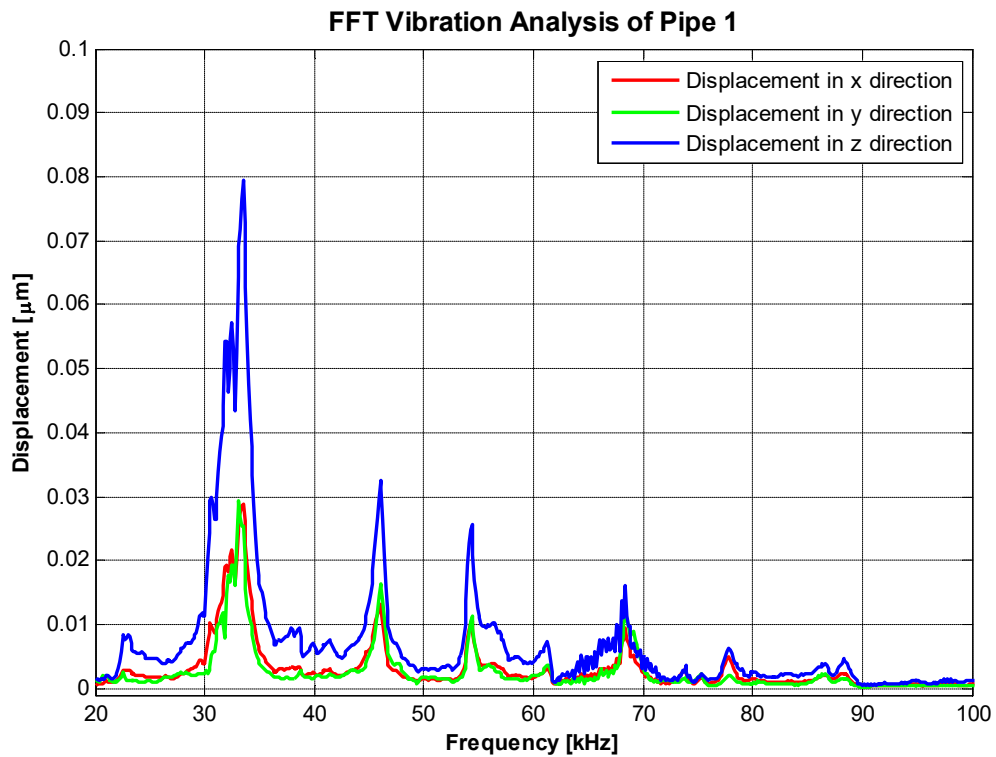


Figure 7.8. FFT analysis of the scanning surface for pipe number 1 to find the frequency that produces the largest displacements in the Z direction.

The cleaning experiment was performed at the same time that the 3DSV measured the actual vibration of the scanning surface. This was done with 2500 scan points on the surface and by

collecting 100 signals per scan point for averaging. The 3DSV sample frequency was established at 512 kHz with a resolution of 125 Hz.

The results of the cleaning are presented in Figure 7.9. As can be seen, the pipe has clear evidence of full cleaning on the opposite side from the HPT location. The rest of the pipe has symptoms of a skin clean in some locations which can be appreciated in Figure 7.10.

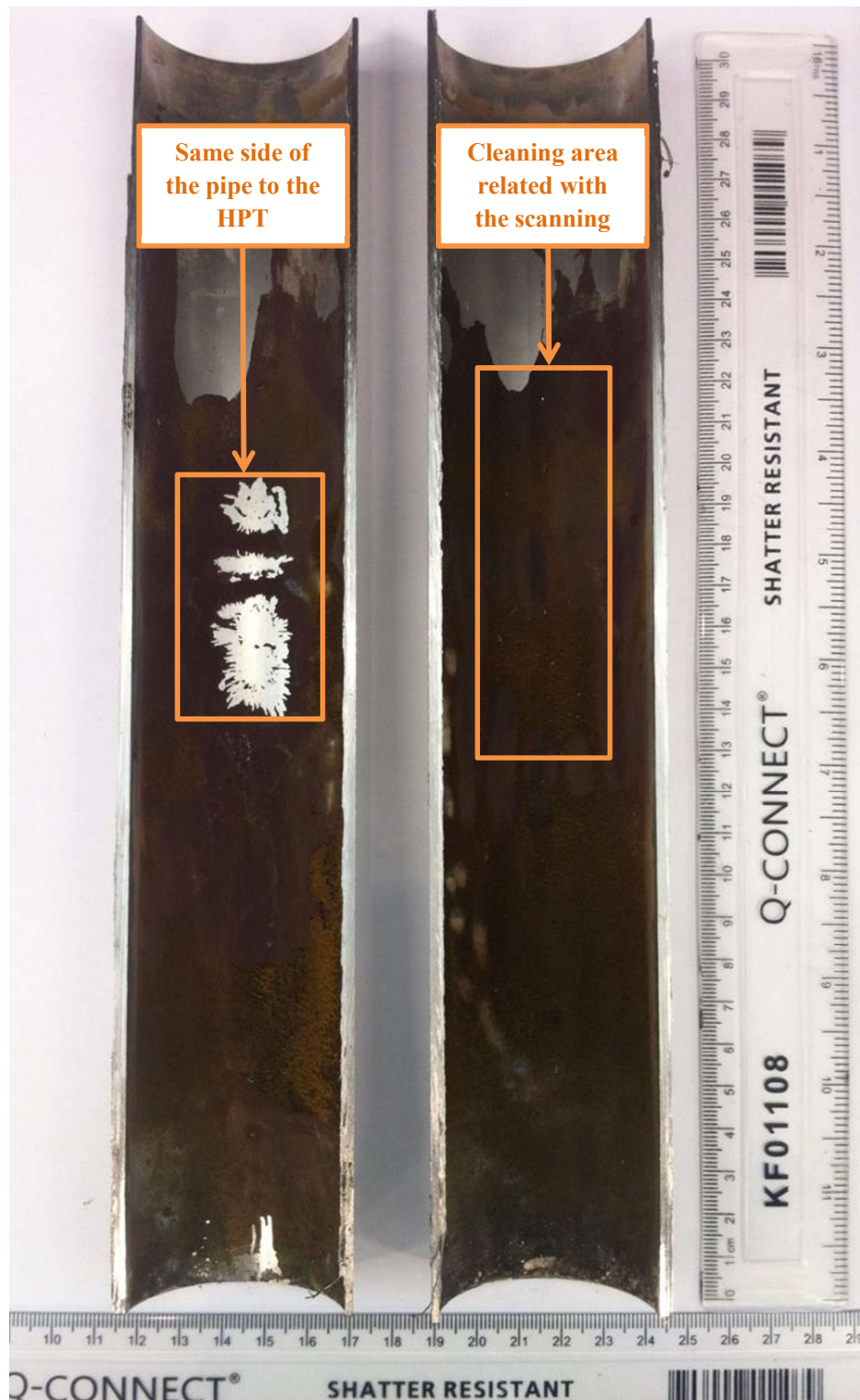


Figure 7.9. Inside wall of pipe number 1 halved after the cleaning.

A focus stacked image of the location related with the cleaned area presents a distribution of removal of soft fouling, Figure 7.10. This was also observed in the location of the nodes and antinodes of the vibration. As it can be seen the nodes present no cleaning evidence in contrast

to the centre of the antinodes in which the maximum cleaning capabilities are presented. Figure 7.10 explains three different amounts of removal.

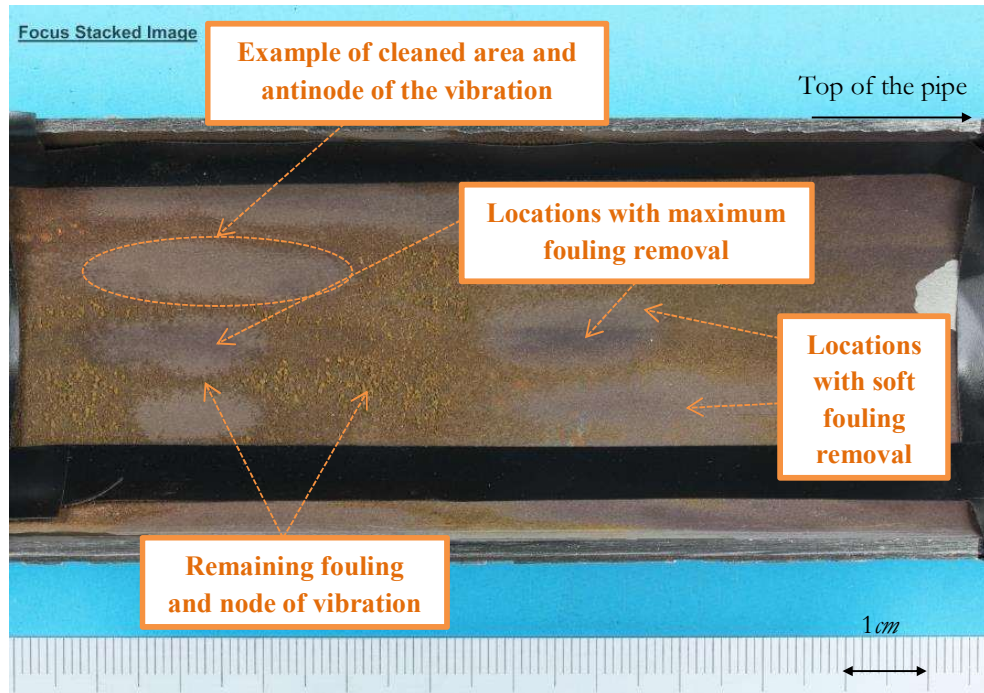


Figure 7.10. Inner surface of the pipe after the cleaning procedure and representation of the cleaning areas related with the nodes and antinodes of the vibration.

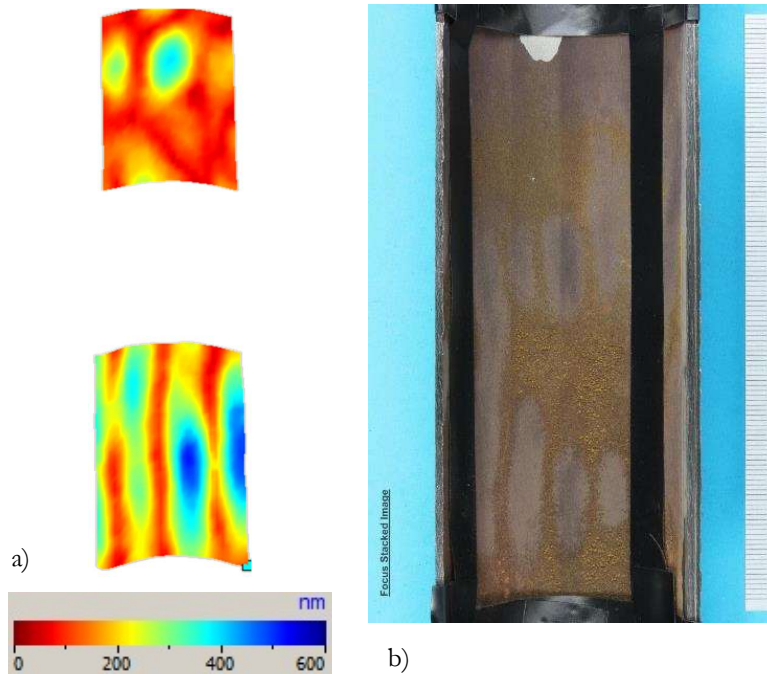


Figure 7.11. Displacement representation obtained with the 3DSV and the relation with the cleaning areas of pipe 1).

Figure 7.11 presents the relation between the cleaning performance and the 3D image of the scanning area and the results of cleaning in pipe 1).

To associate the type of cavitation that is more likely to be connected with the cleaning capability the radial displacement must be calculated. After calculating the radial displacement, the acoustic pressure obtained is compared with the type of cavitation predicted by the plots generated. Figure 7.12 presents the cavitation prediction plots for the experiments executed in pipe 1).

The relation between the cavitation prediction plots and the displacements obtained with the vibrometer can be obtained with equation (4.20) and using the radial displacement D_r as the amplitude A in the equation. Then, with P and knowing the atmospheric pressure P/P_0 it can be calculated for each point of the scanning area. Therefore, it is necessary to know the cavitation prediction plots for each cleaning experiment. Figure 7.12 presents the cavitation prediction plots of pipe 1). All these calculations were explained in Chapter 4. In these cases, the saturation value has been considered 1 since the water used has been exposed to air and is under equilibrium. In addition, it is important to note that this parameter only affects the rectified diffusion threshold which will affect the side of the bubbles that can cavitate depending on the displacement (which is considered out of the scope of this investigation).

Table 7-2. values used of the calculation of the cavitation prediction plots of pipe 1).

Magnitude	Symbol	Value	Units
<i>Surface tension of water at 20 °C</i>	$\sigma_{20\text{ }^{\circ}\text{C}}$	7.20E – 02	N/m
<i>Speed of sound in water at 20 °C</i>	$c_{20\text{ }^{\circ}\text{C}}$	1,482	m/s
<i>Ratio of specific heats at 20 °C</i>	$\kappa_{20\text{ }^{\circ}\text{C}}$	1.401	–
<i>Density of water at 20 °C</i>	$\rho_{\kappa_{20\text{ }^{\circ}\text{C}}}$	997	kg/m ³
<i>Atmospheric pressure at room conditions</i>	$P_{0\text{ }20\text{ }^{\circ}\text{C}}$	101,325	Pa
<i>Saturation on air gases</i>	C	1	–
<i>Frequency of excitation</i>	f	32.75	kHz
<i>Resonance radius</i>	R_{RES}	110	mm

Cavitation prediction plot for pipe 1) experiment

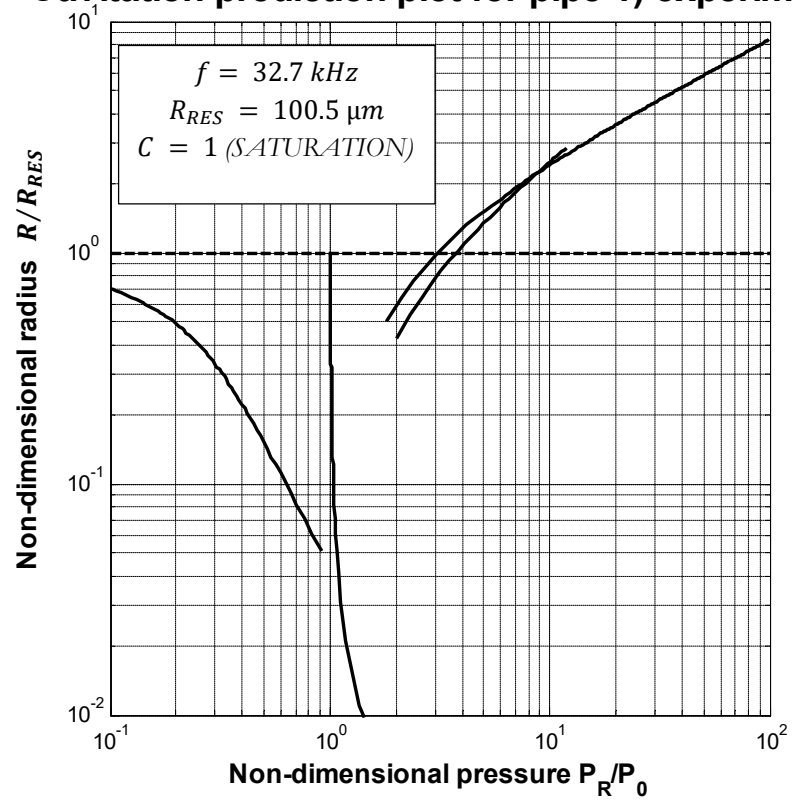


Figure 7.12. Cavitation prediction plot for the conditions applied in the investigation of pipe number 1) experimentation.

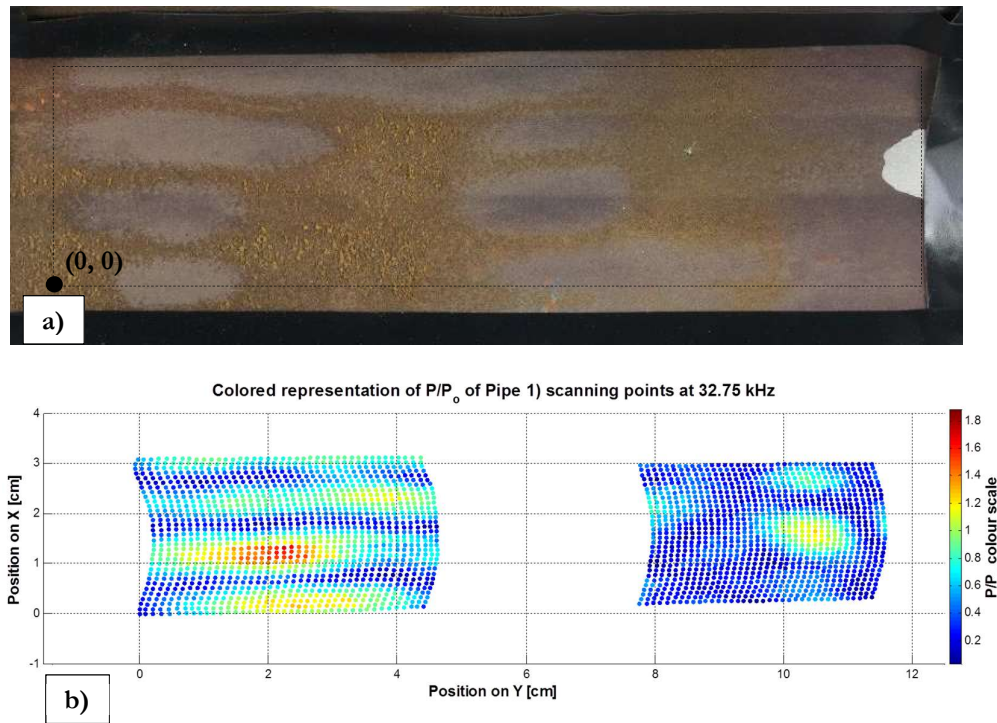


Figure 7.13. Comparison between the cleaning results and its relation with the P/P_0 per point of the scanning area for the pipe 1).

Figure 7.13 a) presents the cleaning results in the inner wall of pipe 1), it also includes the relative location of the origin $(0, 0)$ of the surface. Figure 7.13 b) represents the relation P/P_0 of each of the 2500 scanning points on the scanning surface. As can be seen in the figures the threshold for the cleaning of soft fouling is around $0.7 P/P_0$. This has an associated value of $0.233 \mu\text{m}$ for the displacement in the radial direction. In addition, it can be seen that the highest value of P/P_0 is around 1.7 which has an associated a displacement of $0.57 \mu\text{m}$. It is important to observe that in this case none of the hard scale fouling has been removed from the pipe.

The comparison of the results with the cavitation prediction plots evidence that only some of the points with a value above 1.6 fall in the transient cavitation area. The majority of the values of P/P_0 in this case are located in the regions A and B of the potential types of cavitation which is the type of cavitation used in classic ultrasonic cleaning [202], [203]. In addition, it can be stated that only existing cavities in the liquid above $0.1 R/R_{RES}$, $10.05 \mu\text{m}$ will produce cavitation at the minimum values of displacement measured by the 3DSV that correspond with around $0.6 P/P_0$. Finally, it can be concluded that the cleaning performance has not been sufficient and the pipe is still not visible after the excitation therefore the displacements generated are not able to remove fouling under the conditions applied.

7.3.2 Pipe number 2)

Pipe number 2) was excited also with transducer T43 and with a total power of 65 W for 30 minutes but in this case the frequency used for the excitation was 33.65 kHz and was selected with the same procedure as presented for pipe 1). Figure 7.14 presents the FFT analysis of the contact surface for this experimentation. The excitation results are presented in

Table 7-3.

Table 7-3. Parameters of the excitation of pipe number 2.

	<i>Value of the parameter</i>
<i>Transducer</i>	T43
<i>Power Input</i>	65W
<i>Excitation Frequency</i>	33.6 kHz
<i>Duration of the excitation</i>	30 min

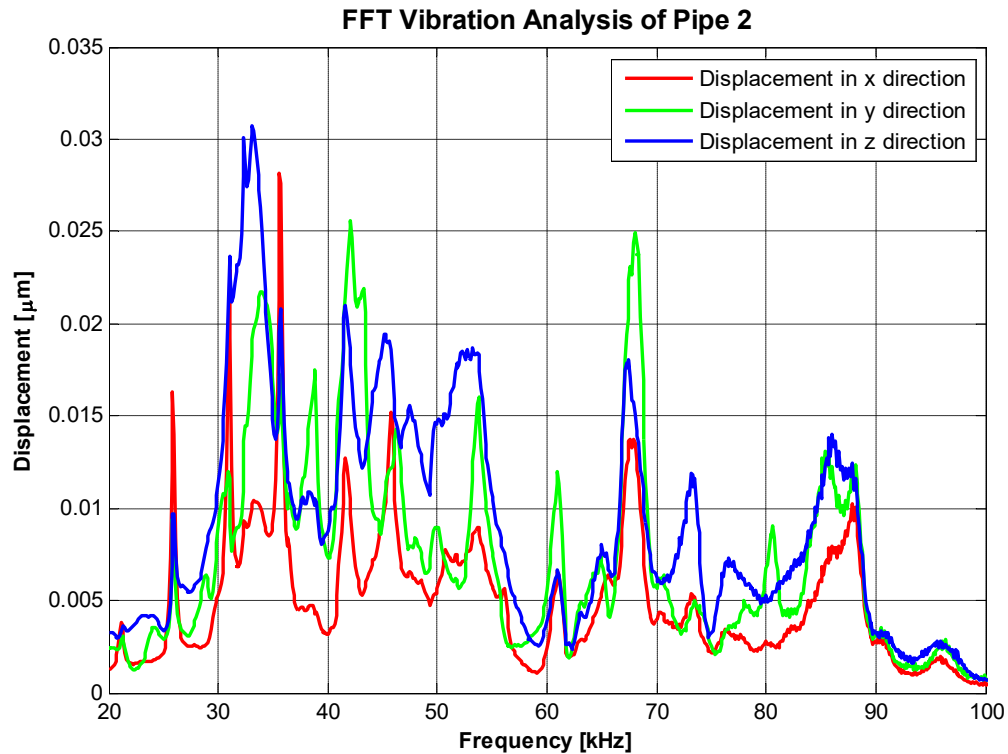


Figure 7.14. FFT analysis of the scanning surface for pipe number 2) to find the frequency that produces the largest displacements in the Z direction.

The number of points in the scanning area measured by the 3DSV is 1625. The number of values taken per point is 100. The 3DSV sample frequency was 512 kHz with a resolution of 125 Hz.

The results obtained after cleaning are presented in Figure 7.15 and Figure 7.16. Similarly, to pipe 1) the clearest cleaning results are in the opposite side of the HPT location. In contrast to pipe 1) there is a location with full removal of fouling.

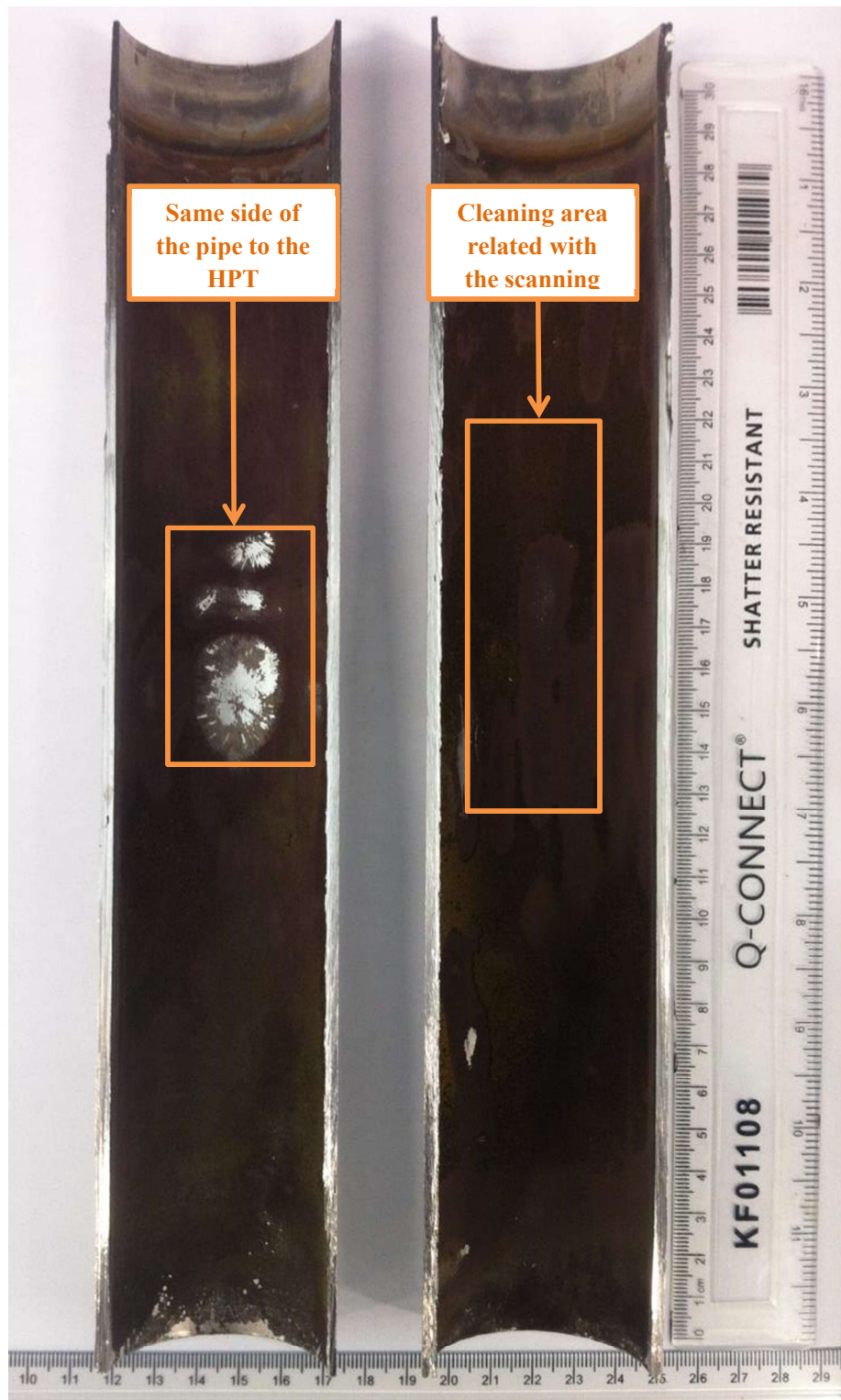


Figure 7.15. results of cleaning in pipe 2).

Figure 7.16 presents the focus stacked image of the cleaning area related to the scanning area of pipe 2). In this case four different types of results can be found; the locations which do not present visible results of cleaning, locations where the softer fouling has been removed, locations where the hard fouling has started to be removed which presents a colour darker that of the surrounding area with soft fouling cleaned, and finally two locations where the hard scale has been completely removed.

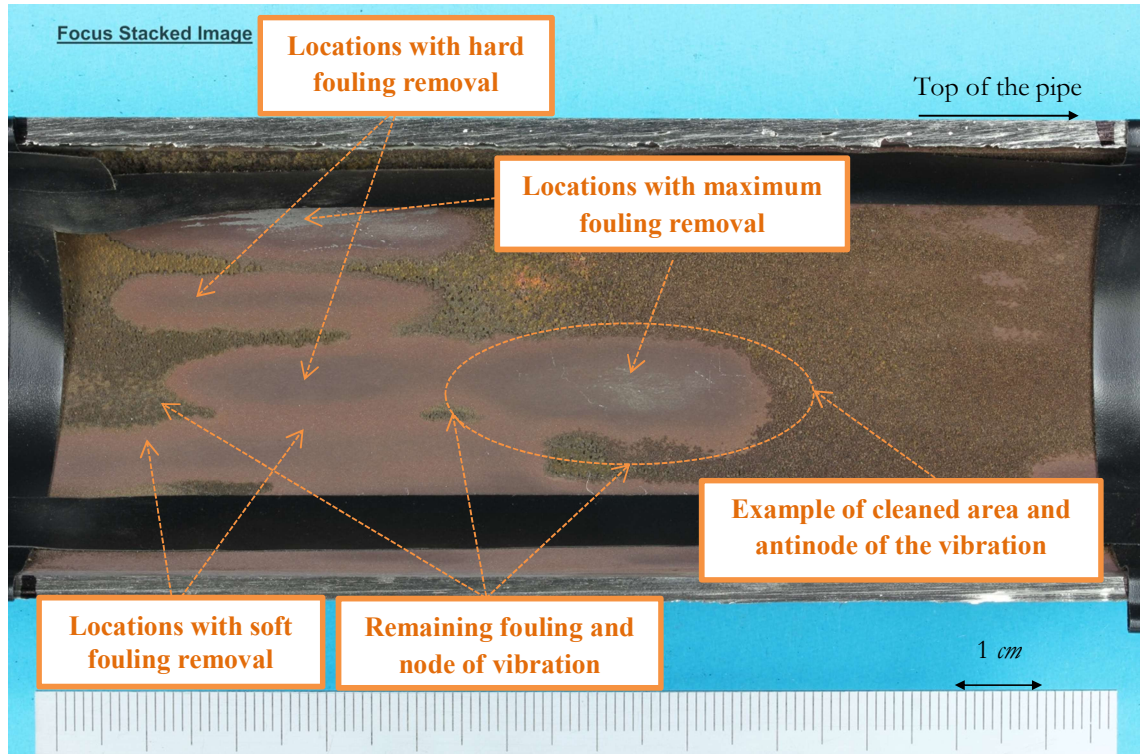


Figure 7.16. Inner surface of the pipe after the cleaning procedure and representation of the cleaning areas related with the nodes and antinodes of the vibration of pipe 2.

The cleaning results of Figure 7.16 can be related with the vibrometer results as per Figure 7.17 for pipe 2).

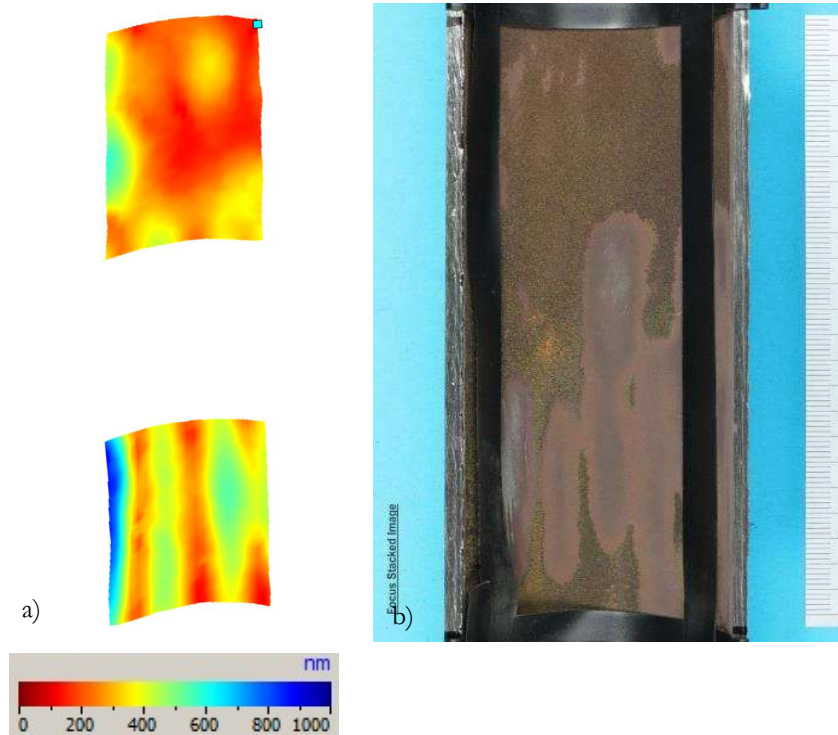


Figure 7.17. Displacement representation and the relation with the cleaning area of pipe 2).

Figure 7.17 presents the total displacement measured by the vibrometer and the corresponding cleaning area. As explained above, this total displacement can be used to calculate the displacement in the radial direction and with this it is possible to calculate the relation P/P_0 and link the cleaning results with the cavitation that is more likely to be produced. The cavitation prediction plots for the experimentation of pipe 2) are presented in Figure 7.18 and the values used for its calculations are included in Table 7-4.

Table 7-4. Values used of the calculation of the cavitation prediction plots of pipe 2) experiments.

Magnitude	Symbol	Value	Units
Surface tension of water at 20 °C	$\sigma_{20\text{ }^{\circ}\text{C}}$	$7.20E - 02$	N/m
Speed of sound in water at 20 °C	$c_{20\text{ }^{\circ}\text{C}}$	1,482	m/s
Ratio of specific heats at 20 °C	$\kappa_{20\text{ }^{\circ}\text{C}}$	1.401	—
Density of water at 20 °C	$\rho_{\kappa_{20\text{ }^{\circ}\text{C}}}$	997	kg/m^3
Atmospheric pressure at room conditions	$P_{0\text{ }20\text{ }^{\circ}\text{C}}$	101,325	Pa
Saturation on air gases	C	1	—
Frequency of excitation	f	33.65	kHz
Resonance radius	R_{RES}	97.7	mm

Cavitation prediction plot for pipe 2) experiment

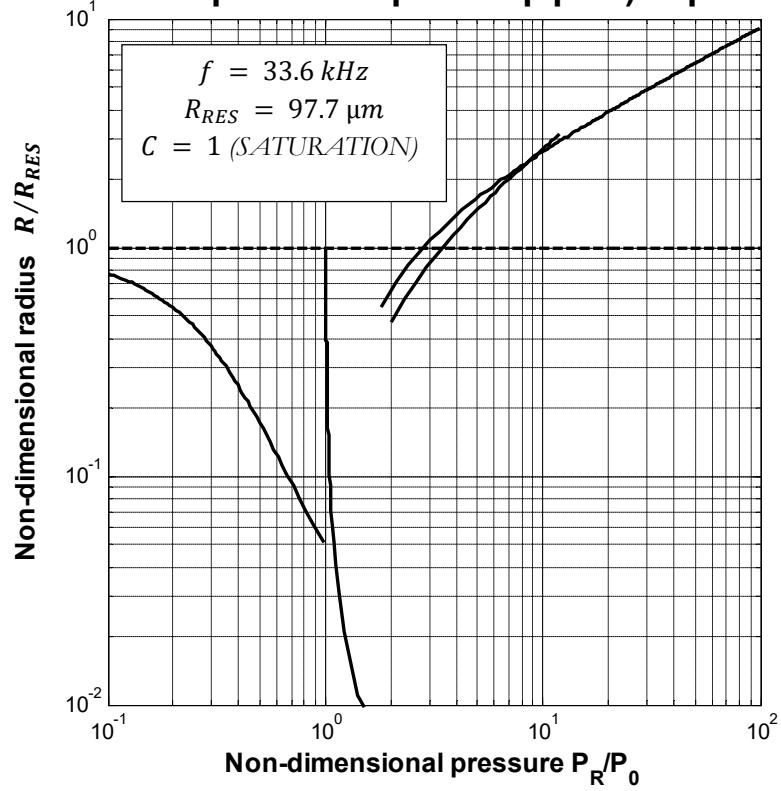


Figure 7.18. Cavitation prediction plot of the conditions applied in the investigation of pipe number 2) experimentation.

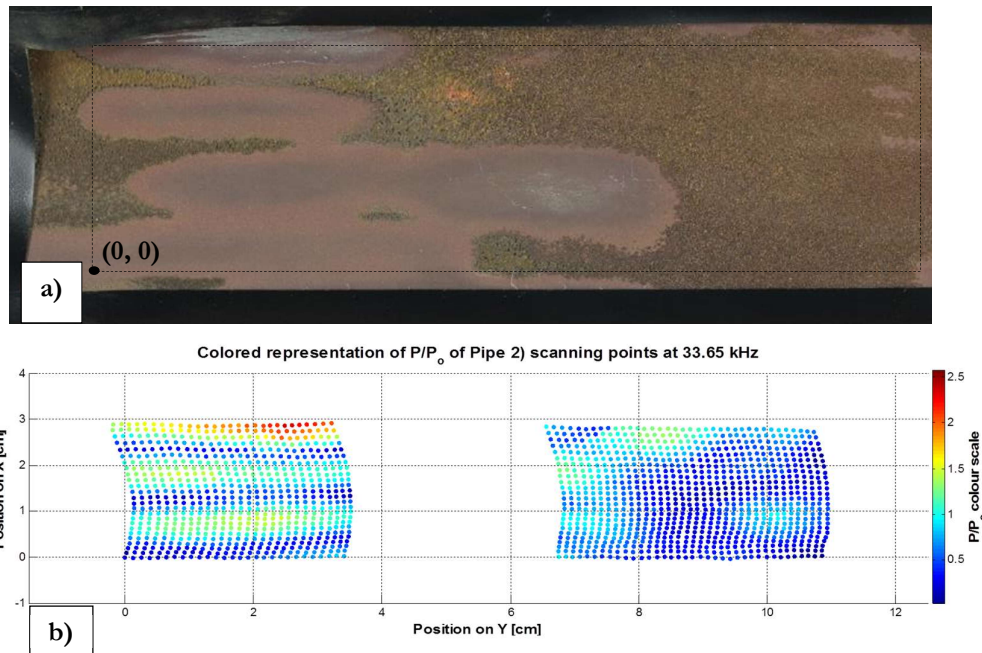


Figure 7.19. Comparison between the cleaning results of and its relation with the P/P_0 per point of the scanning area for pipe 2).

Figure 7.19 a) presents the FSI of the cleaned area of pipe 2) and the location of the reference point (0, 0). Figure 7.19 b) presents a coloured representation of the value of P/P_0 at each point

of the scanning surface and the coordinates of the points to facilitate the relation with the point (0, 0) of Figure 7.19 a). This image is similar to Figure 7.17 a) but the values at each point have been converted to radial displacement and then to the relation P/P_0 of the selected points for the analysis. The colour of each point can be related with the colour scale of Figure 7.19 b) and therefore with P/P_0 and this with the cavitation prediction plots for this experiment, Figure 7.18.

As described above four results in cleaning can be found in this pipe. All the points with values below $0.5 P/P_0$ present no-results in cleaning. The soft fouling is removed with any value above $0.6 P/P_0$ which is represented with light blue.

In the locations with symptoms of hard scale removal appear with values of P/P_0 above 1.4 and these have a displacement of $0.47 \mu\text{m}$. These points are allocated above Blake's threshold. The cleaning has an improvement related with higher amplitude that improves the microstreaming due to the cavity oscillation [202], [203].

Finally, the fully cleaned locations have a value of P/P_0 above 1.9 which has a displacement associated of $0.63 \mu\text{m}$. This falls in the transient cavitation area (figure Chapter 4) and therefore the removal efficiency is increased by the impact of the jets generated by the implosion of surrounding cavities.

7.4 Summary

In this chapter has been demonstrated the concept of the removal of fouling from a pipe in different locations.

The pipe wall displacement measured simultaneously with the cleaning process has been correlated with the ratio P/P_0 , and with the cavitation prediction plots.

It has been established that any type of cavitation can remove soft fouling but the hard scale fouling needs cavitation above Blake's threshold.

It has been demonstrated that the best results of cleaning are presented in the locations where the amplitude of the radial displacement is able to generate transient cavitation.

8 Preindustrial trials

After proving the concept of cleaning small tubes under laboratory conditions it is time to go one step further and demonstrate the concept in an industrial pipe. Here the transducers and the collar developed in a project related with this investigation, UltraCleanPipe (<http://www.ultracleanpipe.com/>), were tested in under laboratory conditions and later industrial food processing plant laboratory.

8.1 UltraCleanPipe collar and transducers test

For the preindustrial experimentation, pipe 3) was excited also with transducer V1 (Appendix A) in the same manner as was used for pipes 1) and 2). In this case also collar produces in the project UCP (Appendix A) is also used to improve the attachment. The specifications of the collar and the transducer can be found in Appendix A. The transducer was excited with a total power of 65 W for 30 min but in this case the frequency used for the excitation was 40.46 kHz and was selected with the same procedure as presented in pipes 1) and 2). The FFT analysis of the contact surface for this experimentation is presented in Figure 8.1. The excitation parameters are presented in Table 8-1.

Table 8-1. Parameters of the excitation of pipe number 2.

	Value of the parameter
Transducer	<i>V1</i>
Power Input	<i>65W</i>
Excitation Frequency	<i>40.46 kHz</i>
Duration of the excitation	<i>30 min</i>

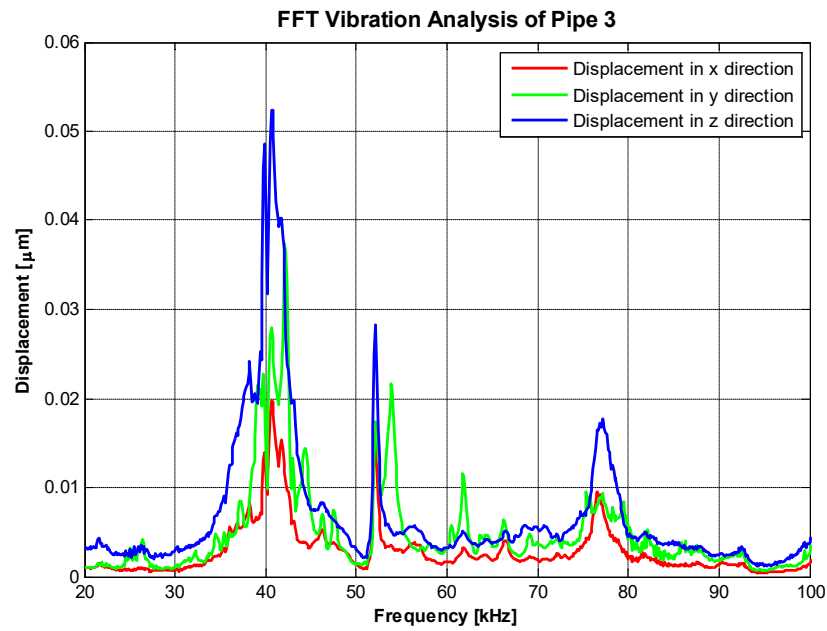


Figure 8.1. FFT analysis of the scanning surface for pipe number 3) to find the frequency that produces the largest displacements in the Z direction.

The cleaning experiment was performed at the same time that the 3DSV measured the actual vibration of the scanning surface. This was done with 2500 scan points on the surface and by collecting 100 signals per scan point for the average. The 3DSV sample frequency was established at 512 kHz with a resolution of 125 Hz.

The results obtained in the cleaning area are presented in Figure 8.2 and Figure 8.3. Figure 8.4 presents the comparison between the cleaning area and the vibrometer results. In this case clear evidence of cleaning is presented along the whole perimeter of the location of the HPT.

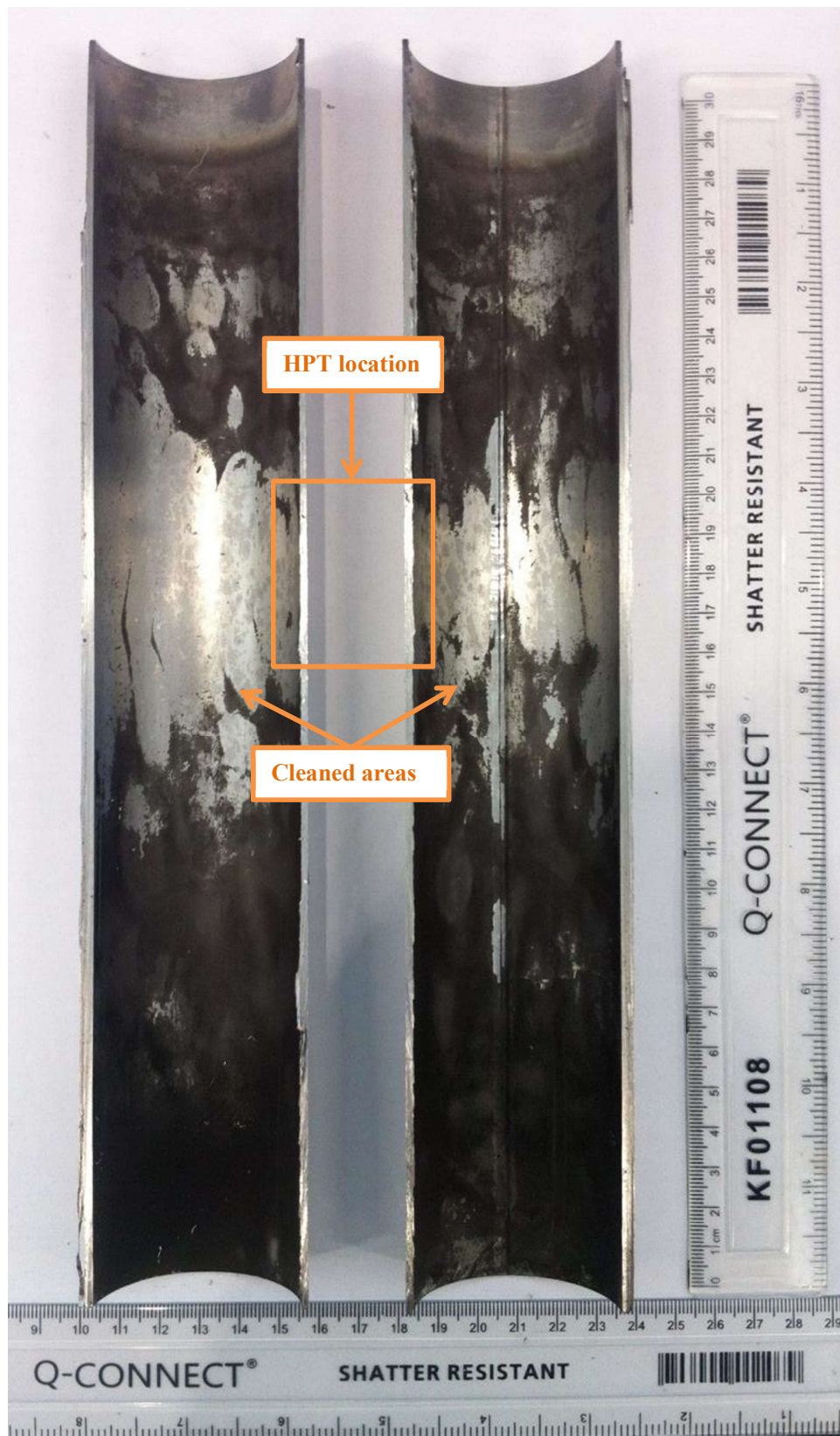


Figure 8.2. Inside wall of pipe number 3 halved after the cleaning.

A FSI image with the cleaning area related with the scanning area is presented in Figure 8.3. It also shows the location of the nodes and antinodes of the vibration. As can be seen, the nodes

show no evidence of cleaning in contrast to the centre of the antinodes in which the maximum cleaning capabilities are presented.

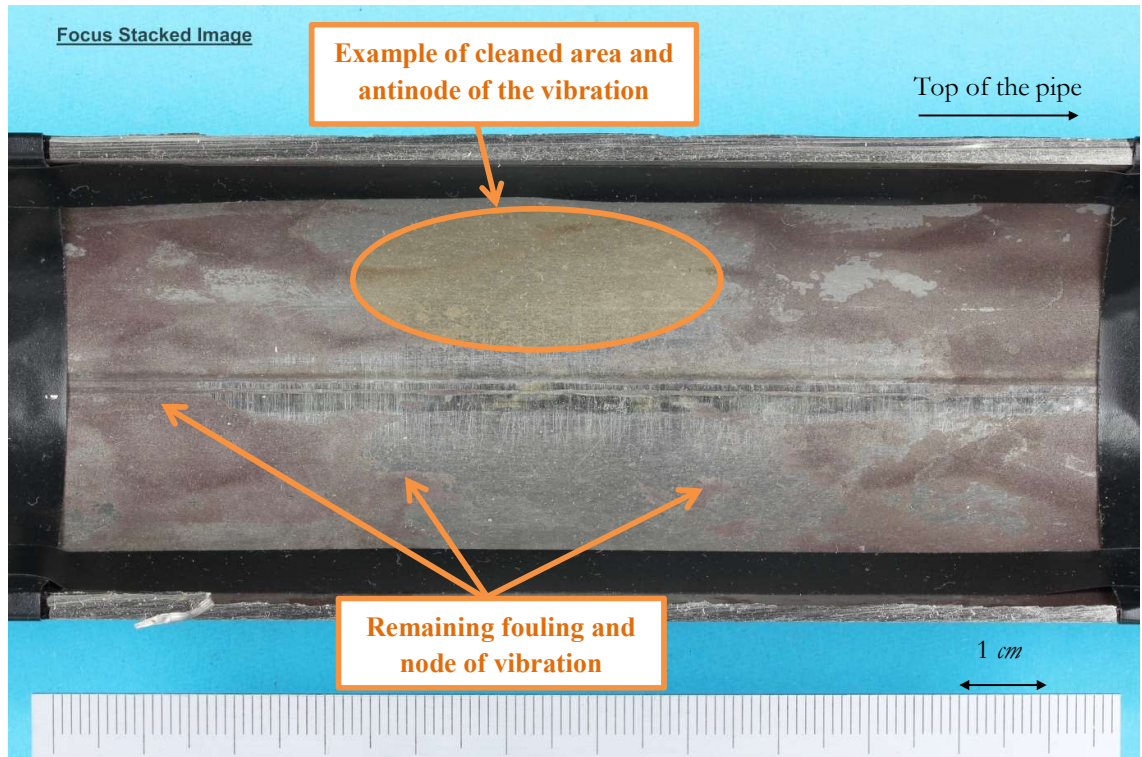


Figure 8.3. Inner surface of the pipe after the cleaning procedure and representation of the cleaning areas related with the nodes and antinodes of the vibration of pipe 3).

Figure 8.3 presents the cleaning results in the opposite side of the scanning surface. As can be seen in the FSI, it can be difficult to determine the boundaries between the cleaned and not cleaned zones. Therefore, modification to colour of the picture is applied in Figure 8.4.

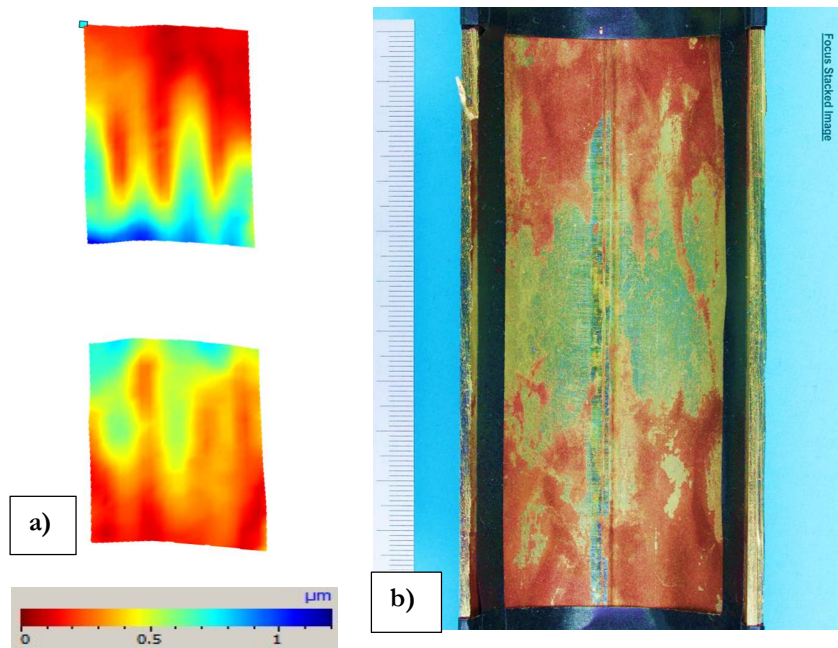


Figure 8.4. Displacement representation and the relation with the cleaning area. Specification of the maximum displacement and the threshold points selected.

Figure 8.5 represents the cavitation prediction plots for the experiments executed in pipe 3) and the parameters for the excitation are presented in Table 8-2.

Table 8-2. Values used of the calculation of the cavitation prediction plots of pipe 3) experiments.

Magnitude	Symbol	Value	Units
Surface tension of water at 20 °C	$\sigma_{20\text{ }^{\circ}\text{C}}$	$7.20E - 02$	N/m
Speed of sound in water at 20 °C	$c_{20\text{ }^{\circ}\text{C}}$	1,482	m/s
Ratio of specific heats at 20 °C	$\kappa_{20\text{ }^{\circ}\text{C}}$	1,401	–
Density of water at 20 °C	$\rho_{\kappa_{20\text{ }^{\circ}\text{C}}}$	997	kg/m^3
Atmospheric pressure at room conditions	$P_{0\text{ }20\text{ }^{\circ}\text{C}}$	101,325	P_a
Saturation on air gases	C	1	–
Frequency of excitation	f	44.46	kHz
Resonance radius	R_{RES}	73.98	mm

Cavitation prediction plot for pipe 3) experiment

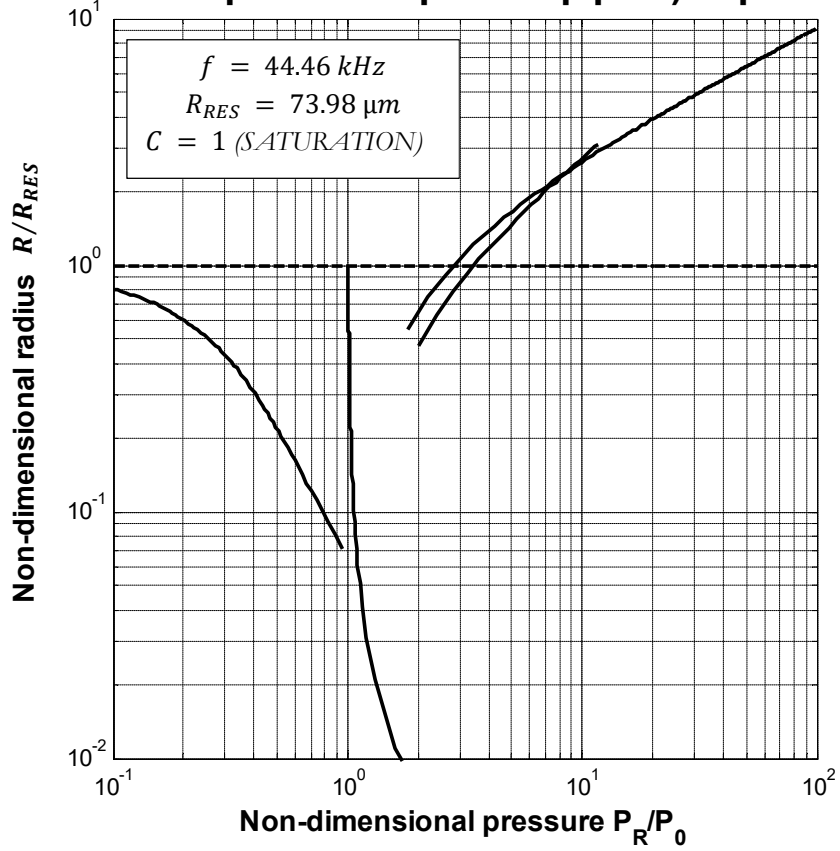


Figure 8.5. Cavitation prediction plot for the conditions applied in the investigation of pipe number 3).

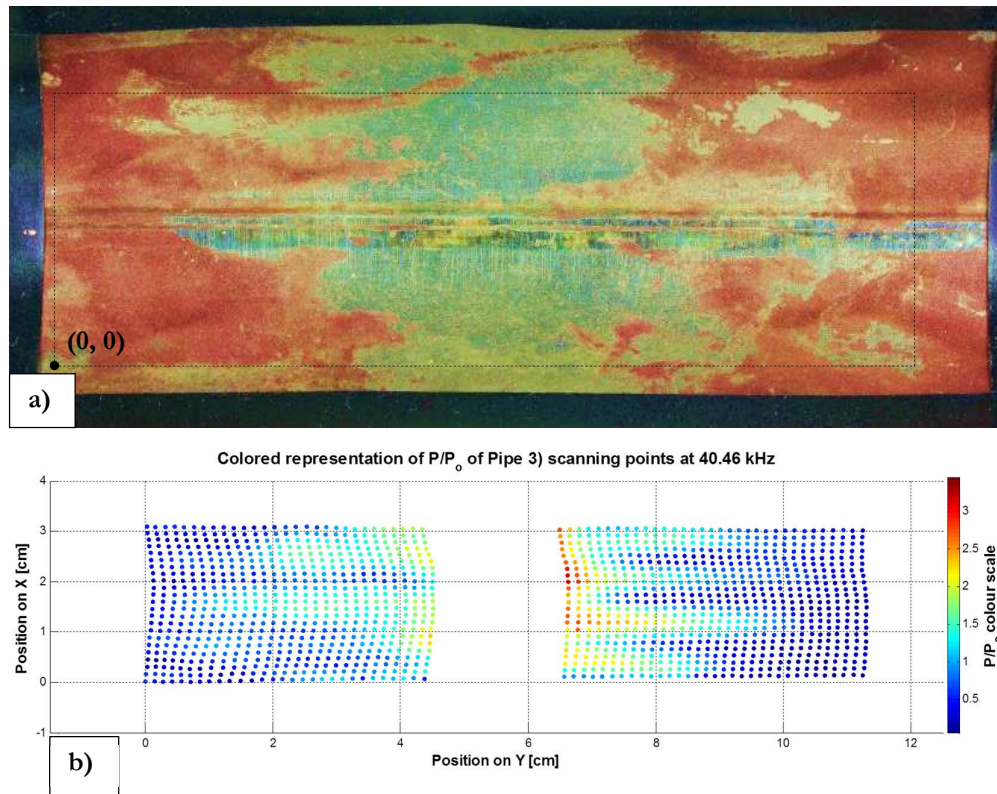


Figure 8.6. Comparison between the cleaning results and its relation with the P/P_o per point of the scanning area for pipe 3).

Figure 8.6 a) presents the cleaning results obtained in pipe 3). It also includes the position of the point (0, 0) on the surface. Figure 8.6 b) is the coloured representation of P/P_o of the scanning points. As can be seen, there are only two patterns of cleaning, the locations with no cleaning evidence and the location on which the pipe wall is visible and therefore the fouling has been removed.

In this case the minimum value of P/P_o from which cleaning results can be seen is around 1.5 having a displacement value that corresponds with $0.40 \mu\text{m}$. This value falls in the transient cavitation area and therefore it can remove Calcite as has been explained above.

Analysis of the pipe wall after cleaning

A further analysis of the pipe's wall integrity has been done using pipe 3). For this SEM images and a metallography of the cross Section area has been obtained from the locations where the cleaning performance has occurred.

Figure 8.7 presents the SEM of the inner wall of the pipe with some remaining fouling as well as the impact of a transient cavitation jet on the Calcite. This type of impacts has been described before in [204].

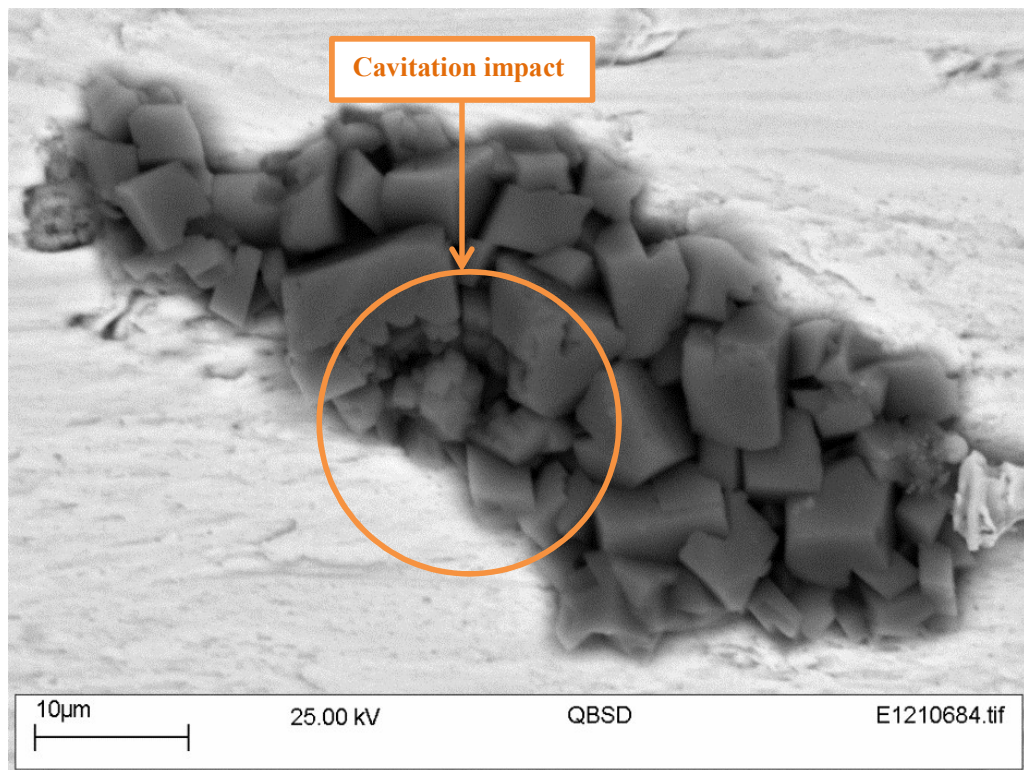


Figure 8.7. Remaining Calcite on pipe 3) inner wall with the impact of a cavitation.

In addition, presents a metallography of the cross Sectional area of the pipe in the antinodes of the cleaning. It can be seen that the wall of the pipe presents no visible cracks or damage due to the cleaning.

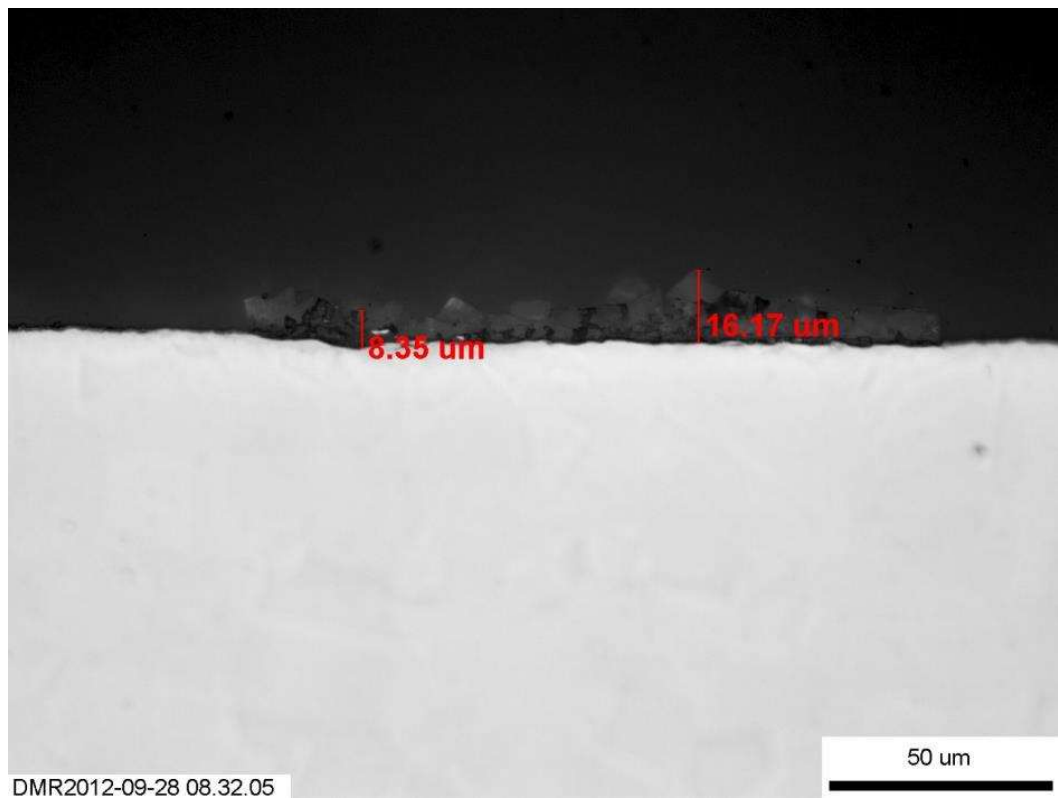
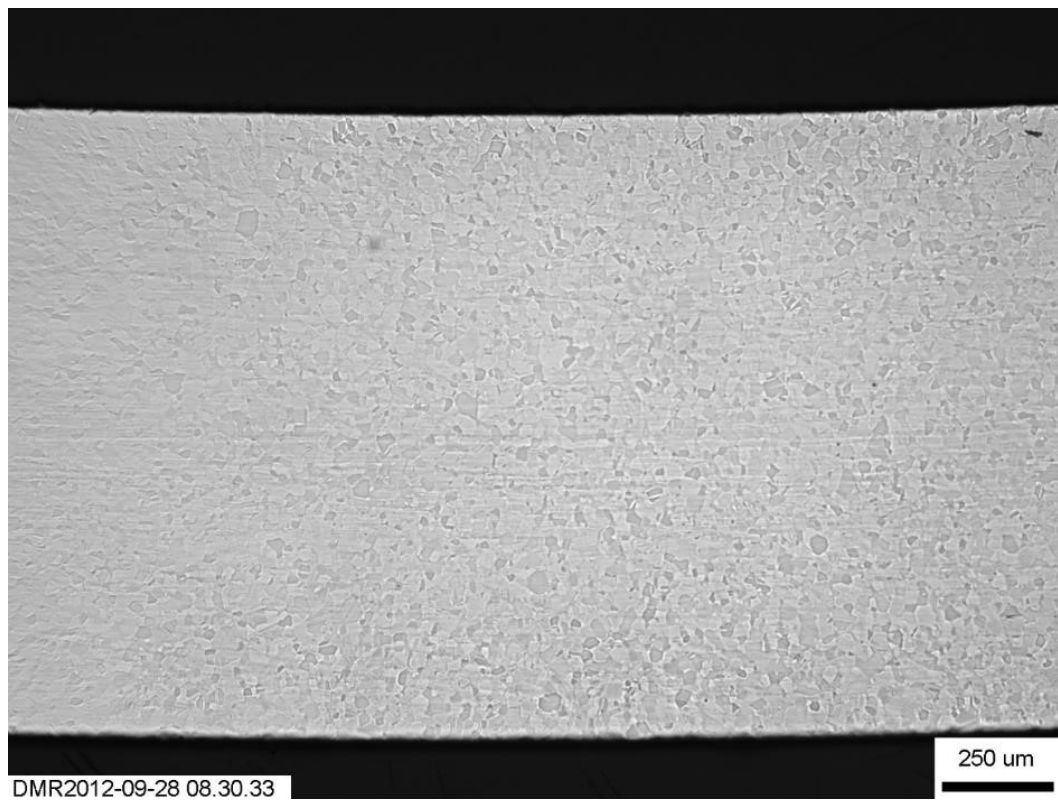


Figure 8.8. Metallography of the cross-section of pipe 3).

8.2 Field trials in an industrial laboratory

After testing the performance of UCP transducers and collar the system was tested under real conditions in an industrial laboratory on a 1.5 m stainless steel.

8.2.1 Fouling creation for the field trials

The fouling was created in a 1.5 m stainless steel pipe with 50 mm OD. This was achieved by heating the pipe to over 100⁰C to ensure that the water boiled, increasing the rate of the deposition process. As explained in Chapter 4 and similarly to the plates created (see Section 3.3.2), Calcite is fouled on the inner wall of an industrial pipe.

8.2.2 Fouling creation setup

- Stainless steel stands.
- 1500 mm length, 50 mm OD, 1.5 mm wall thickness, Stainless steel 316L pipe.
- Wood Stoppers.
- Funnel and hose (to introduce the solution).
- Highly concentrated solution of Calcium carbonate (Sodium hydrocarbonate 1.2g/l, calcium chloride 1.2 g/l).
- Heating plates and power supply.
- Thermocouple.

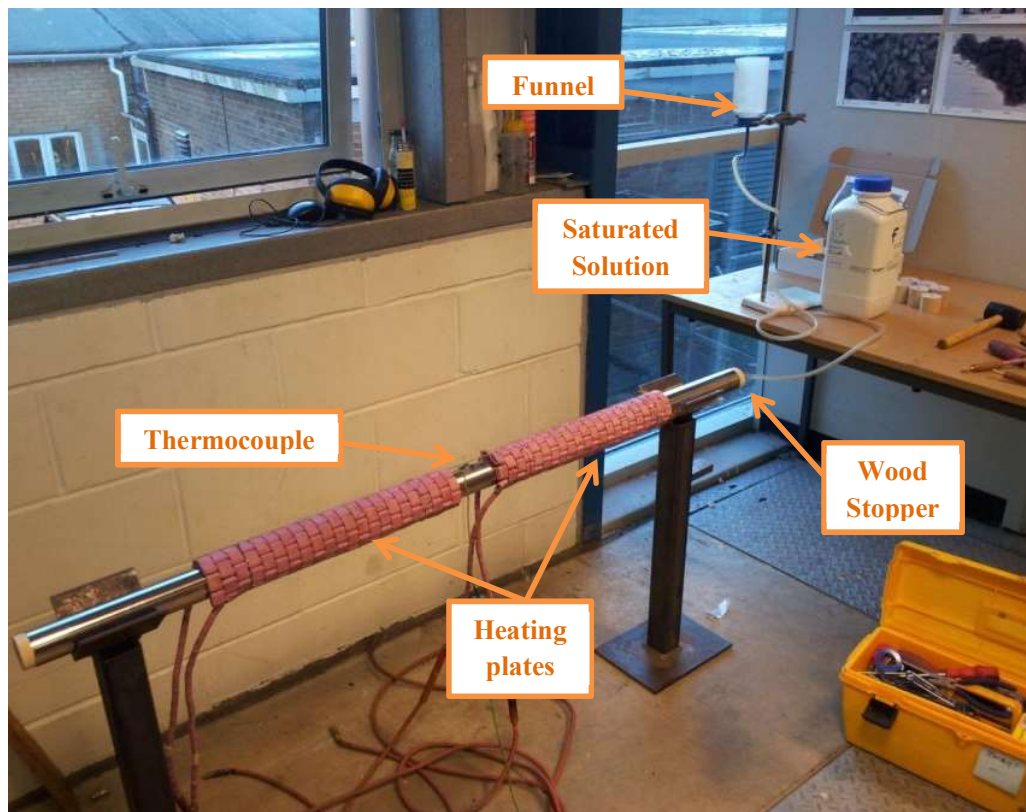


Figure 8.9. Setup for creation of fouling.

8.2.3 Procedure for the fouling creation

The pipe was held by two metal supports on the extremes, while the central part remained free to attach the heating plates. Then two wooden stoppers sealed each end of the pipe. These stoppers had a hole drilled in the middle of each one to allow introduction of water to the pipe, and also to allow the steam created by the heating to escape out of the pipe. The stoppers also ensured that some water always remained inside the pipe as shown in Figure 8.10. The pipe was levelled to ensure an even distribution of the water inside.

Once the pipe was ready with the heating plates and the stoppers it was heated up. This was done using a heat treatment module, whereby heating plates wrapped around the pipe increased the temperature of the pipe up to 120°C . Then, when it reached this temperature, the calcium carbonate solution was introduced using a hose attached to a funnel, as shown in Figure 8.9.

To monitor and control the temperature, a thermocouple was attached to the pipe between the two heating plates. In these experiments the pipe was heated up to 120°C for about 16 hours, rotated around 15° every 5 min, and introducing evenly about 0.15 litres of a calcium carbonate solution every 15 min.

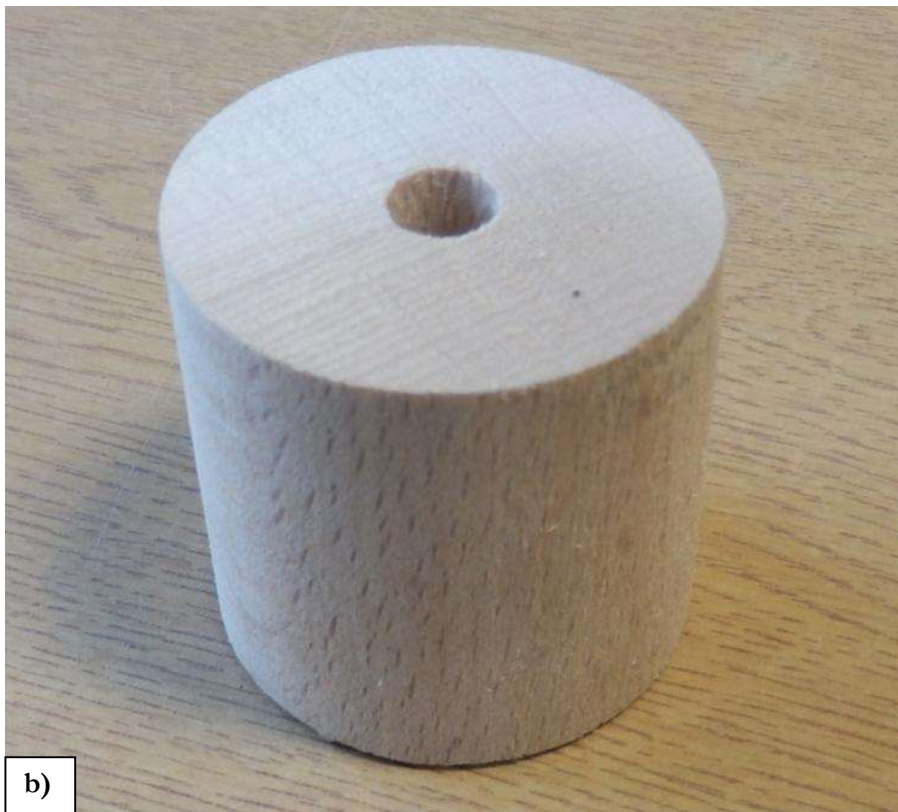


Figure 8.10. Images of the objects used to introduce the solution in the pipe.
a) Funnel, hose and solution.
b) Wood stoppers with a hole in the middle to allow introduction of the high concentration solution.

8.2.4 Fouling creation results

After the fouling creation process, the pipe was left to cool down without any mechanical disturbance to ensure the best formation of crystals of calcium carbonate on the surface of the pipe. The results of this method can be seen in Figure 8.11.

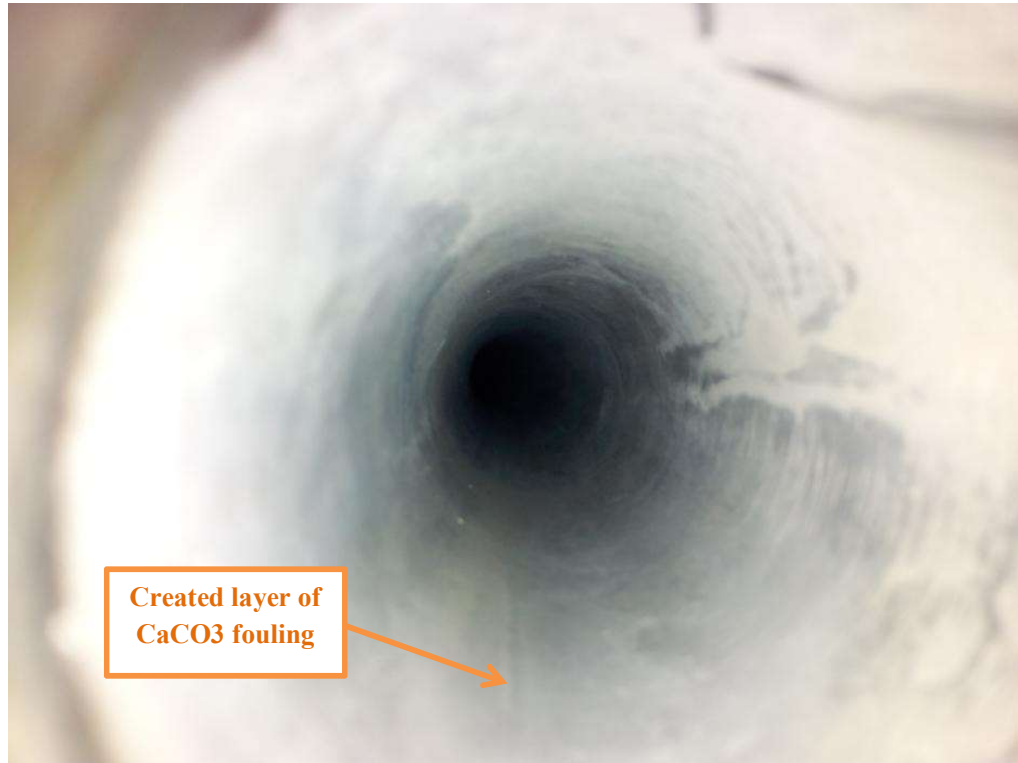


Figure 8.11. Even distributed CaCO_3 on the inner wall of the 1.5 m pipe.

8.3 Field Trials set-up and procedure

The fouled pipes were joined to a closed circuit to simulate an industrial environment. The components of this circuit can be seen in Figure 8.12.

Two different sets of transducers were attached to the pipe for ultrasonic excitation with and without flow. For the attachment, the collar described in Appendix A was used and a low acoustic attenuation couplant silicone was used as couplant (Section 5.2.3), and the following procedure was implemented.

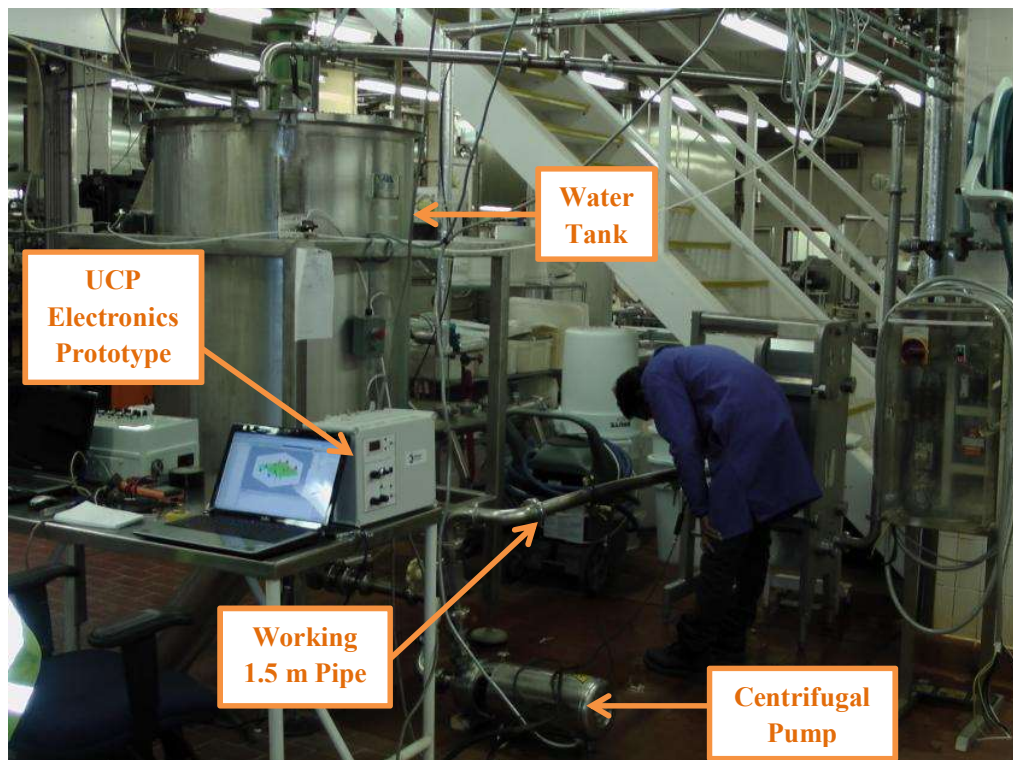


Figure 8.12. Field trials set-up in a real industry laboratory facility.

Frequency sweep

The first measurement was the calculation of the optimal frequency to be applied, for that a frequency sweep, with characteristics represented in

Table 8-3, was carried out to prove that the energy travelling would be higher when closer to the resonant frequency of the transducers. For this a “Teletest MK5” of Pi ltd unit was used for the signal transmission and reception.

Table 8-3. Frequency sweep parameters for the optimal frequency selection.

Pitch-Catch frequency sweep

High power transducer, Transmitting - PZT transducer, Receiving

Frequency Range- 20 kHz – 80 kHz

Steps- 181 (every 0.5 kHz)

Sampling period for each measurement 5000 microseconds

Distance between HPT and PZT: 114cm

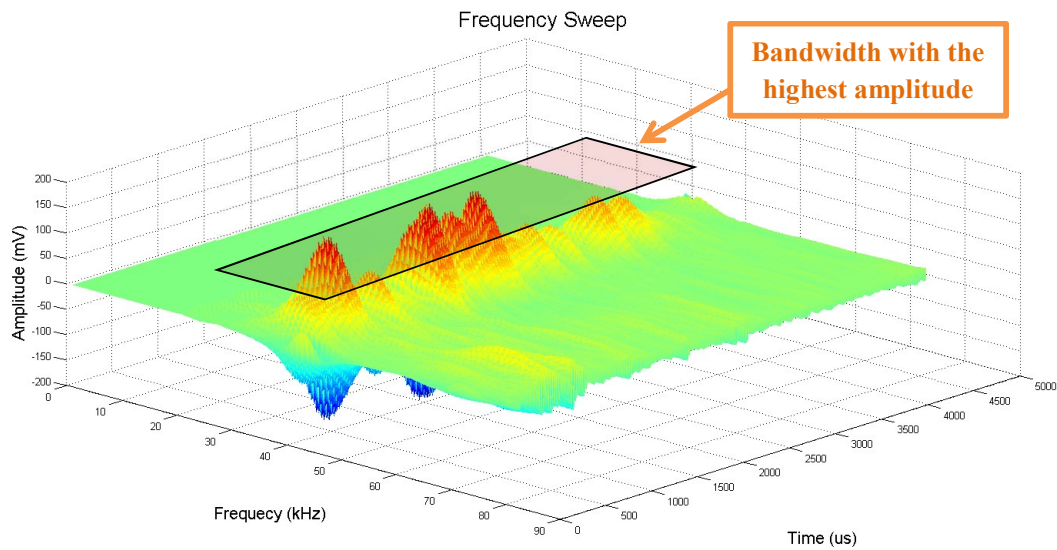


Figure 8.13. Frequency Sweep from 20 kHz to 80 kHz applied on the pipe for the optimal frequency selection.

The results of the frequency sweep are presented in Figure 8.13. It can be seen that frequencies closer to the frequency of 40 kHz have higher amplitude than the rest of the frequencies.

Position of the second transducer

In order to find the optimal position for the second transducer, 32 measurements were taken of the signal produced by an HPT allocated in the position 0 and, received by other HPT allocated in the positions presented in

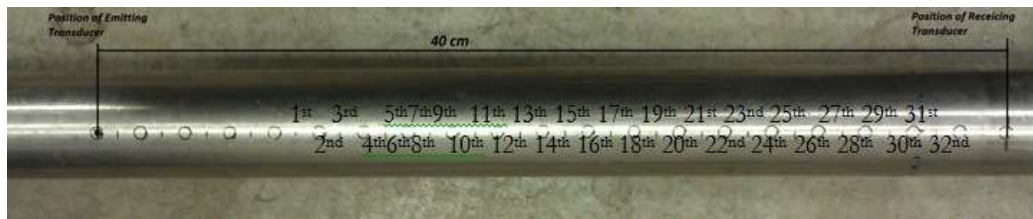


Figure 8.14 with a distance of 1cm per location. The signals were produced and received with “DSO-X 2012A Agilent Oscilloscope”. It is important to note that in the first nine positions the receiving transducer cannot be clamped because of the large size of the supports of both transducers.

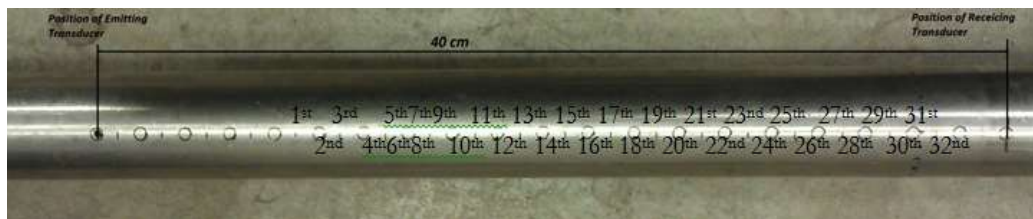


Figure 8.14. Relative position of the second HPT referred to the location of the first HPT for the field trials.

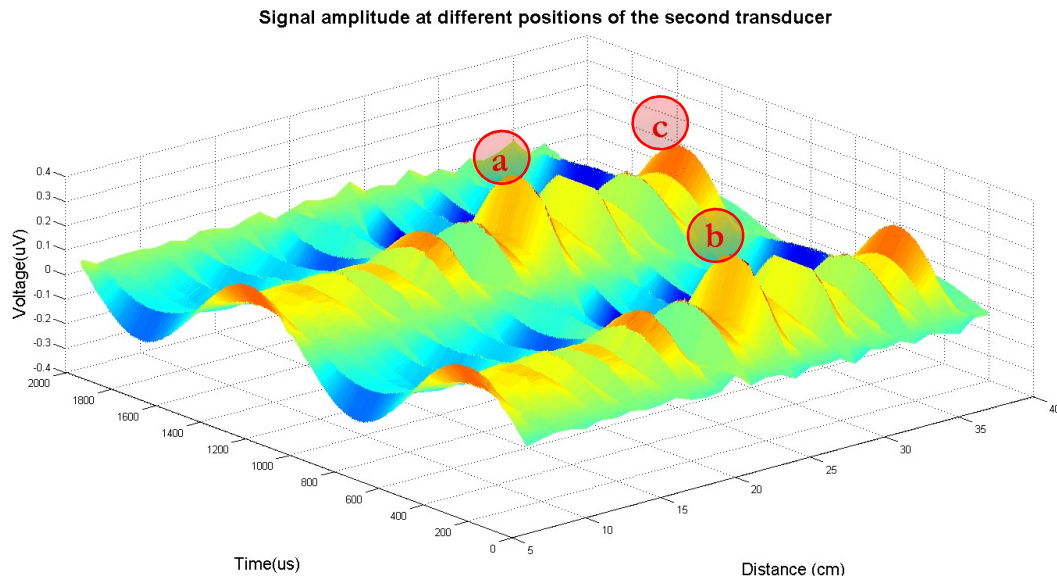


Figure 8.15. Amplitude of the signal for each position of the second transducer.

Figure 8.15 presents the results of the measurements for the optimal location of the transducers. It can be seen that at 25 (a), 28 (b) and 38 (c) cm from the first transducer the signal has larger amplitude than at the other positions, therefore the transducers were placed at that distance for the experiments.

8.4 Final trials procedure

After the pipe is attached to the process and is filled with water two different experiments were performed. The first one with no flow, and the second one with flow to compare the results.

No-water flowing trials

One of the fouled pipes was connected to the circuit presented above and was filled with water to simulate the static pressure of an industrial pipe. Then 5 HPT transducers were attached to the pipe at 25 cm intervals. These transducers were excited with a voltage of 650 V and a current of 1.9 A with the UCP 4 channel prototype driver unit⁵ for 30 minutes. Figure 8.16 illustrates the setup.

The results of this first cleaning in the field trials are shown in Figure 8.17. It can be seen that the cleaning results have an uneven distribution due to the interferences generated by all the waves generated by each of the five HPTs.

⁵ The specifications for the electronics used to excite the transducers can be found in Appendix B.



Figure 8.16. HPT transducers attached with low acoustic attenuation couplant silicone and UCP support clamped to a 1.5 m pipe for the field trials for the non-flow experimentation.

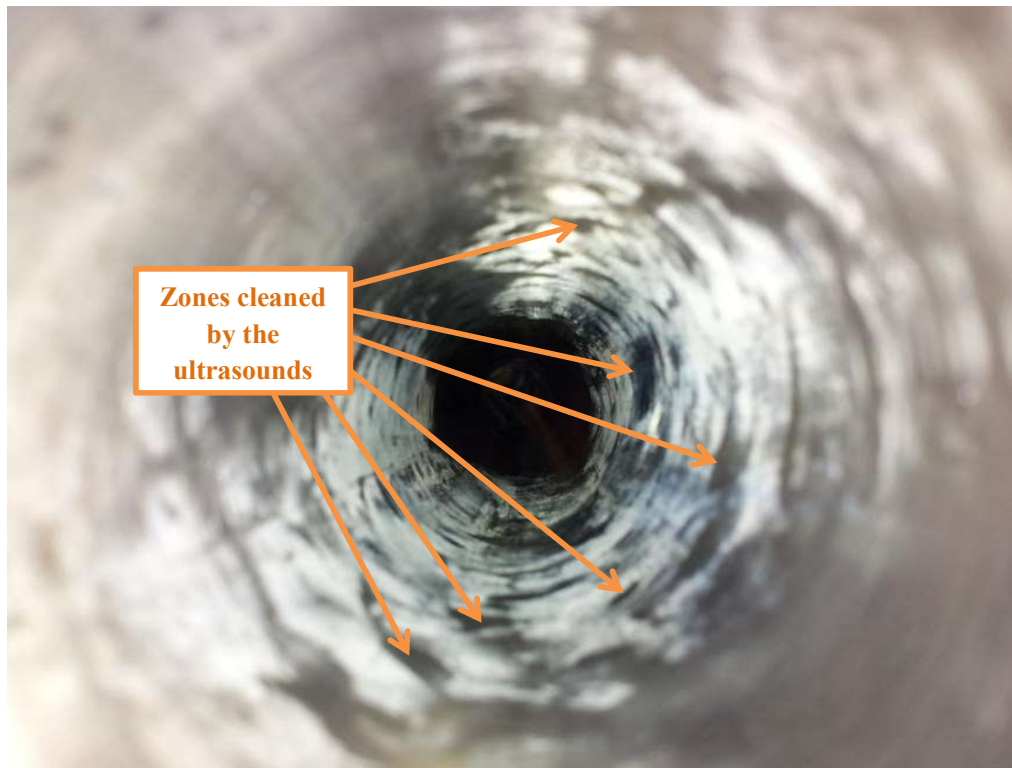


Figure 8.17. Results of the cleaning in the pipe with no flow conditions.

Water flowing trials

For the second experiment a pipe with a thin scale of Calcite fouling was connected to the same circuit. Then four HPT transducers were attached to the pipe and excited with the prototype driver, with a voltage of 650 V and a current of 1.9 A. The transducers were connected in series as Fig. 10 shows.

The pipe was filled with water and the pump of the circuit was turned on, supplying a pressure of 0.5 bar and a constant flow of 230 l/min. Once the flow was running, the HPTs were excited for 30 minutes.

The results taken from this experiment can be seen in Figure 8.19 and in Figure 8.20.

This pipe was cut in different pieces without damaging the cleaning results, in order to analyse the whole inner surface at the same location where the transducers were located.



Figure 8.18. UltraCleanPipe transducers and support attached for the field trials. Flow of 230 l/min.



Figure 8.19. Sections of the pipe cleaning with flow.

The cleaning results obtained with this method can be seen better in Figure 8.19 where it is possible to distinguish the distribution of the cleaned regions, matching with the node distribution of the wave measured with the Vibrometer laser on the pipe. Figure 8.20 shows the distribution of nodes and antinodes of a 40 kHz wave produced in a pipe filled with water.

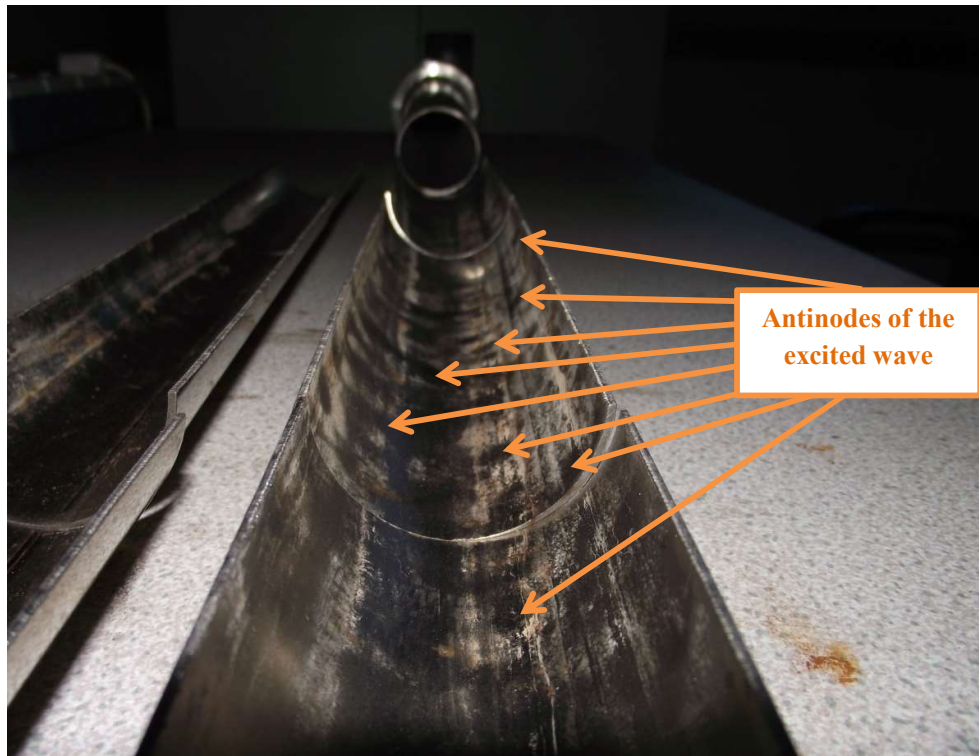
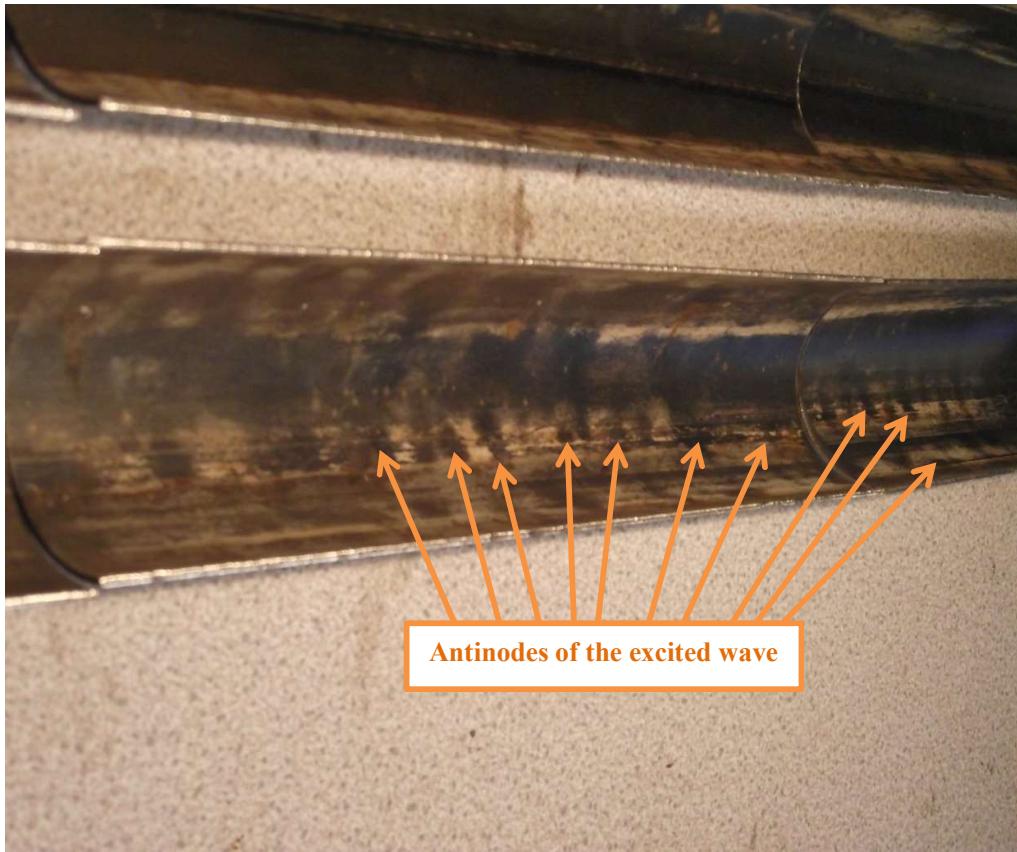


Figure 8.20. Inner section of the pipe cleaned with a flow of 230 l/min and a pressure of 0.5 bar.

8.5 Summary

This chapter contains the pre-industrial experimentation to demonstrate the concept of the use of ultrasound for pipeline cleaning.

The generation of fouling in a 1.5 m 316L stainless steel pipe due to the evaporation of a high concentration solution of calcium carbonate and due to the inverse solubility of calcium carbonate has been presented.

The locations in which signals with higher amplitudes can be found for the location of the second transducer and five and four transducers have been excited under industrial conditions both with non-flow and with flow respectively have been calculated.

The results obtained reveals that the pipe has only been cleaned in some of the locations both with and without flow.

9 Conclusions

This chapter contains the main conclusions obtained from this work, including comparison of the proposed method with classic ultrasonic cleaning and the recommendations for future work.

9.1 Conclusions

It has been proved in this thesis that it is possible to remove hard scale fouling from the inner wall of a pipeline using ultrasonic waves guided. The approach to the solution has been done by using the most common fouling in industrial and domestic pipelines: Calcite. The cleaning occurs in the inner wall of the pipes via its own vibration which generates cavitation whose shock waves of stable cavitation or the impact of jets generated by transient cavitation break the fouling and removes it from the metallic surface. The analysis of the samples cleaned presents no damage to the structural health during or after the cleaning procedure.

A literature review performed at the beginning of the investigation evidences a lack in the knowledge in the current cleaning methods which are still applied in an old-fashioned way and with intervals and durations based on past experiences rather than a meticulous scientific research. Therefore, the productivity of the current processes can be improved significantly by optimising these cleaning methods.

Also, from the literature review some investigations related to the cleaning of pipes with ultrasound were analysed, showing most of them had a common factor, the focus on non-industrial or domestic fouling. Here, to solve this problem which was considered essential for the validation of the method, Calcite was fouled in 30 cm pipes generating samples equivalent to industrial conditions in order to validate the method unambiguously.

In Chapter 4, the relation between displacement and acoustic pressure was presented to compare the displacement produced by a HPT or a pipe wall with the capability of producing the different types of cavitation. In addition, the cavitation prediction plots were presented for the frequencies used later on the investigation for the HPT transducers analysis and validation.

The modification of HPTs existing in the market has been compared with unmodified HPTs. The modification improves the attachment and increases the contact surface HPT-pipe. Also an analysis of the modes of vibration in the two types of transducers has been presented both with impedance analysis and a vibration analysis. It has been shown that the HPT produced even larger displacement than the displacement produced by the existing HPT. This is due to the change on

the mode of vibration. In addition, the displacements measured at the contact surface were compared with the displacements calculated in Chapter 4 that can produce transient cavitation under the conditions applied in the lab experimentation.

The generation of cavitation with the modified HPT in pipes has been detected with acoustic emission. This evidences that cavitation was generated for the fouling removal. For the visualization of the cavitation threshold, a plotting method has been proposed to detect the onset in a more accurate manner (see Chapter 6). In addition, it has been presented that a further analysis of the acoustic emission produced by stable cavitation oscillation by measuring ultraharmonics of high order may be able to present the cavitation onset in a more accurate manner.

The displacement produced in the pipe wall was related to the acoustic pressure generated in the liquid inside the pipe and this to discriminate the type of cavitation that is most likely to occur under the conditions applied in the lab. This relationship between displacement and cavitation was then used to validate the HPTs used and to analyse the cleaning results obtained in Chapter 7.

Also, it has been proved that cavitation is the phenomenon which removes hard fouling by the impact of bursting bubbles on the fouling surface. But, in contrast with classic ultrasonic cleaning, it has been seen that transient cavitation is necessary for the removal, instead of stable cavitation. This has been demonstrated by comparing the cleaning results with the cavitation prediction plots explained in Chapter 4 and produced in Chapter 7 for each cleaning condition.

The discussion in Chapter 4 and in Chapter 7 present the importance of considering only the displacements in the radial direction since they are the only displacements that can produce a compressional wave in the liquid and therefore produce acoustic cavitation.

It is important to highlight as strength of the investigation the use of Calcite as fouling for the validation of the method. Also, the measurement of the real displacement with a 3DSV has given the opportunity to relate the cleaning results with the displacement generated inside the pipelines. This is in contrast to the common practice which relies on the amount of power per surface which has been proven here that is not necessarily related with the rates of cleaning while the displacements, and therefore the acoustic pressure, are strictly related with the type of cavitation generated and hence with the capabilities of cleaning.

The differences between the current ultrasonic cleaning and the new method of cleaning can be summarized in the following table.

Table 9-1. Differences between current ultrasonic cleaning and the new method presented in this thesis.

Classic ultrasonic cleaning	Ultrasonic cleaning with wave guided
<ul style="list-style-type: none">• Components immersed in a tank	<ul style="list-style-type: none">• Equipment in operation
<ul style="list-style-type: none">• Cleaning occurring in a vibration liquid	<ul style="list-style-type: none">• Cleaning performed by the vibration of the structure
<ul style="list-style-type: none">• Need to stop production	<ul style="list-style-type: none">• Can be carried out during production
<ul style="list-style-type: none">• Flat transducers	<ul style="list-style-type: none">• Concave transducers
<ul style="list-style-type: none">• Stable cavitation	<ul style="list-style-type: none">• Transient cavitation

9.2 Recommendation for future work

This research consolidates the basic theory and concepts to be applied for the use of acoustic cavitation for the removal of fouling in pipe lines. Pipeline cleaning with acoustic cavitation is a new type of cleaning and therefore a new field where each part has potential room for further investigation. The most important recommendations for further work are explained below.

High power transducer design to improve the transduction of acoustic energy to the pipe. In Chapter 5 the vibration analysis of HPT has presented the existence of different resonant frequencies and different modes of vibration. These are complex vibrations and are not either a guided wave or a bulk wave. Therefore, a HPT design for better transduction of the acoustic energy could be useful to cover larger distances or larger pipe thicknesses. In addition, the possibility of using the different modes of vibration with different applications could be interesting for other scientific or industrial applications.

Related also with the transduction of acoustic energy, there is a lot of room for the optimisation of the attachment method to maximize the HPT operation. Different parameters such as couplant and optimal pressure on the HPT for the attachment could be considered for further investigation.

This thesis has presented the study related with a concept similar to a guided wave, but only a wave guided (see Section 7.1) by the pipe wall has been achieved. This leads to the study of optimal configuration of a transducer array for guided waves generation for cleaning. This has to consider the modes of propagation with large displacement in the radial direction if acoustic cavitation wants to be achieved. The collar design would need contributions from the HPT design since different shapes could improve the whole section of the pipe excitation and therefore the generation of a guided wave.

The optimisation of the frequency to be applied depending on the type of fouling and the process parameters is recommended. The frequency determines the size of the bubbles generated and the pressure generated by the jets produced by a transient cavitation implosion. This will produce pollution inside the process pipe with different sizes depending on the volume of the bubble.

Therefore an optimum between the minimum pressure to remove the hard scale fouling and the side of the removed fouling into the liquid should be investigated.

Furthermore, the analysis of the capabilities of the method under more challenging conditions should be analysed. Processes with high pressure will decrease the ratio P_a/P_o and therefore the necessary displacements for transient cavitation generation will increase. Other parameters such as viscosity and surface tension of the liquid may need more complex mathematical models than the one presented in this thesis in Chapter 4. For this, a mock-up scale plant would be necessary for the investigation which also will allow controlling other parameters like flow control and temperature.

Regarding the cavitation threshold for stable cavitation, it was presented in Chapter 6 that different ultraharmonics may be presenting the cavitation onset before than the first subharmonic $f/2$. This should be analysed with a validated method for stable cavitation detection i.e. photography method, and by applying small changes in the power to the transducer to see the potential changes in the acoustic emission signal.

References

- [1] P. Hopkins, "Oil and Gas Pipelines: Yesterday and Today," *Pipeline Systems Division (PSD), International Petroleum Technology Institute, American Society of Mechanical Engineers (ASME)*. Available online at http://www.engr.mun.ca/~spkenny/Courses/Undergraduate/ENGI8673/Reading_List/2007/_Hopkins.pdf, 2007.
- [2] U. S. E. P. Agency, "Drinking Water Infrastructure Needs Survey and Assessment," 2009.
- [3] M. M. Awad, "Fouling of heat transfer surfaces," Prof. Aziz Belmiloudi, Ed. http://cdn.intechopen.com/pdfs/13202/InTech-Fouling_of_heat_transfer_surfaces.pdf: INTECH Open Access Publisher, 2011, pp. 505–542.
- [4] B. I. Master, K. S. Chunangad, and V. Pushpanathan, "Fouling mitigation using helixchanger heat exchangers," in *Heat Exchanger Fouling and Cleaning: Fundamentals and Applications*, 2004, p. 317.
- [5] SINTEF, "Getting to the bottom of fouling problems," 2010. [Online]. Available: <http://www.sciencedaily.com/releases/2010/09/100927083905.htm>.
- [6] T. Casanueva-Robles and T. Bott, "The environmental effect of heat exchanger fouling: a case study," in *Proceedings of the 6th International Conference on Heat Exchanger Fouling and Cleaning—Challenges and Opportunities RP2*, 2005, pp. 5–10.
- [7] J. R. Taylor, *Risk analysis for process plant, pipelines and transport*. Taylor & Francis, 2003.
- [8] D. P. Dowling, C. E. Nwankire, M. Riihimäki, R. Keiski, and U. Nylén, "Evaluation of the anti-fouling properties of nm thick atmospheric plasma deposited coatings," *Surface and Coatings Technology*, vol. 205, no. 5, pp. 1544–1551, 2010.
- [9] H. Müller-Steinhagen, *Heat Exchanger Fouling: Mitigation and Cleaning Techniques*, vol. Unit 14. Essex, SS6 9RL: IChemE, 2000.
- [10] W. Marner and J. Suitor, "A Survey of Gas Side Fouling in Industrial Heat Transfer Equipment," *JPL Publication*, pp. 83–74, 1983. Report No: NASA-CR-173469
- [11] P. J. Fryer, P. T. Robbins, and K. Asteriadou, "Current knowledge in hygienic design: can we minimize fouling and speed cleaning?," *Procedia Food Science*, vol. 1, pp. 1753–1760, 2011.
- [12] I. G. De Carellan, P. Catton, C. Selcuk, and T.-H. Gan, "Methods for detection and cleaning of fouling in pipelines," *Emerging Technologies in Non-Destructive Testing V*, p. 231-236, 2012.

- [13] W. Liu, Z. Zhang, and P. Fryer, "Identification and modelling of different removal modes in the cleaning of a model food deposit," *Chemical engineering science*, vol. 61, no. 22, pp. 7528–7534, 2006.
- [14] P. Fryer and K. Asteriadou, "A prototype cleaning map: a classification of industrial cleaning processes," *Trends in Food Science & Technology*, vol. 20, no. 6, pp. 255–262, 2009.
- [15] P. A. Cole, K. Asteriadou, P. T. Robbins, E. G. Owen, G. A. Montague, and P. J. Fryer, "Comparison of cleaning of toothpaste from surfaces and pilot scale pipework," *Food and Bioproducts Processing*, vol. 88, no. 4, pp. 392–400, 2010.
- [16] S. Changani, M. Belmar-Beiny, and P. Fryer, "Engineering and chemical factors associated with fouling and cleaning in milk processing," *Experimental Thermal and Fluid Science*, vol. 14, no. 4, pp. 392–406, 1997.
- [17] W. Benzinger, U. Schygulla, M. Jäger, and K. Schubert, "Anti fouling investigations with ultrasound in a microstructured heat exchanger (pp: 197-201) En," in *Proceedings of 6th International Conference on Heat Exchanger Fouling and Cleaning*, 2005, pp. 5–10.
- [18] N. Nakagawa, M. Fujihara, C. Wu, and J. Satonobu, "Removal of Pipe Fouling Inside Pipes Using Ultrasonic Waves," *JSME International Journal Series C*, vol. 49, no. 3, pp. 713–718, 2006.
- [19] J. Glater, J. L. York, and K. S. Campbell, *Scale formation and prevention*, vol. 627. Academic Press, 1980.
- [20] M. Reddy and G. Nancollas, "Calcite crystal growth inhibition by phosphonates," *Desalination*, vol. 12, no. 1, pp. 61–73, 1973.
- [21] C. Y. Tai, M.-C. Chang, R.-J. Shieh, and T. G. Chen, "Magnetic effects on crystal growth rate of calcite in a constant-composition environment," *Journal of Crystal Growth*, vol. 310, no. 15, pp. 3690–3697, 2008.
- [22] J. Coey and S. Cass, "Magnetic water treatment," *Journal of Magnetism and Magnetic Materials*, vol. 209, no. 1, pp. 71–74, 2000.
- [23] K. H. Schoenbach, R. Alden III, and T. J. Fox, "Biofouling prevention with pulsed electric fields," in *Power Modulator Symposium, 1996., Twenty-Second International*, 1996, pp. 75–78.
- [24] F. Derrien, "Physical treatment of water in buildings," <http://www.irbnet.de/daten/iconda/CIB11807.pdf>, 2009, pp. 151–163.
- [25] D. Ellison and S. Duranceau, *Investigation of pipe cleaning methods*. American Water Works Assoc., 2003.
- [26] J. Chew, W. Paterson, and D. Wilson, "Fluid dynamic gauging for measuring the strength of soft deposits," *Journal of food engineering*, vol. 65, no. 2, pp.

175–187, 2004.

- [27] M. Henningsson, M. Regner, K. Östergren, C. Trägårdh, and P. Dejmek, “CFD simulation and ERT visualization of the displacement of yoghurt by water on industrial scale,” *Journal of food engineering*, vol. 80, no. 1, pp. 166–175, 2007.
- [28] J. Chew, W. Paterson, and D. Wilson, “Fluid dynamic gauging for measuring the strength of soft deposits,” *Journal of food engineering*, vol. 65, no. 2, pp. 175–187, 2004.
- [29] P.-Y. Qian, D. Rittschof, B. Sreedhar, and F. Chia, “Macrofouling in unidirectional flow: miniature pipes as experimental models for studying the effects of hydrodynamics on invertebrate larval settlement,” *Marine Ecology Progress Series*, vol. 191, pp. 141–151, 1999.
- [30] W. Blel, P. Legentilhomme, T. Bénézech, J. Legrand, and C. Le Gentil-Lelièvre, “Application of turbulent pulsating flows to the bacterial removal during a cleaning in place procedure. Part 2: Effects on cleaning efficiency,” *Journal of Food Engineering*, vol. 90, no. 4, pp. 433–440, 2009.
- [31] W. Blel, C. Le Gentil-Lelièvre, T. Bénézech, J. Legrand, and P. Legentilhomme, “Application of turbulent pulsating flows to the bacterial removal during a cleaning in place procedure. Part 1: Experimental analysis of wall shear stress in a cylindrical pipe,” *Journal of Food Engineering*, vol. 90, no. 4, pp. 422–432, 2009.
- [32] A. Pereira, J. Mendes, and L. Melo, “Monitoring cleaning-in-place of shampoo films using nanovibration technology,” *Sensors and Actuators B: Chemical*, vol. 136, no. 2, pp. 376–382, 2009.
- [33] J. N. H. Tiratsoo, *Pipeline pigging technology*, Second edition. Gulf Professional Publishing, 1992.
- [34] B. Nesbitt, *Handbook of Valves and Actuators: Valves Manual International*. Butterworth-Heinemann, 2011.
- [35] W. C. Hull, “Tube cleaning brush,” US Patent 2,559,757, 1951.
- [36] N. M. Redmond, “Pipe and sewer cleaning apparatus,” US Patent 2,481,152, 1949.
- [37] D. R. Smith, “Pig for use in cleaning the interior wall of a pipeline,” US Patent 5,384,929, 1995.
- [38] M. J. Lehtola, T. K. Nissinen, I. T. Miettinen, P. J. Martikainen, and T. Vartiainen, “Removal of soft deposits from the distribution system improves the drinking water quality,” *Water research*, vol. 38, no. 3, pp. 601–610, 2004.
- [39] J. Tiratsoo, *Pipeline pigging technology*. Gulf Professional Publishing, 1992.

- [40] M. Jalalirad, M. Abd-Elhady, and M. Malayeri, "Cleaning action of spherical projectiles in tubular heat exchangers," *International Journal of Heat and Mass Transfer*, vol. 57, no. 2, pp. 491–499, 2013.
- [41] I. Okouchi, S. Takahashi, Y. Mukai, K. Otake, T. Sasaki, and M. Miyai, "Cleaning system for heat conductive conduits of a heat exchanger," 1983.
- [42] L. Zhang, C. Li, C. Liu, T. Qu, and K. Liao, "Reserach on pigging model for the associated gas pipeline," *Natural Gas Industry*, vol. 28, no. 8, pp. 120–122, 2006.
- [43] F. Wang, "Antislip Design of Cleaning Robot for Municipal Drainpipes with Medium/Small Diameter," *Advanced Materials Research*, vol. 472, pp. 917–920, 2012.
- [44] Z. Liu and Y. Kleiner, "State of the Art Review of Inspection Technologies for Condition Assessment of Water Pipes," *Measurement*, vol. 46, no. 1, pp. 1–15, 2013.
- [45] O. Sivacoe, "Method of cleaning a pipe with a cylindrical pipe pig having pins in the central portion," US Patent 5,358,573, 1994.
- [46] G. Quarini, E. Aislie, D. Ash, A. Leiper, D. McBryde, M. Herbert, and T. Deans, "Transient thermal performance of ice slurries pumped through pipes," *Applied Thermal Engineering*, vol. 50, no. 1, pp. 743–748, 2012.
- [47] A. Kitanovski, D. Vuarnoz, D. Ata-Caesar, P. W. Egolf, T. M. Hansen, and C. Doetsch, "The fluid dynamics of ice slurry," *International journal of refrigeration*, vol. 28, no. 1, pp. 37–50, 2005.
- [48] G. Shire, G. L. Quarini, T. Rhys, and T. Evans, "The anomalous pressure drop behaviour of ice slurries flowing through constrictions," *International Journal of Multiphase Flow*, vol. 34, no. 5, pp. 510–515, 2008.
- [49] A. Monteiro and P. K. Bansal, "Pressure drop characteristics and rheological modeling of ice slurry flow in pipes," *International Journal of Refrigeration*, vol. 33, no. 8, pp. 1523–1532, 2010.
- [50] T. Evans, G. L. Quarini, and G. Shire, "Investigation into the transportation and melting of thick ice slurries in pipes," *international journal of refrigeration*, vol. 31, no. 1, pp. 145–151, 2008.
- [51] G. Quarini, E. Ainslie, M. Herbert, T. Deans, D. Ash, D. Rhys, N. Haskins, G. Norton, S. Andrews, and M. Smith, "Investigation and development of an innovative pigging technique for the water-supply industry," *Proceedings of the Institution of Mechanical Engineers, Part E: Journal of Process Mechanical Engineering*, vol. 224, no. 2, pp. 79–89, 2010.
- [52] F. Illán and A. Viedma, "Experimental study on pressure drop and heat transfer in pipelines for brine based ice slurry Part II: Dimensional analysis and rheological model," *International Journal of Refrigeration*, vol. 32, no. 5,

pp. 1024–1031, 2009.

- [53] M. Grozdek, R. Khodabandeh, and P. Lundqvist, “Experimental investigation of ice slurry flow pressure drop in horizontal tubes,” *Experimental thermal and fluid science*, vol. 33, no. 2, pp. 357–370, 2009.
- [54] F. Illán and A. Viedma, “Experimental study on pressure drop and heat transfer in pipelines for brine based ice slurry. Part I: operational parameters correlations,” *International Journal of Refrigeration*, vol. 32, no. 5, pp. 1015–1023, 2009.
- [55] B. McKeon, J. Morrison, B. McKeon, and J. Morrison, “Asymptotic scaling in turbulent pipe flow,” *Philosophical Transactions of the Royal Society A: Mathematical, Physical and Engineering Sciences*, vol. 365, no. 1852, pp. 771–787, 2007.
- [56] K. Morison and R. Thorpe, “Liquid distribution from cleaning-in-place sprayballs,” *Food and bioproducts processing*, vol. 80, no. 4, pp. 270–275, 2002.
- [57] C. Lelièvre, P. Legentilhomme, C. Gaucher, J. Legrand, C. Faille, and T. Bénézech, “Cleaning in place: effect of local wall shear stress variation on bacterial removal from stainless steel equipment,” *Chemical Engineering Science*, vol. 57, no. 8, pp. 1287–1297, 2002.
- [58] C. Gillham, P. Fryer, A. Hasting, and D. Wilson, “Cleaning-in-place of whey protein fouling deposits: mechanisms controlling cleaning,” *Food and bioproducts processing*, vol. 77, no. 2, pp. 127–136, 1999.
- [59] C. Lelievre, G. Antonini, C. Faille, and T. Bénézech, “Cleaning-in-Place: modelling of cleaning kinetics of pipes soiled by Bacillus spores assuming a process combining removal and deposition,” *Food and bioproducts processing*, vol. 80, no. 4, pp. 305–311, 2002.
- [60] G. F. Connelly Jr, “Inhibited acid composition for cleaning water systems,” US Patent 4,025,359, 1977.
- [61] D. P. Salisbury and R. L. Sloan, “Process for cleaning pipe dope and other solids from well systems,” US Patent 5,676,763, 1997.
- [62] G. F. Connelly Jr, “Pipe cleaning composition,” US Patent 3,969,255, 1976.
- [63] H. Martin, “Drain-pipe cleaning composition,” US Patent 2,997,444, 1961.
- [64] G. F. Connelly Jr, “Pumpable pipe cleaning composition,” US Patent 4,222,886, 1980.
- [65] T. Hodgkiess, K. Al-Omari, N. Bontems, and B. Lesiak, “Acid cleaning of thermal desalination plant: do we need to use corrosion inhibitors?,” *Desalination*, vol. 183, no. 1, pp. 209–216, 2005.

- [66] T. Abe and others, "The cleaning and disinfecting of hemodialysis equipment using electrolyzed strong acid aqueous solution," *Artificial organs*, vol. 23, no. 4, pp. 303–309, 1999.
- [67] S. L. Berry, J. L. Boles, G. F. Di Lullo, and others, "Evaluation of a Safe, Slightly Acidic Tubing Clean-Out Fluid," in *SPE Annual Technical Conference and Exhibition*, 2003.
- [68] P. E. Lien and J. H. Ludwig, "Vacuum waste pipe cleaning," U.S. Patent No. 5,873,944, 1999.
- [69] C. Gillham, P. Fryer, A. Hasting, and D. Wilson, "Enhanced cleaning of whey protein soils using pulsed flows," *Journal of Food Engineering*, vol. 46, no. 3, pp. 199–209, 2000.
- [70] M. Frondel, J. Horbach, and K. Rennings, "End-of-pipe or cleaner production? An empirical comparison of environmental innovation decisions across OECD countries," *Business Strategy and the Environment*, vol. 16, no. 8, pp. 571–584, 2007.
- [71] O. Yoffe, A. Wohlfarth, Y. Nathan, S. Cohen, and T. Minster, "Oil shale fueled FBC power plant-Ash deposits and fouling problems," *Fuel*, vol. 86, no. 17, pp. 2714–2727, 2007.
- [72] H. Förch, T. Oliver, and W. Hertle, "Chemical cleaning of PWR steam generators with a low temperature process," *Nuclear engineering and design*, vol. 147, no. 1, pp. 115–118, 1994.
- [73] P. Y. Duggirala, "Formation of calcium carbonate scale and control strategies in continuous digesters," *CD del II Coloquio Internacional sobre Celulosa de Eucalipto, Concepción, Chile, Mayo*, 2005.
- [74] A. C. Hieatt and J. H. Ludwig, "Method of cleaning and maintaining potable water distribution pipe systems," US Patent 5,885,364, 1999.
- [75] L. Brackeen, "Cleaning device for pipelines," US Patent 2,332,984, 1943.
- [76] U. Masaru, "Rotary cleaning device for drain pipe and the like," US Patent 4,687,011, 1987.
- [77] C. A. Prince, "Method of cleaning the inside of pipe," US Patent 2,745,231, 1956.
- [78] S. Probert and C. Chu, "Optimal internal lining of pipes to achieve energy conservation," *Applied Energy*, vol. 6, no. 1, pp. 49–62, 1980.
- [79] T. M. Walski, "Predicting costs of pipe cleaning and lining projects," *Journal of transportation engineering*, vol. 112, no. 3, pp. 317–327, 1986.
- [80] S. E. Jacks, "Method and apparatus for cleaning a pipe with sonic energy," US Patent 3,421,939, 1969.

- [81] B. J. Keenan Jr, "Sonic cleaning of wells," US Patent 3,970,146, 1976.
- [82] A. G. Bodine, "Sonic apparatus for cleaning wells, pipe structures and the like," US Patent 4,280,557, 1981.
- [83] R. A. Loose and W. R. Rice, "Venturi flow nozzle ultrasonic cleaning device," US Patent 4,762,668, 1988.
- [84] D. T. Hutchins Sr, "Method for cleaning water pipe," US Patent 5,178,684, 1993.
- [85] M. Legay, Y. Allibert, N. Gondrexon, P. Boldo, and S. Le Person, "Experimental investigations of fouling reduction in an ultrasonically-assisted heat exchanger," *Experimental Thermal and Fluid Science*, vol. 46, pp. 111–119, 2013.
- [86] V. A. Prisyazhniuk, "Physico-chemical principles of preventing salts crystallization on heat-exchange surfaces," *Applied Thermal Engineering*, vol. 29, no. 14, pp. 3182–3188, 2009.
- [87] B. Niemczewski, "Estimation of the suitability of selected organic solvents for ultrasonic cleaning," *Ultrasonics sonochemistry*, vol. 6, no. 3, pp. 149–156, 1999.
- [88] C. E. Brennen, *Cavitation and bubble dynamics*, vol. 44. Oxford University Press, USA, 1995.
- [89] A. D. Bryden, "Zebra mussel (*Dreissena polymorpha*) and other aquatic organism control," US Patent 5,432,756, 1995.
- [90] R. A. Brizzolara, W. Walch, D. J. Nordham, S. Hoover, M. S. Mazzola, M. Burnett, G. Licina, and R. Bott, "Pulsed acoustics for biofouling control in heat exchangers and piping systems," in *Proceedings of the Engineering Foundation Conference on Mitigation of Heat Exchanger Fouling and its Economic and Environmental Implications. Banff, Canada*, 1999.
- [91] M. Walch, M. Mazzola, and M. Grothaus, "Feasibility Demonstration of a Pulsed Acoustic Device for Inhibition of Biofouling in Seawater Piping," Naval Surface Warfare Center, Carderock Division, 2000.
- [92] R. A. Brizzolara, D. J. Nordham, M. Walch, R. M. Lennen, R. Simmons, E. Burnett, and M. S. Mazzola, "Non-chemical biofouling control in heat exchangers and seawater piping systems using acoustic pulses generated by an electrical discharge," *Biofouling*, vol. 19, no. 1, pp. 19–35, 2003.
- [93] M. Legg, M. Yücel, I. G. de Carellan, V. Kappatos, C. Selcuk, and T. Gan, "Acoustic methods for biofouling control: A review," *Ocean Engineering*, vol. 103, pp. 237–247, 2015.
- [94] R. B. Schaefer, "Pulsed Acoustic Sparker Bio-Fouling Control in Heat Transfer Equipment," Phoenix Science and Technology, Inc, 2002.

- [95] A. C. Miller and P. Lowry, "Controlling Zebra Mussels, Quagga Mussels, and Biofilm Growth with the Plasma Sparker," Zebra Mussel Technical Notes Collection, www.wes.army.mil/el/elpubs/zebtnote.html, 2000.
- [96] G. L. Mackie, P. Lowery, and C. Cooper, "Plasma pulse technology to control zebra mussel biofouling," Army engineer waterways experiment station Vickburg MS engineer research and development center , 2000.
- [97] R. Schaefer, R. Claudi, and M. Grapperhaus, "Control of Zebra Mussels Using Sparker Pressure Pulses.," *J. Am. Water Works Assoc.*, vol. 102, p. 113, 2010.
- [98] I. Mott, D. Stickler, W. Coakley, and T. Bott, "The removal of bacterial biofilm from water-filled tubes using axially propagated ultrasound," *Journal of Applied Microbiology*, vol. 84, no. 4, pp. 509–514, 1998.
- [99] N. Oulahal-Lagsir, A. Martial-Gros, M. Bonneau, and L. J. Blum, "'Escherichia coli-milk' biofilm removal from stainless steel surfaces: Synergism between ultrasonic waves and enzymes," *Biofueling*, vol. 19, no. 3, pp. 159–168, 2003.
- [100] M. Kopel, E. Degtyar, and E. Banin, "Surface acoustic waves increase the susceptibility of *Pseudomonas aeruginosa* biofilms to antibiotic treatment," *Biofouling*, vol. 27, no. 7, pp. 701–711, 2011.
- [101] M. R. Gavand, J. B. McClintock, C. D. Amsler, R. W. Peters, and R. A. Angus, "Effects of sonication and advanced chemical oxidants on the unicellular green alga *Dunaliella tertiolecta* and cysts, larvae and adults of the brine shrimp *Artemia salina*: A prospective treatment to eradicate invasive organisms from ballast water," *Marine pollution bulletin*, vol. 54, no. 11, pp. 1777–1788, 2007.
- [102] T. Bott and L. Tianqing, "Ultrasound enhancement of biocide efficiency," *Ultrasonics sonochemistry*, vol. 11, no. 5, pp. 323–326, 2004.
- [103] A. Watkinson, L. Louis, and R. Brent, "Scaling of enhanced heat exchanger tubes," *The Canadian Journal of Chemical Engineering*, vol. 52, no. 5, pp. 558–562, 1974.
- [104] D. Hasson, M. Avriel, W. Resnick, T. Rozenman, and S. Windreich, "Mechanism of calcium carbonate scale deposition on heat-transfer surfaces," *Industrial & Engineering Chemistry Fundamentals*, vol. 7, no. 1, pp. 59–65, 1968.
- [105] X. Xiaokai, "Research on the electromagnetic anti-fouling technology for heat transfer enhancement," *Applied Thermal Engineering*, vol. 28, no. 8, pp. 889–894, 2008.
- [106] C. Gabrielli, G. Maurin, G. Poindessous, and R. Rosset, "Nucleation and growth of calcium carbonate by an electrochemical scaling process," *Journal of crystal growth*, vol. 200, no. 1, pp. 236–250, 1999.

- [107] F. Alimi, M. Tlili, M. B. Amor, G. Maurin, and C. Gabrielli, "Effect of magnetic water treatment on calcium carbonate precipitation: Influence of the pipe material," *Chemical Engineering and Processing: Process Intensification*, vol. 48, no. 8, pp. 1327–1332, 2009.
- [108] A. Rakitin and V. Kichigin, "Electrochemical study of calcium carbonate deposition on iron. Effect of the anion," *Electrochimica Acta*, vol. 54, no. 9, pp. 2647–2654, 2009.
- [109] E. Dalas and P. G. Koutsoukos, "Calcium carbonate scale formation on heated metal surfaces," *Geothermics*, vol. 18, no. 1, pp. 83–88, 1989.
- [110] J. Chen and L. Xiang, "Controllable synthesis of calcium carbonate polymorphs at different temperatures," *Powder Technology*, vol. 189, no. 1, pp. 64–69, 2009.
- [111] A. Jones, J. Hostomsky, and L. Zhou, "On the effect of liquid mixing rate on primary crystal size during the gas-liquid precipitation of calcium carbonate," *Chemical engineering science*, vol. 47, no. 13, pp. 3817–3824, 1992.
- [112] Y. Liu, Y. Zou, L. Zhao, W. Liu, and L. Cheng, "Investigation of adhesion of CaCO₃ crystalline fouling on stainless steel surfaces with different roughness," *International Communications in Heat and Mass Transfer*, vol. 38, no. 6, pp. 730–733, 2011.
- [113] D. Chakraborty, V. Agarwal, S. Bhatia, and J. Bellare, "Steady-state transitions and polymorph transformations in continuous precipitation of calcium carbonate," *Industrial & engineering chemistry research*, vol. 33, no. 9, pp. 2187–2197, 1994.
- [114] M. E. Berndt and W. E. Seyfried, "Rates of aragonite conversion to calcite in dilute aqueous fluids at 50 to 100 C: experimental calibration using Ca-isotope attenuation," *Geochimica et cosmochimica acta*, vol. 63, no. 3, pp. 373–381, 1999.
- [115] C. Perdikouri, A. Kasiopas, T. Geisler, B. C. Schmidt, and A. Putnis, "Experimental study of the aragonite to calcite transition in aqueous solution," *Geochimica et Cosmochimica Acta*, vol. 75, no. 20, pp. 6211–6224, 2011.
- [116] N. H. de Leeuw and S. C. Parker, "Surface structure and morphology of calcium carbonate polymorphs calcite, aragonite, and vaterite: An atomistic approach," *The Journal of Physical Chemistry B*, vol. 102, no. 16, pp. 2914–2922, 1998.
- [117] M. Dinamani, P. V. Kamath, and R. Seshadri, "Electrochemical synthesis of calcium carbonate coatings on stainless steel substrates," *Materials research bulletin*, vol. 37, no. 4, pp. 661–669, 2002.
- [118] S. Keysar, D. Hasson, R. Semiat, and D. Bramson, "Corrosion protection of mild steel by a calcite layer," *Industrial & engineering chemistry research*, vol. 36, no. 8, pp. 2903–2909, 1997.

- [119] M. A. McClanahan, K. H. Mancy, and others, "Effect of pH on Quality of Calcium Carbonate Film Deposited From Moderately Hard and Hard Water (PDF)," *Journal-American Water Works Association*, vol. 66, no. 1, pp. 49–53, 1974.
- [120] D. Hasson and M. Karmon, "Method for rapid controlled coating of the inner surfaces of pipes with a tenacious calcite lining," US Patent 4,678,685, 1987.
- [121] G. B. Hatch, "Control of calcium carbonate deposition for corrosion inhibition," US Patent 2,299,748, 1942.
- [122] D. Hasson and M. Karmon, "Method for calcite coating on the inner surface of pipes," US Patent 4,264,651, 1981.
- [123] R. Hunhoff and N. S. Primus, "Method for lining pipes with calcite," US Patent 3,640,759, 1972.
- [124] T. Chen, A. Neville, K. Sorbie, and Z. Zhong, "Using in situ synchrotron radiation wide angle X-ray scattering (WAXS) to study CaCO₃ scale formation at ambient and elevated temperature," *Faraday discussions*, vol. 136, pp. 355–365, 2007.
- [125] L. E. Umoru, A. Oladipo, and O. O. Ige, "Carbonate Coatings as Protective Barriers for Pipe Borne Water Transport Material," *Journal of Minerals and Materials Characterization and Engineering*, vol. 11, no. 06, p. 609, 2012.
- [126] S. Muryanto, A. Bayuseno, H. Ma'mun, M. Usamah, and others, "Calcium Carbonate Scale Formation in Pipes: Effect of Flow Rates, Temperature, and Malic Acid as Additives on the Mass and Morphology of the Scale," *Procedia Chemistry*, vol. 9, pp. 69–76, 2014.
- [127] J. Mariin-Cruz, R. Cabrera-Sierra, M. Pech-Canul, and I. González, "Characterization of different allotropic forms of calcium carbonate scales on carbon steel by electrochemical impedance spectroscopy," *Journal of applied electrochemistry*, vol. 34, no. 3, pp. 337–343, 2004.
- [128] J. Watanabe and M. Akashi, "Formation of various polymorphs of calcium carbonate on porous membrane by electrochemical approach," *Journal of Crystal Growth*, vol. 311, no. 14, pp. 3697–3701, 2009.
- [129] E. A. Kulp and J. A. Switzer, "Electrochemical biomineralization: The deposition of calcite with chiral morphologies," *Journal of the American Chemical Society*, vol. 129, no. 49, pp. 15120–15121, 2007.
- [130] J. Martin-Cruz, E. Garcia-Figueroa, M. Miranda-Hernández, and I. González, "Electrochemical treatments for selective growth of different calcium carbonate allotropic forms on carbon steel," *Water research*, vol. 38, no. 1, pp. 173–183, 2004.
- [131] H. Le Chatelier and O. Boudouard, "Limits of flammability of gaseous mixtures," *Bull. Soc. Chim. (Paris)*, vol. 19, pp. 483–488, 1898.

- [132] J. Martín, “Estudio de los procesos de corrosión e incrustación del acero al carbono, en agua de sistemas de enfriamiento,” *Universidad Autónoma Metropolitana-Iztapalapa Ph. D. thesis*, 2004.
- [133] W. M. Haynes, *CRC handbook of chemistry and physics*. CRC press, 2013.
- [134] P. Elstnerová, M. Friák, H. O. Fabritius, L. Lymperakis, T. Hickel, M. Petrov, S. Nikolov, D. Raabe, A. Ziegler, S. Hild, and others, “Ab initio study of thermodynamic, structural, and elastic properties of Mg-substituted crystalline calcite,” *Acta biomaterialia*, vol. 6, no. 12, pp. 4506–4512, 2010.
- [135] E. Loste, R. M. Wilson, R. Seshadri, and F. C. Meldrum, “The role of magnesium in stabilising amorphous calcium carbonate and controlling calcite morphologies,” *Journal of Crystal Growth*, vol. 254, no. 1, pp. 206–218, 2003.
- [136] H. Miley, “Copper oxide films,” *Journal of the American Chemical Society*, vol. 59, no. 12, pp. 2626–2629, 1937.
- [137] J. Johnston, “The several forms of calcium carbonate,” *American Journal of Science*, no. 246, pp. 473–512, 1916.
- [138] Y.-Y. H. Chao and D. R. Kearns, “Electron spin resonance investigation of the soluble blue copper (II) hydroxide complex,” *The Journal of Physical Chemistry*, vol. 81, no. 7, pp. 666–668, 1977.
- [139] E. Brujan, T. Ikeda, and Y. Matsumoto, “On the pressure of cavitation bubbles,” *Experimental Thermal and Fluid Science*, vol. 32, no. 5, pp. 1188–1191, 2008.
- [140] T. Leighton, “Ultrasound in food processing,” Springer, 1998, p. 151.
- [141] M. Kornfeld and L. Suvorov, “On the destructive action of cavitation,” *Journal of Applied Physics*, vol. 15, no. 6, pp. 495–506, 1944.
- [142] P. V. Chitnis, N. J. Manzi, R. O. Cleveland, R. A. Roy, and R. G. Holt, “Mitigation of damage to solid surfaces from the collapse of cavitation bubble clouds,” *Journal of Fluids Engineering*, vol. 132, no. 5, p. 051303, 2010.
- [143] W. Lauterborn, “Optic cavitation,” *Le Journal de Physique Colloques*, vol. 40, no. C8, pp. C8–273, 1979.
- [144] C. Hurren, “A study into the ultrasonic cleaning of wool,” *Deaking University Ph. D. thesis*, 2009.
- [145] D. Heath, B. Sirok, M. Hocevar, and B. Pevcnik, “The use of the cavitation effect in the mitigation of CaCO₃ deposits,” *Strojnikovski vestnik-Journal of Mechanical Engineering*, vol. 59, no. 4, pp. 203–215, 2013.
- [146] A. A. Atchley and A. Prosperetti, “The crevice model of bubble nucleation,” *The Journal of the Acoustical Society of America*, vol. 86, no. 3, pp. 1065–

1084, 1989.

- [147] E. A. Neppiras, “Acoustic cavitation,” *Physics reports*, vol. 61, no. 3, pp. 159–251, 1980.
- [148] R. E. Apfel, “7. Acoustic Cavitation,” *Methods in experimental physics*, vol. 19, pp. 355–411, 1981.
- [149] T. Leong, M. Ashokkumar, and S. Kentish, “The fundamentals of power ultrasound—a review,” *Acoustics Australia*, vol. 39, no. 2, pp. 54–63, 2011.
- [150] P. R. Gogate, R. K. Tayal, and A. B. Pandit, “Cavitation: a technology on the horizon,” *Current Science*, vol. 91, no. 1, pp. 35–46, 2006.
- [151] R. Apfel, “Acoustic cavitation prediction,” *The Journal of the Acoustical Society of America*, vol. 69, no. 6, pp. 1624–1633, 1981.
- [152] L. A. Crum, “Measurements of the growth of air bubbles by rectified diffusion,” *The Journal of the Acoustical Society of America*, vol. 68, no. 1, pp. 203–211, 1980.
- [153] M. Safar, “Comment on papers concerning rectified diffusion of cavitation bubbles,” *The Journal of the Acoustical Society of America*, vol. 43, no. 5, pp. 1188–1189, 1968.
- [154] A. I. Eller, “Growth of bubbles by rectified diffusion,” *The Journal of the Acoustical Society of America*, vol. 46, no. 5B, pp. 1246–1250, 1969.
- [155] D.-Y. Hsieh and M. S. Plesset, “Theory of rectified diffusion of mass into gas bubbles,” *The Journal of the Acoustical Society of America*, vol. 33, no. 2, pp. 206–215, 1961.
- [156] H. Briggs, J. Johnson, and W. Mason, “Properties of liquids at high sound pressure,” *The Journal of the Acoustical Society of America*, vol. 19, no. 4, pp. 664–677, 1947.
- [157] F. G. Blake Jr, “Onset of Cavitation in Liquids,” *Harvard University Ph. D. thesis*, 1949.
- [158] R. P. Taleyarkhan, C. D. West, and F. Moraga, “Experimental determination of cavitation thresholds in liquid water and mercury,” *Transactions of the American Nuclear Society*, vol. 78, CONF-980606, 1998.
- [159] C. K. Holland and R. E. Apfel, “Thresholds for transient cavitation produced by pulsed ultrasound in a controlled nuclei environment,” *The Journal of the Acoustical society of America*, vol. 88, no. 5, pp. 2059–2069, 1990.
- [160] G. Iermetti, P. Ciuti, F. Calligaris, A. Francescutto, and N. V. Dezhkunov, “Cavitation threshold dependence on the rate of the transducer voltage variation,” *Ultrasonics*, vol. 34, no. 2, pp. 193–195, 1996.

- [161] S. Lin and F. Zhang, "Measurement of ultrasonic power and electro-acoustic efficiency of high power transducers," *Ultrasonics*, vol. 37, no. 8, pp. 549–554, 2000.
- [162] M. Prokic and M. Interconsulting, *Piezoelectric transducers modeling and characterization*. MP Interconsulting, 2004.
- [163] J. A. Gallego-Juarez, "High-power ultrasonic processing: recent developments and prospective advances," *Physics Procedia*, vol. 3, no. 1, pp. 35–47, 2010.
- [164] T. Mason, L. Paniwnyk, and J. Lorimer, "The uses of ultrasound in food technology," *Ultrasonics sonochemistry*, vol. 3, no. 3, pp. S253–S260, 1996.
- [165] M. J. Povey and T. J. Mason, *Ultrasound in food processing*. Springer, 1998.
- [166] L. Parrini, "New technology for the design of advanced ultrasonic transducers for high-power applications," *Ultrasonics*, vol. 41, no. 4, pp. 261–269, 2003.
- [167] S. Lin, L. Xu, and H. Wenxu, "A new type of high power composite ultrasonic transducer," *Journal of Sound and Vibration*, vol. 330, no. 7, pp. 1419–1431, 2011.
- [168] J. Gallego-Juárez, G. Rodríguez, V. Acosta, and E. Riera, "Power ultrasonic transducers with extensive radiators for industrial processing," *Ultrasonics sonochemistry*, vol. 17, no. 6, pp. 953–964, 2010.
- [169] J. Tsujino and T. Ueoka, "Characteristics of large capacity ultrasonic complex vibration sources with stepped complex transverse vibration rods," *Ultrasonics*, vol. 42, no. 1, pp. 93–97, 2004.
- [170] Y.-C. Chen, "Langevin Type Piezoelectric Transducer with Different Mass Loading on Both Ends," Department of Electronics Engineering and Computer Science, Tung-Fang Institute of Technology, 2005.
- [171] Morgan Electroceramics, *Piezoelectric Ceramics Properties & Applications*. 2009.
- [172] B. Engineer, "The mechanical and resonant behaviour of a dry coupled thickness-shear PZT transducer used for guided wave testing in pipe line," *Brunel University London Ph. D. thesis*, pp. 2–109, 2013.
- [173] K. Adachi, M. Tsuji, and H. Kato, "Elastic contact problem of the piezoelectric material in the structure of a bolt-clamped Langevin-type transducer," *The Journal of the Acoustical Society of America*, vol. 105, no. 3, pp. 1651–1656, 1999.
- [174] S. Kumar, R. Singh, T. Singh, and B. Sethi, "Surface modification by electrical discharge machining: A review," *Journal of Materials Processing Technology*, vol. 209, no. 8, pp. 3675–3687, 2009.
- [175] L. Svilainis, V. Dumbrava, and G. Motiejunas, "Optimization of the ultrasonic excitation stage," in *Information Technology Interfaces, 2008. ITI 2008. 30th*

International Conference on, 2008, pp. 791–796.

- [176] L. Svilainis and G. Motiejunas, “Power amplifier for ultrasonic transducer excitation,” *Ultragarsas (Ultrasound). Kaunas: Technologija*, vol. 58, pp. 30–36, 2006.
- [177] G. Ter Haar and S. Daniels, “Evidence for ultrasonically induced cavitation in vivo,” *Physics in medicine and biology*, vol. 26, no. 6, p. 1145, 1981.
- [178] J. L. Laborde, C. Bouyer, J.-P. Caltagirone, and A. Gérard, “Acoustic bubble cavitation at low frequencies,” *Ultrasonics*, vol. 36, no. 1, pp. 589–594, 1998.
- [179] D. Yount, E. Gillary, and D. Hoffman, “A microscopic investigation of bubble formation nuclei,” *The Journal of the Acoustical Society of America*, vol. 76, no. 5, pp. 1511–1521, 1984.
- [180] W. Huang, W. Chen, Y. Liu, and X. Gao, “The evolution of the cavitation bubble driven by different sound pressure,” *Ultrasonics*, vol. 44, pp. 407–410, 2006.
- [181] Z. Han, M. Keswani, E. Liebscher, M. Beck, and S. Raghavan, “Use of a Simple Cavitation Cell Set-Up with Replaceable Single Band Filters for Analysis of Sonoluminescence Signal from Megasonic Irradiated Gasified Aqueous Solutions,” *ECS Transactions*, vol. 58, no. 6, pp. 69–76, 2013.
- [182] R. Roy, A. Atchley, L. Crum, J. Fowlkes, and J. Reidy, “A precise technique for the measurement of acoustic cavitation thresholds and some preliminary results,” *The Journal of the Acoustical Society of America*, vol. 78, no. 5, pp. 1799–1805, 1985.
- [183] F. G. Sommer and D. Pounds, “Transient cavitation in tissues during ultrasonically induced hyperthermia,” *Medical physics*, vol. 9, no. 1, pp. 1–3, 1982.
- [184] V. S. Moholkar, S. P. Sable, and A. B. Pandit, “Mapping the cavitation intensity in an ultrasonic bath using the acoustic emission,” *AIChE journal*, vol. 46, no. 4, pp. 684–694, 2000.
- [185] S. Yoshizawa, S. Umemura, and Y. Matsumoto, “Cavitation detection with subharmonic emissions by low intensity sustaining ultrasound,” in *Ultrasonics Symposium, 2008. IUS 2008. IEEE*, 2008, pp. 772–775.
- [186] S. Komarov, K. Oda, Y. Ishiwata, and N. Dezhkunov, “Characterization of acoustic cavitation in water and molten aluminum alloy,” *Ultrasonics sonochemistry*, vol. 20, no. 2, pp. 754–761, 2013.
- [187] M. Strasberg, “Onset of ultrasonic cavitation in tap water,” *The Journal of the Acoustical Society of America*, vol. 31, no. 2, pp. 163–176, 1959.
- [188] E. Neppiras and W. Coakley, “Acoustic cavitation in a focused field in water at 1 MHz,” *Journal of Sound and Vibration*, vol. 45, no. 3, pp. 341–373, 1976.

- [189] R. F. Contamine, A. Wilhelm, J. Berlan, and H. Delmas, "Power measurement in sonochemistry," *Ultrasonics Sonochemistry*, vol. 2, no. 1, pp. S43–S47, 1995.
- [190] C. Campos-Pozuelo and C. Vanhille, "Electrical detection of the ultrasonic cavitation onset," *Ultrasonics sonochemistry*, no. 19, pp. 1266–1270, 2012.
- [191] J. R. Price, K. W. Hylton, K. W. Tobin, P. R. Bingham, J. D. Hunn, and J. R. Haines, "Detection of cavitation pits on steel surfaces using SEM imagery," in *Proceedings of SPIE*, 2003, vol. 5132, pp. 476–484.
- [192] J.-K. Choi, A. Jayaprakash, and G. L. Chahine, "Scaling of cavitation erosion progression with cavitation intensity and cavitation source," *Wear*, vol. 278, pp. 53–61, 2012.
- [193] Y. Gong, D. Zhang, and X. Gong, "Subharmonic and ultraharmonic emissions based on the nonlinear oscillation of encapsulated microbubbles in ultrasound contrast agents," *Chinese Science Bulletin*, vol. 50, no. 18, pp. 1975–1978, 2005.
- [194] C. C. Church, "The effects of an elastic solid surface layer on the radial pulsations of gas bubbles," *The Journal of the Acoustical Society of America*, vol. 97, p. 1510–1521, 1995.
- [195] R. Esche, "Untersuchung der schwingungskavitation in flüssigkeiten," *Acta Acustica united with Acustica*, vol. 2, no. Supplement 4, pp. 208–218, 1952.
- [196] P. D. Welch, "The use of fast Fourier transform for the estimation of power spectra: A method based on time averaging over short, modified periodograms," *IEEE Transactions on audio and electroacoustics*, vol. 15, no. 2, pp. 70–73, 1967.
- [197] R. Schilling and S. Harris, *Fundamentals of digital signal processing using MATLAB*. Cengage Learning, 2011.
- [198] D. Zmarzly and M. Szmechta, "Investigation of acoustic emission generated by cavitation in insulating oils," *Pomiary, Automatyka, Kontrola*, vol. 54, pp. 64–66, 2008.
- [199] J. L. Rose, *Ultrasonic waves in solid media*. Cambridge university press, 2004.
- [200] K. R. Lohr and J. L. Rose, "Ultrasonic guided wave and acoustic impact methods for pipe fouling detection," *Journal of food engineering*, vol. 56, no. 4, pp. 315–324, 2003.
- [201] J. Hua and J. Rose, "Guided wave inspection penetration power in viscoelastic coated pipes," *Insight-Non-Destructive Testing and Condition Monitoring*, vol. 52, no. 4, pp. 195–205, 2010.
- [202] R. E. Apfel, "Sonic effervescence: A tutorial on acoustic cavitation," *The Journal of the Acoustical Society of America*, vol. 101, no. 3, pp. 1227–1237,

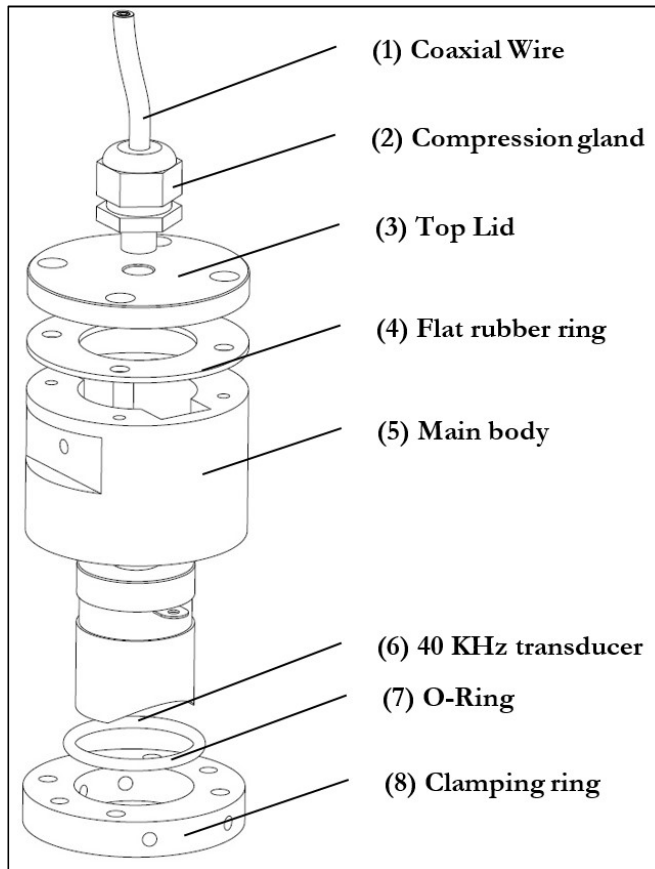
1997.

- [203] J. Collis, R. Manasseh, P. Liovic, P. Tho, A. Ooi, K. Petkovic-Duran, and Y. Zhu, “Cavitation microstreaming and stress fields created by microbubbles,” *Ultrasonics*, vol. 50, no. 2, pp. 273–279, 2010.
- [204] R. Wagterveld, L. Boels, M. Mayer, and G. Witkamp, “Visualization of acoustic cavitation effects on suspended calcite crystals,” *Ultrasonics sonochemistry*, vol. 18, no. 1, pp. 216–225, 2011.
- [205] D. E. Newbury, and N. W. Ritchie, “Is Scanning Electron Microscopy/Energy Dispersive X-ray Spectrometry (SEM/EDS) Quantitative?,” *Scanning*, vol. 35, no. 3, pp. 141–168, 2013.

APPENDIX A

Transducer clamping system (design detail):

The main objective of the system is to guarantee the correct alignment of all the parts attached along the pipe. This is a quite critical issue because the appropriate ultrasound implementation depends on the position and the verticality of the transducers. Relative position between them is an important point also, so, for this purpose, a physical reference which will fix the transducers into the correct position and distance will be used.



The exploded view on the left shows the different parts of the system: Beginning from top to down, the coaxial wire enters into the main body, which wraps the transducer protecting it from water, dust or other external agents.

This main body and the top lid are made in aluminium in order to decrease the weight, having also a cost-effective prototype. Inside, the transducer is clamped by the inner clamping stainless steel Ring, avoiding vertical movements using the radial screws and the lower clamping lid.

Figure A.1. CAD drawing of Clamping system parts version 2.

Rubber rings offer to the assembly an IP68 protection against dust and high pressure cleaning water.

Using a tough material in the Clamping ring part it's a matter of strength, in order to avoid losing its primal shape and clamping power when the screws become tight.

The upper assembly of Figure C.1 has shown the main parts of the transducer clamping system before attaching it to the pipe, but there's another step to do before, as it will be shown below in Figure C.2. The point is to fit the element and the pipe together, in a position referred to the main body in order to clamp it afterwards tightening the clamping lid. For this purpose, a pattern which has the same 50mm diameter shape as the pipe will be used. So, the first assembly will be the reference to the rest of the transducers using the Straightening Rule.

In order to mount the transducer correctly, it will be used a convex pattern with the same circular shape as the 50mm Diameter tube. This is a quite important issue because the other transducers have to be straightened with each other.

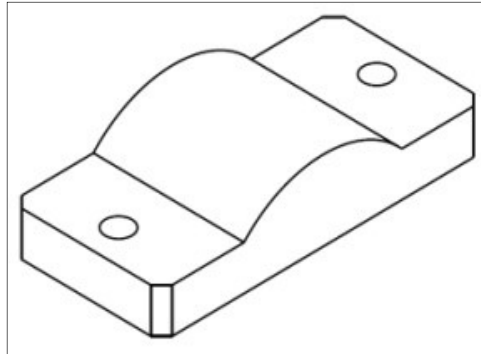


Figure A.2. Alignment Pattern.

Mounting the system

Figure C.3 shows the assembly sequence of the fixation system.

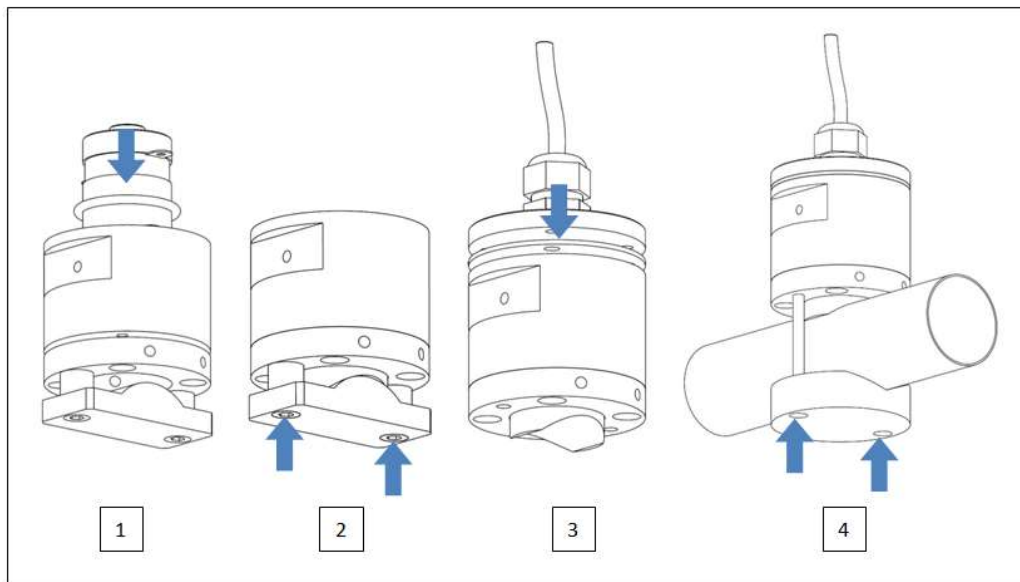


Figure A.3. Drawing of the assembly sequence.

- 1) Firstly, the **Clamping ring** screws have to be only screwed up a few millimeters into the **Main body** part, leaving a clearance and avoiding the compression of the **O-ring** against the **Main body** part. Doing that, the transducer will be easily inserted from above. Afterwards, the pattern from below has to be screwed up against the **Clamping ring** part, using the cylindrical separators.
- 2) Afterwards, the transducer has to be inserted down until it became fitted with the convex pattern; then it's time to screw up the parts in order to fix it well. Now the **O-ring** will compress the transducer, avoiding the possibility of pouring water inside.

- 3) In the third step, the lid, the flat rubber and the compression gland have to be screwed up against the upper side of the main body, completing the assembly. Now the whole system is sealed in both sides, up and down.
- 4) After removing the **Pattern** from below, gel and a 1mm silicone sheet will be applied between the transducer and the tube parts, assuring an optimum contact over the surface and improving the energy transfer through the tube.

Below, the two 80mms DIN912 M6 screws have to be tighten up to 2 Nm of maximum torque. Controlling this action, all the transducers will have, approximately a homogeneous contact with the surface and similar energy transference.

Bellow as shown in Figure C.4, the transducers are fixed and aligned using the ruler. The process of using a fixed reference is an easy way to assure a good alignment and verticality, improving the signal power for the process.

The lateral Straightening Rule is drilled each 20mm, and the transducers can be attached starting at a minimum of 80mm of the separation.

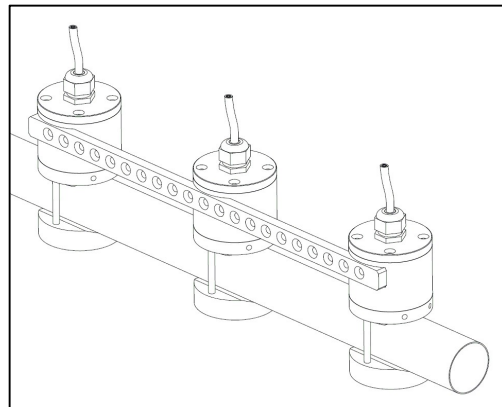


Figure A.4. Assembly with the transducers aligned by the ruler.

UltraCleanPipe HPT

The 40 kHz transducers have been designed, as it's shown in the drawing below of the Figure 5, to fit with the 50mm OD pipe. The maximum energy transference is reached using the stainless steel transducers due to its acoustic impedance which is similar to the pipe material.

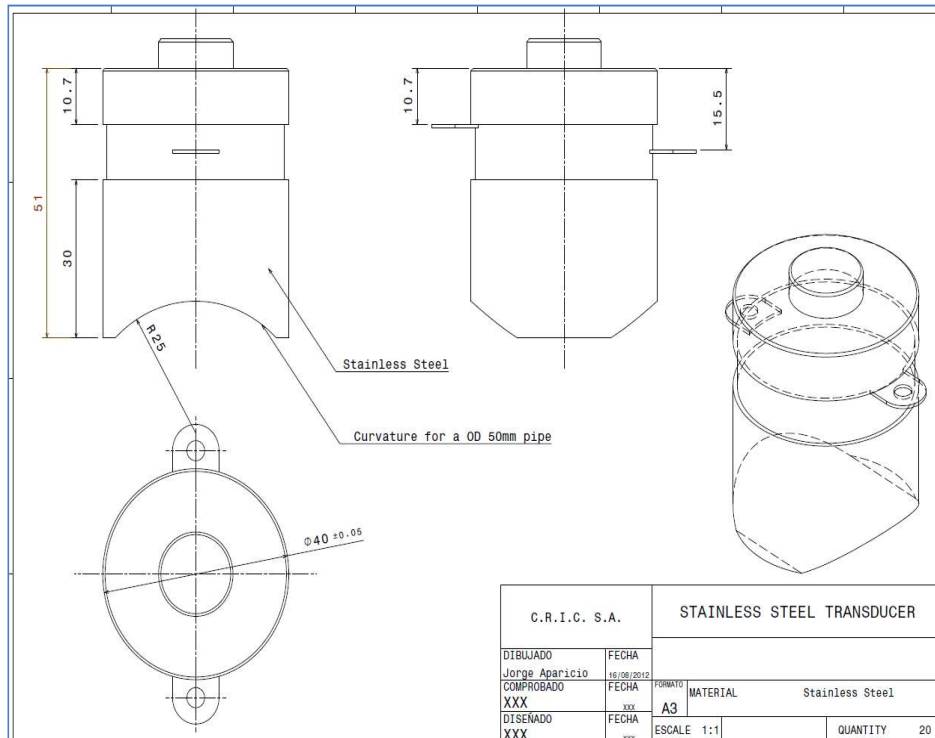


Figure A.5. UCP transducer drawing design



Figure A.6. UCP transducer

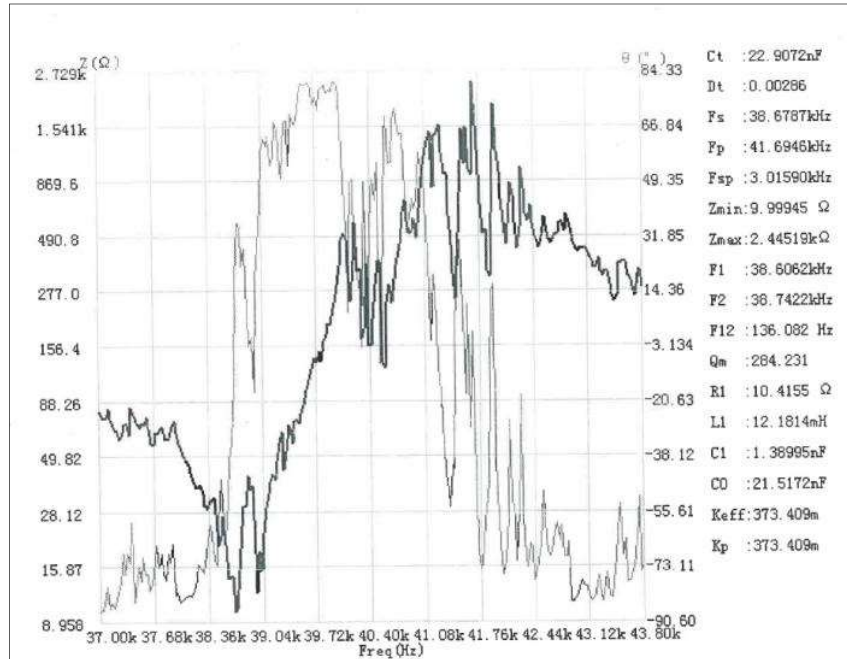


Figure A.6. Picture of the designed power transducers v1

APPENDIX B

Main high power testing, 1st prototype:

This will be a single safe box containing a high power ultrasonic power amplifier for driving one or more high power half wave resonant (Cleaning type transducers).

Specifications:

Input supply: 240V 50Hz.

Output supply: 0 to 300V rms over current protected.

Output Frequency: 20 to 100kHz.

Wave form: (square wave inverter) internal output filter to produce sinewave at transducers.

Output power: 300Watts max (20 to 80kHz), 200Watts (80 to 120kHz).

User Controls: Voltage adjustment knob, Frequency knob and transducer matching switch.

Frequency control: Switch and knob to select adjust, PRF, frequency sweep range and modulation, Ramp up, Ramp down and random.

Auto Frequency control: Circuit to track any changes in transducers, pipe and inverter.

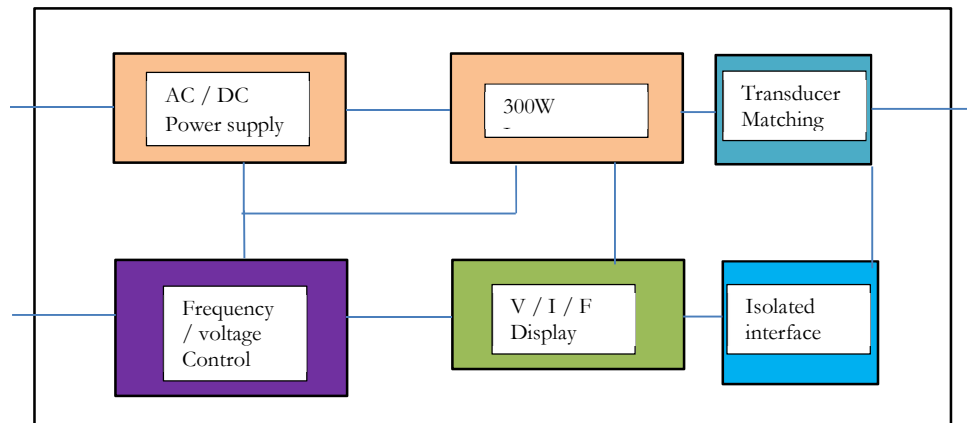


Figure B.1. Test box schematic diagram.

Main high power testing, 2nd prototype:

Box containing:

- Four high power ultrasonic power amplifiers (100W max) for driving one or more high power half wave (Cleaning type transducers) from 20kHz to 60kHz) (80 to 100kHz at reduced power of 60watts).
- A dual channel Teletest to be used with Version 1 TT software.

System integration

The fouling detection performance will depend on the type of transducers used Teletest long range ultrasonic or cleaning transducers.

The fouling removal performance will depend on frequency and transducers / coupling used.

This includes confirmation that the target power level is being generated in standing wave modes in pipes (both modes filling the entire structure for removal of large area fouling as well as localised thickness modes for removal of localised fouling) with the target wall thicknesses and diameters.

Two generators may be needed to supply the 'whole structure' standing wave modes which involve low kHz frequencies and the local thickness modes which involve low MHz frequencies.

Adjustments to the probes may be made as a result of these tests.

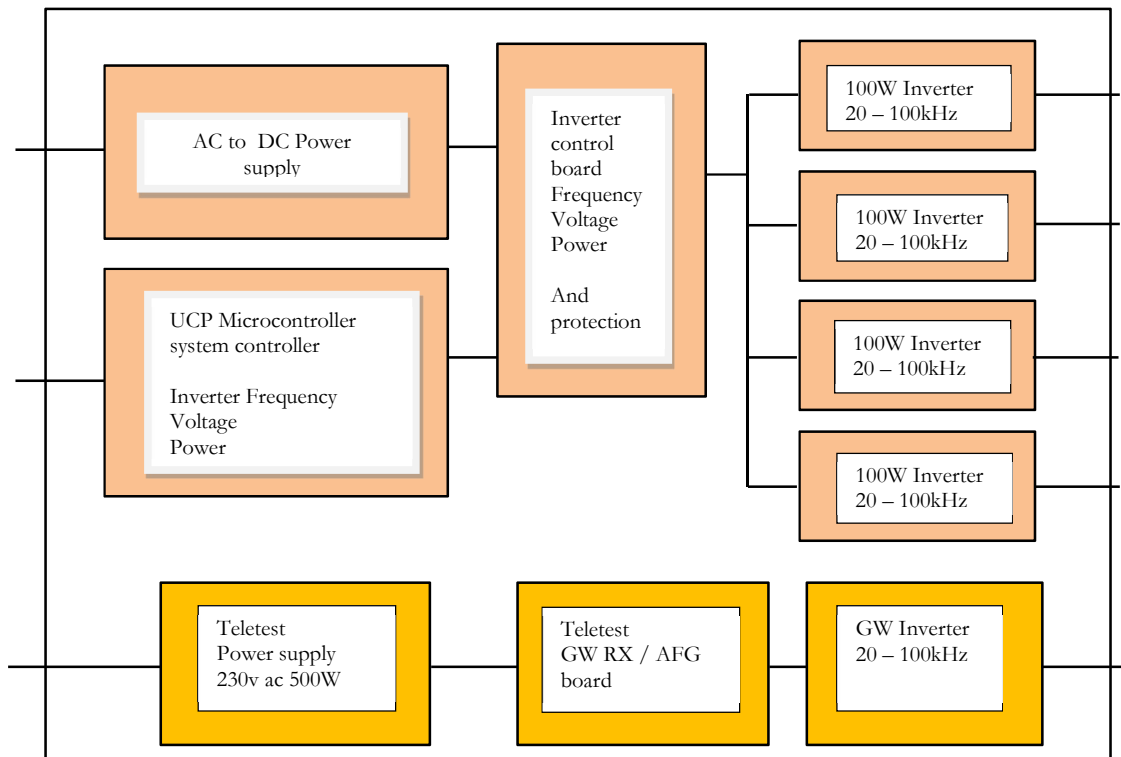


Figure B.2. System box schematic diagram.

Voltage specifications

Cleaning supplies:

4 off Power amplifier either based on linear / switched mode sinewave power variable voltage / frequency.

Square wave FET inverter and output transformer / resonant inductor (tapped).

100 Watts max each output into typical transducer.

Max output voltage: 700 to 1500V (rms) (depending on resonance).

Max output current: 2.0 Amps (rms) power factor depends on resonant frequency (current trip / level).

Controls:

Variable amplitude control.

Variable frequency control (separate outputs).

Possible sweep frequency to prevent standing nodes.

Overload protection (indicators) / reset if manual.

On off button for each output.

Computer control of all of the above (Local / remote).